ANGLIA RUSKIN UNIVERSITY

FACULTY OF HEALTH, EDUCATION,
MEDICINE AND SOCIAL CARE

DEVELOPMENT OF A HIGH-THROUGHPUT, PHENOTYPIC SCREENING ASSAY TO IDENTIFY NOVEL MEDICINES TO PREVENT DERMAL SCARRING

ALICE RUTH LAPTHORN

A thesis in partial fulfilment of the requirements of
Anglia Ruskin University for the degree of Doctor of Philosophy

This research programme was carried out in collaboration with
St. Andrew's Centre for Plastic Surgery and Burns

June 2021

Acknowledgements

It's no hidden secret that I lucked into having an amazing supervisory team. To my first supervisor Prof Selim Cellek, thank you for trusting me with this project, for all the valuable advice throughout my time in your team, and for fighting to make sure I had enough time to get this thesis to the point it is now.

I would like to thank my clinical supervisor Prof Peter Dziewulski for all his support, especially in the initial and latter stages of this project. Your clinical insights into the world of burn injuries and scarring have ensured the project remains focused on helping those affected.

No supervisory team would be complete without a Dr Marcus Ilg. There is so much I need to thank you for. Not only have you been the best lab mentor, but you have become one of my dearest friends. Thank you for putting up with my stupid questions and sharing your snacks/coffee with me. Also, thank you for bringing Alex (and subsequently Pixie) into my life, you guys are the best. P.S. Sorry for never watching Fight Club.

A huge thank you to the Peterborough Burns Unit Appeal Fund for providing the funding for this PhD project. Further, I'd like to thank Dr Justine Sullivan, Natalie Fox, Mr Odhran Shelley and the entire team at St. Andrews Centre for Plastic Surgery and Burns for your support in the recruitment of patients to this project. A special thank you to all the patients who donated their skin to be used in this study, you've made this research possible.

To my MTRC colleagues, Stephen, Jo, Sophie and Sara – thank you for letting me tap into your expertise when needed, and for your kind and motivating words in the final months.

I would not have pursued this PhD if it wasn't for an email one Friday afternoon from my mum. Being the youngest child, my parents and sister have always been my biggest inspirations. Their love and continued support have allowed me to pursue my dreams. Thank you so much for going on this journey with me, I hope I have made you all proud.

To my friends, the majority of who I have not seen in well over a year, thank you, thank you, thank you. I am so grateful for your patience, for the days when you were there to celebrate the good and pick me up on days when nothing went right. A special shout out to Alice, Hannah and Dan. I feel so lucky to have friends who are also entangled in the weird world of research, you have helped me make sense of everything.

A final word to every #PandemicPGR who has navigated the COVID-19 pandemic and shared their struggles on social media. Thank you for providing me with a little corner of solace and reminding me that every emotion I've experienced is completely natural. I stand in solidarity with those of you who are still fighting for funding extensions and support from your institutions.

ANGLIA RUSKIN UNIVERSITY

ABSTRACT

FACULTY OF HEALTH, EDUCATION, MEDICINE AND SOCIAL CARE

DOCTOR OF PHILOSOPHY

DEVELOPMENT OF A HIGH-THROUGHPUT, PHENOTYPIC SCREENING ASSAY TO IDENTIFY NOVEL MEDICINES TO PREVENT DERMAL SCARRING

ALICE RUTH LAPTHORN

JUNE 2021

Introduction: Dermal scarring affects 91% of burn patients every year and yet, there is currently no effective treatment for their prevention. Dermal scarring is often caused by the dysregulation in different stages of the wound healing process – particularly the sustained transformation of fibroblasts to alpha-smooth muscle actin (α-SMA) expressing myofibroblasts. The aim of this thesis was to identify novel drugs that can be re-purposed for the prevention of dermal scar formation, using a phenotypic, high-throughput screening (HTS) assay.

Materials & Methods: Primary fibroblasts, derived from excised scar tissue, were exposed to transforming growth factor beta-1 (TGF-β1) to induce transformation to myofibroblasts. Using the In-Cell ELISA method, a HTS assay was optimised and validated before screening 1,954 approved drugs. Hits were defined as showing >80% inhibition of α-SMA expression, whilst maintaining >80% cell viability. Anti-myofibroblast activity of the candidate drugs was confirmed by construction of concentration response curves, before investigating their effects on cell viability, extracellular matrix (ECM) production and keratinocyte epithelial-mesenchymal transition (EMT).

Results: A HTS assay measuring α-SMA expression was optimised and validated, yielding a Z-factor of 0.59 ± 0.03. The screening of 1,954 approved drugs identified 90 hits (4.6%) that successfully inhibited myofibroblast transformation. 10 hits were identified as having a desirable safety profile and could be used for topical application. The anti-myofibroblast activity of one drug class (hydroxypyridone anti-fungals) was confirmed – ciclopirox (IC_{50} = 16.7 ± 2.3 μM), ciclopirox ethanolamine (IC_{50} = 10.3 ± 0.8 μM) and piroctone olamine (IC_{50} = 1.4 ± 0.1 μM). Secondary assays showed that the hydroxypyridone anti-fungals could reduce ECM production and inhibit keratinocyte EMT, whilst maintaining cell viability.

Conclusions: Using primary fibroblasts, a phenotypic HTS assay identified hydroxypyridone anti-fungals as being able to inhibit TGF-β1-induced myofibroblast transformation. These drugs exhibited further anti-fibrotic effect when measuring for ECM production and keratinocyte EMT. This is the first study to identify and investigate the anti-fibrotic effect of hydroxypyridone anti-fungals in dermal scarring, suggesting that these drugs could be re-purposed as medical therapy to prevent dermal scarring.

Keywords: Fibrosis, phenotypic screening, dermal scarring, myofibroblast transformation

Table of Contents

List of figures

List of tables

List of abbreviations

α-SMA	α-smooth muscle actin
ACE	Angiotensin-converting-enzyme
ACTA2	Gene for α-smooth muscle actin
AML	Acute myeloid leukaemia
ANOVA	Analysis of variance
ARU	Anglia Ruskin University
bFGF	Basic fibroblast growth factor
BMP	Bone morphogenetic protein
BMR	Basal metabolic rate
cAMP	Cyclic adenosine monophosphate
CK-14	Cytokeratin-14
CKD	Chronic kidney disease
CPX	Ciclopirox
CPXO	Ciclopirox ethanolamine
CREB	cAMP response element-binding protein
CTGF	Connective tissue growth factor
CVD	Cardiovascular disease
DAPI	4′,6-diamidino-2-phenylindole
DIEP	Deep inferior epigastric perforator
DKK1	Dickkopf-related protein-1
DMEM	Dulbeccos's Modified Eagle Media
DMSO	Dimethyl sulfoxide
DNA	Deoxyribonucleic acid
EC_{50}	Half maximal effective concentration
ECM	Extracellular matrix
EDTA	Ethylenediaminetetraacetic acid
EGFR	Epidermal growth factor receptor
EGTA	Ethylene glycol-bis(β-aminoethyl ether)-N,N,N′,N′-tetraacetic acid
ELISA	Enzyme-linked immunosorbent assay
EMA	European medicines agency

E_{max}	Maximal effect
EMT	Epithelial-mesenchymal transition
EndMT	Endothelial-mesenchymal transition
ERK	Extracellular signal-regulated kinase
FCS	Foetal calf serum
FDA	Food and Drug Administration
FITC	Fluorescein isothiocyanate
GAPDH	Glyceraldehyde 3-phophate dehydrogenase
h	Hour(s)
H&E	Haematoxylin and Eosin
hBFGF	Human basic fibroblast growth factor
HCl	Hydrochloric acid
HIF-1α	Hypoxia inducible factor-1α
HIV	Human immunodeficiency virus
HKGS	Human keratinocyte growth serum
HSCs	Hepatic stellate cells
HTS	High-throughput screening
IC_{50}	Half maximal inhibitory concentration
ICC	Immunocytochemistry
ICE	In-Cell ELISA
IFNγ	Interferon gamma
IHC	Immunohistochemistry
ILD	Interstitial lung disease
IL	Interleukin
IPF	Idiopathic pulmonary fibrosis
JNK	c-Jun N-terminal kinase
kDa	Kilodalton
KOSR	Knock-out serum replacement
lncRNA	Long non-coding RNA
LoS	Localised scleroderma
LRP	Low-density lipoprotein receptor-related protein

LTBP	Latency associated peptide-latent TGF-β1 binding protein
MAPK	Mitogen-activated protein kinase
MEK	MAPK/ERK kinase
Min	Minute(s)
miRNA	microRNA
MMPs	Matrix metalloproteinases
MTT	3-(4,5-dimethylthiazol-2-yl)-2,5-diphenyltetrazolium bromide
Na_3VO_4	Sodium orthovanadate
$Na_4P_2O_7$	Tetrasodium pyrophosphate
NaCl	Sodium chloride
NADPH	Nicotinamide adenine dinucleotide phosphate
NaF	Sodium fluoride
NFDM	Non-fat dried milk
NHS	National Health Service
OCT	Optimal cutting temperature compound
OPX	Piroctone olamine (Octopirox)
PBS	Phosphate-buffered saline
PD	Peyronie's disease
PDGF	Platelet-derived growth factor
PDGFR	Platelet-derived growth factor receptor
PFA	Paraformaldehyde
PDE5i	Phosphodiesterase type 5 inhibitor
Pen/Strep	Penicillin/streptomycin
PI3K	Phosphoinositide 3-kinases
PMSF	Phenylmethane sulfonyl fluoride
PPARγ	Peroxisome proliferator-activated receptor gamma
PVDF	Polyvinylidene difluoride
RD	Rhabdomyosarcoma
RIPA	Radioimmunoprecipitation assay
RNA	Ribonucleic acid
ROS	Reactive oxygen species

s	Second(s)
SEM	Standard error of the mean
SERM	Selective oestrogen receptor modulator
SSc	Systemic scleroderma
TBS	Tris-buffered saline
TBSA	Total body surface area
TBS-T	Tris-buffered saline with Tween
TGF-β	Transforming growth factor beta
TNF	Tumour necrosis factor
TRITC	Tetramethylrhodamine
UIP	Usual interstitial pneumonia
UK	United Kingdom
V	Volt(s)
VEGF	Vascular endothelial growth factor
Wnt	Wingless-related integration site
Z'	Z-factor

Copyright declaration

Chapter 1: Literature review

1.1. Physiology of the skin

As one of the body's largest organs, the skin, in combination with its specialised appendages, form the integumentary system (Marieb and Hoehn, 2014; Kolarsick, Kolarsick and Goodwin, 2008). The integumentary system is responsible for several functions such as thermoregulation, moisture control, and tissue repair (Marieb and Hoehn, 2014). However, functioning as a protective barrier to protect the inside of the body from the external environment, is widely regarded as the skins most vital function (Boer et al., 2016).

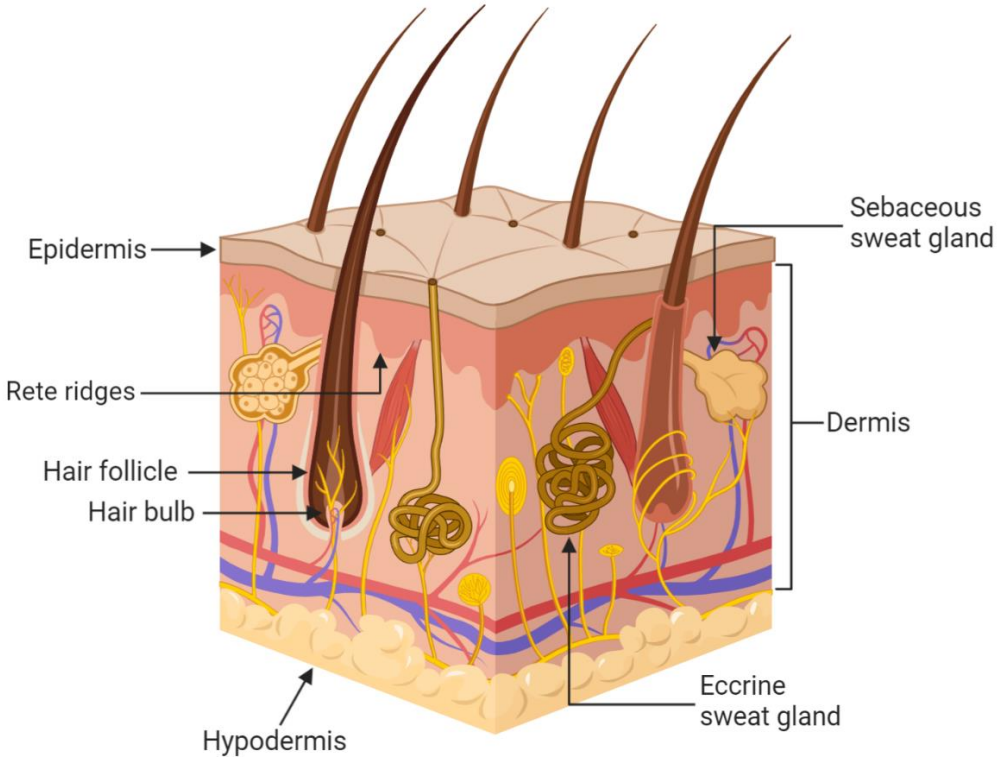

Figure 1-1: Cross-section of the skin showing all major components. Skin is composed of three layers – epidermis, dermis, and hypodermis, which house the main skin appendages such as hair follicles and sweat glands. Image created using BioRender.

The skin is composed of three different layers, all with distinct cell populations and functions. The top layer of the skin is known as the epidermis, which acts as the immediate barrier to the external environment (Marieb and Hoehn, 2014). The epidermis consists of five individual layers termed the stratum basale (bottom layer), spinosum, granulosum, lucidum and corneum (the uppermost layer), of which approximately 80% of the cell population are keratinocytes (Kolarsick, Kolarsick and Goodwin, 2008). Keratinocytes are responsible for the production of keratin, an intermediate filament protein which forms part of the epidermal cytoskeleton and helps to ensure mechanical stability of the epidermis (Moll, Divo and Langbein, 2008; Bragulla and Homberger, 2009). Keratinocytes undergo a process called keratinization, where the cytoplasmic levels of keratin accumulate as keratinocytes migrate from the bottom layer of the epidermis (stratum basale) to the uppermost layer (stratum corneum) (Kolarsick, Kolarsick

and Goodwin, 2008). This accumulation of keratin results in the flattening of the cells and loss of cellular components, as keratin bundles form attachments with the plasma membrane (Kolarsick, Kolarsick and Goodwin, 2008; Bragulla and Homberger, 2009). One of the unique features of the epidermis is that it is self-renewing, a process that will occur thousands of times over someone's life (Leary et al., 1992; Alberts et al., 2014). As cells in the top layer of the epidermis are eventually shed from the skin, to compensate for this loss, cells in the stratum basale are highly proliferative and are responsible for producing new cells that go on to differentiate into keratinocytes (Alberts et al., 2014).

Melanocytes are responsible for the production of melanin and can be found in the stratum basale and in hair follicles (Kolarsick, Kolarsick and Goodwin, 2008). Melanocytes play a vital role in the pigmentary system of the skin and therefore not only determine the colour of a person's skin, but also their hair and iris colour (Tsatmali, Ancans and Thody, 2002; Cichorek et al., 2013). Keratinocytes form close interactions with neighbouring melanocytes in the epidermis, to facilitate the movement of melanin via melanosomes, which is achieved through dendrites formed by melanocytes (Tsatmali, Ancans and Thody, 2002; Cichorek et al., 2013).

Two other cell types that are found in the epidermis are Merkel, and Langerhans cells. Merkel cells, like melanocytes, can be found in both the basal layer of the epidermis and in the hair follicle (Moll, 1994). Merkel cells form synaptic junctions with dermal sensory axons, which allows them to function as mechanoreceptors and are often found in abundance in the fingertips (Kanitakis, 2002; Kolarsick, Kolarsick and Goodwin, 2008). Langerhans cells are dendritic in nature, often described as mononuclear phagocytes that reside in the stratum granulosum and spinosum (West and Bennett, 2018). Langerhans cells are responsible for identifying foreign antigens in the skin and polarising $CD4^+$ T cells to initiate an immune response and cell migration (West and Bennett, 2018; Kanitakis, 2002).

The next layer of the skin, the dermis, is primarily composed of filamentous connective tissue, providing the skin with elasticity and support (Rippa, Kalabusheva and Vorotelyak, 2019). The dermis makes up most of the skin, acting as a scaffold for sweat glands, vascular networks, and hair follicles (Rippa, Kalabusheva and Vorotelyak, 2019). Furthermore, the dermis plays vital roles in thermoregulation, wound healing, and moisture control (Kolarsick, Kolarsick and Goodwin, 2008). The dermis has two distinct layers – the papillary and reticular dermis, which are distinguished by the architecture of the extracellular matrix (ECM) present in each layer (Rippa, Kalabusheva and Vorotelyak, 2019). The ECM is composed of multiple components, such as collagens (typically type I/III) which provide tensile strength, elastin which provides the skin with elasticity, and fibronectin which helps fibroblasts and keratinocytes attach to the ECM for migration (Uitto, Olsen and Fazio, 1989). The most abundant cells in the dermis are

fibroblasts, which are responsible for co-ordinating the production of ECM and wound contraction, during wound healing (Tracy, Minasian and Caterson, 2016). In their resting state, the key role of fibroblasts is the remodelling and organisation of the ECM (Sorrell and Caplan, 2004).

The final layer of the skin is the hypodermis, which is primarily formed of loose connective tissue and pockets of white adipose tissue (Wong et al., 2016). This subcutaneous fat is often described as an endocrine organ, as it is responsible for the conversion of androstenedione to estrone (Wong et al., 2016). Furthermore, the hypodermis is home to adipocytes and lipocytes which are responsible for stimulating the process of thermogenesis of fat and for playing a vital role in adipose homeostasis (Wong et al., 2016; Driskell et al., 2014).

1.2. Wound Healing

The process of wound healing in humans is highly conserved and is defined as the process by which the body resolves any injury or trauma that occurs to its tissues (Gonzalez et al., 2016; Sorg et al., 2017; Wynn and Vannella, 2016). In the skin, the main aim of wound healing is to restore it to its key function as a protective barrier (Boer et al., 2016). Wound healing is achieved by three distinct phases, which are often identified by the cell populations present during these stages (Li, Chen and Kirsner, 2007). Figure 1-2 outlines the normal wound healing process which works towards the complete repair of the injured tissue, and what cells are present in those stages.

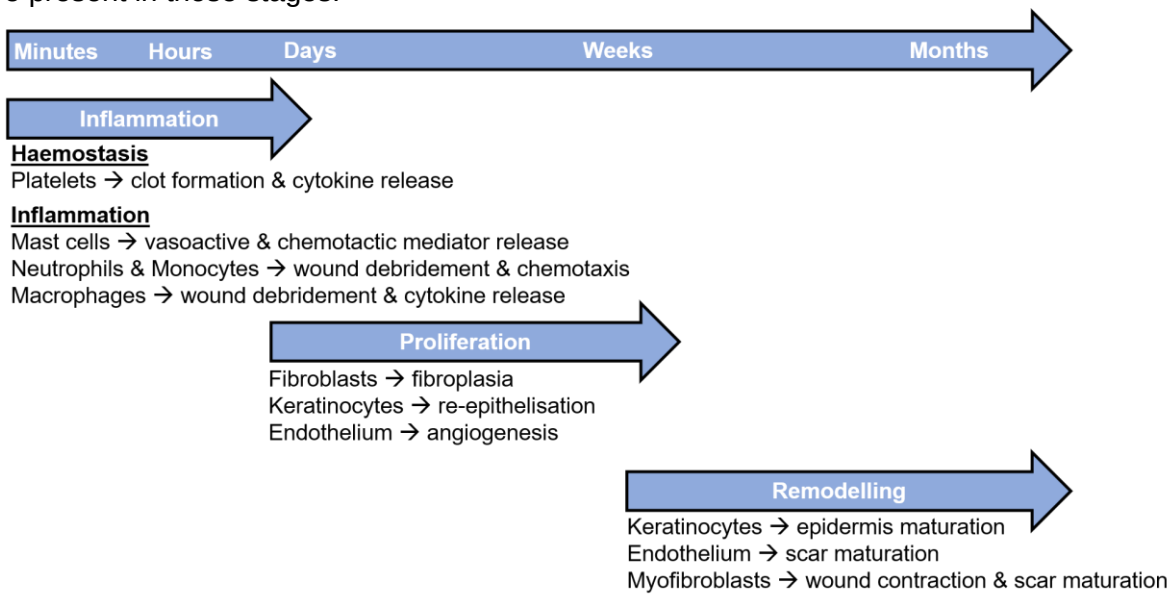

Figure 1-2: Schematic of the stages of wound healing, identifying the key cells/components responsible and how long each stage occurs for. The first stage of wound healing is inflammation where platelets and immune cells are responsible for co-ordinating the inflammatory response. Proliferation begins towards the end of the inflammatory stage, in which epithelial cells and fibroblasts are responsible for wound closure. Finally, the remodelling stage is responsible for maturation of the scar/epidermis. Image adapted from (Li, Chen and Kirsner, 2007)

Within minutes of an injury occurring, the wound healing process is initiated, with the primary aim to restore the integrity of the tissue (Martin, 1997; Singer and Clark, 1999). To prevent excessive bleeding at the wound site, the process of haemostasis is initiated and will last until a sufficient immune response has been activated – usually for no more than 24 hours (Gale, 2011). During haemostasis, platelets become activated upon exposure to ECM components (e.g. fibronectin) allowing them to aggregate within the wound (Gale, 2011). Platelet aggregation, combined with the production of other ECM components (e.g. fibrin and vitronectin), creates a temporary barrier that prevents both excessive bleeding and the entry of microorganisms into the wound (Kahaleh and Mulligan-Kehoe, 2012). During this process, tissue resident mast cells are responsible for the production of pro-inflammatory cytokines initiating the recruitment of immune cells to the wound site. Mast cells also aid in fibroblast activation, later in the wound healing process (Eming, Krieg and Davidson, 2007; Trautmann et al., 2000).

The inflammatory response is established within the first 24 hours after initial injury and can last for up-to 72 hours after (Gonzalez et al., 2016). Inflammation is initially co-ordinated in the latter stages of haemostasis, in which immune cells are recruited to the wound site. Both a local tissue and systemic inflammatory response is initiated, with neutrophils and monocytes recruited first from the surrounding vasculature. Macrophages are then recruited when neutrophil numbers start to decline (Li, Chen and Kirsner, 2007). Neutrophils play a key role in the initial inflammatory response, as they are responsible for protecting against infection, and killing any foreign microbes that have penetrated the skin (Wilgus, Roy and McDaniel, 2013; Gonzalez et al., 2016). Neutrophils also produce key pro-inflammatory cytokines and proteases, which aid in the activation of cells during the proliferation stage (Theilgaard-Mönch et al., 2004; Dalli et al., 2013). Monocytes that are recruited to the wound site differentiate into macrophages and continue to aide in the removal of debris and microorganisms (Sindrilaru et al., 2011). Furthermore, macrophages also help to prepare the wound for closure, by debriding the wound site and removing damaged matrix (Frykberg and Banks, 2015).

Following inflammation, the next step of the wound healing process is known as proliferation. As the name suggests, a key part of this stage is the proliferation of different cell populations (e.g. fibroblasts and keratinocytes), with the aim to achieve wound closure (Li, Chen and Kirsner, 2007). The proliferation stage of wound healing typically begins 72 hours following initial injury, however the time frame for the resolution of this stage is dependent on the size of the wound (Sorg et al., 2017). Proliferation can be broken down into different stages that occur in parallel. One of these stages is angiogenesis, the process by which new blood vessels are formed in tissues. Macrophages release cytokines such as vascular endothelial growth factor (VEGF) to stimulate the process of angiogenesis and increase blood flow in that area

(Kumar et al., 2015; Brem et al., 2009). During wound healing this is beneficial, as the increased blood flow allows for the infiltration of cells and proteins that aid in the wound healing process (Kumar et al., 2015).

The next stage of proliferation is known as fibroplasia, which sees the transformation of resting fibroblasts in the dermis to activated myofibroblasts (Falke et al., 2015). Myofibroblasts are the cells responsible for the formation of necessary granulation tissue, allowing for cell migration across the wound bed (Tracy, Minasian and Caterson, 2016). As shown in Figure 1-3, in the presence of mechanical stress (such as the initial injury itself) fibroblasts begin their transformation process and become proto-myofibroblasts, where they begin to express the ECM component fibronectin (Falke et al., 2015). Following exposure to inflammatory cytokines (e.g. transforming growth factor beta-1; TGF-β1) and further mechanical stress, fibroblasts complete full transformation to alpha-smooth muscle actin (α-SMA) expressing myofibroblasts. Myofibroblasts are responsible for the increased biosynthesis of key extracellular matrix proteins (e.g. collagen and elastin) which forms the granulation tissue (Caves et al., 2011; Petrov, Fagard and Lijnen, 2002). Furthermore, following transformation to activated cells, these myofibroblasts also significantly increase the production of key collagens (e.g. collagen I) in the wound area (Wynn, 2007; Herum et al., 2017).

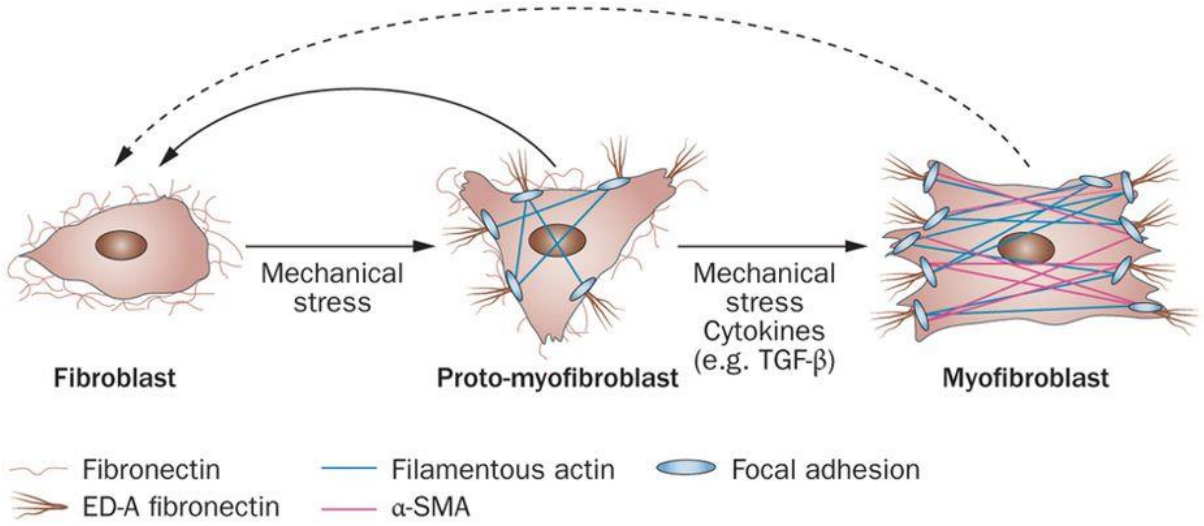

Figure 1-3: Schematic of myofibroblast transformation. During the initial trauma, quiescent fibroblasts transform into proto-myofibroblasts and start expressing ECM components such as fibronectin. Upon further trauma and the expression of TGF-β1 from immune/epithelial cells, proto-myofibroblasts transform into activated myofibroblasts. Myofibroblasts express α–SMA and are responsible for aiding in wound closure. Fibroblast to proto-myofibroblast transformation is reversible (as indicated by the solid arrow) however, it is unknown whether myofibroblast transformation can be completely reversed. Image taken from (Falke et al., 2015).

The process of re-epithelisation allows for the restoration of the skin to its full function as a protective barrier. Re-epithelisation of a wound occurs via a process known as epithelial-mesenchymal transition (EMT) whereby resident epithelial cells (e.g. keratinocytes) undergo several phenotypic changes and begin to resemble mesenchymal cells, as shown in Figure 1-4 (Barriere et al., 2015; Stone et al., 2016). During EMT, cells lose several of their epithelial characteristics, including the loss of epithelial-cadherin (E-cadherin) expression and loss of cell-cell interactions (Aban et al., 2021). Instead, the cells begin to express typical mesenchymal markers, such as vimentin and fibronectin (Stone et al., 2016). The aim of this transition is to increase epithelial cell motility, allowing epithelial cells to migrate across the wound bed and aid in the closure of the wound (Coulombe, 2003). Furthermore, these cells secrete collagenases into the wound bed which allows for the dissection of the damaged eschar tissue from the underlying viable tissue (Riley and Herman, 2005). Whilst re-epithelisation is taking place, activated myofibroblasts increase their contractile forces and induce a centripetal movement towards the middle of the wound (Arif, Attiogbe and Moulin, 2021). This contraction brings the edges of the wound together, which combined with keratinocyte migration across the wound bed allows the wound to close.

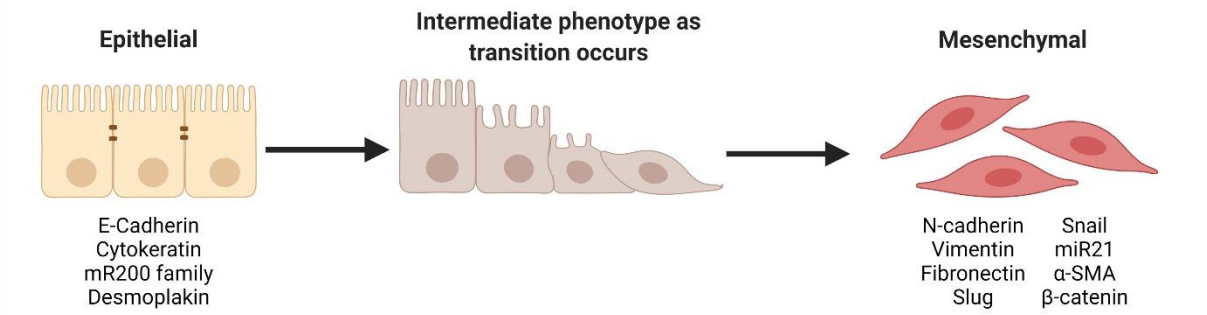

Figure 1-4: Schematic of epithelial mesenchymal transition (EMT). In the presence of inflammatory cytokines, keratinocytes will undergo EMT, adopting a migratory phenotype. As part of this process, keratinocytes will lose their key epithelial markers (e.g. E-cadherin and laminin-1) and as the cell transitions, will start to express key mesenchymal markers (e.g. vimentin and fibronectin). Image created using BioRender, adapted from (Kalluri and Weinberg, 2009).

The final stage of wound healing is known as remodelling, where the immature tissue is restructured and fully matures. It is believed that the process of remodelling continues for many months after initial wound closure, but typically the tissue is considered ‘mature’ 12 months following initial injury (Li, Chen and Kirsner, 2007). During this time, the extracellular matrix is degraded and resynthesized by enzymes called matrix metalloproteinases (MMPs), producing a highly dense ECM that resembles the skin original tissue structure (Bonnans, Chou and Werb, 2014; Xue and Jackson, 2015). Furthermore, remodelling allows for clearance of components that are no longer required via apoptosis and emigration, such as myofibroblasts and immune cells (Desmoulière et al., 1995; Darby, Skalli and Gabbiani, 1990).

1.3. Fibrosis

Fibrosis can be defined as the excessive accumulation of fibrous tissue in an organ or tissue, following injury or trauma (Wynn and Ramalingam, 2013; Nanthakumar et al., 2015; Prakash and Pinzani, 2017). The excessive accumulation of ECM in the wound bed can be attributed to a multitude of underlying cellular and molecular mechanisms that drive the fibrotic response.

1.3.1. Cellular pathology of fibrosis

Aberrations in the wound healing response can result in two scenarios, the first being excessive wound healing leading to scar formation and the second being chronic wound healing, leading to wounds that never fully heal. For the purpose of this thesis, the aberrations in the wound healing process that lead to excessive wound healing and scar formation will be discussed. As shown previously in Figure 1-2, the wound healing process is well regulated with the different stages following each other in a particular pattern. During excessive wound healing, it is believed that the stages of wound healing overlap with one another, often occurring for extended periods of time and therefore exaggerating the effects of each stage (Gauglitz et al., 2011). Previous work has investigated the dysregulation in the stages of the wound healing process which drives excessive wound healing.

In the latter stages of haemostasis, platelets will degranulate, releasing a variety of growth factors and clotting factors to initiate the rest of the wound healing process. One of these growth factors is platelet-derived growth factor (PDGF), which during normal wound healing, plays a role in the regulation of ECM deposition and the activation of fibroblasts (Pierce et al., 1991). During excessive wound healing PDGF is overexpressed, with studies showing that this increases the expression of TGF-β1 type I and II receptors on fibroblasts in the wound bed (Bonner, 2004; Zhou et al., 2002). Furthermore, PDGF is associated with the transformation of fibroblasts to myofibroblasts, contributing to the overproduction of ECM (Tan et al., 1995). Platelets also release VEGF during their degranulation, which helps to stimulate the process of angiogenesis (Carmeliet, 2005). Studies have shown that increased levels of circulating VEGF during excessive wound healing, drives the increased infiltration of inflammatory cells into the wound bed, contributing to the chronic inflammation associated with fibrosis (Zhang et al., 2016a; Huang and Ogawa, 2020). Furthermore, inhibition of VEGF using *in vivo* models, led to the reduction in the severity of scarring (Kwak et al., 2016).

One of the key differences between normal and excessive wound healing is the length of time the inflammatory response occurs for. The inflammatory response is exaggerated during excessive wound healing and does not resolve until just after remodelling begins (Gauglitz et al., 2011). As a result, this chronic inflammation increases the intensity of the immune response which has shown to drive scar formation (Zhu, Ding and Tredget, 2016). Part of this

is due to the populations of immune cells that are recruited to the wound site. It is well established that an increase in Th2 $CD4^+$ T cells causes an overexpression of fibrogenic cytokines (e.g. IL-4, IL-5 and IL-13), whereas increased infiltration of Th1 $CD41^+$ T cells has been shown to attenuate the formation of scars (Hoffmann, Cheever and Wynn, 2000; Wynn, 2004). Furthermore, chronic inflammation affects the macrophage population in the wound bed. In the initial stages of inflammation, M1 macrophages are recruited to the wound bed to help regulate ECM deposition and degradation, but due to the stress of the microenvironment, they transform into M2 macrophages (Delavary et al., 2011; Song et al., 2000). This sub-population of macrophages has been shown to drive scar formation as they contribute to the increased expression of TGF-β1 (Song et al., 2000). TGF-β1 is one of the cytokines that initiates myofibroblast transformation, therefore increased TGF-β1 results in more myofibroblasts, and subsequently leads to excessive ECM production (Zhu, Ding and Tredget, 2016; Lijnen and Petrov, 2002).

The majority of the aberrations seen during haemostasis and inflammation have a knock-on effect, causing dysregulation during the proliferative phase of wound healing. This is partially due to the overexpression of fibrogenic cytokines, which causes the transformation of resting cells to active ECM-producing cells (Borthwick, Wynn and Fisher, 2013). It has been suggested that spontaneous transformation of quiescent fibroblasts to myofibroblasts happens more frequently during excessive wound healing, due to the fibroblasts being more sensitive to the required stimuli needed for transformation (Zhu, Ding and Tredget, 2016; Schmid et al., 1998). This can be explained by the increased expression of the receptors for the cytokines that induce transformation (e.g. TGF-β1) (Bonner, 2004; Schmid et al., 1998). Epithelial keratinocytes have been shown to overexpress cytokines which activate both fibroblasts and endothelial cell proliferation, aiding in the hyper-cellularisation that is often seen in these scars (Niessen et al., 2004; Andriessen et al., 1998). Furthermore, during normal wound healing, epithelial keratinocytes will express basic fibroblast growth factor (bFGF), a natural TGF-β1 inhibitor, which is significantly downregulated in excessive wound healing (Tiede et al., 2009). Studies that increased bFGF levels during wound healing and used it as a therapeutic tool, showed a reduction in the severity of the scarring associated with decreased collagen deposition in the wound (Xie et al., 2008; Ono et al., 2007). Another cell type that has been associated with increased fibroblast proliferation are mast cells, which have also been indicated in the promotion of angiogenesis and chronic inflammation (Smith, Smith and Finn, 1987). Further, increased infiltration of mast cells and release of histamine has been identified during the active phase of scarring (Moyer, Saggers and Paul Ehrlich, 2004; Noli and Miolo, 2001).

The main issue during the remodelling phase of excessive wound healing is the overproduction of ECM. This is not helped by the delay in the start of the remodelling process, which does not occur until approximately 12 months after the initial injury (Gauglitz et al., 2011). As the inflammatory and proliferative responses are exaggerated, the remodelling response is subsequently hampered, and often full scar maturation is not achieved for many years (Armour, Scott and Tredget, 2007). MMPs are the proteins responsible for remodelling of the ECM have been found to be significantly downregulated during excessive wound healing (Ghahary et al., 1996). MMP-1, MMP-8 & MMP-13 are responsible for the remodelling of collagen I, II and III, however as they are regulated in part by TGF-β signalling, when TGF-β1 is overexpressed these MMPs are downregulated (Bran et al., 2009). Typically, cell clearance during wound healing would occur 3 weeks following initial injury, whereas in excessive wound healing, maximum cell clearance can occur anywhere between 19-30 months after the initial injury (Armour, Scott and Tredget, 2007). Histology of early scars further confirms the presence of hypercellular nodules in the dermis of the skin, with immunohistochemistry confirming that myofibroblasts account for the majority of these cells (Sorg et al., 2017; Gauglitz et al., 2011). Studies have identified that the myofibroblasts present during excessive wound healing are resistant to apoptosis, which is said to be mediated by several different mechanisms. For cutaneous scars (e.g. hypertrophic and keloid scars) the mechanism by which myofibroblasts become evade apoptosis has been suggested to be due to the overexpression of p53, or myofibroblasts become resistant to Fas-3 ligand mediated apoptosis (Lu et al., 2007; de Felice et al., 2009). Another possible mechanism that could be mediating apoptosis resistant in myofibroblasts is the activation of Toll-like receptor 4, which has been reported in idiopathic pulomary fibrosis myofibroblasts (Hanson et al., 2019).

1.3.2. Signalling pathways in fibrosis

As described in the above section, cytokines and growth factors expressed during fibrosis are responsible for inducing much of the fibrotic response, through their downstream signalling effects. TGF-β signalling is believed to be one of the most important signalling pathways involved in the progression of fibrosis. The TGF-β superfamily consists of approximately 30 different proteins, including the three TGF-β isoforms (TGF-β1, TGF-β2 and TGF-β3) which have been identified as being key mediators in wound healing and fibrosis (Biernacka, Dobaczewski and Frangogiannis, 2011). In particular, TGF-β1 induces transformation of fibroblasts to myofibroblasts, a process that is upregulated during fibrosis (Borthwick, Wynn and Fisher, 2013). TGF-β1 has been shown to induce the expression of α-SMA (the myofibroblast marker), through the upregulation of *ACTA2*, the gene that encodes for α-SMA (Desmouliere et al., 1993). Furthermore, TGF-β1 has also been shown induce EMT in

epithelial cells during the wound healing process, through the upregulation of the transcription factors Slug (SNAI2) and Snail (SNAI1) (Naber et al., 2013). TGF-β1 exerts its effects through Smad signalling (canonical signalling pathway; Fig 1-5) or crosstalk with our signalling pathways in a Smad-independent manner (non-canonical signalling pathway; Fig 1-6). In both types of signalling, TGF-β1 is made available through expression by circulating cells or through its cleavage from the latency associated peptide-latent TGF-β1 binding protein (LTBP) (Biernacka, Dobaczewski and Frangogiannis, 2011). Latent TGF-β1 is typically found stored in the extracellular matrix, and following mechanical stress caused by injury, it is cleaved and released from the LTBP (Wipff et al., 2007).

The canonical TGF-β1 signalling pathway involves the formation of a Smad complex, which mediates the transcription of numerous pro-fibrotic molecules. TGF-β1 binds first to TGF-β receptor 2, which in turn recruits and activates TGF-β receptor 1. TGF-β receptor 1 recruits the Smad2/3 complex to its cytoplasmic domain, phosphorylating the complex (Kamato et al., 2013). Smad2/3 is then able to bind with Smad4, which allows the complex to translocate into the nucleus (Kamato et al., 2013). Here, the phosphorylated Smad3 is able to bind to the gene promoters and initiate the transcription of pro-fibrotic molecules such as α-SMA, fibronectin and pro-fibrotic microRNAs (miRNA) (Kamato et al., 2013). In fibroblasts, this process ultimately leads to myofibroblast transformation and the production of ECM (Massagué, 1998, 2012). In epithelial cells, the Smad2/3 complex is able to induce the transcription of genes such as slug/snail, which initiate the EMT process (Naber et al., 2013). Smad7 acts as an internal negative regulator and is anti-fibrotic in nature, as it is able to inhibit the binding of Smad4 to the Smad2/3 complex and subsequently prevent translocation to the nucleus, and all downstream effects (Meng, Nikolic-Paterson and Lan, 2016).

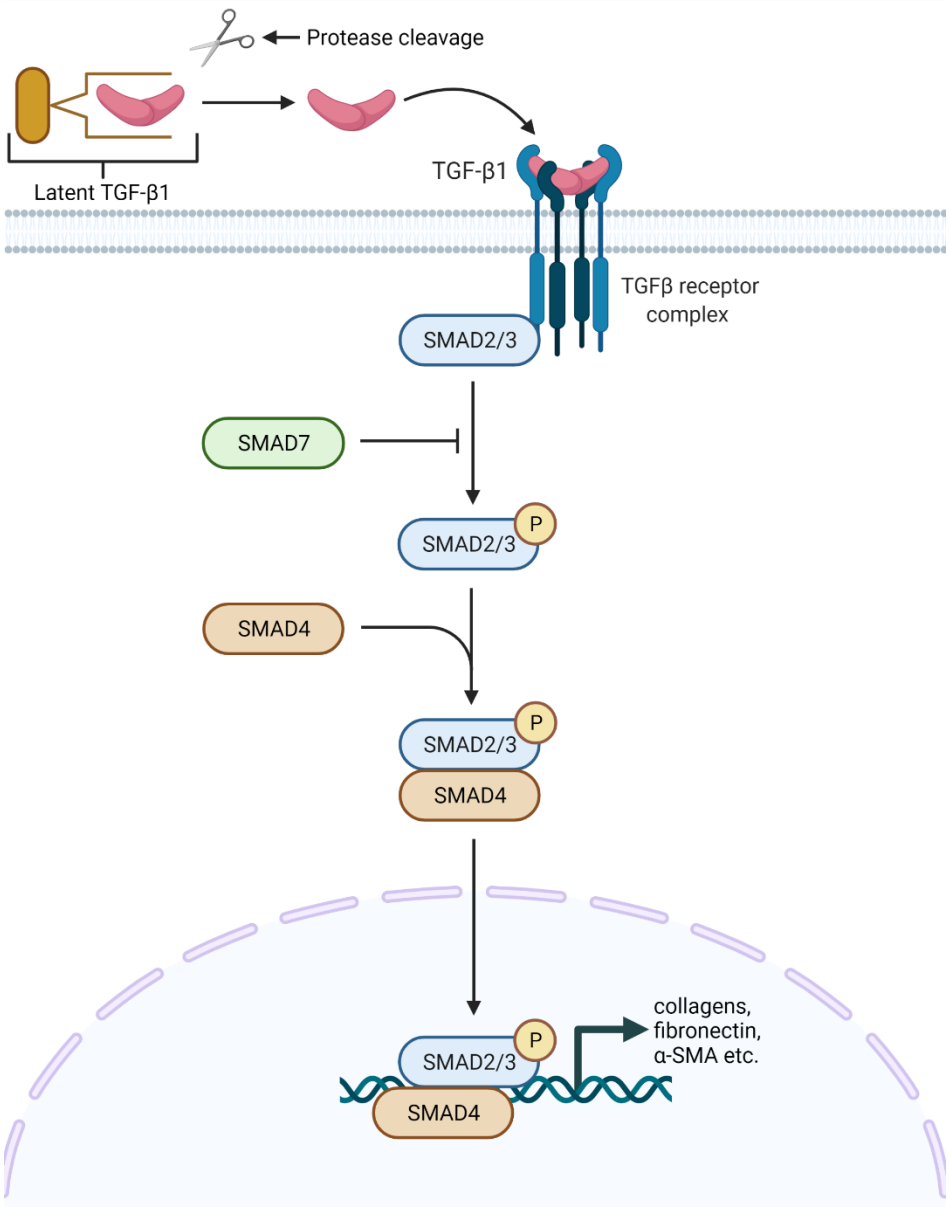

Figure 1-5: Canonical TGF-β1 signalling. Following cleavage from the Latency-associated peptide, latent TGF-β1 binding protein (LTBP), TGF-β1 binds to TGF-β receptor 2 before recruiting TGF-β receptor 1 to form the full complex. Smad2 and Smad3 are then phosphorylated by the activated receptor and form a complex with Smad4. This allows nuclear translocation, whereby it binds directly to the gene promotors and induces transcription of the genes encoding for different fibrotic proteins (e.g. α-SMA and fibronectin). Smad7 acts by inhibiting the Smad2/3 complex and is anti-fibrotic in nature. Image created using BioRender, adapted from (Meng, Nikolic-Paterson and Lan, 2016).

The effects of TGF-β1 can also be induced via crosstalk with other signalling pathways, otherwise known as the non-canonical TGF-β signalling pathway (Figure 1-6). The interactions between mitogen-activated protein kinases (MAPK) and TGF-β signalling is so far the best understood. The MAPK family are made up of three signalling molecules, p38, JNK and ERK, which have all been indicated in the progression of fibrosis. Like TGF-β1, the MAPK family are able to phosphorylate the linker regions of Smad2/3 initiating their downstream effects (Kamato et al., 2013). TGF-β1 is able to initiate MAPK signalling in a Smad-independent manner, through either TGF-β receptor 1 becoming an active tyrosine receptor kinase (for

ERK signalling) or through the recruitment of tumour necrosis factor (TNF) receptor associated factor-6 and TGF-β activated kinase I/M3K7 (for p38/JNK signalling) (Sorrentino et al., 2008; Lee et al., 2007). Upregulation of MAPK signalling during fibrosis has shown an increase in α-SMA expression and ECM production in fibroblasts, with EMT also being induced through ERK mediated decrease in E-cadherin expression (Gui et al., 2012; Bakin et al., 2002). Furthermore, pharmacological inhibition of MAPK (particularly p38) has been shown to attenuate the fibrotic response, with studies having shown a decrease in myofibroblast transformation, collagen production and TGF-β1 expression (Dolivo, Larson and Dominko, 2019; Sato et al., 2002).

Canonical Wnt/β-catenin signalling has been indicated to play a role in the progression of different fibrotic disorders. Wnt glycoproteins bind to membrane bound receptor Frizzled and low-density lipoprotein receptor-related protein 5/6 (LRP5/6), which stabilises cytoplasmic β-catenin, preventing it from being phosphorylated and subsequently degraded (MacDonald, Tamai and He, 2009). Stabilisation of β-catenin allows for its translocation to the nucleus, where it is able to induce transcription of its target genes (MacDonald, Tamai and He, 2009). Up-regulation of β-catenin and its target genes have been identified in unresolved injury, with the majority of β-catenin's target genes being pro-fibrotic (e.g. fibronectin, Snail and MMP7) (Zhou et al., 2016). Further research into the potential crosstalk between Wnt/β-catenin and TGF-β signalling still needs to be conducted, however one study has suggested that the suppression of Dickkopf-related protein 1 (DKK1; an inhibitor of Wnt) via p38, exacerbates the fibrotic response in skin fibrosis (Akhmetshina et al., 2012). Furthermore it is believed that β-catenin and downstream Smads interact with one another to mediate EMT via cAMP response element (CREB)-binding protein, with one study suggesting a potential synergy between the two in order to maintain the mesenchymal phenotype in epithelial cells undergoing EMT (Eger et al., 2004).

Finally, the role of oxidative stress and the production of reactive oxygen species (ROS) has been associated with TGF-β signalling. TGF-β1 has been shown to increases levels of NADPH oxidases, the enzymes responsible for cleaving ROS, with increased ROS levels associated with increased fibroblast proliferation (Barnes and Gorin, 2011). Further, TGF-β1 has been shown to signal using ROS to initiate the phosphorylation of Smad2/3 and induce the transcription of plasminogen activator inhibitor-1, a protein which acts to suppress ECM degradation (Higgins et al., 2011; Chuang-Tsai et al., 2003). The other role of ROS in fibrosis is in the initiation and upregulation of the tumour suppressor gene, p53. Aside from its potential role in the apoptotic resistance seen in myofibroblasts during fibrosis, phosphorylation of p53 by the serine protein kinase ARM allows it to form complexes with Smad3 influencing the transcription of the Smad target genes (de Felice et al., 2009; Overstreet et al., 2014, 2015).

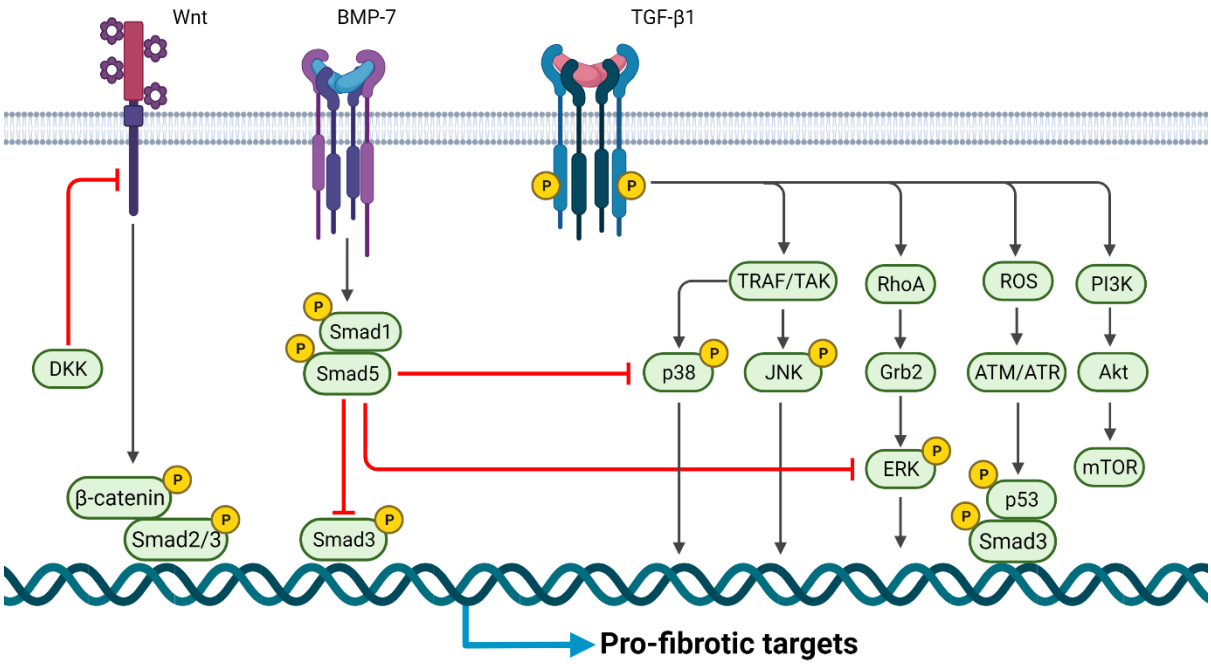

Figure 1-6: Non-canonical TGF-β1 signalling. TGF-β1 is able to initiate the transcriptional activities of the Smad2/3/4 complex, through crosstalk with other signalling pathways. Smad phosphorylation can be mediated through the mitogen-activated protein kinase (MAPK) pathway (ERK, p38 and JNK) which are able to modulate the transcriptional activity of the Smad 2/3/4 complex. Furthermore, MAPKs can be activated in this way through other signalling pathways (such as oxidative stress) which also contributes to Smad phosphorylation. The Wnt/β-catenin signalling pathway has also been indicated in the upregulation of pro-fibrotic factors, through the complexing of β-catenin with Smads. Reactive oxygen species (ROS) are also induced by TGF-β, subsequently causing the phosphorylation of p53 and aiding with the translocation of Smad3 into the nucleus. There are also a number of pathways that act as negative regulators of Smad3 by reducing the nuclear accumulation of phosphorylated Smad3, including bone morphogenic protein-7 (BMP-7). Image created using BioRender, adapted from (Meng, Nikolic-Paterson and Lan, 2016).

Other growth factors and their downstream signalling cascades have been associated with driving fibrosis. Connective tissue growth factor (CTGF) is a matricellular protein that has been identified as a central mediator in activating many of the pro-fibrotic signalling cascades (Lipson et al., 2012). CTGF has been shown to exacerbate the effects of TGF-β1, and a lack of CTGF prevents many of these TGF-β1 effects from occurring (Kok et al., 2014). For example, CTGF has been shown to bind tyrosine receptor kinase A which subsequently suppresses the expression of Smad7 and prevents the inhibition of TGF-β1 induced Smad signalling (Wahab, Weston and Mason, 2005). Further, CTGF is able to inhibit bone morphogenetic protein 7 (BMP7) signalling, a negative regulator of Smad3 (Nguyen et al., 2008). As CTGF is a downstream target of TGF-β1 signalling it is expressed in both fibroblasts and epithelial cells, and therefore contributes to myofibroblast transformation and EMT of these cells, respectively (Shi-Wen, Leask and Abraham, 2008).

PDGF is released by platelets during their degranulation to help initiate the inflammatory phase of wound healing. Following binding of PDGF to the PDGF receptor (PDGFR), autophosphorylation of Ras and phosphatidylinositol 3-kinase (PI3K) occurs, activating their signalling cascades (Ying et al., 2017). Autophosphorylation of Ras subsequently leads to the initiation of the MAPK signalling cascade via MEK/ERK, although other studies have shown that PDGF can also activate the p38 and p42/44 MAPK (Ying et al., 2017; Deng et al., 2015). Autophosphorylation of PI3K leads to downstream activation of NF-κβ, a pro-inflammatory transcription factor which contributes to chronic inflammation (Kok et al., 2014; Ying et al., 2017). In fibroblasts, PDGF signalling has been shown to induce myofibroblast transformation and the expression of α-SMA, along with the increased production of collagen (Deng et al., 2015). No expression of the PDGFR has been found on keratinocytes, indicating that PDGF signalling does not play a role in EMT during fibrosis. However, keratinocytes are a key source of PDGF and therefore contribute to the fibrotic effects of fibroblasts (Ansel et al., 1993).

1.4. Fibrotic disorders of major organs

Fibrosis can affect almost any tissue and organ in the body, with the pathology accounting for 45% of mortality worldwide (Distler et al., 2019; Wynn, 2004). Fibrosis in the major organs is often driven by underlying aetiologies including viral infection, autoimmune conditions, ischaemia, and repetitive physical or chemical injury (Li et al., 2017). Figure 1-7 shows the major organs and tissues that fibrosis can affect, along with the common underlying diseases that fibrosis can be associated with, such as carcinoma.

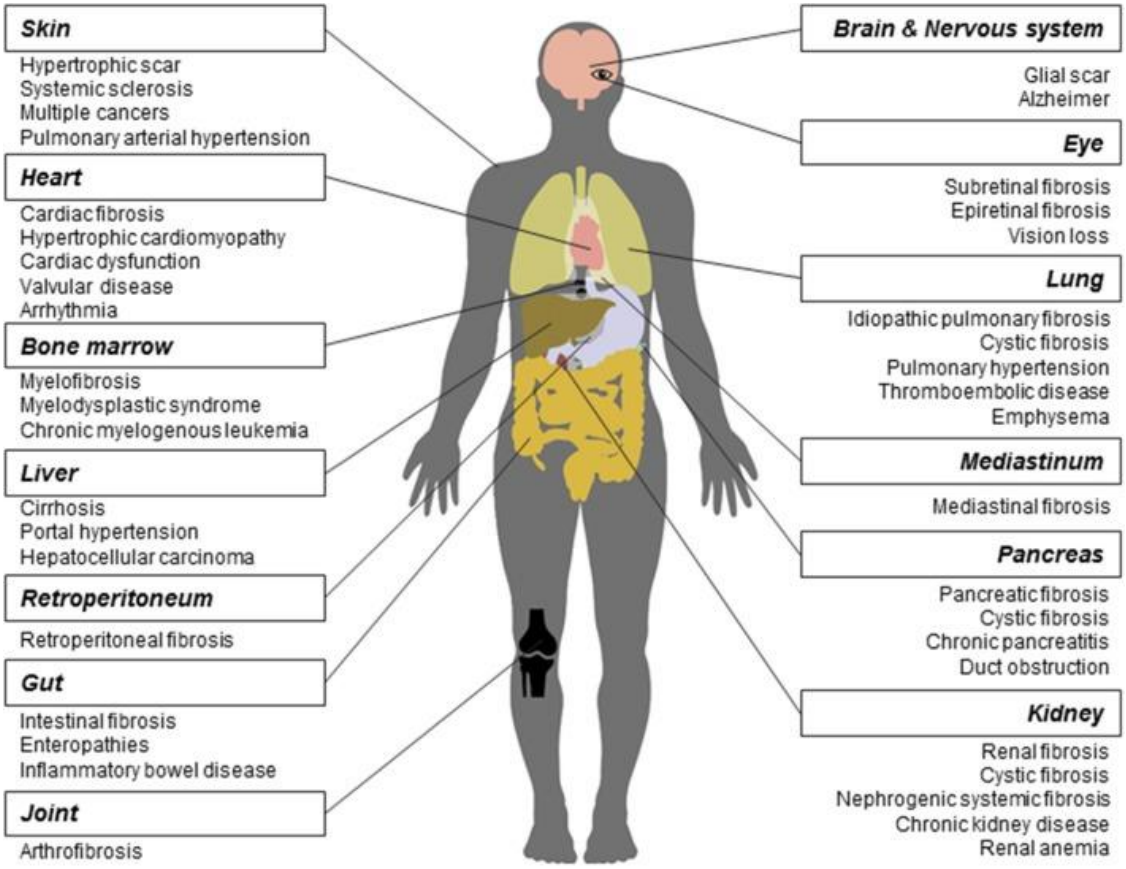

Figure 1-7: Fibrosis of major organs and tissues. Fibrosis often associated with the progression of several diseases and underlying conditions, affecting almost all organs and tissues. Further, fibrosis can cause several consequences including vision loss and obstruction of ducts and vessels. Image taken from (Li et al., 2017).

As discussed previously, the cellular and molecular pathways that drive fibrosis are thought to be commonly shared amongst the different fibrotic disorders (Distler et al., 2019). Therefore, the following sections describe some of the key fibrotic disorders of the major organs (particularly those with the highest mortality rates), before focussing on fibrotic disorders of the skin.

1.4.1. Idiopathic pulmonary fibrosis

Pulmonary fibrosis is the endpoint for many respiratory diseases, with 6,000 patients in the UK diagnosed with idiopathic pulmonary fibrosis (IPF) per year (Martinez et al., 2017; Olson et al., 2018). Unfortunately, IPF comes with a high mortality rate with patients only having a survival rate of 3-5 years following their initial diagnosis (Datta, Scotton and Chambers, 2011). IPF is the most severe form of the interstitial pneumonias, presenting with similar radiology and histology as usual interstitial pneumonia (UIP) and only affects the lungs (Tzouvelekis, Bonella and Spagnolo, 2015). Although similar to UIP, the progression of IPF usually sees periods of stability, followed by periods of severe decline in the patients' health (Tzouvelekis, Bonella and Spagnolo, 2015). Histologically, thickening of the interstitial space can be seen, along with cystic remodelling of the ECM and the presence of fibroblastic foci (Rabeyrin et al., 2015). As the term idiopathic suggests, no underlying aetiology has been linked to the progression of IPF. However, recent advancements have identified that persistent injury and inflammation to the alveolar epithelium, may be responsible for exacerbating the fibrotic response (Selman et al., 2004). There are currently two medical therapies approved for IPF treatment – pirfenidone (a pyridone) and nintedanib (a tyrosine-kinase inhibitor) (Somogyi et al., 2019). Although the exact mechanism of action of each drug is incompletely understood, both drugs have been shown to be anti-fibrotic and slow the progression of fibrosis in the lungs (Somogyi et al., 2019). Unfortunately, these therapies do not completely stop or reverse the fibrosis, and both drugs have been shown to exhibit worrying adverse effects (e.g. changes to liver function, photosensitivity and hypertension) (Lancaster et al., 2017; Noth et al., 2018). Further research is being undertaken to identify novel therapies that could potentially stop or reverse the fibrosis, particularly identifying drugs that are able to inhibit fibroblast proliferation and migration (Mora et al., 2017).

1.4.2. Cardiac fibrosis

Worldwide, cardiovascular disease (CVD) is the leading cause of mortality, causing significant financial burden on healthcare providers with an estimated cost of 210 billion euros per year in Europe alone (Murtha et al., 2017; Wilkins et al., 2017). Cardiac fibrosis is the subsequent endpoint of many different types of CVD and can be categorised into two different types of fibrosis – replacement and interstitial fibrosis (Liu et al., 2017). Replacement fibrosis occurs after injury to the tissue, such as in myocardial infarction where ECM is laid down to replace the dead myocytes (Liu et al., 2017). Interstitial fibrosis is a more progressive pathology, usually a result of ageing and hypertension. Interstitial fibrosis can also lead to replacement fibrosis as the more severe pathology causes myocyte cell death (Hashimura et al., 2017). In physiological conditions, one of the key roles of cardiac fibroblasts is to maintain the ECM homeostasis in the heart, as the ECM acts as a scaffold for myocytes (Hinderer and Schenke-

Layland, 2019). However following injury, ECM is produced excessively, replacing the dead cells, and ultimately resulting in impaired heart function (Hinderer and Schenke-Layland, 2019). One of the underlying factors which drives this excessive accumulation of ECM is that cardiac fibroblasts are not the only cells responsible for producing the ECM. Following injury, vascular endothelium and epicardial cells undergo a process called endothelial-mesenchymal transition (EndMT), in which they transition to mesenchymal-like cells, and begin producing ECM (Davis and Molkentin, 2014). The current treatment for CVD and subsequent cardiac fibrosis is known as the 'golden-triangle' of medications, including beta blockers, angiotensin-converting enzyme (ACE) inhibitors and aldosterone antagonists (Liu et al., 2017; Hinderer and Schenke-Layland, 2019). Although none of these medications directly target the molecular mechanisms behind fibrosis, emerging therapies are looking into this with particular interest in targeting collagen production and degradation (Liu et al., 2017).

1.4.3. Liver fibrosis

Fibrosis of the liver (usually presenting as cirrhosis) is the 11th biggest killer worldwide, accounting for approximately one million deaths each year (Asrani et al., 2019). It is a result of chronic inflammation and persistent cell death in the liver, with repeated exposure to the cause of injury resulting in more advanced disease states (e.g. cirrhosis and hepatocarcinoma) (Mehal and Imaeda, 2010). It is believed that the early stages of fibrosis in the liver may be beneficial, as the liver aims to contain the injury (Bonis, Friedman and Kaplan, 2001; Ebrahimi, Naderian and Sohrabpour, 2016). Like any other type of fibrosis, liver fibrosis is defined by the excessive accumulation of ECM, especially as ECM usually only makes up 3% of the liver itself (Bedossa and Paradis, 2003). Furthermore, it has been shown that the main source of ECM producing cells in the liver are hepatic stellate cells (HSCs), which in the presence of inflammatory cytokines transform into myofibroblasts (de Oliveira da Silva, Ramos and Moraes, 2017). Unfortunately, there is no standardised treatment for liver fibrosis with most clinicians choosing to treat the underlying aetiology that may be driving the fibrosis (e.g. viral infection) or opting for transplantation in the most severe cases (Bataller and Brenner, 2005). Emerging treatments for liver fibrosis aim to target cell senescence, apoptosis of ECM producing cells, and the transformation of HSCs to myofibroblasts (de Oliveira da Silva, Ramos and Moraes, 2017).

1.4.4. Kidney fibrosis

Kidney fibrosis is the main endpoint of chronic kidney disease (CKD), typically affecting the ageing population (Humphreys, 2018). Histological analyses of the different stages of CKD show a progressive accumulation of ECM in the parenchyma of the kidneys (Efstratiadis et al., 2009; Liu, 2006). This build-up of ECM overtime disrupts the kidney architecture, compromising the functional components and resulting in end-stage renal failure (Liu, 2006). There is evidence to suggest that the excessive accumulation of ECM in the kidneys is a result of a diverse population of ECM producing cells – not just myofibroblasts (Kuppe et al., 2020; Falke et al., 2015). In the presence of inflammatory cytokines, epithelial and endothelial cells undergo phenotypic changes which allow them to start depositing ECM (Falke et al., 2015). This process of EMT and EndMT, along with the transformation of interstitial fibroblasts to myofibroblasts, are of interest to those trying to discover new anti-fibrotic therapies, to prevent excessive ECM production (Kuppe et al., 2020; Efstratiadis et al., 2009). Currently the standard care for those with CKD and subsequent kidney fibrosis is dialysis and transplantation, for those with end-stage renal failure (Hewitson, 2012).

1.4.5. Peyronie's disease

Peyronie's disease (PD) is a fibrotic disorder of the penis which is caused by the formation of a fibrous plaque in the tunica albuginea (Garaffa et al., 2013). PD is typically characterised by pain during erection and the curvature of the penis, which can eventually lead to erectile dysfunction (Smith, Walsh and Lue, 2008; Hussein, Alwaal and Lue, 2015). There are two distinct phases to the progression of PD – the acute phase describes the inflammatory, unstable nature of the disorder and is commonly associated with pain and the beginnings of penile deformity (Mulhall, Schiff and Guhring, 2006). The stable phase of PD occurs approximately 12-18 months following the initial injury, at which point the plaque itself has stabilised, as well as any penile curvature (Mulhall, Schiff and Guhring, 2006). Typically, early diagnosis of PD is rare, and the patients tend to seek medical help once the plaque has progressed into the stable phase. As with many fibrotic disorders, the treatment options for PD are extremely limited and usually, surgical intervention is the gold standard (Hellstrom and Usta, 2003). In recent years, non-surgical treatment options have become available - in particular, the FDA- and EMA-approved the use of collagenase injections for PD (Honig, 2014). Collagenases are enzymes that are responsible for breaking down excess collagen and although they were shown to reduce the size of the plaque and penile curvature, they have been associated with some significant side effects (e.g. haematoma and ecchymosis) (Levine et al., 2015; Levine, 2017). Nevertheless, collagenase injection has been withdrawn from the European market for the treatment of PD leaving surgery as the only option for the patients in the UK and Europe (Cocci et al., 2020). Recent advances have shown that the

combination of selective estrogen receptor modulators (SERMs) and phosphodiesterase type 5 inhibitors (PDE5i) are not only effective in preventing the formation of the PD plaque but have also shown to exert a synergistic effect in *in vitro* and *in vivo* studies (Ilg et al., 2019, 2020).

1.4.6. Dupuytren's contracture

Dupuytren's contracture is a progressive fibroproliferative disorder, which causes the bending of the fingers due to the excessive formation of collagen in the palmar fascia (Hart and Hooper, 2005). Duputryens' contracture was first described by Guillaume Duputryen in 1831, and today has an incidence of 20% in those over 65 years old, affecting mainly white men (Murrell and Hooper, 1992; Bayat, Cunliffe and McGrouther, 2007). Dupuytren's contracture consists of a dense matrix, which forms collagen knots and histology shows anywhere between a 6- and 20-fold increase in fibroblast population (Murrell and Hooper, 1992). There are three grades of Dupuytren's contracture (as shown in Fig 1-8), with the first grade limited to a knot in palmar fascia with some skin puckering, the second grade showing limited extension and the third grade the most severe with full contracture (Lex Medicus Pathologies, 2021; Hart and Hooper, 2005).

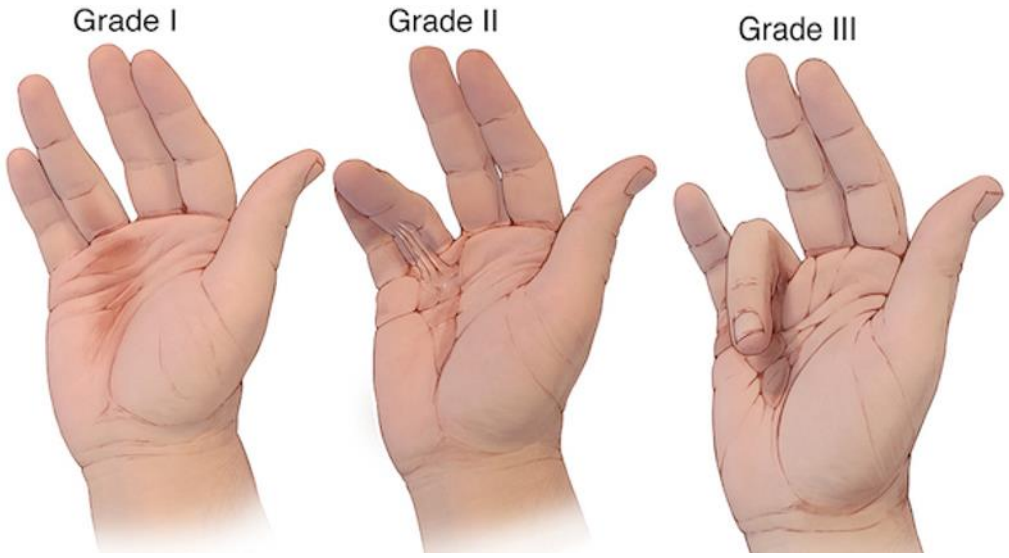

Figure 1-8: Grades of Dupuytren's contracture. Grade I presents as pitting of the skin, as well as slight curvature of the ring finger. Grade II shows the formations of a collagen knot, with further curvature of the ring finger. Finally Grade III presents with full curvature of the affected finger. Image taken from (Lex Medicus Pathologies, 2021).

Dupuytren's contracture can often be associated with other conditions such as diabetes mellitus and human immunodeficiency virus (HIV). In diabetes, the incidence of Dupuytren's contracture is much higher compared with the general population (63% vs. 13%) however, it is said to be a much milder disease in diabetics (Noble, Heathcote and Cohen, 1984; Smith, Burnet and McNeil, 2003). The relation between the two conditions is largely unknown, with scientists debating whether diabetes is an underlying initiator of Dupuytren's contracture, or if

they are inherited together (Hart and Hooper, 2005). One theory suggests that the vascular changes that occur as a side effect of diabetes are like that of the vascular changes seen in Dupuytren's contracture, which drives hypoxia in the affected tissue (Hart and Hooper, 2005).

Another association is the prevalence of Dupuytren's in HIV patients, with a 36% incidence rate having been identified (Bower, Nelson and Gazzard, 1990). As suggested with other conditions, it has been reported that the underlying mechanism that links Dupuytren's and HIV is the increased production of free oxygen radicals in both conditions (Bower, Nelson and Gazzard, 1990). Furthermore, it is believed that the incidence of Dupuytren's in HIV patients can be used as an indicator of the disrupted oxygen metabolism, and therefore act as a measure for AIDS development (Bower, Nelson and Gazzard, 1990).

The link between alcoholism and Dupuytren's contracture has been longstanding, with the first case described back in the 1950s (Hart and Hooper, 2005; Bayat, Cunliffe and McGrouther, 2007). Studies have showed that for Dupuytren's contracture to develop in these patients a degree of liver damage (whether this is full cirrhosis or non-cirrhotic) must have occurred. Incidence of Dupuytren's contracture increases in a dose-dependent manner with increasing levels of alcohol consumption (Godtfredsen et al., 2004; Attali, 1987). The underlying mechanisms that link alcoholism and Dupuytren's contracture are not well understood, however it is believed that changes to the vasculature and the incidence of ischaemia in the palmar fascia and fatty tissue promotes a fibrotic response (Attali, 1987; Hart and Hooper, 2005).

It has been reported that approximately 3-15% of men that present with Dupuytren's contracture, will at some point also develop Peyronie's disease (PD) (Nugteren et al., 2011). Unfortunately, it is not well understood how these two disorders are linked. Some have suggested that Dupuytren's and PD share similar pathomechanisms, as both are caused by the formation of a fibrous nodule in the respective tissue which subsequently causes curvature of the affected appendage (Shindel et al., 2017). Gene expression analysis of cells from PD and Dupuytren's patients showed similar changes in the expression of key fibrosis markers, providing evidence that the pathomechanisms of these two disorders may be linked (Qian et al., 2004).

There are a wide range of treatments available for Dupuytren's including non-surgical interventions such as physiotherapy to help maintain function of the affected hand (Ball et al., 2016). The gold-standard treatment is the surgical release of the contracture and the removal of the excessive fibrotic tissue (Rodrigues et al., 2015). Although this is a highly effective treatment, the recurrence rate is high with 66% of patients reporting formation of new contractures following surgery (Rodrigues et al., 2015). Recently, collagenase injections have

been approved as a therapy for Dupuytren's contracture, which involves injecting enzymes into the affected site that break down the excessive collagen directly (Fletcher et al., 2019). Although collagenase injections have been shown to be effective in the early disease, significant side effects (e.g. oedema and tendon rupture) have been reported (Alberton et al., 2014; Fletcher et al., 2019).

1.4.7. Fibrotic skin disorders

1.4.7.1. Scleroderma

Scleroderma is a chronic connective tissue disorder, characterised by fibrosis of the skin and other major organs (Distler and Cozzio, 2016; Wei et al., 2011; Careta and Romiti, 2015). There are two main types of scleroderma – localised scleroderma (LoS) which is exclusive to the skin and underlying tissue and systemic scleroderma (SSc) which manifests as cutaneous sclerosis in the initial stages of the disease, before affecting the major organs (e.g. lungs and oesophagus) (Careta and Romiti, 2015). Sclerosis of the skin is a key component of both versions of scleroderma and is often described as being the key factor in the diagnosis of SSc as this develops before the systemic component (Krieg and Takehara, 2009). Despite their similarities, many clinicians and scientists view LoS and SSc as separate disorders, as their underlying cellular and molecular mechanisms differ greatly (Fett, 2013).

LoS is exclusively confined to the skin and its underlying tissues. Often termed 'morphea,' LoS is characterised by the thickening of the skin due to the increased production of collagen in the dermis and hypodermis, typically affecting the trunk and limbs of the patient (Krieg and Takehara, 2009). It is a very rare disease with an incidence rate of 0.4 - 2 per 100,000 individuals, and 90% of cases are diagnosed in children (Careta and Romiti, 2015; Distler and Cozzio, 2016). LoS can be subdivided into five types of morphea, each type affecting the layers of the skin and its surrounding tissues differently – this has been summarised in Table 1-1 (Careta and Romiti, 2015; Distler and Cozzio, 2016). The identification of novel therapeutics for LoS is often stunted due to the inability to carry out full standardised clinical trials, as the incidence rate of the disease is so low (Fett, 2013). Despite this the most common treatment given for LoS are potent, topical corticosteroids while the use of phototherapy is also being investigated (Krieg and Takehara, 2009).

Table 1-1: Subdivisions of morphea seen in localised scleroderma. Adapted from (Careta and Romiti, 2015; Distler and Cozzio, 2016)

Morphea classification	Lesion features	Affected tissues
Plaque	• Round lesions • Skin appears shiny/hard	Dermis
Bullous	• Advanced form of plaque morphea • Characterised by presence of 'erosions' on plaques	Dermis
Deep	• Lesions appear depressed • Asymptomatic	Dermis & subcutaneous tissue
Generalised	• Affects 2 or more areas of the body • Plaques appear inflamed and pigmented	Dermis, rare to be seen in subcutaneous tissue
Linear	• Can affect whole body • Linear indurations across the skin	Dermis, subcutaneous tissue, bone, and muscle (most advanced cases)

SSc is a far more severe disease due to the pronounced effect it has on major organs. Patients with SSc have a survival rate of 62%, with interstitial lung disease (ILD) the greatest cause of death (Corbella and Fonollosa, 2014). Despite its high morbidity and mortality, SSc remains a rare disease with an incidence rate of 0.7 – 53 per 100,000 individuals (Corbella and Fonollosa, 2014). SSc can be generally categorised by the presence of the following three factors – vascular injury, tissue fibrosis, and immune activation (Wei et al., 2011). The early stages of SSc begin with cutaneous sclerosis of the fingers, starting with significant oedema and inflammation before developing thick scarring of the inflamed area (Krieg and Takehara, 2009). Other manifestations of cutaneous sclerosis noted in SSc patients include changes to pigmentation of the skin and the loss of hair follicles and sebaceous glands (Krieg and Takehara, 2009).

As the disease progresses, fibrosis is noted in the major organs. As mentioned previously, ILD is responsible for the majority of SSc related deaths and is said to develop in approximately 20% of all SSc patients (Wei et al., 2011). Fibrosis of the lungs in SSc patients is often characterised by the presence of interstitial inflammation and with even distribution of fibrosis across the organ (Wei et al., 2011). In almost all SSc cases, there is fibrosis of the oesophagus which extends down through the lamina propria to the underlying muscular layers (Wei et al., 2011; Fett, 2013). Due to its heterogenous nature the disease manifestation can vary drastically from patient to patient, resulting in lack of a generalised treatment strategy for SSc (Fett, 2013). Treatment for SSc is limited, with no approved therapies to tackle the fibrotic

effects. However, methotrexate and cyclophosphamide are both recommended for the skin and lungs, respectively (Distler and Cozzio, 2016). Typically, clinicians will also aim to treat the underlying co-morbidities (e.g. Raynaud's and ILD) caused by SSc (Fett, 2013).

1.4.7.2. Hypertrophic scars and keloids

The scars that form after burn injury are often described as one of the greatest unmet challenges in the treatment of these injuries (Finnerty et al., 2017). Scarring after trauma usually manifests as hypertrophic scarring, however in some cases patients can develop keloid scars. In the most severe cases, hypertrophic scarring can manifest as contractures. These scarring types exhibit similar physical symptoms after their formation, with patients experiencing severe pain, intense pruritus and in the worse cases, loss-of-function of the affected area (Bayat, McGrouther and Ferguson, 2003). Most patients also suffer from psychological stress following scarring, as most are dissatisfied with their appearance (Wolfram et al., 2009). Although many treatments have been used clinically over the years to manage scarring, none are able to prevent scar formation regardless of how early the treatment is given (Finnerty et al., 2017).

Most deep partial/full thickness burn wounds will form hypertrophic scars, with scar formation occurring 4-8 weeks after the initial trauma (Gauglitz et al., 2011). Studies have shown that the size of the wound and the time it takes for the wound to heal, can influence the risk of hypertrophic scarring significantly (Cubison, Pape and Parkhouse, 2006; Chipp et al., 2017). Wounds that took 2 weeks to heal had an 8% risk of hypertrophic scarring, whereas wounds that took more than 4 weeks weeks to heal have a risk of 68% (Cubison, Pape and Parkhouse, 2006). Maturation of hypertrophic scars occur over 6 months after the initial injury and once fully matured, hypertrophic scars enter a 'regression phase,' where the nodular, raised scar will flatten out and become symptomless (Gauglitz et al., 2011; Bayat, McGrouther and Ferguson, 2003; Wolfram et al., 2009). These scars usually occur over areas of high tension, such as the shoulders, legs, and the chest, with the scar remaining within the original wound boundary (Figure 1-9A) (Niessen et al., 1999; Atiyeh, Costagliola and Hayek, 2005). Histologically, hypertrophic scars can be distinguished by the presence of 'wavy' type III collagen bundles, which lie parallel to the epidermis of the skin (Ehrlich et al., 1994). Furthermore, nodules containing myofibroblasts and glycosaminoglycans can be observed (Gauglitz et al., 2011; Ehrlich et al., 1994).

Regarding the management of hypertrophic scarring, clinicians widely agree that the identification of preventative strategies are key to reduce the severity of the scarring. If preventative measures fail, scar modulation and surgery are the next steps. Pressure therapy is currently used as a first line prophylaxis for hypertrophic scars, with pressure garments having been shown to also help reduce pruritis and associated pain (Arno et al., 2014). There is limited scientific evidence behind the use of pressure therapy for scars, however some studies have shown that compression of the wound area leads to a reduction in collagen production, due to the activation of collagenase and decreased production of MMPs (Renò, Grazianetti and Cannas, 2001). Another preventative treatment is the use of topical silicone gel and silicone gel sheeting, which are commonly used following closure of the wound (Arno et al., 2014). Silicone treatment aims to increase the hydration of the wound, counteracting the extreme water loss seen in full thickness wounds. Furthermore, silicone is thought to have a direct chemical action on scars, whilst preventing the stimulation of keratinocytes and subsequent activation of fibroblast through cytokine-mediated signalling (Mustoe, 2008; Mokos et al., 2017). Despite these preventative advancements, surgical excision of the scars and grafting of the affected area, continues to be the most effective treatment (Chiang et al., 2016). However, the recurrence of these scars is common (Griffith, Monroe and McKinney, 1970; Kiil, 1977), and patients may need to undergo several surgeries in their lifetime. Furthermore, recovery can take a long time depending on the size of the wound (Lee and Jang, 2018). Other established and emerging treatment strategies are summarised in Table 1-2.

Table 1-2 Current and emerging treatment options for hypertrophic scars. Adapted from (Gauglitz et al., 2011; Arno et al., 2014; Mokos et al., 2017)

Therapy	Mechanism of action	Advantages/ Disadvantages	Reference
Laser therapy	• Increase in MMPs • Collagen production altered • Capillary destruction	• Very effective as a first line treatment • Erythema seen after treatment • Can be expensive	(Bellew, Weiss and Weiss, 2005; Hultman et al., 2013)
Cryotherapy	• Causes tissue necrosis and anoxia. • Damages the vasculature of the surrounding tissue.	• Very low cost and easy to perform • Increased pain after treatment • Only effective on small scars	(Har-Shaii, Amar and Sabo, 2003; O'Boyle, Shayan-Arani and Hamada, 2017)
Intralesional corticosteroid injections	• Antimitotic – inhibits fibroblast and keratinocyte proliferation • Anti-inflammatory • Immunosuppressant	• Very successful when used in combination with other therapies • Reduces pruritus and pain • Can cause skin atrophy	(Atiyeh, 2007; Jalali and Bayat, 2007)
Intralesional 5-fluorouracil injections	• Induce fibroblast apoptosis • Inhibition of cell proliferation	• Significant side effects (e.g. significant pain and hyperpigmentation) • Very successful when used in combination with corticosteroid	(Larrabee Jr et al., 1990; Asilian, Darougheh and Shariati, 2006)
Interferon therapy	• Inhibits Smad7 signalling • Inhibits TGF-β/ECM production	• Flu-like symptoms common • May require need for local anaesthetic	(Larrabee Jr et al., 1990; Tredget et al., 1998)
Bleomycin injections	• Induces apoptosis • Inhibition of TGF-β1	• Used as therapy for scars that do not respond to steroid treatment • Not a very common treatment option due to toxicity issues	(Espana, Solano and Quintanilla, 2001; Naeini, Najafian and Ahmadpour, 2006)
Botulinum toxin A injections	• Decreases tension of wound edges, by immobilisation of the underlying muscle	• Patient satisfaction very high – also popular with clinicians • Expensive • Larger studies still need to be carried out	(Xiao, Zhang and Cui, 2009; Freshwater, 2013)

Contractures are a further manifestation of hypertrophic scars, occurring in areas of high tensions, such as around joints (Figure 1-9B). Contractures are caused by increased cross-linking and contraction of the collagen fibres, a result of the differing growth rate between the scar tissue and the healthy underlying tissue (Stekelenburg et al., 2015; Hayashida and Akita, 2017). Although full-thickness skin grafts can prevent contracture formation, this therapy is not commonly used as it is hard to receive good quality grafts and hence the waiting time for this treatment is prolonged (Hayashida and Akita, 2017). Common practice for contracture treatment involves the 'release' of the contraction via excision, before being covered with a split-thickness skin graft (Hayashida and Akita, 2017; Stekelenburg et al., 2015; Goel and Shrivastava, 2010).

Figure 1-9: Clinical presentation of different scars. A) Hypertrophic scar across the chest, B) scar contracture of the wrist and c) keloid scar on the back. Images taken from (Goel and Shrivastava, 2010; Bayat et al., 2005; Aarabi, Longaker and Gurtner, 2007).

Keloid scars are defined as benign fibrous tumours, which infiltrate the tissue surrounding the original wound (Figure 1-9C) (Kim, 2021). They appear as firm, protruding tumours, commonly occurring on the earlobes, neck and shoulders and are purple/pink in colour (Bayat et al., 2005). Unlike hypertrophic scars, keloid scars never enter a 'regression' phase and after excision, they have a 45-100% recurrence rate (Gauglitz et al., 2011). Studies have been carried out to investigate whether individuals who develop keloid scars have a genetic predisposition (Bayat et al., 2005). One study showed that in African populations 6-16% of individuals have a higher risk of developing keloid scars, with another study showing that of the patients studied, more than 50% showed a positive family history for keloid scarring (Niessen et al., 1999; Bayat et al., 2005). The histology of keloid scars shows a disorganized collagen structure with thick type I and type III collagen bundles, whilst the scars are also hypocellular with no increased myofibroblast presence (Atiyeh, Costagliola and Hayek, 2005). Due to their persistent nature, therapy of keloid scars is limited and are usually treated using pressure therapy or corticosteroids (Ud-Din and Bayat, 2013; Kim, 2021). Both therapies however have controversial success rates, with pressure therapy having low patient compliance and corticosteroid treatment still having to be combined with other therapies to show success (Ud-Din and Bayat, 2013).

1.5. Burn Injuries

It is believed that 6 million people per year seek medical care for burn injuries, with approximately 250,000 seeking medical care in the UK (Stylianou, Buchan and Dunn, 2015). Since 2003 there has been a rise in the incidence of burn injuries across the UK each year, with a difference of an extra 10,000 cases in 2017 compared to 2003 according to data collated by the international burn injury database (Stylianou, Buchan and Dunn, 2015; Riviera, 2018). Furthermore, complex burn injuries are a huge financial burden on healthcare systems, costing the NHS >£20 million per year (Riviera, 2018). There are multiple causative agents for burn injuries, with thermal causes (e.g. scalds or open flame) accounting for approximately 70% of hospital admissions (Grundlingh, Payne and Hassan, 2017). In recent years, NHS hospitals have seen an influx in admissions for chemical burns because of a rise in acid attacks across the country (Stylianou, Buchan and Dunn, 2015; Brusselaers et al., 2010). Other causes of burn injuries include radiation and electrical sources, although these account for very few burn cases seen (Jeschke et al., 2020). As a result of the first national lockdown during the COVID-19 pandemic, burn units reported a 30-fold increase in the number of patients presenting with scalds and other burn injuries due to spending more time at home (Brewster et al., 2020).

The severity of a burn injury is categorized by the skin layers that are affected by the trauma (Fig 1-10) – for example, a first-degree burn is superficial and does not extend past the epidermis, compared to a third degree burn where the injury extends to deeper tissue layers and destroys the dermis (Bayat, McGrouther and Ferguson, 2003). Scarring after burn injury has been reported to occur after all burns which are classed as second degree or worse, therefore the injury must extend beyond the epidermis to induce scar formation (Hettiaratchy and Dziewulski, 2004). Following the initial injury, the body initiates both local and systemic responses. The local response to a burn injury was previously described by Jackson in 1947, by identifying the zones of a burn (Lang et al., 2019). The zones of a burn are as followed:

1. Zone of coagulation – this is the area which has immediate contact with the cause of the burn, resulting in irreversible tissue loss.
2. Zone of stasis – this is the tissue surrounding the zone of coagulation, which can be characterised by a reduction in tissue perfusion.
3. Zone of hyperaemia – this consists of the outermost tissue, which should remain mostly unaffected, however may be compromised due to severe infection.

The systemic response to burn injury will only be initiated by the inflammatory response once the burn covers >30% of the total body surface area (TBSA) (Kaddoura et al., 2017). The systemic response involves changes in multiple systems, including the cardiovascular and respiratory systems, along with metabolic changes. One of the greatest concerns following complex burn injury is 'burn shock,' which is caused by a cardiovascular impairment, resulting in oedema of the affected area and significant water loss (Rae, Fidler and Gibran, 2016). Cytokines released by immune cells induce bronchoconstriction and capillary leak, which in adult burn patients can lead to respiratory distress syndrome (Kaddoura et al., 2017). Previous studies have shown that burn patients require huge amounts of energy, specifically patients suffering from burns of TBSA >40% have a 2-fold increase in their basal metabolic rate (BMR) (Rutan et al., 1986; Clark et al., 2017). This increase in BMR has been suggested to help maintain gut integrity, however this has disastrous effects on other organs, as the hypermetabolic response has been shown to impair wound healing and increase the risk of infection (Jeschke et al., 2020).

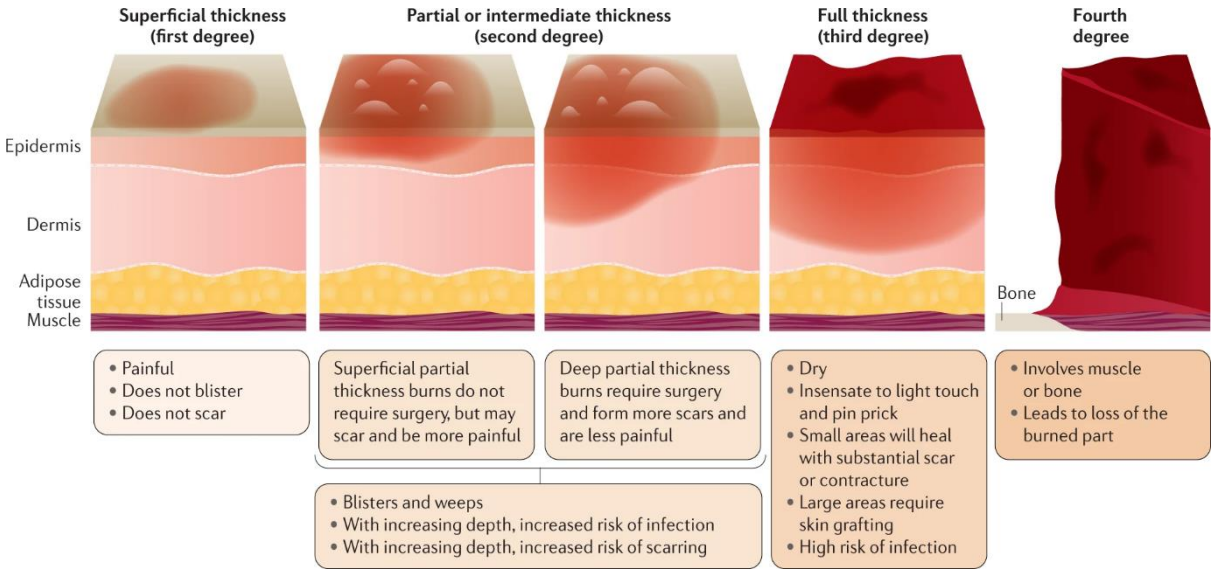

Figure 1-10: Schematic showing the consequences of different burn depths. First degree burns are superficial and do not extend past the epidermis. Second degree burns damage the epidermis and expose the dermis, it is at this degree of burn injury that the risk of scarring increases. Third degree burns extend down to the dermis and will heal with substantial scarring. Fourth degree burns destroy the dermis and hypodermis, exposing the underlying bone. Such significant damage may lead to loss of the affected area. Image taken from (Nielson et al., 2017)

The management of complex burns is imperative to reduce the incidence of scarring and infection, protect any remaining viable tissue and reduce the mortality rate (Nielson et al., 2017; Kaddoura et al., 2017). This is particularly important in the first 48-72 hours following injury. As previously described, complex burns can be characterised by significant water loss and so, fluid resuscitation is critical to enable the optimal environment for wound healing to take place (Faldmo and Kravitz, 1993; Rae, Fidler and Gibran, 2016). Furthermore, all necrotic eschar tissue that has formed in the zone of coagulation is removed, before grafting the area

with autologous split-thickness grafts from healthy tissue on the patients' body (DeSanti, 2005). Antibiotics are topically administered to the patient, to help prevent the formation of bacterial biofilms in the wounded area (Nielson et al., 2017). Finally, burn wounds are then dressed with a non-adherent dressing, to allow the wound to heal without the worry of the dressing sticking to the wound (Nielson et al., 2017). Despite these measures and those described in Section 1.3.4.3., 91% of all deep partial thickness and full thickness burn injuries will result in hypertrophic scarring. Unfortunately, no current prevention or treatment strategy aims to target the underlying causes that drive scar formation.

1.6. Drug discovery in fibrosis

Discovering new medicines is a complex process, that includes the expensive and time-consuming endeavour of taking a drug from development to market (Hughes et al., 2011). Over the years the pharmaceutical industry has adopted two models for the discovery of new medicines – phenotypic and target-based approaches (outlined in Figure 1-11) (Terstappen et al., 2007). The phenotypic (or systems-based) approach involves the development of assays which measure a key phenotype associated with a disease (O'Connor and Roth, 2005). A large number of compounds are then screened against the selected phenotype, and following the identification of candidate compounds, target deconvolution can be carried out to identify their cellular/molecular target (Swinney, 2013; Terstappen et al., 2007).

Vorinostat, a histone deacetylase inhibitor, is an example of a drug identified using phenotypic screening. In 1971, erythroleukemia cells were placed in culture with DMSO and their differentiation to functional cells was noted, due to a change in colour of the cell (Friend et al., 1971). Further research into this identified polar amides as the factor that induced this differentiation, which eventually lead to the discovery of the first-generation compounds (Grant, Easley and Kirkpatrick, 2007; Marks, 2007). Although these compounds showed good efficacy in clinical trials, the compounds were not tolerated well by patients (Andreeff et al., 1992). Studies into the structure and subsequently the derivatives of these compounds, lead to the synthesis of vorinostat, which not only showed greater potency in clinical trials, but was also well tolerated by patients (Kelly et al., 2003). It wasn't until the late 1990s when the mechanism of action of vorinostat was identified, 20 years after the initial phenotype was discovered (Tanaka et al., 1975; Yoshidas et al., 1990; Richon et al., 1998). More recently the use of phenotypic screening is gaining popularity for the discovery of therapeutic antibodies (Gonzalez-Munoz, Minter and Rust, 2016).

In vivo models can also be utilised for phenotypic screening, albeit with less throughput compared to cell-based models. Several non-mammalian models such as zebrafish, murine and fruit-fly have been used for phenotypic screening, as well as using models of multiple different disease states (Reaume, 2011). An example of *in vivo* phenotypic screening is the discovery of proton pump inhbitors (PPI) to suppress gastric acid production. The first PPI, omeprazole, was discovered in the 1960s using a conscious dog model where gastric juice acidity was measured with a nasogastric cannulla, at a time when the acid producing enzyme in the stomach was not yet discovered (Olbe, Carlsson and Lindberg, 2003). More recently, the concept of testing a library of drugs using phenotypic *in vivo* models have gained more traction and was successfully utilised in the re-purposing of the antihistamine astemizole, as an anti-malarial (Chong et al., 2006; Chen et al., 2006).

The other approach to drug discovery is known as a target-based approach, in which the molecular target is identified first, before developing assays to modulate this target and then screening millions of compounds for hit identification (Terstappen et al., 2007). Raltegravir, an anti-viral used in the treatment of HIV, is one example of a medicine discovered using a target-based approach (Swinney, 2013). Prior to its discovery, three enzymes were identified as being key factors in the regulation and replication of HIV. One of these enzymes is known as integrase, which aids in the integration of the viral DNA into the host cell genome (Deeks et al., 2008; Hazuda et al., 2000). Integrase became the focus of many studies to identify any inhibitors that could potentially be used therapeutically, eventually leading to the discovery of raltegravir and its drug class known as diketo acids (Summa et al., 2008; Rowley, 2008). In clinical trials, raltegravir was shown to significantly reduce viral load in patients and no severe adverse effects were identified (Summa et al., 2008).

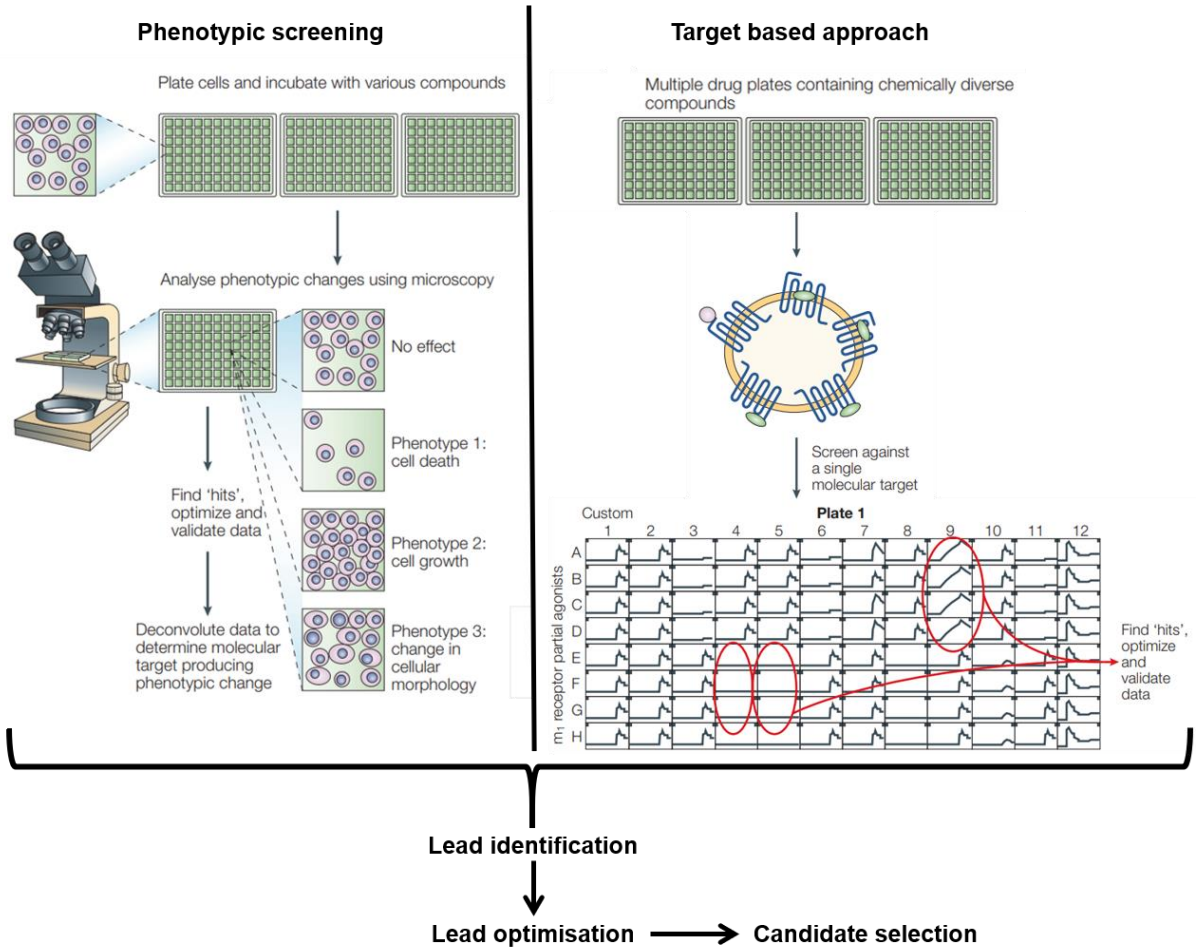

Figure 1-11: The drug discovery process, highlighting the different steps between phenotypic and target-based approaches. The phenotypic approach works by developing an assay to measure a functional phenotype associated with the disease, and once hits have been identified the process of target identification is carried out. In comparison, the target-based approach screens compounds against a specific molecular target, to identify those that are able to modulate this target. Image adapted from (O'Connor and Roth, 2005).

Over the last three decades, the pharmaceutical industry has invested heavily in adopting the target-based approach to discover new medicines. However, the effectiveness of this method has been questioned, as the cost to take a drug from target identification to market is exponentially increasing (Drews and Ryser, 1997). In 2011, Swinney and Anthony published the landmark paper which looked at how first-in class drugs were discovered over a 10-year period. This study identified that of the 45 first-in class drugs discovered, phenotypic approach was used to discover 28 with only 17 discovered using target-based approach (Swinney and Anthony, 2011). Further reviews looking into this have also highlighted that many drugs discovered using target-based approaches are failing in the early stages of clinical trials due to safety and efficacy issues (Swinney and Lee, 2020). This raised questions over whether the shift in drug discovery towards target-based approaches was worth it, and whether returning to a more traditional approaches should be considered (Sams-Dodd, 2005; Eder, Sedrani and Wiesmann, 2014).

The discovery of new medicines to combat fibrosis has proven challenging. Many of the drugs that have been discovered using target-based approaches have exhibited safety and tolerability issues, whilst also exhibiting limited efficacy (Datta, Scotton and Chambers, 2011). Recent examples of drugs that failed in clinical trials for the treatment of fibrosis include Interferon gamma (IFNγ)-1β and peroxisome proliferator-activated receptor gamma (PPARγ) agonists for IPF and endothelin receptor antagonists for liver fibrosis – all of which showed little to no improvement in patient survival and disease progression compared to the placebo (Raghu et al., 2013; King et al., 2009; Ratziu et al., 2010). Regarding dermal scarring, there has also been limited success in identifying an effective therapeutic. In the 1990s, Ferguson et al., developed a neutralising TGF-β1/2 antibody which was able to improve scar appearance in both rodent and rabbit animal models (Shah, Foreman and Ferguson, 1992; Lu et al., 2005). Despite success in clinical trials for surgical scars, there has been no reported trials on patients who developed scars following severe injury (e.g. burns) (Durani et al., 2008). Currently researchers are taking a more systems-based approach to discover new treatments for fibrosis, by investigating the key phenotypes that drive its progression. This has included addressing the excessive ECM production, promoting the production of anti-fibrotic cytokines, inducing apoptosis and cell clearance, and preventing the sustained transformation of fibroblasts to myofibroblasts (Mora et al., 2017; Falke et al., 2015). Lack of progress in finding novel anti-fibrotic drugs using target-based approach stimulated a switch to the phenotypic approach.

1.7. Rationale

Unmet need: Combatting excessive scarring of the skin is considered as the greatest unmet need following burn injury. Fibrosis, the process by which these scars form, can affect many of the major organs (e.g. lungs, kidney, and liver), subsequently causing irreversible damage and potentially resulting in organ failure. Despite fibrosis being responsible for an estimated 45% of all deaths in the Western world, the treatment options for this underlying pathology are limited. Hypertrophic scarring seen after severe injury is a fibrotic disorder of the skin, characterised by the presence of a raised area of skin, which remains within the margins of the initial wound. Side effects of these scars include pruritus, pain, and loss-of-function of the affected area. Furthermore, due to the disfiguration, the individual can suffer from significant mental health disorders. There are currently no therapeutics available to prevent the formation of scars after severe injury, with current treatment strategies focussing on relieving the associated clinical sequele.

Target-based approach has failed: The current treatment strategy for dermal fibrosis involves surgical excision of the scars, with patients encouraged to massage the affected area. At this moment in time, there are only two FDA-approved medical therapies on the market for fibrosis (specifically idiopathic pulmonary fibrosis), highlighting the need to identify novel therapeutics that can tackle the underlying cellular and molecular mechanisms that drive fibrosis. One of the issues surrounding drug discovery for fibrosis is the multiple factors driving its progression, suggesting that the classical target-based approach might not lead to success. Therefore, a phenotypic approach could be more productive in finding novel treatements for scar prevention.

Phenotype: For the phenotypic approach, a disease relevant phenotype first needs to be identified. One of the key elements that drives fibrosis is the persistent nature of cells known as myofibroblasts. During wound healing, resting fibroblasts transform into contractile and migratory myofibroblasts in the presence of inflammatory cytokines. These cells are responsible for the production of essential granulation tissue, consisting of ECM components, allowing for the migration of cells across the wound bed to facilitate wound closure. During fibrosis however, the stages of wound healing are prolonged with myofibroblasts becoming highly proliferative and resistant to apoptosis. This subsequently leads to the excessive accumulation of ECM and scar formation. It is well known that myofibroblasts found in the dermis of the skin are responsible for driving the formation of hypertrophic scars.

Assay: There are many issues which have prevented the identification of novel therapeutics to prevent dermal scarring, the first being the lack of reliable and physiologically relevant models of skin fibrosis *in vitro* and *in vivo*. Although in recent years more models have been developed, with the rise in popularity of *ex vivo* culture and 3D human skin equivalents, a model that is reliable and rapid enough to be used for high-throughput screening has not been identified. The previous work of other PhD students in the lab had focussed on developing an assay that used fibroblasts isolated from the tunica albuginea of Peyronie's disease patients, a fibrotic disorder that affects the penis. This assay utilised the In-Cell ELISA (ICE) method which could quantify the expression of α-SMA in fibroblasts that underwent myofibroblast transformation, after exposure to TGF-β1 in a multi-well format. This developed assay was used as the basic starting blocks, to develop a similar assay using fibroblasts derived from the skin. The assay was taken through a series of optimisation steps, to ensure that the best output was achieved, before being rigorously validated to ensure that it is suitable for high-throughput screening. The assay was then utilised to screen a drug library of 1,954 approved drugs to identify any that can inhibit TGF-β1-induced myofibroblast transformation, whilst maintaining suitable cell viability. Further investigation into the anti-fibrotic activity of any identified candidate drugs was carried out, using a battery of secondary screening assays that measured other phenotypic hallmarks of fibrosis, and the effect of the candidate drugs on aspects of cell viability.

Therefore, in this thesis I aim to identify drugs through phenotypic approach that can ultimately be developed as anti-scarring agents.

1.7.1. Research questions

This thesis set out to investigate the following research questions:

1. Could a high-throughput, phenotypic screening assay be developed and optimised for use with primary human skin fibroblasts?
2. Can this assay identify any drugs that can inhibit TGF-β1-induced myofibroblast transformation?
3. Are any of the hits identified from the screening assay capable of showing other anti-fibrotic effects?

1.7.2. Aims & Objectives

The aim of this thesis was to identify novel drugs that can prevent myofibroblast transformation in fibroblasts isolated from the scars of burn patients, using a high-throughput phenotypic screening assay to measure α-SMA expression. The objectives were:

1. Isolate and culture of primary human dermal fibroblasts, from the scars of burn patients.
2. Develop, optimise and validate a cell-based, high-throughput phenotypic screening assay which measures myofibroblast transformation.
3. Screen 1,954 approved drugs to identify any drugs that prevent myofibroblast transformation.
4. Develop secondary screening assays, to measure other common hallmarks of fibrosis and assess cell viability.
5. Investigate the anti-fibrotic activity of the candidate drugs using the secondary assays.

Chapter 2: Development and validation of a phenotypic, high-throughput screening assay

2.1. Introduction

When developing an assay for phenotypic screening, the 'rule of three' should be considered to ensure that the assay remains relevant for the disease that it is being used for. The criteria listed in the 'rule of three' focus on the the tissue or cells used, stimulus used and the endpoint of the assay (Vincent et al., 2015). Therefore, for the assay being developed in this thesis, the rule of three was followed while determinining which aspect of the fibrosis phenotype would be used. Burn wound healing and scar formation is a complex process, co-ordinated by several different cell populations. However, as these scars are often characterised by a significant increase in extracellular matrix in the wound bed (Xue and Jackson, 2015), it is clear that the cells responsible for producing the majority of ECM during wound healing/fibrosis (myofibroblasts) are the key culprit in burn scar development (Zhu, Ding and Tredget, 2016). Therefore, the transformation of fibroblasts to myofibroblasts was selected as the phenotype to be used in the screening assay.

Targeting myofibroblast transformation has been suggested previously as a potential target for anti-fibrotic therapies. In these studies, a target known for inducing myofibroblast transformation (e.g. growth factor receptors and integrin receptors) was identified and drugs screened/developed to inhibit these. For example, the tyrosine kinase inhibitor imatinib was found to inhibit both TGF-β1 and PDGF-induced transformation by inhibiting downstream signalling pathways involving c-abl (Jang et al., 2014; Wang et al., 2005). Another example is through the activation of the prostaglandin receptors EP2/4. Agonists for these receptors have been developed (e.g. butaprost) and have been shown to attenuate myofibroblast transformation through the upregulation of cAMP (Kolodsick et al., 2003).

The first aspect of the rule of three to be considered was the tissue or cells used in the assay itself. The more relevant the cells to the disease, the stronger the assay in identifying translatable hits. For that reason, primary human dermal fibroblasts were isolated from patient tissue. The tissue donated to the study were the scars of burn patients undergoing excision surgery.

The second aspect of the 'rule of three' to be considered is the endpoint of the assay. The more proximal and functionional the readout, the higher the relevance and translatibility of the screen. Burn scars are often characterised histologically by an overabundance of myofibroblasts in the dermis, identified from high levels of α-SMA expression (Zhu, Ding and Tredget, 2016). As α-SMA is only expressed by myofibroblasts and not fibroblasts (Desmouliere et al., 1993), this acts as the best measurement for the assay.

The final aspect of the ‘rule of three’ to be considered was which stimulus would be used to invoke the phenotypic change. The more phyisologically relevant the stimulus, the higher the chance of the assay to identify hits that translate to the clinic. It is known that a number of factors involved in the burn scar pathophysiology can initiate myofibroblast transformation and so careful consideration was needed to identify the ‘best’ stimulus to be used *in vitro*. One stimulus that could be used is inducing oxidative stress in the cells. Due to significant cellular injury occuring immediately after burn injury, there is increased oxidative stress and production of reactive oxygen species (ROS) in the cells surrounding the wound site (Simpson et al., 1993; Hernandez et al., 1987). This increased ROS presence can induce myofibroblast transformation in resting fibroblasts, by activating the transcription factor, NF-κβ (Wang et al., 2017). Other stimuli that would be easier to use *in vitro* are the cytokines and growth factors expressed by the several cell populations involved in the scarring response. As discussed in Chapter 1.2., PDGF, TGF-β1 and IL-6 are all expressed during burn injury and have been associated with inducing myofibroblast transformation (Xue et al., 2000; Ghahary et al., 1995; Mori, Shaw and Martin, 2008). Significantly, there is evidence that TGF-β1 may be the key cytokine mediator of myofibroblast transformation, particularly when looking specifically at burn wound pathophysiology. TGF-β1 has been shown to be overexpressed in full thickness/deep dermal burn wounds (Honardoust et al., 2012), with ~67% of all full thickness burns resulting in some form of scarring (van Baar, 2020). Furthermore, higher levels TGF-β1 have been shown to be circulating in burn patients both systemically and in the local tissue (Tredget et al., 1998). For this reason TGF-β1 was chosen as the stimulus.

2.2. Materials and Methods

2.2.1. Tissue Acquisition

Skin samples were obtained from St. Andrews Centre for Plastic Surgery and Burns, Broomfield Hospital, Chelmsford, UK with ethical approval from NHS East of England – Cambridge Central Research Ethics Committee (REC 18/EE/0072) and Anglia Ruskin University Faculty Research Ethics Panel (FMSFREP/17/18 187). The samples were otherwise surgical discard tissue and were collected from fully informed and consented patients undergoing either burn scar excision or deep inferior epigastric perforator (DIEP) flap reconstruction. Patients who were age 16-75, listed for either burn scar excision or DIEP flap reconstruction surgery, and understood the patient information sheet were recruited for the study by Prof Dziewulski or a member of his surgical team. Patients under the age of 16, or over the age of 75 and who were not able to understand the patient information sheet were excluded from this study. The consent was obtained by the surgical team and the samples were transferred to Anglia Ruskin University (ARU) in fully anonymized form with the following information: age, surgery underwent, co-morbidities, and medications. In total, three different types of skin samples were collected – late stage burn scars, normal skin from burn patients and abdominal skin from DIEP patients.

In total 20 patients were recruited to the study and donated tissue - 13 were patients undergoing surgery for burn scar excision and 7 were patients undergoing DIEP flap reconstruction. Of the 13 patients undergoing burn scar excision surgery, 3 patients also donated normal tissue as well (unaffected, non-burn scar tissue). The average age of the burn patients was 30 years old and 59 years old for the DIEP patients. Table 2-1 summarises the co-morbidities and co-medication of each patient recruited to the study.

Table 2-1: Co-morbidities and co-medications of the patients recruited to the study.

Patient #	Co-morbidities	Co-medications
Burn scar patients		
1	None	None
2	None	None
3	None	None
4	None	None
5	None	None
6	None	None
7	Asthma (Mild), Hypothyroidism, Hypertension, Atrial Fibriliation, Stage III Chronic Kidney Disease, Bilateral Total Knee Replacement	Amitriptyline, Chlorphenamine, Levothyroxine, Gabapentin, Ramipril, Zopiclone, Adcal D3, Moricol, Salbutamol, Omeprazole, Tiramadol
8	Psychiatric problems	None
9	Osteoarhtiritis, IBS & Psoriatic arthitis	Amitryptyline, Desgestorel
10	None	None
11	None	None
12	None	None
13	None	None
DIEP patients		
1	None	None
2	Breast cancer	None
3	Breast cancer and arthritis	Overcounter vitamin and tumeric tablet
4	None	None
5	Breast cancer, bowel cancer and pulmonary embolism	None
6	Breast Cancer	None
7	Breast Cancer	None

2.2.2. Fibroblast cell culture

2.2.2.1. Isolation of primary human fibroblasts

Skin samples were kept on ice and transferred to ARU in media which consisted of DMEM-F12 (Gibco Invitrogen, UK), 20% foetal calf serum (FCS; Fisher Scientific, UK) and 1% penicillin/streptomycin (Pen/Strep; Gibco Invitrogen, UK) – this media will hereby be referred to as '20% FCS media'. After the skin samples were transferred to the lab, they were first washed in phosphate-buffered saline (PBS; previously warmed to 37°C) and then all subcutaneous tissue was removed. Mechanical separation of the dermis and epidermis was carried out using forceps and scissors, with the dermis then cut into smaller sections for explantation. Using a scalpel, dermal explants (approximately $1cm^2$ in size), were scratched into the bottom of a 6-well plate (Nunc Fisher Scientific, UK) to anchor them in place. 2 mL of 20% FCS media was then carefully added into each well and the plate incubated at 37°C, 5% CO_2 for 5-7 days.

After 5 days, fibroblast growth was monitored using a light microscope (Nikon Instruments Europe, UK) and if fibroblast outgrowth was observed, the tissue was removed from the wells. All explant tissue was placed into cryotubes (Nunc Fisher Scientific, UK) and stored at -80°C. The cells were washed twice with warm PBS, before being given fresh 20% FCS media and incubated at 37°C, 5% CO_2. Once the cells had reached 70-90% confluency, old media was removed, and the cells washed twice with warm PBS. Cells were detached using 500 µl of 0.25% trypsin/0.03% EDTA (Gibco Invitrogen, UK), which was neutralised with 1 mL 20% FCS media. The cell suspension was transferred to a T75 flask (Nunc Fisher Scientific, UK), containing 11 mL of 20% FCS media, and incubated at 37°C, 5% CO_2.

At this point (passage 0; P0), each primary cell line was labelled with a specific code to ensure that they were identifiable. The code was made up of the tissue type (Late stage burn scar – L; Normal tissue from burn patient – LN; Abdominal tissue from DIEP patients – BR), the patient number and then the well number the explants were put in. For example, L10FA1, indicates fibroblasts grown from burn scar patient #10, in well A1 of the six well plate.

Once attachment of the P0 cells was observed (usually the next day), the old media was removed, and the cells washed with warm PBS. The media was switched to media consisting of DMEM-F12, 10% FCS, 1% Pen/Strep and 4 ng/mL of human basic fibroblast growth factor (hBFGF; Sigma-Aldrich, UK) – this media will hereby be referred to as complete media.

2.2.2.2. Passage and maintenance

Whilst in culture, fibroblasts were maintained in 12 mL of complete media, with media changes occurring every 2-3 days until cells reached 80% confluency. At this point, fibroblasts would be passaged and split at a 1:4 ratio. For this, the old media was removed from the flask and the cells washed in 10 mL of warm PBS, before adding 2 mL of trypsin/EDTA to the flask and incubation at 37°C, 5% CO_2 for 5 min. During this time 4 new T75 flasks were labelled and filled with 10 mL of complete media. The flask in the incubator was checked under the microscope to ensure detachment of the cells. Once this was achieved trypsin/EDTA was neutralised with 6 mL of complete media. The cell suspension was transferred to the new T75 flasks, with 2 mL placed in each flask. The flasks were placed in the incubator at 37°C, 5% CO_2. Fibroblasts were maintained in this way until they reached passage 6.

2.2.2.3. Freezing and storage

For long term storage, cells were frozen and stored at -80°C. Fibroblasts were washed with 10 mL of warm PBS and detached using 2 mL trypsin/EDTA. The trypsin was neutralised using complete media, and the cell suspension transferred to a 15 mL Falcon tube (Nunc Fisher Scientific, UK). The cell suspension was subjected to centrifugation at 400 x g for 5 min

at 4°C using the Multifuge™ X1R (ThermoFisher Scientific, UK). The supernatant was discarded, and the cell pellet was resuspended in 1 mL of freezing media, consisting of 10% dimethyl sulfoxide (DMSO; Fisher Scientific, UK) in FCS. The cell suspension was transferred to a cryotube and stored at -80°C.

2.2.2.4. Defrosting cells

When lower passage fibroblast stocks were required for experiments, cells were defrosted from the stocks at -80°C. To do this, the desired cryotube was chosen from the stocks and defrosted in the water bath (set to 37°C). Once defrosted, the cryotube was transferred to the culture hood, where the cell suspension was diluted in 5 mL of complete media and transferred to a 15 mL Falcon tube. The cell suspension was centrifuged at 400 x g for 5 min at 4°C using the Multifuge™ X1R, before removal of the supernatant. The cell pellet was resuspended in 1 mL of fresh complete media and transferred to a T75 flask containing 12 mL of complete media. Cells were incubated at 37°C, 5% CO_2.

2.2.2.5. Seeding of fibroblasts for experiments

Fibroblasts were seeded for experiments once they had reached 70-90% confluency. In preparation for this, fibroblasts were washed twice with 10 mL of warm PBS and then serum starved, using 10 mL of serum free media (DMEM-F12 and 1% pen/strep). The fibroblasts were serum starved for 30 mins at 37°C, 5% CO_2. The cells were washed again with 10 mL of PBS and then detached as explained previously (section 2.2.2.1). Once the trypsin/EDTA was neutralised with complete media, the cell suspension was transferred to a 15 mL Falcon tube. The tube was inverted and 500 µl of the cell suspension transferred to a 1.5 mL microtube. Using the Scepter 2.0 handheld automated cell counter (Scepter; Merck Millipore, UK), the cell number was counted. Once the cell number had been determined, it was diluted to the cell density required for the experiment using complete media (without bHFGF). The cells were seeded onto the desired plasticware and then left overnight at 37°C, 5% CO_2. Table 2-2 summarises which patient tissue and cells were used for the experiments in this chapter.

Table 2-2: Summary of patient tissues and/or cell lines used in the development, optimisation and validation of the screening assay. 'X' indicates which experiments the tissue/cells were used for.

Patient #	Whole tissue or cell line used?	Characterisation experiments						Assay optimisation	Assay validation		
		Histology – H&E	Histology – IHC	TGF-β1 CRC	ICC	ICE	Western blot		Z-Factor	SB-505124 CRC	Vehicle CRC
Burn Patient											
2	Whole tissue	X									
7	Whole tissue	X	X								
10	L10FA1			X		X	X	X	X	X	X
	LN10FB1			X							
11	L11FB1					X	X			X	X
12	L12FB1				X	X	X			X	X
DIEP Patient											
4	Whole tissue	X	X								
6	BR6FA3			X							

2.2.3. Keratinocyte cell culture

2.2.3.1. Passage and maintenance

Primary adult human epithelial keratinocytes (catalogue #C0055C – ThermoScientific, UK) were maintained in 13 mL of media consisting of EpiLife® basal media, human keratinocyte growth supplement (HKGS; Gibco Invitrogen, UK) and 1% pen/strep – this media will hereby be referred to a Epilife media. Growth was monitored using a light microscope. Cells were given fresh Epilife media every 2 days until they reached 50% confluency, after this point the media was changed daily until cells were ready to be sub-cultured. Once the cells reached 80% confluency, all media was removed from the flask and 3 mL of trypsin/EDTA was used to wash the cells. This trypsin/EDTA was discarded and 1 mL of fresh trypsin/EDTA was added the flask, before leaving the flask at room temperature for 7-8 min. Once the cells had detached, 6 mL of a trypsin neutralizer solution (PBS with 0.5% FCS) was used to neutralise the trypsin/EDTA and the cell suspension transferred into a 15 mL Falcon tube. Cells were centrifuged at 180 x g for 7 min at 4°C using the Multifuge™ X1R. Supernatant was removed from the tube and the cells re-suspended in 4 mL of Epilife media. The cell suspension was equally divided into new T75 flasks containing 12 mL of Epilife media.

2.2.3.2. Freezing and storage

Once the cells reached 80% confluency, cells were detached from the flask as described previously with the cell suspension transferred to a 15 mL Falcon tube. Cells were centrifuged at 180 x g for 7 min at 4°C using the Multifuge™ X1R. Supernatant was removed from the tube and the cells re-suspended in 1 mL of freezing media. The cell suspension was transferred to a cryotube and then stored at -80°C.

2.2.3.3. Defrosting cells

When lower passage keratinocyte stocks were required for experiments, cells were defrosted from the stores at -80°C. To do this, the desired cryotube was chosen from the stocks and defrosted in the water bath (set to 37°C). Once defrosted, the cryotube was transferred to the culture hood, where the cell suspension was diluted in 5 mL of Epilife media and transferred to a 15 mL Falcon tube. The cell suspension was centrifuged at 180 x g for 7 min at 4°C using the Multifuge™ X1R, before removal of the supernatant. The cell pellet was resuspended in 1 mL of fresh Epilife media and transferred to a T75 flask containing 12 mL of Epilife media. Keratinocytes were incubated at 37°C, 5% CO_2.

2.2.3.4. Seeding of keratinocytes for experiments

When the cells reached 80-90% confluency, the cells were seeded for experiments. In preparation for this, keratinocytes were detached as explained previously. Once the trypsin/EDTA was neutralised with the trypsin neutraliser, the cell suspension was transferred to a 15 mL Falcon tube and centrifuged at 180 x g for 7 min at 4°C using the Multifuge™ X1R. The supernatant was removed, and the cell pellet resuspended in 10.5 mL of Epilife media. The tube was inverted and 500 µl of the cell suspension transferred to a 1.5 mL microtube. Using the Scepter, the cell number was counted. Once the cell number had been determined, it was diluted to the cell density required for the experiment using Epilife media. The cells were seeded onto the desired plasticware and then left overnight at 37°C, 5% CO_2.

2.2.4. Histology

2.2.4.1. Sample preparation

During the processing of the tissue samples, following removal of all subcutaneous tissue, the sample was split into two pieces – one half used for fibroblast isolation and the second half was processed for histology. The tissue was carefully cut into 3x3 cm pieces using forceps and scissors. These were transferred into 50 mL Falcon tubes and fixed with 4% paraformaldehyde (PFA), for 24 h at 4°C. Samples were then transferred to fresh 50 mL Falcon tubes containing a dehydrating solution (30% sucrose in 0.1 M phosphate buffer), and left for 48 h at 4°C. Following dehydration, samples were placed into plastic molds and submerged in optimal cutting temperature compound (OCT; VWR, UK) before being frozen and stored at -80°C until use. Using the Leica CM1860 Cryostat, the frozen tissue was sectioned in 10 µm slices at -28°C. The tissue sections were placed onto SuperFrost Ultra Plus™ GOLD Adhesion Slides (Fisher Scientific, UK) and left to dry at room temperature for 2 h.

2.2.4.2. Haematoxylin & Eosin staining

The tissue sections were washed in distilled water for 25-30 dips, before being submerged in haematoxylin (Fisher Scientific, UK) for 10 min. The slides were washed in running tap water for 30 s and then submerged in eosin (Fisher Scientific, UK) for 30 s, before being washed again in running tap water for a further 30 s. The slides were then dehydrated in 95% alcohol for 1 min, 100% alcohol for 1 minute and finally placed in xylene for 1 minute. Coverslips were mounted onto the slides with VectaMount® Permanent Mounting Medium (Vector Laboratories, UK) and left to dry in a fume hood overnight. Haematoxylin & eosin (H&E) staining was observed using light microscopy (AXIO Lab.A1; Zeiss, Germany) and images taken using the Axiocam ERc 5s (Zeiss, Germany).

2.2.4.3. Immunohistochemistry (IHC)

Once the tissue sections had dried, a border was drawn around the tissue sections using a hydrophobic pen (Vector Laboratories, UK). 200 µl of a blocking solution (10% donkey serum in 0.1% Triton X-100 in PBS) was placed onto each slide. Slides were incubated for 90 min at room temperature in a humidified chamber. The blocking solution was removed from the slides and replaced with 100 µl of the desired antibody diluted in PBS (Table 2-3). The slides were incubated overnight at 4°C, in a humidified chamber. The following day, the slides were washed three times with 600 µl of PBS, before adding 100 µl of the desired secondary antibody (diluted in PBS) to each slide (Table 2-3). The slides were incubated with the secondary antibody for 2 h at room temperature, in a humidified chamber. The slides were then washed three times with PBS, before removing excess buffer from the slide using tissue. To help reduce autofluorescence caused by formaldehyde fixation, the slides were incubated with the TrueVIEW™ autofluorescence quenching kit (Vector Laboratories, UK) for 4 min at room temperature. The solution was removed from the slides, followed by a 5 min washing step using PBS. Excess buffer was removed from the slides, before mounting coverslips onto the slides using VECTASHIELD® antifade mounting medium with DAPI (Vector Laboratories, UK). The slides were visualised using a fluorescence microscope (Olympus IX71) and images captured using a Leica DFC3000G camera.

Table 2-3: Primary and secondary antibodies used in IHC.

Antibody		Dilution
Primary antibody	Anti-vimentin raised in mouse (Abcam, UK - cat #ab8069)	1:500
	Anti-cytokeratin-14 raised in rabbit (CK-14; Abcam, UK – cat #ab181595)	1:1,000
Secondary antibody	Donkey anti-mouse IgG antibody, fluorescein isothiocyanate conjugate (FITC; Millipore, UK – cat #AP192F)	1:3,000
	Donkey anti-rabbit IgG antibody, tetramethylrhodamine conjugate (TRITC; Millipore, UK – cat #AP182R)	1:3,000

2.2.5. Immunocytochemistry (ICC)

Prior to seeding, coverslips were washed with ethanol and left to dry, before being placed in the wells of a 6-well plate. The coverslips were submerged in 2 mL of media (complete media for fibroblasts or Epilife for keratinocytes) and a pipette used to remove any air bubbles under the coverslips. The plates were kept at 37°C, 5% CO_2 for 2 h. Having diluted the cells to the desired cell density of 1.0 x10^5 per well, the cells were seeded onto the coverslips. The cells were left to adhere to the coverslips for 24 h in the incubator. The following day, the cells were either given fresh blank media or fresh media containing 10 ng/mL TGF-β1 (Sigma Aldrich, UK – cat #T7039). The plates were incubated for 72 h at 37°C, 5% CO_2.

The coverslips were submerged in ice cold methanol for 10 s, before being washed three times in PBS. Coverslips were placed on glass slides and left to dry. The coverslips were incubated with 200 µl of a blocking solution (10% donkey serum in PBS) for 1 h at room temperature in a humidified chamber. Primary antibodies were diluted in PBS to the desired concentration (Table 2-4), using 100 µl of the antibody to replace the blocking solution on the coverslips. The primary antibody was incubated for 2 h at room temperature in a humidified chamber. Coverslips were washed three times with PBS, before incubation with 100 µl of the secondary antibody (Table 2-4) for 2 h at room temperature. The coverslips were washed three times with PBS, before being mounted onto slides using VECTASHIELD® antifade mounting medium with DAPI. The cells were visualised using a fluorescence microscope (Olympus IX71) and images captured using a Leica DFC3000G camera.

Table 2-4: Primary and secondary antibodies used in ICC.

Antibody		Dilution
Primary antibody	Anti-vimentin raised in mouse (Abcam, UK - cat #ab8069)	1:1,000
	Anti-desmin raised in mouse (Abcam, UK – cat #ab6322)	1:500
	Anti-CK-14 raised in rabbit (Abcam, UK – cat #ab181595)	1:1,000
	Anti-α-SMA raised in mouse (Sigma-Aldrich, UK – cat #A5228)	1:1,000
Secondary antibody	Donkey anti-mouse IgG antibody, FITC conjugate (Millipore, UK – cat #AP192F)	1:250
	Donkey anti-rabbit IgG antibody, FITC conjugate (Millipore, UK – cat #AP182F)	1:250

2.2.6. In-Cell ELISA (ICE)

Fibroblasts and keratinocytes were seeded at a density of 4,000 cells per well into black optical 96-well plates (Nunc Fisher Scientific, UK) and left to adhere for 24 h in the incubator. The next day, cells were either given fresh blank media or incubated with media containing 10 ng/mL TGF-β1 and/or the desired compounds. The plates were incubated for at 37°C and 5% CO_2 for 72 h. The cells were fixed by incubating the cells with 4% PFA at room temperature for 20 min. After the PFA was removed, the plates were washed three times for 5 min using 0.1% Triton X-100 in PBS, before a blocking solution of 10% donkey serum in 0.1% Triton X-100 in PBS was added. The plates were incubated for 90 min at room temperature on an orbital shaker.

The blocking solution was then removed from the wells and replaced with the desired primary antibody in PBS (Table 2-5). The plates were incubated at room temperature on an orbital shaker for 2 h. The cells were washed three times with 0.1% Tween 20 in PBS, with each

wash lasting for 5 min. The secondary antibody (800 nm IRdye donkey anti-mouse/anti-rabbit, 1:500 dilution; Li-Cor, UK) and nuclear stain (DRAQ5, 1:1,000 dilution; Biostatus, UK) were diluted in PBS and incubated with the cells for 60 min at room temperature on an orbital shaker. The plates were washed three times with 0.1% Tween 20 in PBS, then once with blank PBS. All liquid was removed from the wells before scanning. The plates were scanned using a near-infrared scanner (Odyssey CLx imager; Li-Cor, UK), in the 700 nm and 800 nm channels.

Table 2-5: Primary antibodies used in ICE.

Antibody		Dilution
Primary antibody	Anti-α-SMA raised in mouse (Sigma-Aldrich, UK – cat #A5228)	1:3,000
	Anti-vimentin raised in mouse (Abcam, UK - cat #ab8069)	1:3,000
	Anti-desmin raised in mouse (Abcam, UK – cat #ab6322	1:500
	Anti-CK-14 raised in rabbit (Abcam, UK – cat #ab181595)	1:1,000

2.2.7. Western blotting

2.2.7.1. Protein isolation

Fibroblasts and keratinocytes were seeded at a density of 1.0 x10^5 per well into 6-well plates and left to adhere overnight in the incubator. The next day, the cells were given either fresh blank media or incubated with media containing 10 ng/mL TGF-β1 (fibroblasts only). The plates were incubated for 72 h at 37°C and 5% CO_2. Prior to isolating the protein, the lysis buffer (Radio Immuno Precipitation Assay (RIPA) buffer) required for this was prepared following the recipe in Table 2-6 and kept on ice for the rest of the protocol. The plates were removed from the incubator and the old media removed from each well. The cells were washed with 1 mL of warm PBS and then detached using 500 µl of trypsin/EDTA. After the cells were detached, the cell suspensions from the same condition were all pooled together and transferred to a 1.5 mL microtube. The cells were subjected to centrifugation at full speed 21,000 x g for 10 min, at 4°C using the Fresco™ 21 Microcentrifuge (ThermoFisher Scientific, UK). The supernatant was removed, and the cell pellet resuspended in 200 µl of radioimmunoprecipitation assay (RIPA) lysis buffer. The suspension was left to incubate for 20 min on ice, vortexing the samples every 5 min. Following the incubation period, the tubes were centrifuged at 21,000 x g for 10 min, at 4°C using the microcentrifuge. After centrifugation, the supernatant was carefully removed and split into 50 µl aliquots. The isolates were stored at -80°C until use.

Table 2-6: Contents of RIPA lysis buffer.

Chemical	Supplier	Final Concentration	Volume required
10% NP-40	Fisher Scientific	1%	1 mL
1 M Tris-HCl, pH 7.4	Fisher Scientific	10 mM	100 µl
1 M NaCl	Fisher Scientific	0.15 M	1.5 mL
0.1 M EGTA	Sigma Aldrich	1 mM	100 µl
100 mM EDTA	Fisher Scientific	10 mM	1 mL
100 mM PMSF	Fisher Scientific	1 mM	100 µl
1 mg/mL Aprotinin	Fisher Scientific	2 µg/mL	20 µl
10 mg/mL Leupeptin	Fisher Scientific	2 µg/mL	2 µl
10 mg/mL Pepstatin A	Fisher Scientific	2 µg/mL	2 µl
0.5 M NaF	Fisher Scientific	50 mM	1 mL
0.1 M $Na_4P_2O_7$	Sigma Aldrich	20 mM	2 mL
100 mM Na_3VO_4	Sigma Aldrich	100 µM	10 µl
Distilled Water	-	-	Adjust to 10mL

2.2.7.2. Protein concentration measurement

To determine the concentration of protein present in the isolated samples, the Bio-Rad *DC* Protein Assay kit II was used. 5 µl of protein standards ranging from 0.0625 - 2 mg/mL were transferred in duplicate into a clear 96-well plate; these standards were used to construct the standard curve required to calculate the protein concentration. The samples were defrosted on ice, before 5 µl of the sample was diluted 1 in 3, in distilled water. 5 µl of the diluted sample was transferred in duplicate into the 96-well plate, changing tips for each different sample. The required amount of working reagent (Reagent S + Reagent A) was prepared, and 25 µl of the working reagent was added to each well. 200 µl of Reagent B was added to each well, before gently agitating the plate to mix the contents. The plate was placed on an orbital shaker for 15 min at room temperature. The absorbance was then read using the iMark™ Microplate Absorbance Reader (Bio-Rad, UK) in the 750 nm wavelength. The protein concentration was calculated using the standard curve generated, using Microsoft Excel.

2.2.7.3. Western blot

20 µg of the protein isolate was mixed in a 1:1 ratio with Laemmli buffer (Bio-Rad, UK), before heat denaturing the mixture at 95°C for 5 min. Samples were kept on ice before being centrifuged at 21,000 g for 15 s at 4°C using the microcentrifuge. 5 µl of a protein ladder (Precision Plus Protein™ Dual Color Standards, 10 -250 kD; Bio-Rad, UK) was loaded into the first lane of a Mini-PROTEAN TGX Precast Protein Gel (Bio-Rad, UK) and 40 µl of the samples were loaded into the subsequent lanes. Electrophoresis was carried out at 120 V for 10 min, to allow separation through the stacking layer, before increasing the voltage to 200 V for a further 50 min to allow complete molecular weight separation. This was carried out using a PowerPac Basic Power Supply (Bio-Rad, UK). Samples were transferred onto a polyvinylidene fluoride (PVDF) membrane (Millipore, UK). After initial polarization of the membrane with methanol, samples were transferred via wet blotting for 1 h at 350 mA using the PowerPac Basic Power Supply. After transfer, the membranes were marked to ensure correct orientation and washed using 1x tris-buffered saline (TBS) four times for 5 min. Membranes were blocked using 10% non-fat dried milk (NFDM) in 1x TBS for 1 h, at room temperature on a shaker. Prior to incubation, primary antibodies were diluted to their desired concentration (Table 2-7) in 5% NFDM in 0.1% TBS-T (0.1% Tween20 in 1x TBS). Membranes were incubated with the primary antibodies overnight, at 4°C on a shaker. The following morning, the membranes were washed 4 x with 0.1% TBS-T before blocking with 10% NFDM in TBS for a further 15 min. The secondary antibodies (Table 2-7) were diluted to a concentration of 1:3,000 in 5% NFDM in 0.1% TBS-T, before incubating the membranes for 1 h at room temperature, in the dark and on a shaker. The membranes were washed 4 x for 5 min using 0.1% TBS-T. The membranes were scanned using a near-infrared scanner (Odyssey CLx imager; Li-COR, UK) in both the 700 nm and 800 nm wavelengths.

Table 2-7: Primary and secondary antibodies used in Western blots.

Antibody		Dilution
Primary antibody	Anti-CK-14 raised in rabbit (Abcam, UK – cat #ab181595)	1:1,000
	Anti-α-SMA raised in mouse (Sigma-Aldrich, UK – cat #A5228)	1:1,000
	Anti-GAPDH raised in rabbit (Abcam, UK – cat #ab9485)	1:10,000
Secondary antibody	800nm IRdye donkey, anti-mouse (Li-COR, UK – cat #926-32212)	1:3,000
	800nm IRdye donkey anti-rabbit (Li-COR, UK – cat #926-32213)	1:3,000
	700nm IRdye donkey anti-rabbit (Li-COR, UK – cat #926-68073)	1:3,000

2.2.7.4. Western blot quantification

ImageJ software (National institute of health, version 1.8.0_172) was utilised to quantify the protein blots and determine the ratio of the desired protein to the loading control. The blot images were first converted to black and white, before highlighting the area where the desired protein bands were, and the loading control bands were (Fig 2-1A). This generated a 2D image of the blot (Fig 2-1B), whereby peaks indicated an area of higher density. Using the wand tool, the area of each peak was calculated, and these results transferred into a Microsoft Excel spreadsheet.

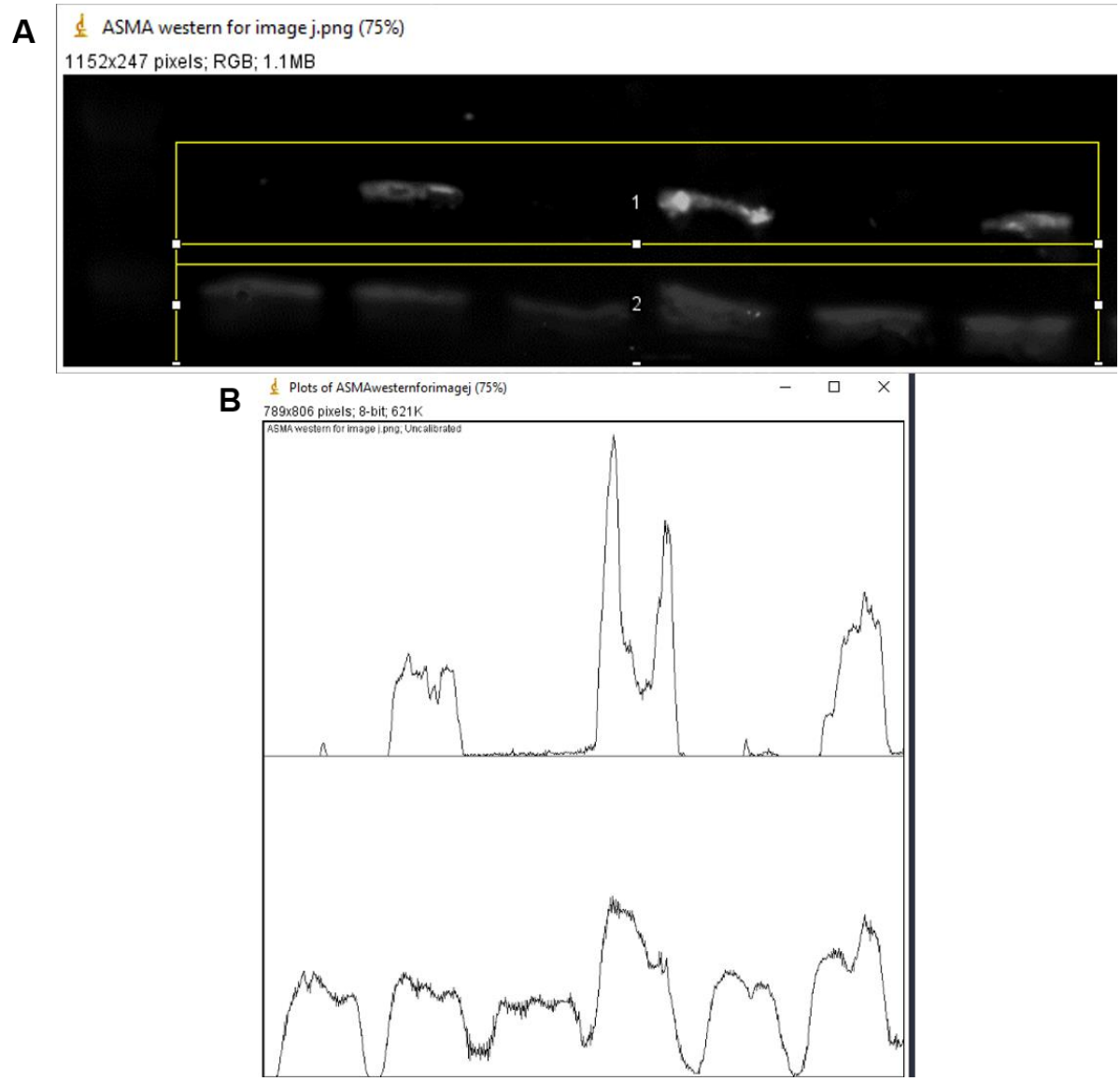

Figure 2-1: Quantification of western blot image, using ImageJ software. A) Blot was converted to black and white, desired protein and loading control lanes were highlighted. B) 2D image of blot, with peaks indicating protein expression.

Finally, for relative protein expression to be calculated, the ratio of the desired protein to loading control was calculated using the following formula:

$$Relative\ protein\ expression = \frac{Area\ density\ (desired\ protein)}{Area\ density\ (loading\ control)}$$

2.2.8. Data analysis

Microsoft Excel 2016 and GraphPad Prism 8 programmes were utilised for all data and statistical analysis, throughout the thesis.

For all ICE experiments where protein expression was measured, protein expression was first normalised to the cell number by calculating the ratio between the 800 nm channel and 700 nm channel (see equation below).

$$\frac{Protein\ expression\ (800\ nm\ channel)}{DRAQ5\ nuclear\ staining\ (700\ nm\ channel)}$$

To ensure the robustness and reliability of the high-throughput screening assay, Z-factor (Z') analysis was used. Z' is able to statistically measure the size of the effect that TGF-β1 has on myofibroblast transformation. Z' is calculated using the following equation:

$$1 - \frac{3 - (\sigma p + \sigma n)}{(\mu p - \mu n)}$$

Where p refers to the positive controls (TGF-β1-treated) and n refers to the negative controls (untreated). σp and σn are the standard deviations of the positive and negative controls, and μp and μn are the means of the positive and negative controls.

To calculate the biological response of SB-505124, DMSO and PBS in their respective concentration response curves, the percentage of the maximum TGF-β1 response was calculated using the equation below:

$$\frac{Sample}{Postive\ Control\ (TGF - \beta 1\ response)}\ x\ 100$$

To calculate the IC_{50} of SB-505124, DMSO and PBS, a second set of concentration response curves were constructed to show their pharmacological response – these graphs can be found in appendix I. The curves were constructed between 0% – 100% so that the IC_{50} could be accurately calculated at 50%. To calculate this, the delta between the positive control and the sample, was normalised to the delta between the positive and negative controls (see equation below).

$$\frac{Postive\ Control - Sample}{Positive\ Control - Negative\ Control}\ x\ 100$$

The positive control refers to the concentration of the drug that had the smallest effect on protein expression, and the negative control refers to the concentration of the drug that had the greatest effect on protein expression.

Statistical difference was calculated using either one-way analysis of variance (ANOVA) test or Student's t-test for unpaired means. A p-value less than 0.05 was found to be statistically significant. ANOVA was utilised for statistical analysis of any experiments where multiple groups were compared, and Student's t-test was utilised for experiments with only two groups. Normal distribution of the data was confirmed by construction of Q-Q probability plots and use of the Shapiro-Wilkes test. All data points were plotted as mean ± SEM, where all experiments were done in triplicates (n=3) and where possible, more than one patient sample (N) was used.

2.3. Results

2.3.1. Histological comparison between normal skin and scar tissue

Histological staining of different tissue types was carried out to identify the key histological changes that occur during the scarring process. Haematoxylin and eosin (H&E) staining of normal skin (Fig 2-2A), <5-year-old burn scar (Fig 2-2B), and >10-year-old burn scar (Fig 2-2C) was carried out to show the changes in skin architecture. All tissue sections in Figure 2-2 show the distinct epidermal and dermal layers, with the normal skin and >10-year-old burn scar showing presence of epidermal rete ridges and disorganised collagen structure in the dermis (Fig 2-2A/C). The <5-year-old scar tissue shows organised collagen structure in the dermis, with the distinct loss of blood vessels and epidermal rete ridges (Fig 2-2B).

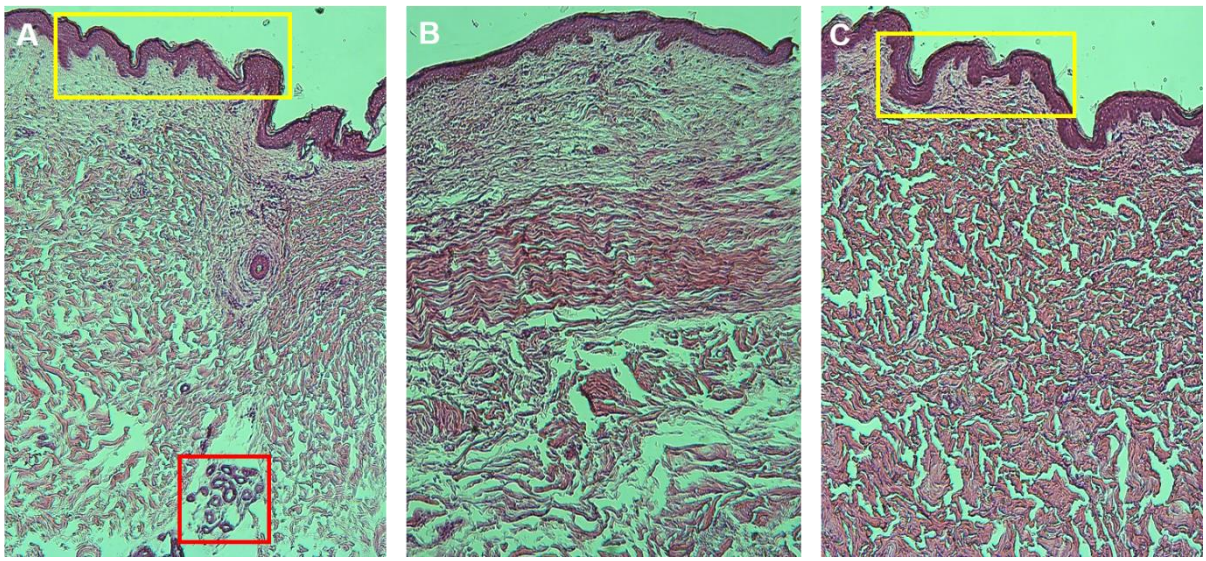

Figure 2-2: Representative images of H&E staining of skin samples obtained from three patients – A) Normal abdominal skin from DIEP patient, B) burn scar <5-years-old and C) burn scar >10-years-old. In A&C the yellow box indicates the presence of rete ridges in the epidermis, and in A, the red box indicates the presence of blood vessels. Images were obtained using brightfield microscopy at 40X magnification.

To confirm the presence of fibroblasts in the obtained skin samples, immunohistochemical staining was carried out prior to isolation of the cells. For this, the tissue samples were stained for the mesenchymal marker vimentin (fibroblasts are of mesenchymal lineage) and epithelial marker cytokeratin-14 (CK-14) to distinguish between the epidermis and dermis. As seen in Figure 2-3, both the normal and burn scar tissue show expression of vimentin in the dermis, confirming the presence of fibroblasts in the tissue. Further, an increase in vimentin expression in the burn scar tissue can be observed.

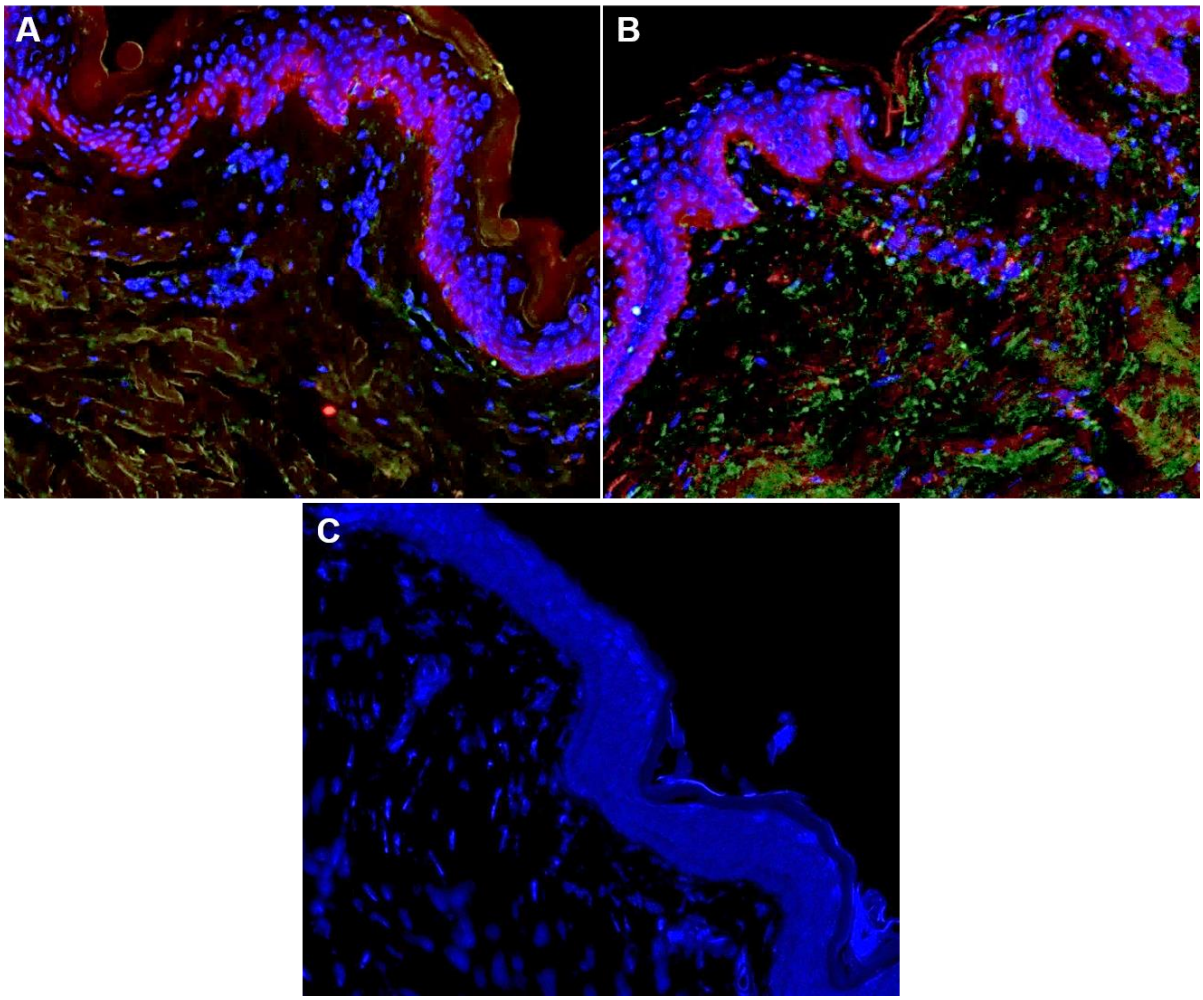

Figure 2-3: Immunohistochemical staining of skin samples obtained from A) normal abdominal skin from DIEP patient, B) >10-year-old burn scar, stained for vimentin and CK-14 and C) no primary control. Cell nuclei were stained DAPI shown in blue, vimentin expression shown in green and CK-14 expression shown in red. Images were obtained at 100X magnification.

2.3.2. Isolation of primary human fibroblasts

One issue that can occur during fibroblast isolation using the explant method is the contamination of other cell types, typically keratinocytes from the epidermis. To prevent this from happening the epidermis and dermis were mechanically separated, before culturing the dermal explants in 20% FCS media.

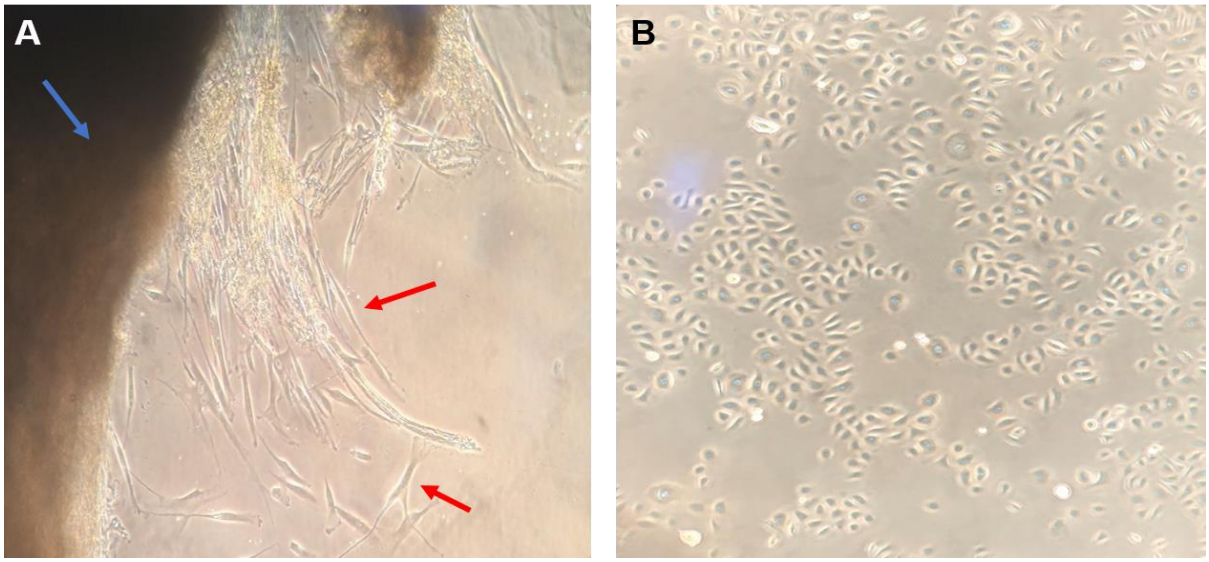

Figure 2-4: Representative images of fibroblasts and keratinocytes in culture. A) Fibroblast outgrowth from dermal explant at day 5 (blue arrow indicates dermal explant; red arrows indicate fibroblast outgrowth, B) commercial primary keratinocytes in culture. Images were obtained using brightfield microscopy at 100X magnification.

In Figure 2-4 fibroblast outgrowth can be confirmed by the observed morphology of the cells. Fibroblasts have a long, spindle like morphology (Fig 2-4A), compared to the keratinocyte morphology, which is commonly described as being cobblestone like (Fig 2-4B).

2.3.4. Characterisation of isolated cells

2.3.4.1. TGF-β1 induces fibroblast to myofibroblast transformation

TGF-β1 is a key factor in the development of the fibrotic phenotype. Since TGF-β1 is responsible for the transformation of fibroblasts to myofibroblasts, it is important to verify this in skin fibroblasts *in vitro.* Fibroblasts from normal skin (burn patient and DIEP patient) and burn scars, were treated with varying concentrations of TGF-β1 (0.01 ng/mL – 30 ng/mL) and full concentration response curves were constructed (Fig 2-5). This generated sigmoid curves for all three cell types, with both upper and lower plateaus. Maximum α-SMA expression was seen at 3 ng/mL for burn scar fibroblasts, with an EC_{50} of 0.5 ± 0.07 ng/mL. Maximum α-SMA expression was also seen at 3 ng/mL for normal fibroblasts from a burn patient and from a DIEP patient, with an EC_{50} of 0.8 ± 0.14 ng/mL and 0.68 ± 0.23 ng/mL, respectively. One-way ANOVA analysis of the EC_{50} of each fibroblast cell line showed no significance difference ($p = 0.44$).

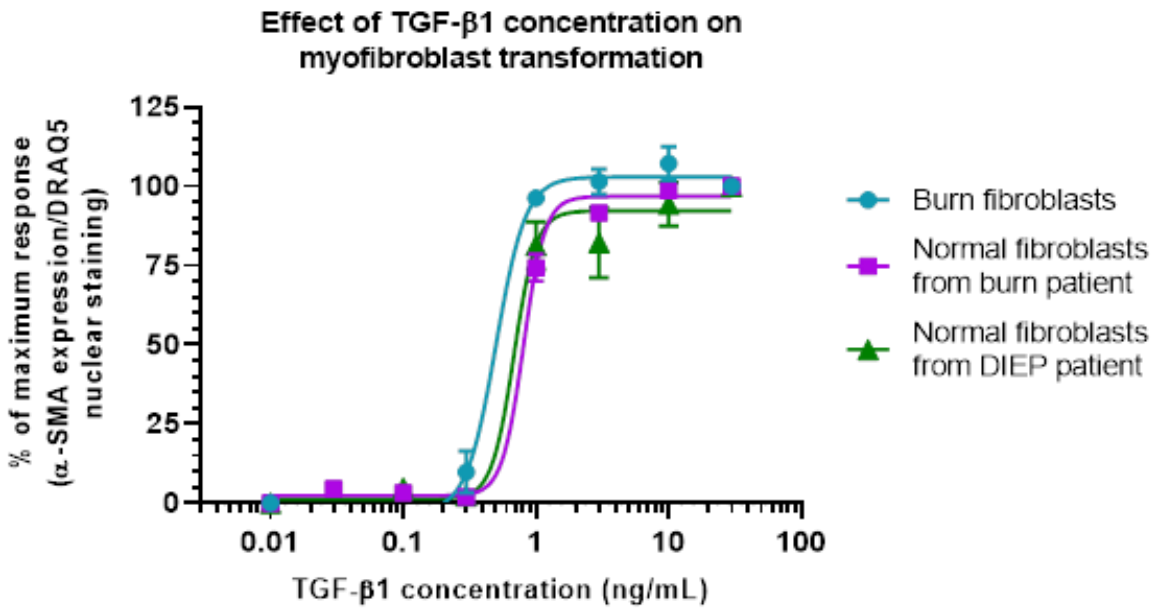

Figure 2-5: Effect of TGF-β1 concentration on myofibroblast transformation. Fibroblasts from burn scars, normal tissue from a burn patient and normal tissue from a DIEP patient were incubated with TGF-β1 at varying concentrations (0.01 ng/mL – 30 ng/mL) for 72 h, before measuring α-SMA expression using the In-Cell ELISA method. Data points are plotted as average ± SEM, N=1, n=3.

Following this, fibroblasts from all three tissue types were incubated with 10 ng/mL TGF-β1 (to ensure maximum transformation) and immunocytochemistry (ICC) was used to visualise α-SMA expression in TGF-β1-treated fibroblasts (Fig 2-6).

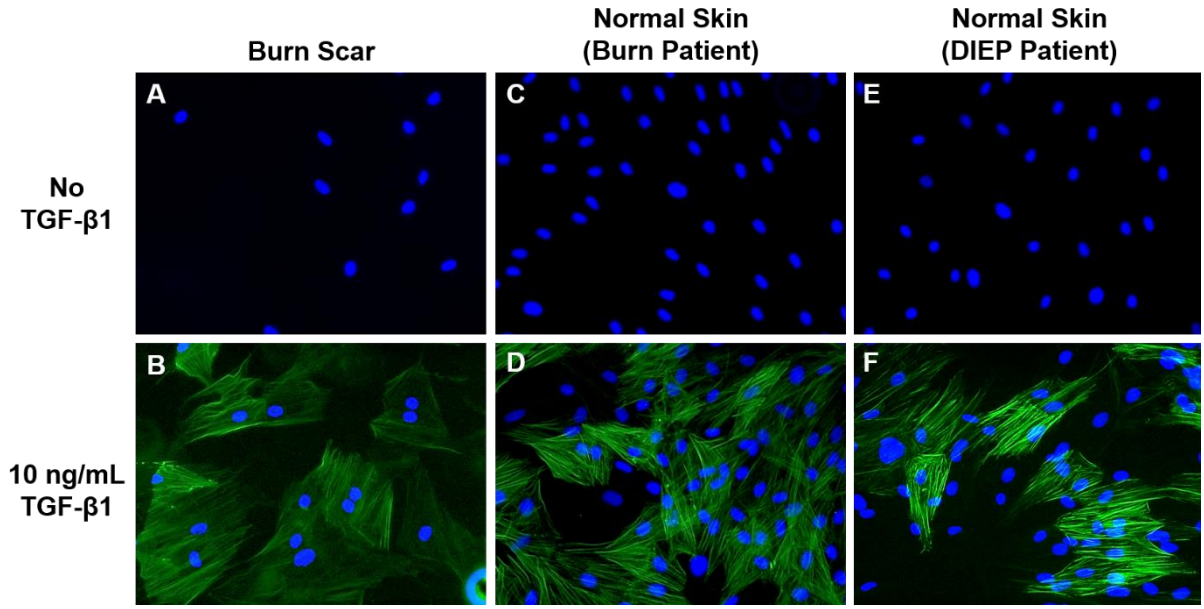

Figure 2-6: Immunocytochemical stainings of fibroblasts for α-SMA expression**.** A&B: burn scar cells, C&D: cells from normal skin of a burn patient, E&F: cells from normal skin of a DIEP patient. Cells were either left untreated (A, C & E) or treated with 10 ng/mL TGF-β1 for 72 h (B, D & F). Cell nuclei were stained blue using DAPI and α-SMA stained green. Images were obtained using 100X magnification.

When stained for α-SMA, the TGF-β1-treated fibroblasts (Fig 2-6B/D/F) shows increased expression of α–SMA expression, compared to the untreated fibroblasts (Fig 2-6A/C/E) which show nuclear staining only. As there was no significant difference in response to TGF-β1 (EC_{50} and cell morphology) between the cells from the three tissue types, burn scar fibroblasts were chosen for the experiments going forward, to create a more biologically relevant disease model.

To quantify α-SMA expression fully and confirm that α-SMA could be used as a reliable myofibroblast marker, Western blot analysis was carried out on protein lysates isolated from burn scar fibroblasts that were untreated and treated with 10 ng/mL TGF-β1. Western blotting confirmed that TGF-β1-treated fibroblasts express α-SMA with the presence of bands at 42 kDA in lanes 2, 4 & 6 (Fig 2-7A). GAPDH was used as a loading control, with all samples showing bands at 37 kDa. Quantification of this data confirmed that TGF-β1-treated fibroblasts have a significantly higher α-SMA/GAPDH ratio, compared to the untreated fibroblasts (Fig 2-7B).

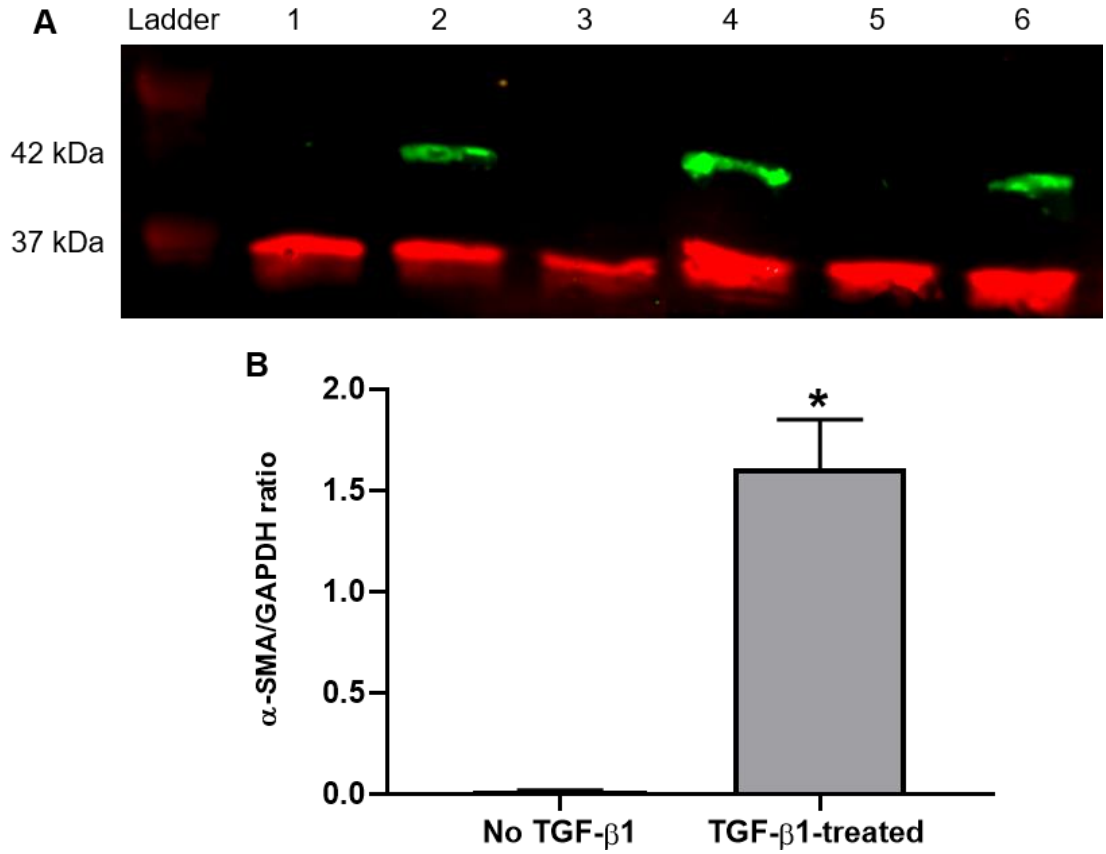

Figure 2-7: Western blot analysis of α-SMA expression in fibroblasts derived from burn scar tissue. A) Odyssey output image of α-SMA Western blot for protein lysates isolated from fibroblast treated with 10 ng/mL TGF-β1 for 72 h and untreated fibroblasts. 5 µl of a protein ladder was loaded, along with 20 µg of protein under reducing conditions. Lanes 1, 3 & 5: untreated fibroblasts. Lanes 2, 4 & 6: fibroblasts treated with 10 ng/mL TGF-β1. The bands seen at 42 kDa confirm α-SMA expression and bands at 37 kDa confirm GAPDH expression, used as a loading control. B) Quantification of Western blot analysis by measuring the α-SMA/GAPDH ratio. Data points plotted as mean ± SEM, N=3 n=1. Statistical analysis carried out using Student's t-test of unpaired means, *$p<0.05$ vs untreated cells.

2.3.4.2. Confirmation of fibroblast identity

Due to the possibility of contamination occurring during the isolation process, it was important to confirm the identity of the cells isolated from the dermal explants. Various methods to detect protein expression were carried out to confirm that the cells isolated from the dermal explants were fibroblasts.

Despite no specific fibroblast marker existing, it is well known that fibroblasts are of a mesenchymal lineage and so, the isolated cells were stained for the mesenchymal marker vimentin (McAnulty, 2007). Cells were either untreated or treated with 10 ng/mL TGF-β1 for 72 h. Figure 2-8A/B show that both untreated and TGF-β1-treated cells express vimentin, confirming their mesenchymal lineage.

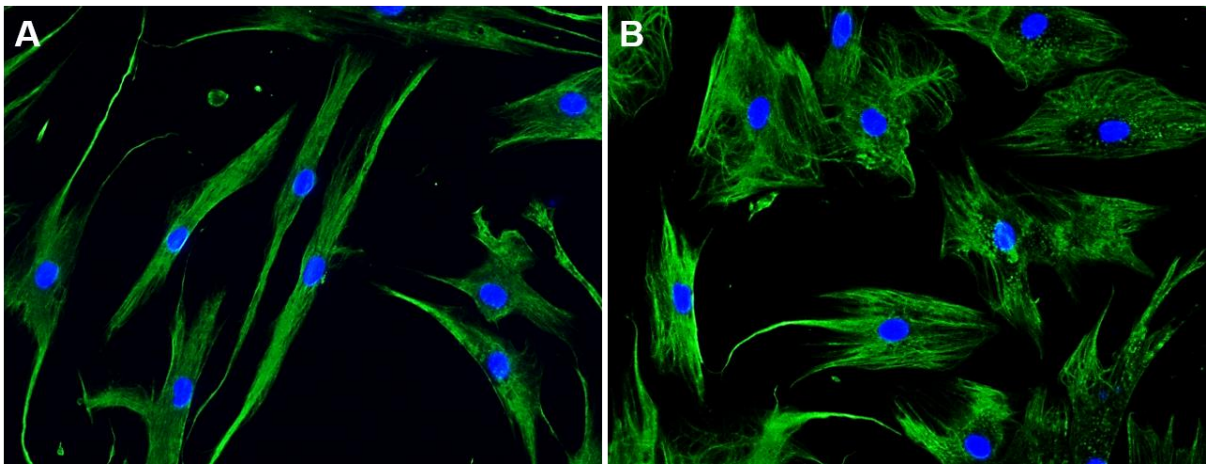

Figure 2-8: Immunocytochemical staining of cells from burn scar tissue for vimentin expression. A) untreated cells and B) cells treated with 10 ng/mL TGF-β1 for 72 h. Cell nuclei were stained blue using DAPI, with vimentin stained green. Images were obtained using 100X magnification.

To quantify vimentin expression fully the ICE method was utilised, where fibroblasts were seeded and treated with 10 ng/mL TGF-β1 for 72 h or left untreated. Cells were stained for vimentin and cell number measured by staining with DRAQ5. Quantification of this data further confirmed expression of vimentin in both untreated and TGF-β1-treated fibroblast, with no significant difference between the two treatment groups, where p = 0.66 (Fig 2-9).

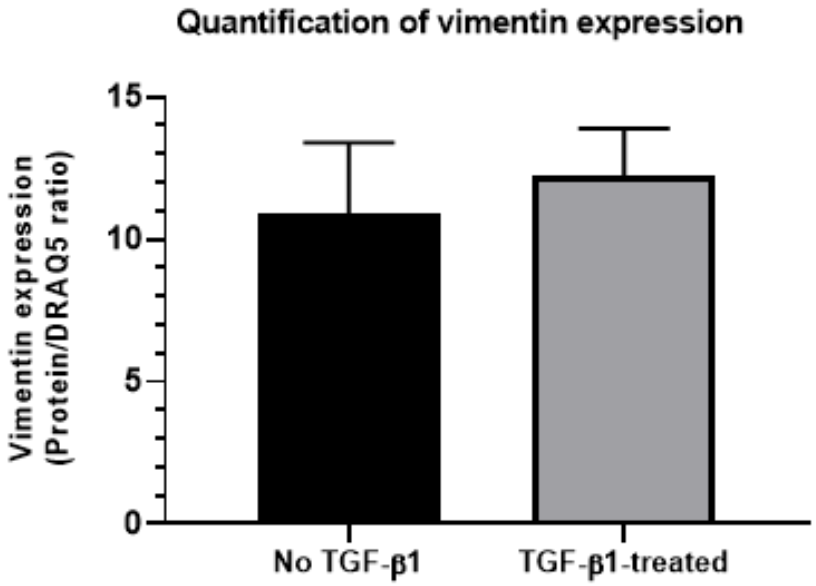

Figure 2-9: Quantification of vimentin expression in untreated cells and cells treated with 10 ng/mL TGF-β1 for 72 h, using the In-Cell ELISA method. Data points are plotted as the average ± SEM, where N=3, n=9. Statistical analysis carried out using Student's t-test of unpaired means.

To confirm that no smooth muscle cells had contaminated the fibroblast cultures, the cells were stained for the smooth muscle marker desmin. Figure 2-10A/B shows that both untreated and TGF-β1-treated cells were desmin negative, as only the nuclear staining was visible. Rhabdomyosarcoma (RD) cells were used as a positive control, with Figure 2-10C confirming desmin expression in these cells.

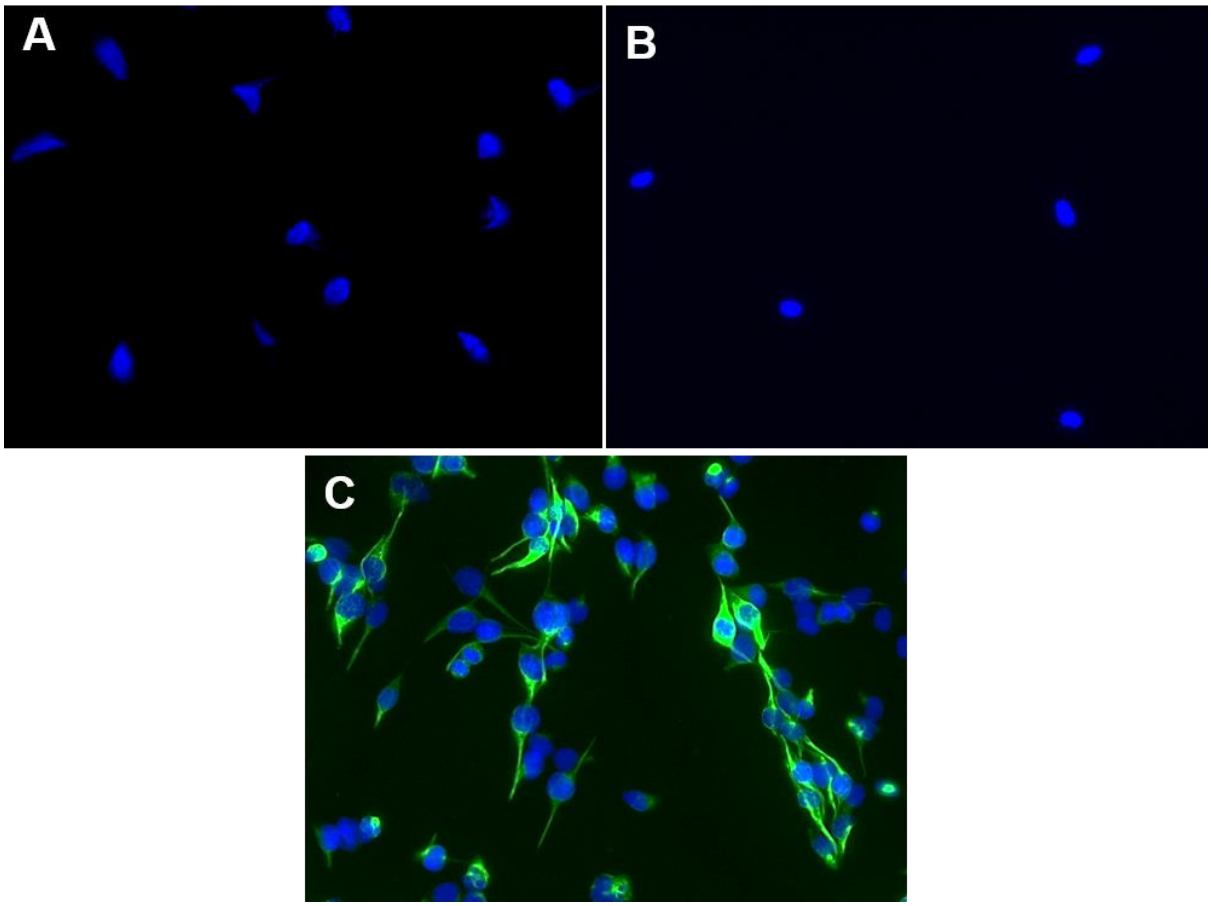

Figure 2-10: Immunocytochemical staining of cells from burn scar tissue for desmin expression. A) untreated cells, B) cells treated with 10 ng/mL TGF-β1 for 72 h and C) rhabdomyosarcoma cells. Cell nuclei were stained blue using DAPI, with desmin stained green. Images were obtained using 100X magnification.

To quantify desmin expression fully, the ICE method was utilised, where fibroblasts were seeded and treated with 10 ng/mL TGF-β1 for 72 h or left untreated, with RD cells seeded as a positive control. Cells were stained for desmin, and cell number measured by staining with DRAQ5. Quantification of this data further confirmed that both untreated and TGF-β1-treated fibroblasts do not express desmin, with no significant difference between the two treatment groups and the no primary control (Fig 2-11).

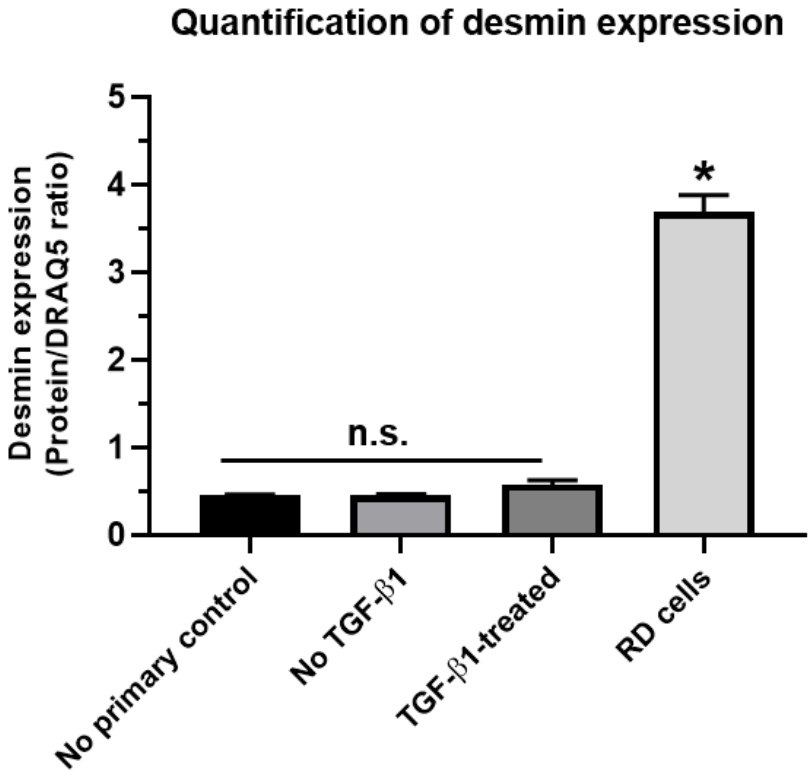

Figure 2-11: Quantification of desmin expression in untreated cells, cells treated with 10 ng/mL TGF-β1 for 72 h and rhabdomyosarcoma (RD) cells using the In-Cell ELISA method. Data points are plotted as the average ± SEM, where N=3, n=9. Statistical analysis using ANOVA multiple comparisons. *p < 0.05 vs untreated or TGF-β1 treated.

To ensure there was no keratinocyte contamination in the cell cultures, the cells were stained for CK-14, a type 1 keratin, which is commonly expressed by basal keratinocytes but not expressed in fibroblasts. Figure 2-12A/B show that both the untreated and TGF-β1-treated cells did not express CK-14, indicated by only the nuclear stain being visible. A commercially available human keratinocyte cell line (Fisher Scientific, UK) was used as a positive control, with Figure 2-12C showing CK-14 expression in these cells.

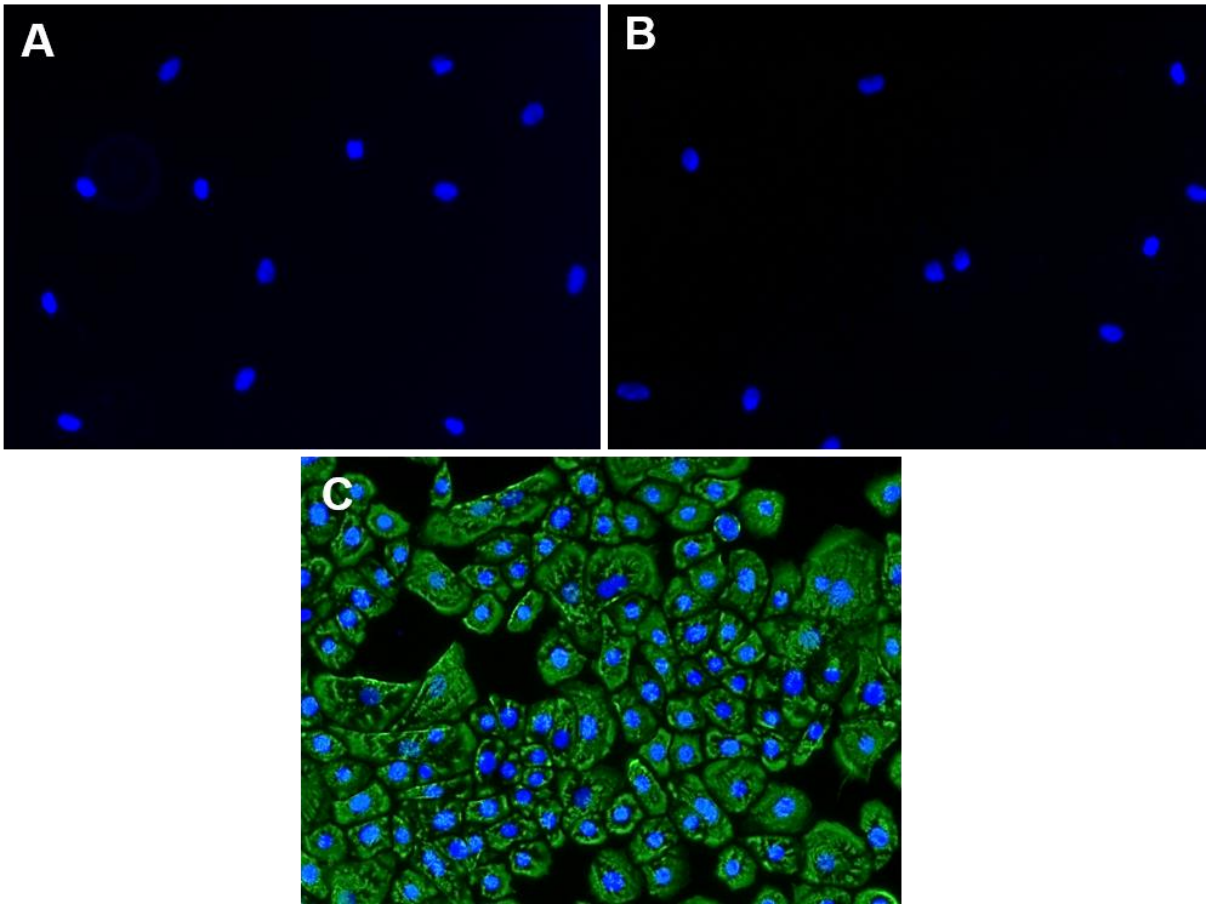

Figure 2-12: Immunocytochemical staining of cells from burn scar tissue for CK-14 expression. A) untreated cells, B) cells treated with 10 ng/mL TGF-β1 for 72 h and C) keratinocytes. nuclei were stained blue using DAPI, with CK-14 stained green. Images were obtained using 100X magnification.

To quantify CK-14 expression fully, Western blot analysis was carried out on protein lysates isolated from fibroblasts that were untreated and treated with 10 ng/mL TGF-β1. Western blotting confirmed that untreated and TGF-β1-treated fibroblast do not express CK-14, with the lack of bands at 50 kDA in lanes 1-6 (Fig 2-13A). Protein lysates from keratinocytes were used as a positive control and CK-14 expression can be seen by the presence of a band at 50 kDa in lane 7. GAPDH was used as a loading control, with the bands at 37 kDa seen in all lanes. Quantification of this data confirmed no significant difference between the CK-14/GAPDH ratio of both untreated and TGF-β1-treated fibroblasts (Fig 2-13B).

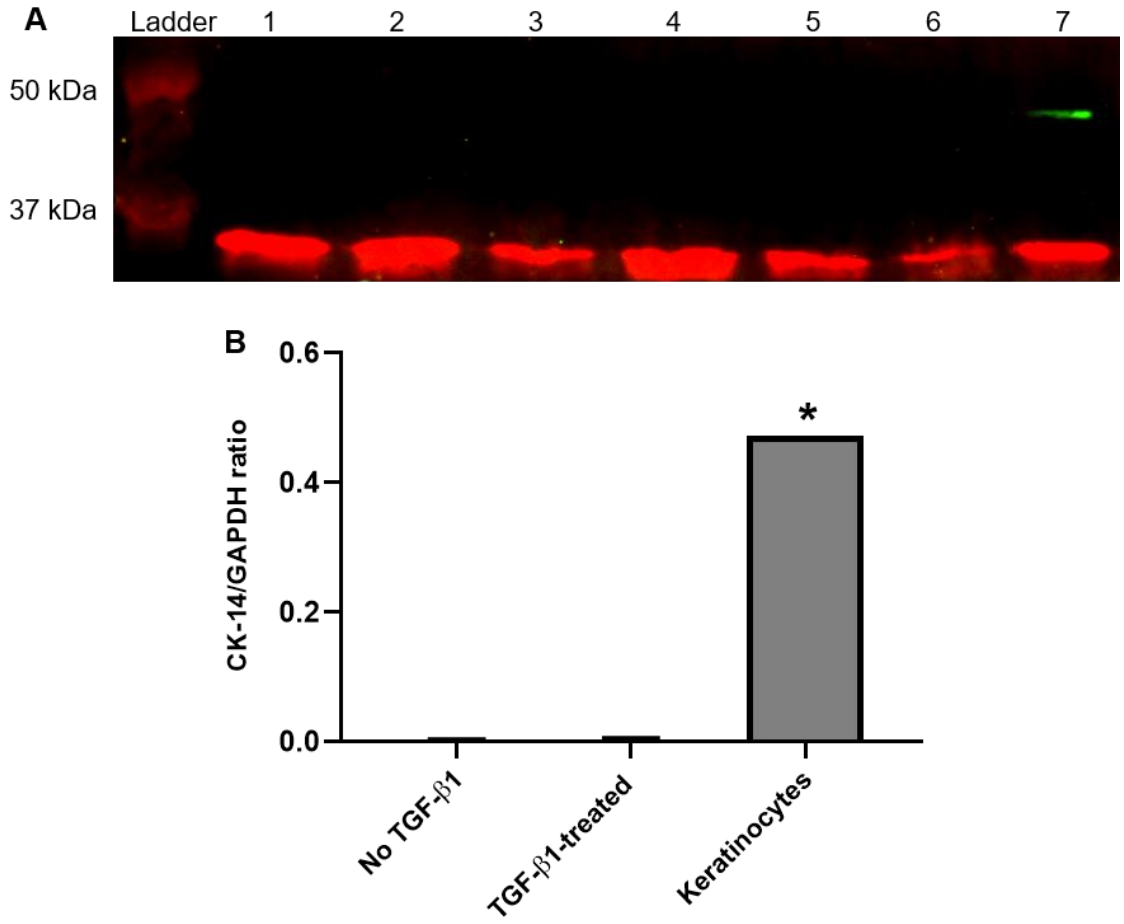

Figure 2-13: Western blot analysis of CK-14 expression in fibroblasts derived from burn scar tissue. A) Odyssey output image of desmin Western blot for protein lysates isolated from fibroblast treated with 10 ng/mL TGF-β1 for 72 h and untreated fibroblasts. 5 µl of a protein ladder was loaded, along with 20 µg of protein under reducing conditions. Lanes 1, 3 & 5: untreated fibroblasts. Lanes 2, 4 & 6: fibroblasts treated with 10 ng/mL TGF-β1. Lane 7: keratinocytes. The band seen at 50 kDa confirms CK-14 expression and bands at 37 kDa confirming GAPDH expression, used as a loading control. B) Quantification of Western blot analysis by measuring the CK-14/GAPDH ratio. Data points plotted as mean ± SEM, N=3 n=1 Statistical analysis using ANOVA multiple comparisons, *p < 0.05 vs untreated or TGF-β1-treated.

CK-14 expression was also quantified using the ICE method, where fibroblasts were seeded and treated with 10 ng/mL TGF-β1 for 72 h or left untreated, with keratinocytes seeded as a positive control. Cells were stained for CK-14 and cell number measured by staining with DRAQ5. Quantification of this data further confirmed that both untreated and TGF-β1-treated fibroblasts do not express CK-14, with no significant difference between the two treatment groups and the no primary control (Fig 2-14).

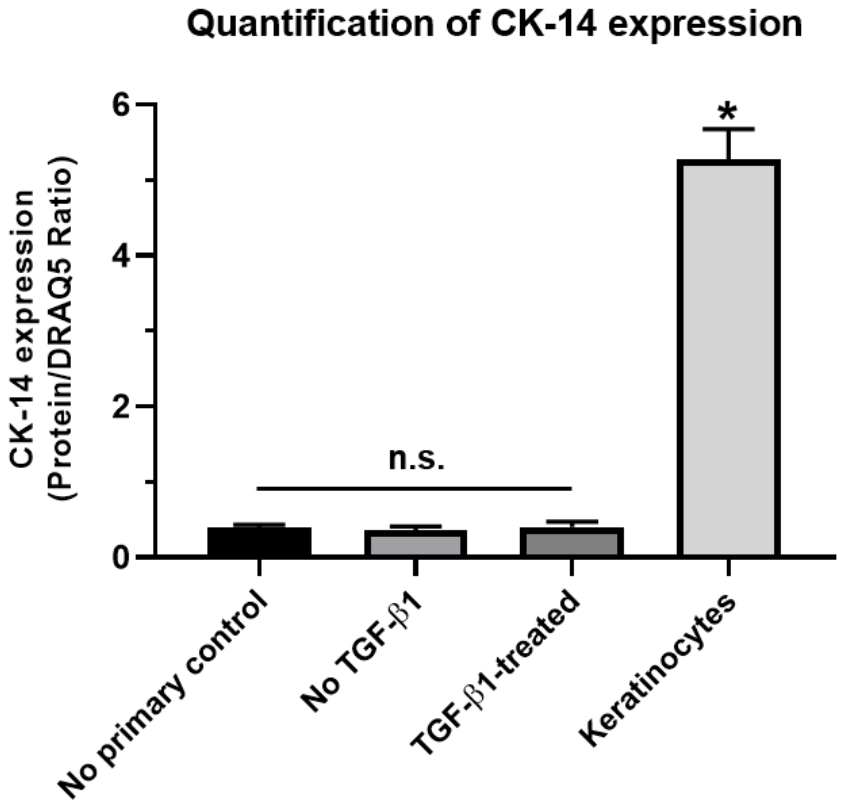

Figure 2-14: Quantification of CK-14 expression in untreated cells, cells treated with 10 ng/mL TGF-β1 for 72 h and keratinocytes, using the In-Cell ELISA method. Data points are plotted as the average ± SEM, where N=3, n=9. Statistical analysis using ANOVA multiple comparisons. *p<0.05 vs untreated or TGF-β1-treated.

2.3.5. Optimisation of the assay

The screening assay used in this project was previously developed using fibroblasts from the tunica albuginea of Peyronie's disease patients (Stebbeds, 2015; Ilg et al., 2019). Therefore, it was important to adapt and fully optimize the assay for the fibroblasts isolated from burn scars.

2.3.5.1. Effect of culture conditions on myofibroblast transformation

Previous studies have identified that the media conditions used when culturing fibroblasts, may induce myofibroblast transformation in untreated groups. Therefore, the optimal culture conditions that should be used for this assay were identified. Experiments were carried out to observe the effects of different concentrations of FCS and a Knock-Out Serum Replacement (KOSR) on myofibroblast transformation, and subsequent α-SMA expression. The conditions used for these experiments were 10% FCS media (the conditions used in the original protocol), serum free media, 1% FCS media and 10% KOSR media.

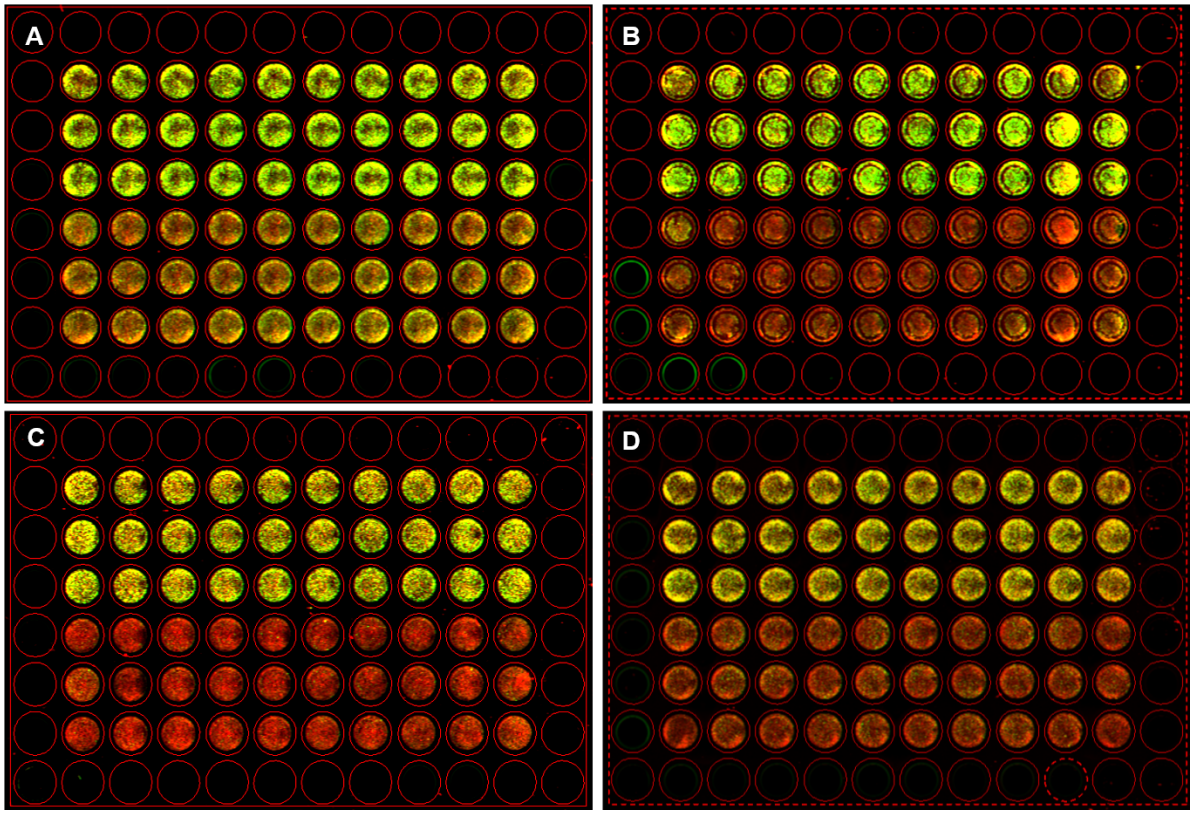

Figure 2-15: Optimisation of the In-Cell ELISA screening assay, measuring the effect of different cell culture conditions on myofibroblast transformation. Odyssey output images, where burn scar fibroblasts were cultured using A) 10% FCS media, B) serum free media, C) 1% FCS media and D) KOSR. In each plate, the top half was treated with 10 ng/mL TGF-β1 for 72 h and the bottom half was left untreated. Cell nuclei was stained red using DRAQ5 and α-SMA expression stained green.

When using 10% FCS media (Fig 2-15A), α-SMA expression can be seen in both treatment groups. When the data was quantified, lower expression of α-SMA expression was seen in the TGF-β1-treated cells, compared to the other culture conditions used (Fig 2-16). Fibroblasts were also incubated with serum free media (Fig 2-15B) and 1% FCS media (Fig 2-15C), which showed a reduction in background α-SMA expression in the untreated fibroblasts (Fig 2-16). 1% FCS media showed a significantly higher expression of α-SMA compared to the cells cultured with 10% FCS media. Fibroblasts cultured using serum-free media (Fig 2-15B) showed reduced cell viability compared to the other conditions.

KOSR is commonly used in stem cell culture as it is a defined, serum-free media component that can be used as a replacement for FCS. TGF-β1-treated fibroblasts showed a significant increase in α-SMA expression compared to the 10% FCS media (Fig 2-16). The untreated cells which were given blank 10% KOSR media show a similar background expression of α-SMA compared to the 10% FCS media (Fig 2-16). Further analysis between the 1% FCS and KOSR media identified a significant increase in α-SMA expression in the TGF-β1-treated group using 1% FCS media (Fig 2-16). It was therefore decided that 1% FCS media would be used in the screening assay to culture fibroblasts.

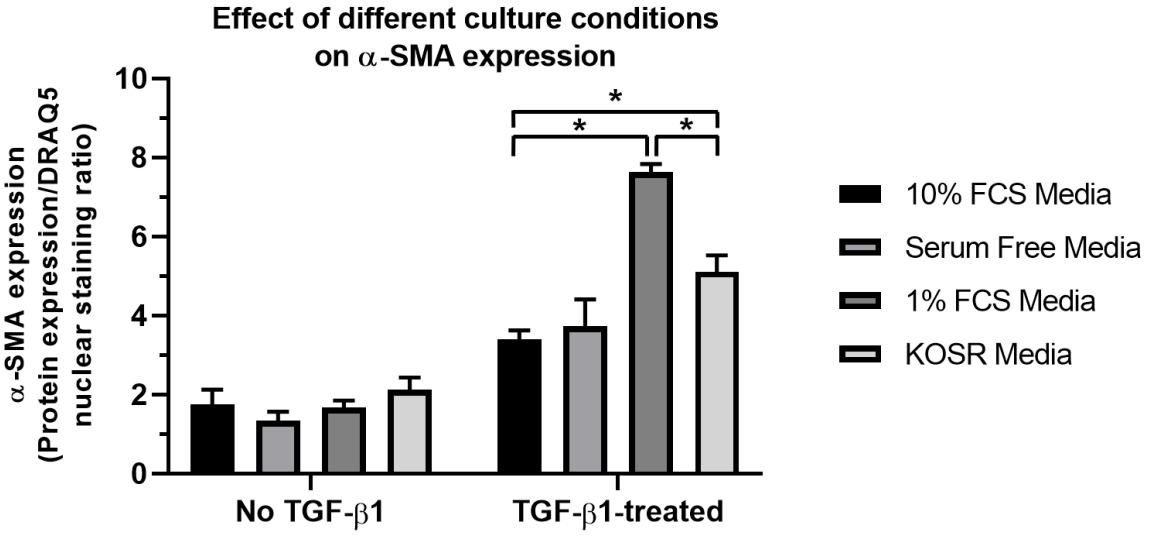

Figure 2-16: Optimisation of the In-Cell ELISA screening assay, measuring the effect of different cell culture conditions on α-SMA expression. Fibroblasts were either untreated or treated with 10 ng/mL TGF-β1, using one of the following media conditions: 10% FCS media, serum free media, 1% FCS media and KOSR media. Data presented as fluorescence intensity of α-SMA expression normalised to DRAQ5 nuclear staining, N=1, n=4. Statistical analysis carried out using ANOVA multiple comparisons. *p<0.05 vs 1% FCS or KOSR media.

2.3.5.2. Effect of TGF-β1 exposure time on myofibroblast transformation

The next step in the optimisation process was to identify how long the fibroblasts needed to be exposed to TGF-β1 to ensure complete transformation to myofibroblasts. The previously developed assay had identified 72 h as the optimal time for TGF-β1 exposure (Stebbeds, 2015), with 48 h also reported to be enough time to induce maximum myofibroblast transformation.

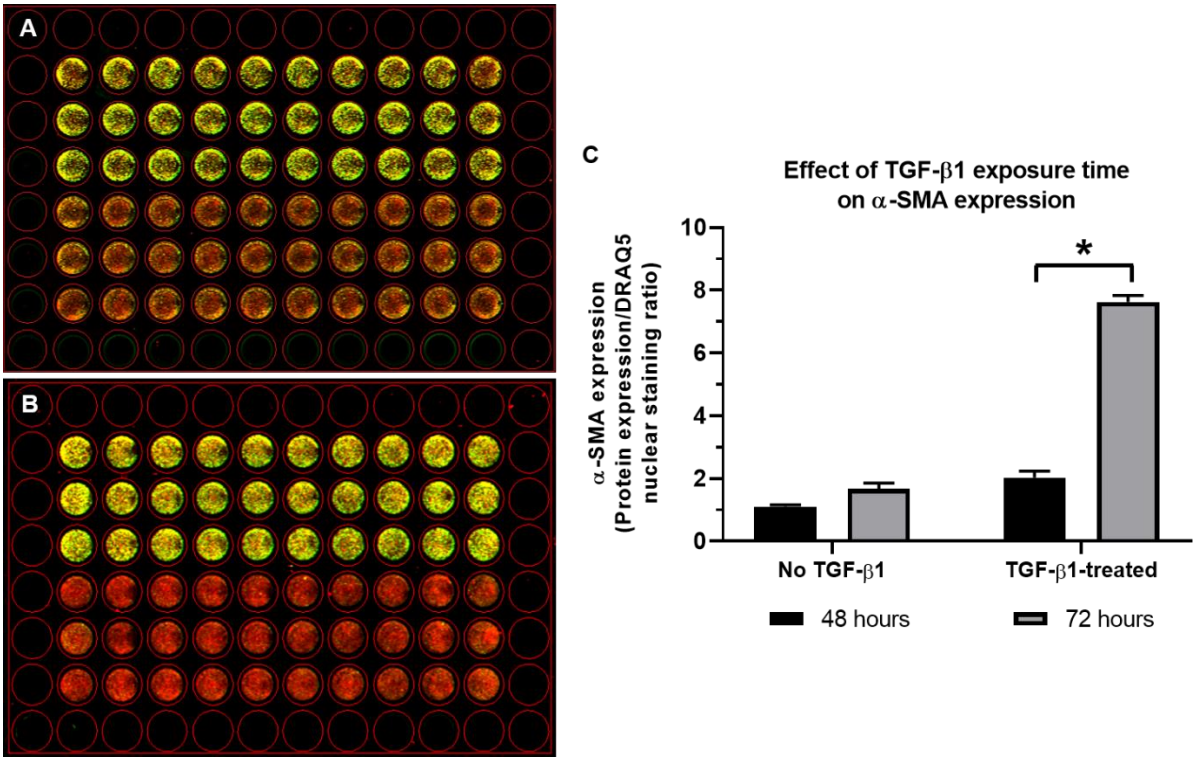

Figure 2-17: Optimisation of the In-Cell ELISA screening assay, measuring the effect of TGF-β1 exposure time on myofibroblast transformation. Odyssey output images where burn scar fibroblasts were either exposed to blank media or exposed to 10 ng/mL TGF-β1 for A) 48 h and B) 72 h. C) Quantification of scanned plates. Data is presented as fluorescence intensity of α-SMA expression normalised to DRAQ5 nuclear staining, N=1, n=4. Statistical analysis carried out using Student's t-test of unpaired means, *p<0.05.

Exposure to TGF-β1 after 48 h showed some transformation in the fibroblasts, however once the data was quantified the expression of α-SMA expression was significantly lower compared to the fibroblasts exposed to TGF-β1 for 72 h (Fig 2-17). Therefore, exposure to TGF-β1 for 72 h was used for all future experiments.

2.3.5.3. Cell density

The final step in the optimisation process was to identify the best cell density to be used for the assay, to ensure appropriate cell confluency in the 96-well plate format. For this, three different cell densities (3,000, 4,000 and 5,000 cells per well) were tested, with 5,000 cells being the cell density used in the original protocol.

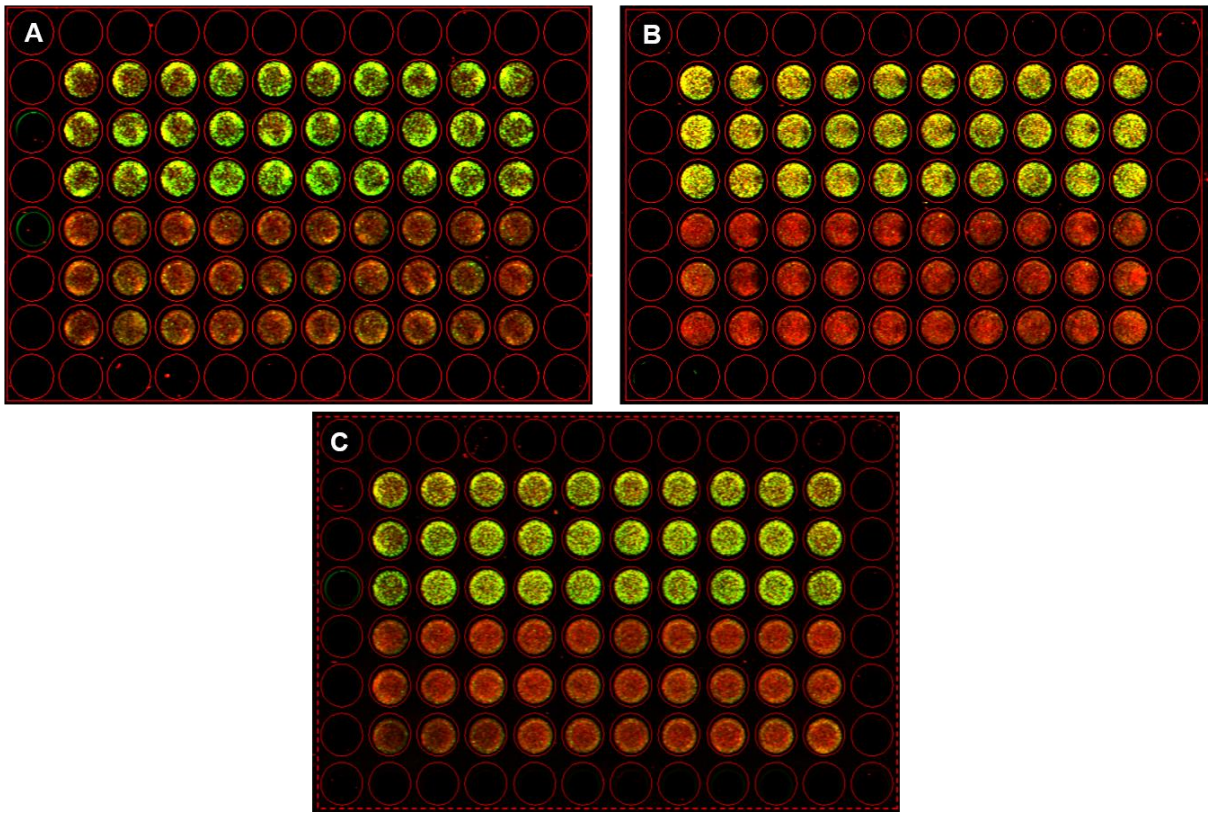

Figure 2-18: Optimisation of In-Cell ELISA screening assay, measuring the effect of cell density on TGF-β1 induced myofibroblast transformation. Odyssey output image, where burn scar fibroblasts were seeded at A) 3,000 cells per well, B) 4,000 cells per well and C) 5,000 cells per well. In each plate, the top half was treated with 10 ng/mL TGF-β1 for 72 h and the bottom half was left untreated. Cell nuclei were stained using DRAQ5 (red) and α-SMA expression stained in green.

The plates where cells were seeded at 4,000 and 5,000 cells per well (Fig 2-18C/E) show a more uniform expression of α-SMA in the TGF-β1-treated cells, compared to the 3,000 cell per well plate (Fig 2-18A). When this data was quantified, the 4,000 cells per well showed a significant increase in α-SMA expression compared to the 5,000 cells per well plate (Fig 2-19). Overall, it was decided that a density of 4,000 cells per well would be used for experiments going forward.

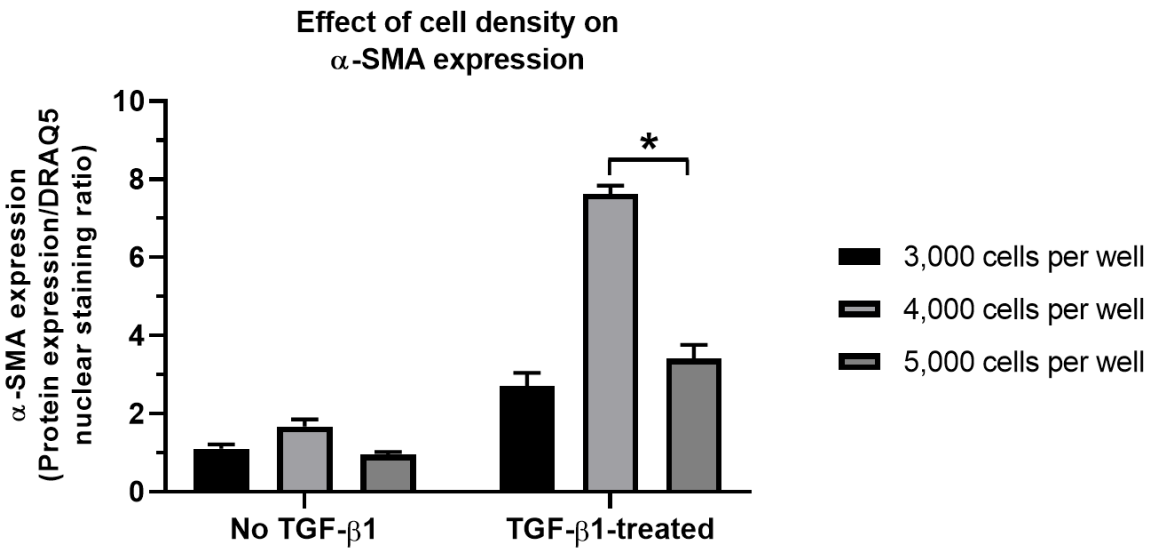

Figure 2-19: Optimisation of In-Cell ELISA screening assay, measuring the effect of cell density on α-SMA expression. Fibroblasts were seeded at 3,000, 4,000 and 5,000 cells per well, and either left untreated or treated with 10 ng/mL TGF-β1 for 72 h. Data presented as fluorescence intensity of α-SMA expression normalised to DRAQ5 nuclear staining, N=1, n=4. Statistical analysis carried out using ANOVA multiple comparisons. *p<0.05 vs 5,000 cells per well.

2.3.6. Assay validation

The next step in the assay development process was to validate the assay, to ensure its reproducibility and that it can be used for its required purpose – the detection of drugs that are able to prevent myofibroblast transformation.

2.3.6.1. Statistical validation

Statistical validation of the assay is key to confirm that the assay itself is robust and reproducible. To investigate this, fibroblasts were given either blank media or treated with 10 ng/mL TGF-β1, both manually and using an automated liquid handling system (Fig 2-20). To calculate the Z-factor (Z'), the α–SMA/DNA staining ratio was compared in the treated (positive control) and untreated cells (negative control).

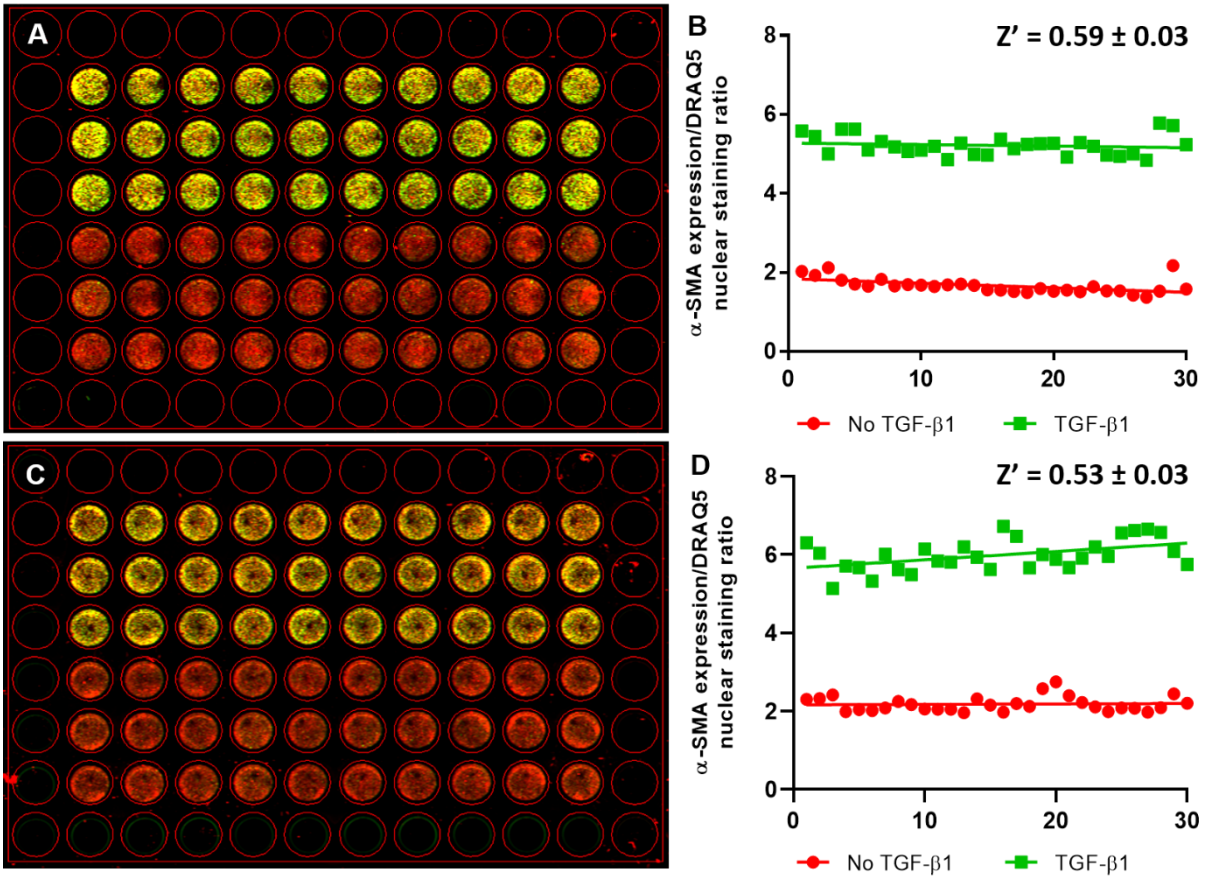

Figure 2-20: Statistical validation of ICE screening assay, measuring the effect of TGF-β1-induced myofibroblast transformation. A&C: Odyssey output image, in each plate, the top half was treated with 10 ng/mL TGF-β1 for 72 h and the bottom half was left untreated., A) using manual pipetting and C) using automated liquid handling. B&D: Quantification of the In-Cell ELISA, with resulting Z-factor from the assay for both B) manual pipetting and D) automated liquid handling. The positive controls are TGF-β1-treated cells, and the negative controls are untreated cells. Data is presented as mean ± SEM, N=1 n=4.

When carrying out the assay using manual pipetting, this generated a Z-factor of 0.59 ± 0.03, with a fold-change of 3.0 in α-SMA expression (Fig 2-20B). When carrying out the assay using the automated liquid handling system, this generated a Z-factor of 0.53 ± 0.03, with a fold-change of 2.5 in α-SMA expression (Fig 2-20D). Statistical analysis using a Student's t-test of unpaired means showed no statistical difference (p=0.25) between using manual and automated pipetting.

2.3.6.2. Identification of hit drugs

To confirm the ability of the assay to successfully detect drug-induced inhibition of myofibroblast transformation, the compound SB-505124 was used as a positive control. SB-505124 is a selective type I TGF-β1 receptor inhibitor which can prevent TGF-β1-induced myofibroblast transformation (Au and Ehrlich, 2010; Sapitro et al., 2010; DaCosta Byfield et al., 2004). A full concentration response curve for SB-505124 was generated (Fig 2-21), where the compound was applied in co-incubation with 10 ng/mL TGF-β1. Concentrations ranged from 0.03 µM – 100 µM. This generated an inverse sigmoid curve, with both upper and lower plateaus, where an IC_{50} of 1.22 ± 0.14 µM was calculated.

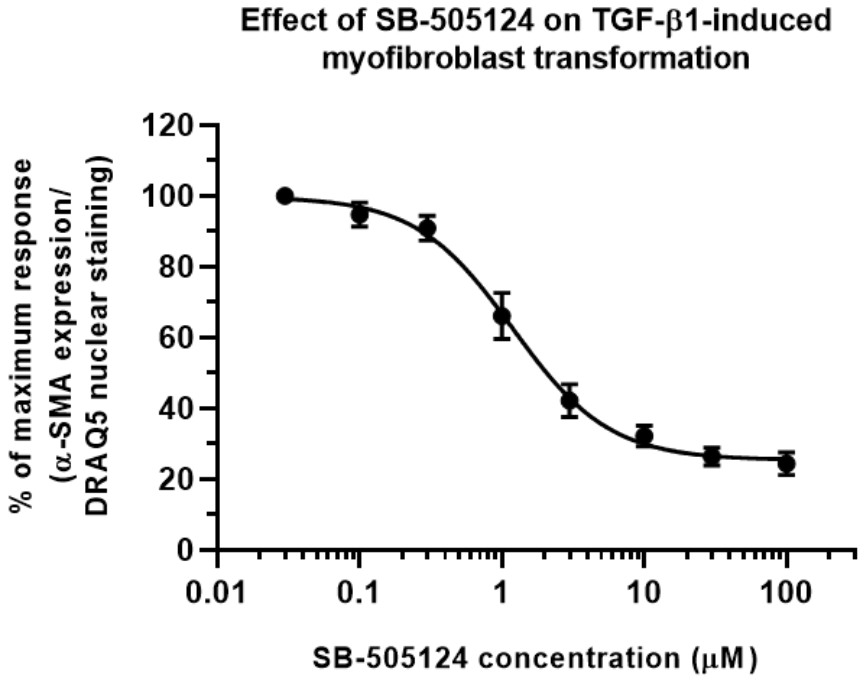

Figure 2-21: Effect of SB-505124 on TGF-β1-induced myofibroblast transformation. Burn scar fibroblasts were co-treated with 10 ng/mL TGF-β1 and a range of SB-505124 concentrations (0.03 µM – 100 µM) for 72 h, before measuring α-SMA expression using the In-Cell ELISA method. A full concentration response curve was generated. Data points are plotted as average ± SEM of the percentage of maximum response, N=3, n=9.

2.3.6.3. Effect of vehicle control

With many drugs in the drug library (SelleckChem, US) pre-dissolved in DMSO or PBS as a vehicle, it was important to check that the final vehicle concentration (<0.1%) during the drug screen would not have any major effect on myofibroblast transformation. A full concentration response curve for DMSO and PBS was constructed, where a range of concentrations (0.001% - 5%) were applied in co-incubation with 10 ng/mL TGF-β1. Figure 2-22 shows that DMSO concentrations of 1% and above affected myofibroblast transformation, as the α-SMA expression decreases beyond this point. Further, PBS was found to have no effect on α-SMA expression.

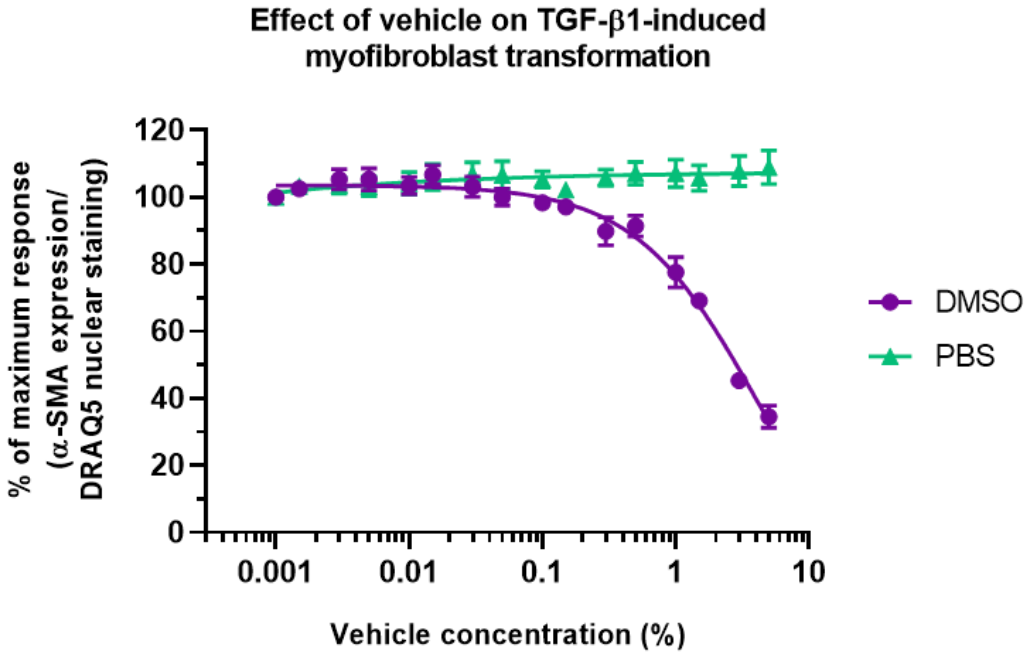

Figure 2-22: Effect of DMSO and PBS on TGF-β1-induced myofibroblast transformation. Burn scar fibroblasts were co-treated with 10 ng/mL TGF-β1 and a range of concentrations (0.001% – 5%) of DMSO and PBS for 72 h, before measuring α-SMA expression using the In-Cell ELISA method. Full concentration response curves were generated. Data points are plotted as average ± SEM of the percentage of maximum response, N=3, n=9.

2.4. Discussion

This section of the thesis set out to investigate whether a phenotypic, high-throughput screening assay could be optimised for use with primary human dermal fibroblasts, isolated from burn scars. The following objectives were set out to investigate the above research question:

1. Isolate and culture of primary human dermal fibroblasts, from the scars of burn patients.
2. Optimise and validate a cell-based, high-throughput phenotypic screening assay which measures myofibroblast transformation.

2.4.1. Tissue characterisation

It is well documented that following partial/full thickness injuries to the skin, the architecture changes due to the increased ECM deposition and cell infiltration (Gauglitz et al., 2011). To characterise the different tissue samples that were collected as part of this project, different histological techniques were carried out to visualise the tissue architecture and cell populations in these tissues. Skin from normal tissue and burn scars (<3-years and >10-years post-injury) were used for haematoxylin & eosin (H&E) staining, to identify the changes in tissue architecture throughout the wound healing and scarring process. H&E staining of all samples showed clear distinction between the epidermis and dermis, with a higher cell population noted in the epidermis as indicated by the denser haematoxylin staining (Fischer et al., 2008). Noticeable changes in the tissue architecture were identified between the different tissue types. H&E staining of normal skin tissue shows the presence of rete ridges across the epidermis, disorganised collagen structure throughout the dermis and blood vessels in the deep dermis. These observations are in line with previous histological analysis of the skin, with the normal skin tissue used in the assay exhibiting the expected architecture (Yu-Yun Lee et al., 2004). In the younger scar tissue complete flattening of the epidermis, attributed to the loss of rete ridges, can be noted along with the highly organised structure of collagen in the dermis, which lies in parallel to the epidermis. In comparison, the older scar tissue exhibits clear signs of remodelling and resembles the normal skin architecture more clearly, with the re-establishment of rete ridges in the epidermis and collagen bundles showing disorganised structure. The observations seen in the tissue architecture at different stages of the scarring process, have also been identified in previous work (Ehrlich et al., 1994). Vasculature cannot be found in either scar tissue sample, which is in line with the observations described in the literature for the younger scar tissue however, vasculature is usually present in mature hypertrophic scars (Connolly, Chaffins and Ozog, 2014; Huang and Ogawa, 2020). The lack of vasculature in the mature scar (Fig 3-1C) may be due to the plane of sectioning of the tissue and if the correct tissue orientation had been achieved, then vasculature may be

noticeable. Further staining and microscopy methods could also be considered to help distinguish the differences between normal skin and scar tissue architecture. For example, Picrosirius red staining could have been utilised to observe the composition of different collagen types in tissues, and Masson's trichrome staining could have been used to distinguish cells from the surrounding ECM (Limandjaja et al., 2021; Lattouf et al., 2014; Vogel et al., 2015). Further, scanning electron microscopy has been used successfully to help distinguish between different types of dermal scars (e.g. hypertrophic and keloid scars) (Harvey-Kemble, 1976).

IHC was carried out to identify if the desired cell population (fibroblasts) were present in the tissue samples, to allow isolation of the cells to take place. Due to the lack of a specific cell marker for fibroblasts, the normal skin tissue and burn scar tissue were stained using the mesenchymal marker vimentin, which is ubiquitously expressed by fibroblasts (McAnulty, 2007). The tissue sections were also stained for the basal keratinocyte marker CK-14, to distinguish between the epidermal and dermal layers. Abundant vimentin expression was observed in the dermis of both the normal skin and scar tissue, indicating the likely presence of fibroblasts in these tissue types. Further, a no primery control was carried out to ensure no unspecific binfing of the secondary antibody. Given that vimentin is a marker for many cells of a mesenchymal lineage, it is also possible that some of the expression seen in Figure 3-2 may be due to the presence of other mesenchymal cells (e.g. macrophages and endothelium) (Mor-Vaknin et al., 2003; Liu et al., 2010). However, given fibroblasts are considered to be the most abundant cell type in the dermis of normal skin and increased fibroblast populations have been identified in scar tissue, it is appropriate to assume that a large proportion of the vimentin expressed is due to the fibroblast population (Tracy, Minasian and Caterson, 2016; Sorg et al., 2017). Further, the increased vimentin expression observed in the burn scar tissue could be directly related to the increased fibroblast populations that have been seen in previous studies (Sorg et al., 2017).

2.4.3. Characterisation of primary human fibroblasts

The recruitment of patients to the study and collection of their tissue ran smoothly from May 2018 – March 2020, when tissue collection was no longer possible due to restrictions with the COVID-19 pandemic. Three different tissue types were collected - scar tissue and normal skin from burn patients, plus normal skin from patients undergoing DIEP reconstruction. Dermal fibroblasts were isolated from from each tissue type using an isolation protocol which was adapted from a number of previously established protocols with the main aim to create an environment that promotes fibroblast growth (Takashima, 1998; Keira et al., 2004; Villegas and McPhaul, 2005; Vangipuram et al., 2013). The most important factor in the isolation process was to ensure a 'pure' fibroblast culture, especially as the skin contains multiple cell

types and so, the risk of contamination was high (Kolarsick, Kolarsick and Goodwin, 2008). Firstly, as the epidermis is home to the majority of the other cell populations, the epidermis and dermis were mechanically separated before isolating fibroblasts using explant culture. Although tissue explantation for the isolation of cells does take a substantial amount of time to generate the required cell number, overall it provides a 'purer' fibroblast culture (Khan and Gasser, 2016). Enzymatic digestion of the tissue has also been suggested as another method for both the separation of the epidermis and dermis, and the isolation of fibroblasts, however there is evidence that shows an increase in the amount of cell debris in the culture causing infiltration of other cell types (Khan and Gasser, 2016). Although care was taken to ensure that the majority of the epidermis was removed from the tissue samples, to prevent potential keratinocyte contamination from any remaining epidermis, media using a high concentration of FCS (20%) was utilised. This was decided from the previous established protocols, but also from the knowledge that keratinocytes are usually cultured in serum-free media on their own or in 10% FCS media when grown on a fibroblast feeder layer (Rhelnwald and Green, 1975; Coolen et al., 2007). Further, the high FCS concentration has also been shown to promote fast fibroblast outgrowth (Vangipuram et al., 2013). To initially confirm fibroblast outgrowth, fibroblasts were characterised by their spindle-like morphology using light microscopy and any explants that showed suspected keratinocyte outgrowth (characterised by the presence of cobblestone like morphology) were not used (Häkkinen, Koivisto and Larjava, 2001; Ravikanth et al., 2011).

As the explant method was used, there was always a risk that fibroblasts would not grow out from the tissue. This may be due to issues with tissue viability, as the tissue begins to die the second it is removed from the patient or issues with the anchoring of the tissue to the 6-well plate. Due to this, fibroblasts did not grow out from the following patient tissues and were not able to be used for experiments in this thesis:

- DIEP normal tissue: patient number 1, 2, 5 and 7
- Burn scar tissue: patient number 2, 9 and 13
- Normal tissue from burn scar patients: patient number 12 and 13

Another cell culture issue that occurred during this project was spontaneous myofibroblast transformation of the cells in normal cell culture conditions. This issue and its solution will be explained in more depth in Chapter 2.4.4., however as a result of these issues it meant that all cell lines grown prior to July 2019 could not be used going forward as they were no longer a 'pure' fibroblast culture. All characterisation experiments that had been completed prior to July 2019 were redone using new patient tissue (burn patient number 10, 11 and 12; DIEP patient number 6) and cell culture method.

TGF-β1 is considered the master regulator of the fibrosis phenotype (Meng, Nikolic-Paterson and Lan, 2016). In particular, it has been shown to play a significant role in myofibroblast transformation, and the subsequent upregulation of the myofibroblast marker α-SMA (Meng, Nikolic-Paterson and Lan, 2016; Biernacka, Dobaczewski and Frangogiannis, 2011; Desmouliere et al., 1993). As part of the characterisation process, the isolated cells were exposed to TGF-β1 to see if myofibroblast transformation was induced. Cells isolated from the three previously described tissue types were exposed to a range of TGF-β1 concentrations (0.01 ng/mL – 30 ng/mL) for 72 h, before staining for α-SMA expression. In all three cell types, TGF-β1 exhibited a concentration-dependent effect on α-SMA expression with an EC_{50} of 0.5 ± 0.07 ng/mL for burn scar fibroblasts, 0.8 ± 0.14 ng/mL for normal fibroblasts from a burn patient and 0.68 ± 0.23 ng/mL for normal fibroblasts from a DIEP patient. Further, maximum expression of α-SMA can be seen at TGF-β1 concentrations >3 ng/mL in all three cells lines. ICC staining of these cells for α-SMA expression was also carried out, to observe any morphological change in the cells. Myofibroblasts have a distinct morphology compared to fibroblasts, where they are larger cells and appear more spread out (Ravikanth et al., 2011). Following exposure to 10 ng/mL TGF-β1 for 72 h, the isolated cells were shown to lose their typical spindle-shape morphology associated with fibroblasts and instead the cells were much larger with clear expression of filamentous α-SMA. As there was no significant difference in the TGF-β1 response between the cells isolated from each tissue type nor any difference in the cell morphology, it was decided that the burn scar fibroblasts would be utilised in future experiments. Evidence from the clinical team at St. Andrew's Centre for Plastic Surgery and Burns has suggested that if a clinical trial for any candidate drug were to go ahead, the drug would not be given until approximately 2 weeks following the initial injury. Therefore, at this time point it must be assumed that the wound would be in the active scarring phase and the cells present would have adopted the fibrotic phenotype (Li, Chen and Kirsner, 2007; Gauglitz et al., 2011). Therefore, this allowed for the generation of a more biologically relevant disease model.

To fully confirm fibroblast identity, cells isolated from burn scar tissue were stained for a panel of different markers due to the lack of specific fibroblast marker. Cells were either untreated or treated with TGF-β1 for 72 h and then stained for the desired proteins. Protein expression was first visualised using ICC, before fully quantifying protein expression using Western blot or ICE analysis. Vimentin is a type III intermediate filament protein, which is expressed by cells of a mesenchymal lineage, such as fibroblasts and myofibroblasts (Ivaska, 2011). ICC and ICE analysis confirmed ubiquitous vimentin expression in both the untreated and TGF-β1-treated cells, isolated from burn scar tissue. Further, quantification of vimentin expression using ICE showed no significant difference in the expression of vimentin between

the two treatment groups, confirming their mesenchymal lineage. The ICC data not only confirmed vimentin expression in these cells but allowed better visualisation of changes to the cell morphology, following TGF-β1 treatment. Untreated cells showed the expected fibroblast spindle shape morphology, with TGF-β1-treated cells appearing much larger and spread out, confirming the morphological changes observed in the α-SMA staining (Ravikanth et al., 2011).

Desmin is another type III filament protein, however it is only expressed by smooth muscle cells (Paulin and Li, 2004). Given that smooth muscle cells also express α-SMA, it was important to ensure that the α-SMA expression seen in the TGF-β1-treated cells was not due to smooth muscle cell contamination (Wang, Zohar and McCulloch, 2006). As part of these experiments, rhabdomyosarcoma cells were used as a positive control. ICC and ICE showed no expression in the untreated and TGF-β1-treated cells. When using ICE analysis, there was no significant difference between the untreated and TGF-β1 treated cells, and the no primary control, indicating that the minimal expression seen in the two treatment groups was just background fluorescence. Furthermore, desmin expression in the RD cells was significantly higher than the untreated and TGF-β1-treated cells, confirming that the isolated cells were not smooth muscle cells.

Despite several attempts, Western blot analysis for vimentin and desmin expression could not be carried out. In these attempts, GAPDH expression could be seen when the blots were scanned, however no expression of vimentin (in untreated and TGF-β1-treated fibroblasts) and no expression of desmin (in RD cells) could be detected. The Western blot is widely considered the ‘gold-standard’ for protein detection and quantification, however the process itself has many drawbacks and often requires significant amounts of troubleshooting (Moritz, 2020; Bass et al., 2017). In this instance, as GAPDH could be detected in both blots, it is likely that the antibodies used for vimentin and desmin were not suitable for use in Western blotting. As both antibodies had been validated by the supplier using knock-out models, this confirms their reliability and specificity for the desired target protein (Bordeaux et al., 2010; Zhong et al., 2018). Further, previous studies have also used these antibodies to measure vimentin and desmin expression in fibroblasts (Kin, Maziarz and Wagner, 2014; Sakamoto et al., 2020). This, along with the antibodies having been successfully used in other techniques (ICC and ICE) to detect vimentin and desmin expression, confirms the specificity of these antibodies.

Although confirmation of vimentin expression and absence of desmin expression is enough to confirm fibroblast identity, staining for a keratinocyte marker was also carried out to ensure that no epidermal cells were present in the fibroblast cultures. Cytokeratin-14 (CK-14) is a type II keratin, intermediate filament protein that is expressed by basal keratinocytes (Yang et al.,

2016). For these experiments, a commercial primary human keratinocyte cell line was used as a positive control. Untreated and TGF-β1-treated cells showed no CK-14 expression, in all three techniques. ICC allowed for visualisation of the keratinocyte morphology, showing their distinct cobblestone morphology. When using ICE analysis, there was no significant difference between the untreated and TGF-β1-treated cells, and the no primary control, indicating that the minimal expression seen in the two treatment groups was just background fluorescence. Furthermore, CK-14 expression in the keratinocytes was significantly higher than the untreated and TGF-β1-treated cells, confirming no keratinocyte contamination of the fibroblast cultures. Other keratinocyte markers such as a pan-cytokeratin antibody could have been utilised, however as basal keratinocytes are found in the epidermal layer adjacent to the dermis and are reported to have increased motility (Häkkinen, Koivisto and Larjava, 2001; Yang et al., 2016). Therefore, basal keratinocytes were more likely to contaminate the fibroblast culture.

With the isolated cells shown to be vimentin positive, desmin negative and CK-14 negative, their fibroblast identity could be confirmed. Furthermore, following treatment with TGF-β1, α-SMA expression confirms the transformation of fibroblasts to myofibroblasts.

2.4.4. Development of a phenotypic, high-throughput screening assay

With only two FDA-approved drugs currently available for the treatment of fibrosis (nintedanib and pirfenidone), a single-target approach for identifying novel therapeutics for fibrosis is not working. This can be partially explained by the multifactorial nature of fibrosis, with a multitude of underlying cellular and molecular mechanisms driving its progression (Eming, Martin and Tomic-Canic, 2014; Wynn and Ramalingam, 2013). In recent years, the target-based approach to drug discovery has come under scrutiny for delivering fewer first-in class-drugs, compared to phenotypic screening (Swinney and Anthony, 2011). Therefore, it is unsurprising that there has been a re-emergence in the use of phenotypic drug screening for identifying new medicines to treat fibrotic conditions (Nanthakumar et al., 2015). For an *in vitro* phenotypic screening assay to be deemed suitable for drug discovery, it typically needs to consider and meet a set of criteria (Vincent et al., 2015). These criteria confirm that the developed assay is a biologically relevant model of the disease, with the criteria that the designed assay met described below:

1. Utilise cells that have a clear link to the disease (e.g. using primary cells or stem cells).
2. Any stimulus used has been identified as an intrinsic disease stimulus or a physiologically relevant stimulus.
3. Phenotypic changes are measured using a functional disease manifestation or biomarker.

The screening assay that was designed for this project, met the above criteria. Primary human dermal fibroblasts from burn scars were used, TGF-β1 was used to induce myofibroblast transformation and α-SMA expression was measured. The assay itself was adapted from a high-throughput screening assay that was developed by previous members of the laboratory, for identifying novel therapeutics for the treatment of Peyronie's disease (PD) (Stebbeds, 2015; Mateus, 2016; Ilg et al., 2019). This utilised the ICE method, to investigate the effect of approved drugs on TGF-β1-induced myofibroblast transformation in fibroblasts isolated from the tunica albuginea. To ensure that the assay protocol was able to elicit the best response from the burn scar fibroblasts, optimisation of the assay protocol was carried out.

Initial experiments using the original protocol used in PD cells showed high levels of background α-SMA expression in the untreated fibroblasts. This also coincided with issues experienced in normal cell culture of the fibroblasts, whereby the cells were spontaneously transforming whilst in culture. Following an extensive review of the literature, it became evident that the FCS concentration in the media may be having an effect. FCS is a non-defined media component, containing several different growth factors required for the growth of cells *in vitro* (Shah, 1999). A study carried out by Siani et al., measured TGF-β1 levels in the FCS from three different manufacturers. The results showed varying concentrations of TGF-β1 in the FCS, ranging from 0.66 ng/mL – 3.48 ng/mL (Siani et al., 2015). Further, the cells that had been cultured with the FCS that had higher basal levels of TGF-β1 showed significantly lower α-SMA expression when exogenous TGF-β1 was added (2-fold increase vs. 7-fold increase in serum free conditions) (Siani et al., 2015). This highlighted a link between the spontaneous transformation seen in the burn scar fibroblasts and the cell culture conditions. To overcome this issue in general cell culture, 4 ng/mL of basic human fibroblast growth factor (bHFGF) was added to the culture media. bHFGF has been previously identified as a natural inhibitor of TGF-β1 signaling and is often used in cell culture to support fibroblast growth (Shimbori et al., 2016). As TGF-β1 was used to induce myofibroblast transformation in the screening assay, all bHFGF had to be removed prior to this. bHFGF has a half-life of 6.3 hours (Ding and Peterson, 2021), and so, given that fresh doses of bHFGF would be given no later than the day prior to seeding, it is believed that the fibroblasts would have metabolized the majority of bHFGF in that time. Further, the fibroblasts were extensively washed with PBS and serum starved for 30 min before trypsinization, a process which allows the cells to synchronise to the same stage in the cell cycle (Chen et al., 2012; Gilroy, Saunders and Wu, 2001).

To combat the FCS issue in the screening assay, the first stage of assay optimisation was to identify the optimal concentration of FCS to be used in the culture media. The aim of this optimisation was to identify the concentration of FCS that would maintain good cell viability and cell confluency, whilst allowing for a high fold change in α-SMA expression between the

untreated and TGF-β1-treated cells. For this, a series of experiments were carried out whereby burn scar fibroblasts were seeded into a 96-well plate, with half the plate (30 wells) treated with 10 ng/mL TGF-β1 and the other half (30 wells) left untreated, and then stained for α-SMA expression 72 h later. The media used in these experiments were serum free media, 1% FCS media and 10% FCS media (used as a control). In addition to testing the different concentrations of FCS, a serum replacement was also tested. KOSR is typically used in stem cell research, as it is a fully defined serum alternative, allowing the researcher to fully control what components are added into their culture media (Zhang et al., 2016b). For this purpose, the fibroblasts were cultured in media containing 10% KOSR.

The results of these experiments confirmed that when 10% FCS media was used the α-SMA/DRAQ5 ratio in the TGF-β1-treated cells was significantly lower compared to the other culture conditions tested. Only a 2-fold change in α-SMA expression between the untreated and TGF-β1-treated fibroblasts was observed when using 10% FCS media. When using serum free media, there was no significant difference in the α-SMA/DRAQ5 ratio of the TGF-β1-treated cells compared to the 10% FCS media. As the α-SMA/DRAQ5 ratio was slightly lower in the untreated fibroblasts, this resulted in a 4-fold change in α-SMA expression between the untreated and TGF-β1-treated fibroblasts when using serum free media. Despite this, the fibroblasts cultured using serum free media showed decreased cell viability after the 72 h incubation period, which is in line with observations made in the literature (Chen et al., 2012). When 1% FCS media was used to culture the fibroblasts, there was a significant increase in the α-SMA/DRAQ5 ratio in the TGF-β1-treated cells compared to the 10% FCS media control. Furthermore, this resulted in a much higher fold change between the untreated and TGF-β1-treated cells (5-fold change using 1% FCS media vs. 2-fold change using 10% FCS media). The KOSR media also showed a significantly higher α-SMA/DRAQ5 ratio in the TGF-β1-treated fibroblasts, compared to the 10% FCS media, with a 3-fold change in α-SMA expression between the untreated and TGF-β1-treated fibroblasts. When the 1% FCS media and KOSR media were compared, the 1% FCS media showed a significantly higher α-SMA/DRAQ5 ratio in the TGF-β1-treated cells compared to the KOSR media. Despite no significant difference between the background expression of α-SMA expression in the untreated fibroblasts of both groups, the fibrobasts cultured with KOSR exhibited a slightly higher α-SMA/DRAQ5 ratio in the untreated fibroblasts, compared to those cultured in 1% FCS. Furthermore, culturing the fibroblasts with 1% FCS media exhibited a higher fold change in α-SMA expression between the two treatment groups (3-fold change using KOSR media vs. 5-fold change using 1% FCS media). For these reasons, 1% FCS media was used for the culturing of fibroblasts during the high-throughput screening assay.

To ensure the appropriate cell density had been chosen for the screening assay, fibroblasts were seeded at 3,000, 4,000 and 5,000 cells per well to observe the effect on α-SMA expression and response to TGF-β1. When cells were seeded at 5,000 cells per well (density used in original PD protocol), the fibroblasts showed a good response to TGF-β1, with a 4-fold change in α-SMA expression between the untreated and TGF-β1-treated cells. When 3,000 cells per well were seeded, there was no significant difference between the α-SMA/DRAQ5 ratio in the TGF-β1-treated cells and showed a similar fold-change in α-SMA expression (3-fold change). However, what is noticeable in the image of the scanned plate is that α-SMA expression across the TGF-β1-treated cells is not uniform, which could be explained due to reduced cell confluency. Finally, when cells were seeded at 4,000 cells per well there was a significant increase in the α-SMA/DRAQ5 ratio in the TGF-β1-treated cells, compared to the 5,000 cell per well plates. Both 4,000 and 5,000 cells per well resulted in the same fold change in α-SMA expression between the untreated and TGF-β1-treated cells. Therefore 4,000 cells per well was chosen for the protocol due to the significant increase in α-SMA expression in response to TGF-β1.

The final step in the optimisation process was to ensure that the 72 h exposure time to TGF-β1 was the appropriate amount of time to induce maximum α-SMA expression. Although 72 h had been used for the previous experiments, and shown to induce maximum α-SMA expression, previous studies had shown that 48 h was sufficient to induce maximum expression (Sieber et al., 2018a). Following exposure to TGF-β1 for 48 h, there was a significant decrease in the α-SMA/DRAQ5 ratio in the TGF-β1-treated cells compared to the 72 h exposure time. Furthermore, the cells that had been exposed to TGF-β1 for 48 h exhibited a 2-fold change in α-SMA expression compared to the 72 h exposure time, which exhibited a 4-fold change in α-SMA expression between the untreated and TGF-β1-treated fibroblasts. Therefore, this data confirmed that 72 h was the appropriate exposure time to ensure maximum α-SMA expression in these cells.

Following optimisation of the assay, validation was the next necessary step to ensure that the assay was robust and reliable for the application of high-throughput screening. Many factors can affect the reliability and reproducibility of high-throughput/high-content assays, ranging from human error (e.g. variability between manual pipetting and automated liquid handling) to different batches of reagents. This variability is known as the spatial uniformity across the plate, which shows if there is drift or an edge effect (Iversen et al., 2012). Drift across the plate refers to the signal uniformity across the plate, identifying if there is a higher signal from right to left, or from top to bottom (Iversen et al., 2012). To prevent drift from occurring, constant agitation of the reservoir and mixing of solutions before aliquoting into the 96-well plate was carried out. This ensured equal seeding of cells and equal distribution of TGF-β1 and drug

solutions. Edge effect is commonly seen in the outer wells of a multi-well plate, whereby a lower signal is seen in these wells (Iversen et al., 2012). To prevent edge effect from happening in this assay, the outer wells were not used, and PBS was placed in any unused wells.

The Z-factor analysis is used for the statistical validation of high-throughput screening assays, by confirming the assays reproducibility. The Z-factor equation measure the difference between the means and standard deviations of the negative and positive controls, with values below 0.5 indicating an assay with high variability and values above 0.5 indicating low variability/high reproducibility (Zhang, Chung and Oldenburg, 1999). For this, Z-factor analysis was used on experiments whereby the TGF-β1 treatment had been carried out manually and carried out by an automated liquid handling system. For the drug screening process, the Gilson PipetMAX would be utilised for the dilution of the 1,954 drugs and the subsequent transfer of these drugs onto the fibroblasts. It was therefore important to ensure that the PipetMAX did not affect the assay in anyway, and the assay would still be highly reproducible and robust when using automation. When using manual pipetting, a Z-factor of 0.59 ± 0.03 was achieved, whilst automated pipetting yielded a Z-factor of 0.53 ± 0.03. As both Z-factors were above 0.5, this indicates that the developed assay is both robust and highly reproducible and therefore can be used for high-throughput screening.

To ensure that inhibition of TGF-β1-induced myofibroblast transformation could be detected, a full concentration response curve for the compound SB-505124, a selective type I TGF-β1 receptor inhibitor, was generated. SB-505124 has been suggested as an effective compound for reducing the presence of myofibroblasts in rat open wound models, however failed to be translated to use *in vivo* due to being pharmacokinetically unstable in humans (Sapitro et al., 2010; Akhurst and Hata, 2012; Au and Ehrlich, 2010). SB-505124 was used at concentrations ranging from 0.03 μM – 100 μM and was used in co-incubation with 10 ng/mL TGF-β1. SB-505124 was shown to inhibit α-SMA expression in a concentration-dependent manner and an IC_{50} of 1.22 ± 0.14 μM could be calculated. Further, SB-505124 was shown to have maximum inhibition of α-SMA expression at ~75%. This data validates that the assay can reliably measure inhibition of TGF-β1-induced myofibroblast transformation.

Given that many of the drugs in the library would be pre-dissolved in a vehicle, concentration response curves for both DMSO and PBS were constructed to ensure that the final concentration would not influence α-SMA expression. Full concentration response curves for DMSO and PBS were constructed, with concentrations ranging from 0.001% - 5% in co-incubation with 10 ng/mL of TGF-β1. PBS was shown to have no effect on the α-SMA/DRAQ5 ratio in the fibroblasts, with α-SMA expression remaining at 100% for all

concentrations. The concentration response curve for DMSO showed that at concentrations above 1%, DMSO caused a reduction in the α-SMA/DRAQ5 ratio in fibroblasts, which is in line with observations made in the literature (Xu et al., 2013). This data confirmed that at higher concentrations of DMSO, there would be an effect on the results of the screening assay. Given that the final concentrations of DMSO and PBS that would be used in the screening assay would be ~0.1%, following the two-step dilution of the drug library, no vehicle effect should be seen.

Chapter 3: Screening of 1,954 approved drugs

3.1. Introduction

High-throughput screening remains a dominant approach to drug discovery and a well established process within the field, whereby large libraries of compounds of varying categories (e.g. small molecules, biologics) are tested to identify novel therapeutics. The basic premise of high-throughput screening is to test large numbers of compounds against a specific target known to the disease or a disease phenotype and see what compounds are able to affect this and elicit biological activity (Swinney, 2013). For the majority of high-throughput screens, pharmaceutical companies will screen novel compounds that have been designed specifically for the target in question. However, in recent years, especially in light of the COVID-19 pandemic, the sector has started moving towards repurposing already approved drugs for new indications (NHS England and Improvement et al., 2019; Safe and Timely Access to Medicines for Patients (STAMP) expert group, 2019; European Comission, European Medicines Agency and Heads of Medicines Agencies, 2021). As these drugs have already been approved for use in humans, the repurposing process allows for a significant reduction in the time (from decades to 12-18 months) and cost (50% reduction) associated with conventional drug discovery (Chong and Sullivan, 2007; Sultana et al., 2020).

The library used in this thesis was the Selleck Chemicals FDA-approved drug library of 1,954 drugs (at the time of purchase April 2019 – the library contains 3,008 drugs at the time of writing this thesis), which is one of the largest libraries of approved drugs available commercially. All drugs in the library have been approved by various regulatory authorities and have had their bioactivity and safety confirmed in clinical trials. The library has been used many times for various screening assays for many different diseases and disorders, with citations in over 420 publications. The drugs available in this library cover a wide range of different indications including drugs for cancer treament, cardiovascular and neurological diseases. Pirfenidone and nintedanib, the only drugs approved for the treatment of fibrotic diseases, are in the drug library, along with a number of emerging therapies for hypertrophic scars (e.g. 5-flurouracil and various corticosteroids).

Prior to the screening campaign being carried out in the burn scar fibroblasts, a similar screening campaign was carried out in fibroblasts from Peyronie's diease plaques (Cellek Lab, unpublished observations). The PD screen used the same drug library as above and found 27 hits in total (1.4% hit rate), suggesting that screening this library using burn scar fibroblasts would be feasible..

3.2. Materials and Methods

For the primary screening assay, fibroblasts were cultured and maintained as previously explained in Chapter 2.2.2. Fibroblasts from one patient cell line were utilised (cell line: L10FA1). Fibroblasts were seeded at a density of 4,000 cells per well into black optical 96-well plates (Nunc Fisher Scientific, UK), according to the layout in Figure 3-1. The plates were incubated overnight at 37°C and 5% CO_2 to allow cell adherence to the plates. A library of 1,954 approved drugs (Selleck Chemicals, US – cat no #L1300) was tested in the screening assay. The Gilson PIPETMAX® automated liquid handling system (PipetMAX; Gilson, UK) was utilised to ensure accurate dilution of the drugs and minimise human error. The following protocol which outlines the process of the drug dilutions and subsequent incubation of the drugs with the fibroblasts was written and programmed for the PipetMAX, by the author in collaboration with the Gilson team.

Initially, the stock plates were defrosted at room temperature on an orbital shaker and the DMEM conditions listed in Table 3-1 were prepared. Following this, the PipetMAX platform was set up and the different DMEM conditions were dispensed into a 12-column reservoir (Aglient Technologies, UK). For preparation of the stamp plate, 247.5 µl of blank serum free DMEM was aliquoted into each well of a clear 96-well plate, according to the layout in Figure 2-2. The drugs underwent an initial 1:100 dilution (10 mM to 100 µM), by mixing 2.5 µl of the drug stock with the blank media in the stamp plate. When not being used, the stamp plates were sealed with an aluminium microplate seal (Corning, US) and stored at -80°C.

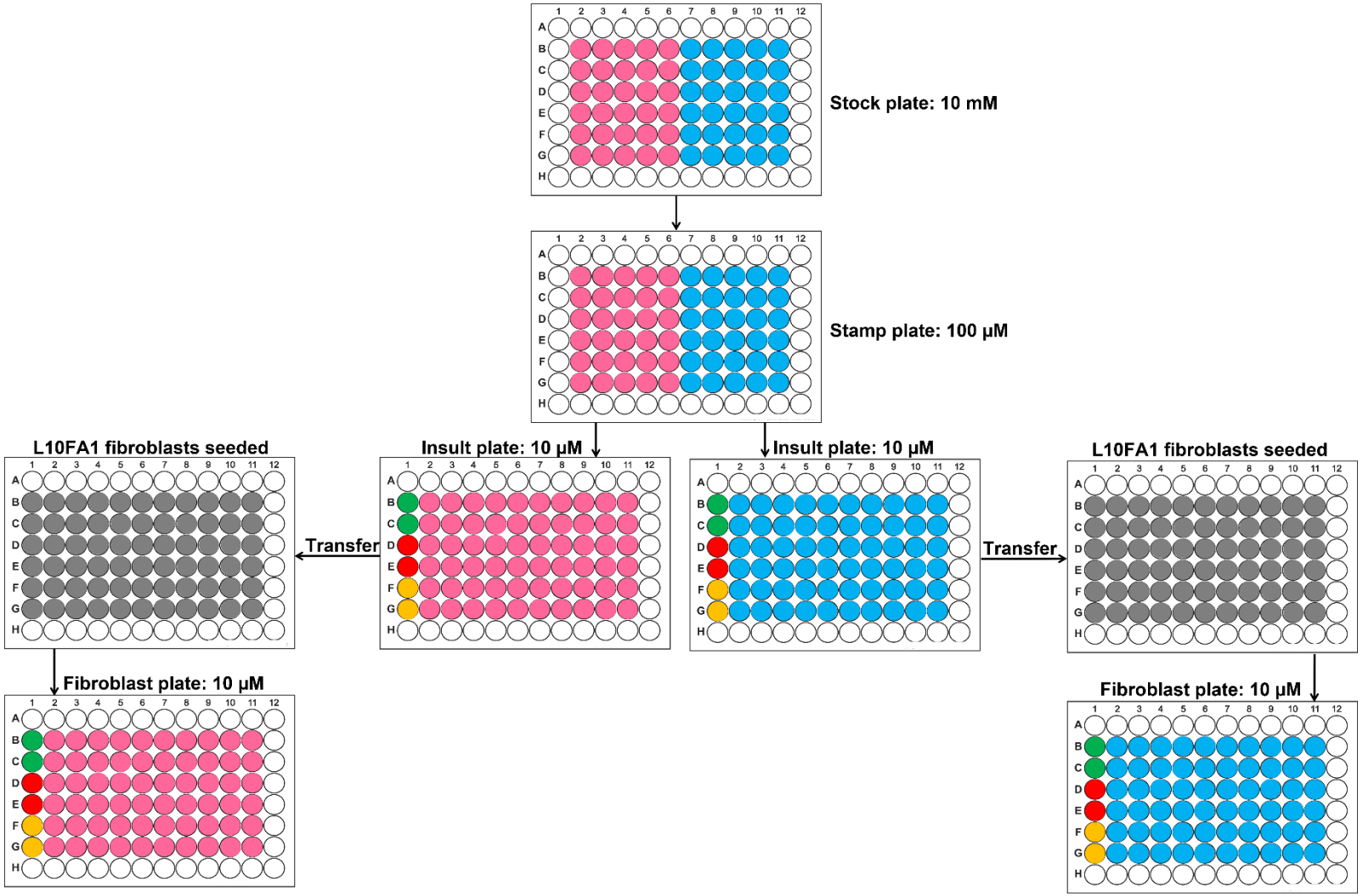

Figure 3-1: Schematic of the screening assay protocol. The drug library was first diluted from 10 mM to 100 µM in serum free media, before being diluted again to a working concentration of 10 µM in TGF-β1 media. Burn scar fibroblasts (cell line L10FA1) were seeded onto plates prior to incubation with the drugs. Each drug was tested in duplicate (pink = drugs 1 – 30, blue = drugs 31 – 60). Three sets of controls (also tested in duplicate) were included in each plate – blank DMEM (green), 10 ng/mL TGF-β1 (red) and 10 ng/mL TGF-β1 + 1 µM SB-505124 (orange).

The next step was the preparation of the stimulation plates, where the drugs underwent a further 1:10 dilution to a working concentration of 10 µM. For this, 225 µl of TGF-β1 media was aliquoted into each well of a clear 96-well plate (pink and blue wells, stimulation plate; Fig 3-1), before mixing 25 µl of drug (100 µM from stamp plate) into the corresponding well, in duplicate. This dilution step also diluted the concentration of TGF-β1 from 11.1 ng/mL to the working concentration of 10 ng/mL. At this point, the controls for the screening assay are also added to the stimulation plates. 250 µl of blank DMEM (green wells), TGF-β1 media (red wells) and TGF-β1 + SB-505124 media (orange wells) were added in duplicate to the plates, for the controls. The last step of the process was the transfer of the drug solutions to the fibroblast plates. The plates were removed from the incubator and the old media discarded, before transferring 200 µl of media from each well of the stimulation plate to the corresponding well on the fibroblast plate. The plates were returned to the incubator and left for 72 h at 37°C and 5% CO_2. Following the 72 h incubation period, the plates were stained for α-SMA expression using the ICE method (outlined in Chapter 2.2.6.).

Table 3-1: DMEM conditions used during the drug screen.

Stage of drug screen (as stated in Fig. 2-2)	DMEM conditions	Concentration of compounds
Stamp plate	Serum free DMEM	-
Stimulation plate	1% FCS DMEM	-
	1% FCS DMEM + TGF-β1	11.1 ng/mL
	1% FCS DMEM + TGF-β1+ SB-505124	10 ng/mL + 1 µM

3.2.1. Identification of candidate drugs

To assess whether the drugs in the approved drug library were able to prevent TGF-β1-induced α-SMA expression, the percentage inhibition of each drug was calculated. The ratio of α-SMA expression to cell number was generated (see Chapter 2.2.8. for eequation) and the duplicate ratios for each drug averaged, before calculating the percentage inhibition of each drug, using the equation below:

$$\frac{(Positive\ control - Sample)}{(Positive\ control - Negative\ control)}\ x\ 100$$

Whereby the positive control refers to fibroblasts treated with TGF-β1 only media, and the negative control refers to fibroblasts given blank media. Hits were identified as showing >80% inhibition of α-SMA expression, whilst maintaining >80% cell viability.

Figure 3-2 shows the process used to identify the candidate drugs, once their percentage inhibition and effect on cell viability was determined. Candidate drugs were identified as those with a desirable safety profile (limited adverse effects and low incidence) and those that did cause any severe cutaneous reactions. This left the hits with the most desirable safety profile, and so those that had been formulated for topical application were identified. Finally, literature and patent searches were carried out to identify if the anti-fibrotic effect of any of the hits had been reported previously.

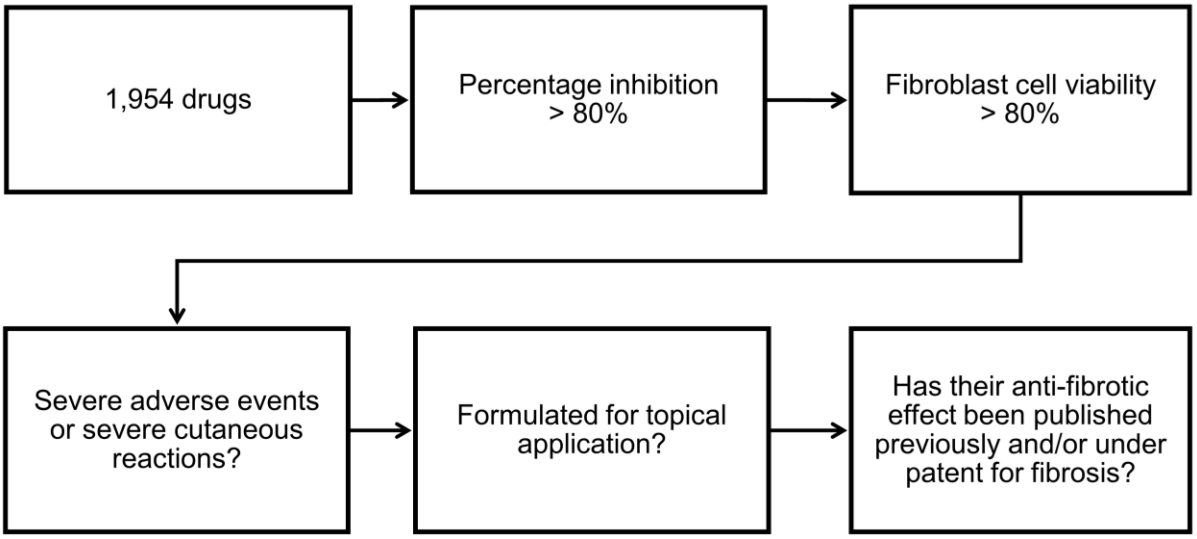

Figure 3-2: Criteria used to identify candidate drugs following hit identification. Those hits with a number of significant adverse effects were first excluded, along with any hits that caused severe cutaneous reactions. This left hits with a desirable safety profile, of which, those that have been previously formulated for topical application were identified. Finally, a literature/patent search was carried out to see if any of the remaining hits have had their anti-fibrotic effect reported, or if they were under patent for hypertrophic scarring or fibrosis.

3.3. Results

For the screening campaign, fibroblasts were seeded into 96-well plates following the layout as described previously (Fig 3-1). The following day, the drugs underwent a two-step dilution, from a stock concentration of 10 mM to a working concentration of 10 µM. The drugs were applied to the fibroblasts, in combination with 10 ng/mL TGF-β1, with each drug tested in duplicate. Control conditions included untreated fibroblasts, fibroblasts treated with 10 ng/mL TGF-β1, and fibroblasts treated with 10 ng/mL TGF-β1 and 1 µM SB-505124. Expression of α-SMA was measured and then normalised to the DRAQ5 nuclear staining, before calculating the percentage inhibition of each drug.

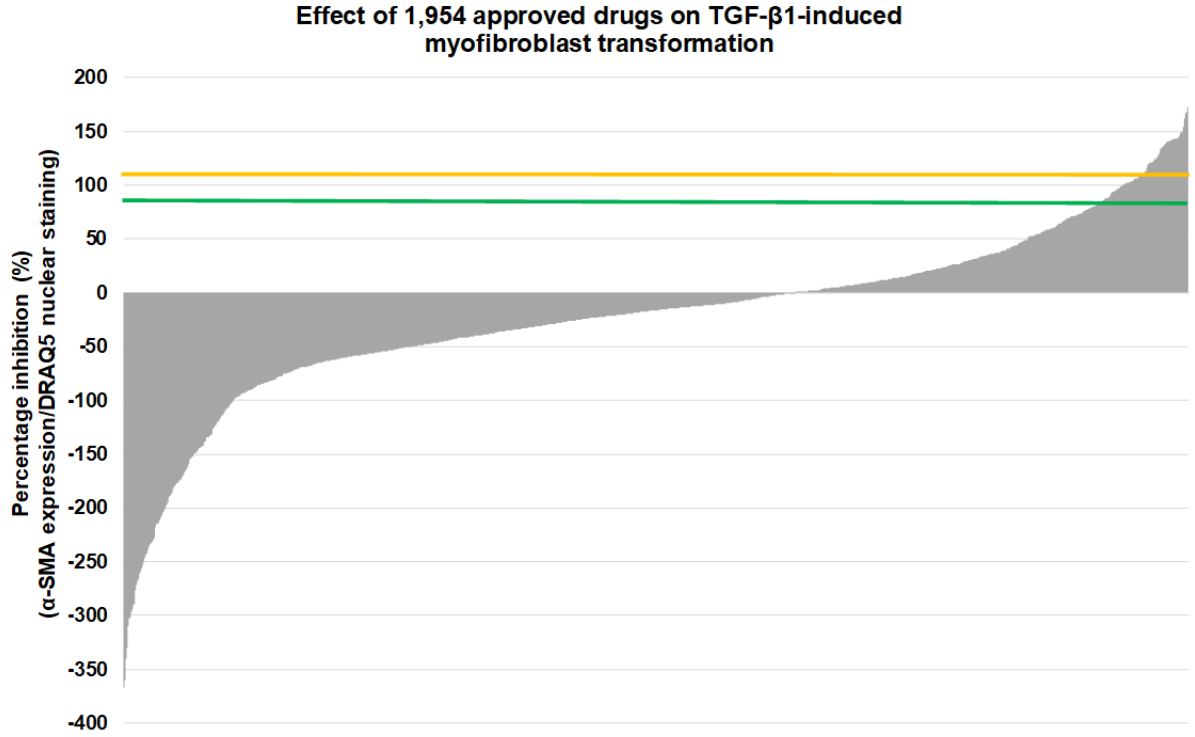

Figure 3-3: Effect of 1,954 approved drugs at 10 µM on TGF-β1-induced myofibroblast transformation. Percentage inhibition of each drug was calculated. An increase in α-SMA expression (as shown by negative inhibition in the graph) indicates that some of the drugs can potentially increase myofibroblast transformation. The green line denotes drugs with >80% inhibition of α-SMA expression, a criterion used to define a hit. The amber line denotes the average percentage inhibition exhibited by the TGF-β1 + 1 µM SB-505124 positive control.

Figure 3-3 represents the inhibitory effect of all 1,954 drugs in the library on TGF-β1-induced myofibroblast transformation. A 'hit' was defined as having >80% percentage inhibition, whilst maintaining >80% cell viability. Furthermore, >80% cell viability ensured that the effect seen was due to inhibition of myofibroblast transformation and not due to cytotoxicity. In total, 90 drugs were identified as hits from the screening assay. Table 3-2 lists all 90 hits, along with the current indication they are approved for, their mechanism of action, target receptor affinity, any severe adverse events, percentage inhibition of α-SMA expression and cell viability. For the target receptor affinity of each drug, this information was obtained via the IUPHAR/BPS

‘Guide to Pharmacology’ database for which the references from the database are given in the table. For the severe adverse events of each drug, this information was obtained via the British National Formulary (BNF) website. In the instance where the drug was not present on the BNF website, references have been provided for either clinical trial data or other health organisation websites.

Table 3-2: List of 90 hits from the primary screening assay. Hits are listed alphabetically, with their indication, mechanism of action, target receptor affinity and severe adverse events. The percentage inhibition and cell viability is also listed.

Drug name	Indication category	Mechanism of action	Target receptor affinity	Severe adverse events	Percentage inhibition	Fibroblast viability
Abemaciclib	Cancer	Cell cycle inhibitor for CDK4/6	IC_{50} of 2 nM for CDK4 and 10 nM for CDK6 (Gelbert et al., 2014)	Haematological disorders (e.g. neutropenia and thrombocytopenia), embolism/thrombosis andskin reactions	93%	133%
Abexinostat	Cancer	Pan-HDAC inhibitor	IC_{50} of 7 nM for HDAC1 and 8.2 nM for HDAC3 (Buggy et al., 2006)	Thrombocytopenia, neutropenia and anaemia (Ribrag et al., 2017)	100%	91%
Afatinib	Cancer	EGFR/Erb-β inhibitor	IC_{50} of 0.5 - 11 nM for EGFR and 14 nM for Erb-β2 (Li et al., 2008; Davis et al., 2011)	Severe cutaneous reactions, interstitial lung disease and pancreatitis	99%	95%
Alimemazine tartrate	Anti-allergy	H1-receptor antagonist	K_i of 0.72 nM in bovine brain preparations (Kubo et al., 1987)	N/A	84%	106%
Amlodipine	Cardiovascular	Calcium channel blocker	IC_{50} of 9.3 nM for $Ca_v1.2$ and 60.1 nM for $Ca_v1.3$ (Hughes and Wijetunge, 1993; Sinnegger-Brauns et al., 2009)	Cardiac disorders (e.g. palpitations and tachycardia)	91%	93%

Amlodipine besylate	Cardiovascular	Calcium channel blocker	IC_{50} of 9.3 nM for $Ca_v1.2$ and 60.1 nM for $Ca_v1.3$ (Sinnegger-Brauns et al., 2009; Hughes and Wijetunge, 1993)	Cardiac disorders (e.g. palpitations and tachycardia)	85%	97%
Amonafide	Cancer	Topoisomerase II inhibitor	IC_{50} of 2.8 - 9.24 µM (Zhu et al., 2007)	Granulocytopenia, neurotoxicity and orthostatic hypotension (Kornek et al., 1994)	93%	88%
Atorvastatin calcium	Cardiovascular	3-hydroxy-3-methyl-glutaryl-coenzyme A reductase (HMG-CoA-reductase) inhibitor	IC_{50} of 8 nM (Istvan and Deisenhofer, 2001)	Severe cutaneous reactions, peripheral oedema, hypo/hyperglycaemia	105%	106%
Azelastine HCl	Anti-allergy	H1-receptor antagonist	K_i of 1.26 nM for H1 receptor (Procopiou et al., 2011)	N/A	96%	97%
Balofloxacin	Antibiotic	Topoisomerase II and IV inhibitor	Unknown – data not available	Severe cutaneous reactions and light sensitivity (Rubinstein, 2001)	103%	82%
Bazedoxifene acetate	Osteoporosis	Selective estrogen receptor modulator	IC_{50} of 23 nM for estrogen receptor-α and 85 nM for estrogen receptor-β (Miller et al., 2001)	Thrombotic events (e.g. deep venous thrombosis and pulmonary embolism) (Gennari, 2008)	127%	87%
Benidipine HCl	Cardiovascular	Calcium channel blocker	IC_{50} of 4.9 µM for $Ca_v1.2$ (Wiśniowska et al., 2012)	New-onset diabetes and bradycardia (Umemoto et al., 2013)	121%	101%

Bithionol	Anti-bacterial/parasitic	NAPE-PLD inhibitor	IC_{50} of 10.7 µM (Aggarwal et al., 2020)	Severe cutaneous reactions and anorexia (Schlossberg and Rafik, 2017)	110%	87%
Cabazitaxel	Cancer	Pan-tubulin inhibitor	IC_{50} of 0.73 – 0.84 nM (Chen et al., 2018)	Kidney injury, sepsis, arrhythmias and deep vein thrombosis	88%	100%
Chloroquine phosphate	Anti-malarial	Haeme polymerase inhibitor	IC_{50} of 8.8 nM - 304 nM in Plasmodium organism assays and EC_{50} of 297 µM for MRGPRX1 in humans (Delves et al., 2012)	Cardiomyopathy, hepatitis and severe cutaneous reactions	95%	112%
Chlorpromazine HCl	Central Nervous	Dopamine receptor antagonist	K_i of 73 nM for D1 receptors and 7.0 - 7.6 nM for D2 receptors in human (Sokoloff et al., 1992; Sunahara et al., 1991b)	Atrioventricular block, cardiac arrest and systemic lupus erythematosus	94%	101%
Chlorprothixene	Central Nervous	Dopamine and histamine receptor antagonist	K_i of 18 nM for D1, 2.96 nM for D2, 4.56 nM for D3, 9 nM for D5 and 3.75 nM for H1 receptors (von Coburg et al., 2009)	Obstructive jaundice, neuroleptic malignant syndrome and tachycardia (Karimi and Vahabzadeh, 2014)	87%	114%
Ciclopirox	Anti-fungal	Chelator of trivalent cations	Unknown – data not available	N/A	99%	106%
Ciclopirox ethanolamine	Anti-fungal	Chelator of trivalent cations	Unknown – data not available	N/A	88%	93%

Clindamycin palmitate HCl	Antibiotic	Inhibitor of bacterial protein synthesis	IC_{50} of 3.12 nM – 8.81 nM (Dahl and Rosenthal, 2007)	Antibiotic associated colitis, severe cutaneous reactions and agranulocytosis	103%	81%
Clofarabine	Cancer	Ribonucleotide reductase inhibitor	IC_{50} of 5 nM for the M1 and M2 subunits (Parker et al., 1991)	Multi-organ failure, severe cutaneous reactions, sepsis and sinusoidal obstruction syndrome	83%	85%
Clomipramine HCl	Central Nervous	Serotonin, norepinephrine and dopamine transporter blocker	K_d of 0.28 nM for SERT, 38 nM for NET and 2.19 µM for DAT (Tatsumi et al., 1997)	Arrhythmias, exacerbated depression, aggression and hallucinations	97%	104%
Dabrafenib	Cancer	BRAF-V600 inhibitor	IC_{50} of 3.2 nM (Laquerre et al., 2009)	Alopecia, hypophosphatemia and neoplasms	110%	120%
Dabrafenib mesylate	Cancer	BRAF inhibitor	IC_{50} of 3.2 nM (Laquerre et al., 2009)	Alopecia, hypophosphatemia and neoplasms	106%	115%
Dacomitinib	Cancer	Pan-Erbβ inhibitor	IC_{50} of 6 nM for EGFR, 46 nM for Erb-β2 receptor tyrosine kinase 2 and 74 nM for Erb-β2 receptor tyrosine kinase 4 (Barf and Kaptein, 2012)	Interstitial lung disease, pneumonitis, increased risk of infection and hypokalaemia	117%	91%
Dapoxetine HCl	Urological	Selective serotonin reuptake inhibitor	IC_{50} of 1.12 nM (Gengo et al., 2005)	Arrhythmias, hypertension and behavioural changes	91%	112%

Dasatinib hydrochloride	Cancer	AblWT and Src dual inhibitor	IC_{50} of 0.27 nM for ABL proto-oncogene 1 and 0.8 nM for Src (O'Hare et al., 2005; Kitagawa et al., 2013)	Hepatitis B reactivation, severe cardiac changes (e.g. heart failure, cardiomyopathy and myocardial dysfunction)	103%	86%
Desloratidine	Anti-histamine	H1-receptor antagonist	K_i of 0.97 nM (Lewis et al., 2004)	N/A	93%	96%
Dichlorophene	Anti-microbial	Vitamin D receptor antagonist	Unknown – data not available	Contact allergic dermatitis and urticaria, jaundice and hepatic necrosis occurs with larger doses (Aronson, 2016)	94%	104%
Diethylstilbestrol	Pregnancy	Estrogen receptor agonist	K_i of 10.4 nM for ER-α and 9.8 nM for ER-β (Kuiper et al., 1997)	Depression, thrombosis, hypercalcaemia and hypertension	111%	101%
Duloxetine	Central Nervous	Serotonin-norepinephrine reuptake inhibitor	K_i of 5 nM for SERT and 5.97 nM for NET (Fish et al., 2008; Pechulis et al., 2012)	Bleeding disorders, cardiac disease, hepatic disorders and increased risk of infection	85%	123%
Duloxetine HCl	Central Nervous	Serotonin-norepinephrine reuptake inhibitor	K_i of 5 nM for SERT and 5.97 nM for NET (Pechulis et al., 2012; Fish et al., 2008)	Bleeding disorders, cardiac disease, hepatic disorders and increased risk of infection	101%	105%
Dyclonine HCl	Anaesthetic	Sodium channel blocker	IC_{50} of 6 µM for type II alpha subunit (Sahdeo et al., 2014)	N/A	84%	102%

Encorafenib	Cancer	BRAF kinase inhibitor	IC_{50} of 4 nM for BRAF V600E (Stuart et al., 2012)	Intracranial haemorrhage, cardiac disease (heart failure, hypertension and thrombosis) and lip squamous cell carcinoma	94%	82%
Entinostat	Cancer	Class I histone deacetylase inhibitor	EC_{50} of 181 nM for HDAC1, 1.15 µM for HDAC2, 2.3 µM for HDAC3 and 505 nM for HDAC9 (Khan et al., 2008)	Neutropenia, leukopenia, hypophosphatemia and hyponatremia (Connolly, Rudek and Piekarz, 2017)	84%	88%
Enzalutamide	Cancer	Androgen receptor antagonist	IC_{50} of 36 - 219 nM (Tran et al., 2009)	Ischaemic heart disease, increased risk of fractures and cognitive disorders	87%	83%
Flupenthixol dihydrochloride	Central Nervous	Dopamine receptor antagonist	K_i of 7.0 - 8.4 nM for D1 and 1.5 nM for D2 receptors (Freedman et al., 1994; Sunahara et al., 1991a)	Cardiovascular disease, cerebral arteriosclerosis, hyperthyroidism and hypothyroidism	106%	108%
Fluvastatin sodium	Cardiovascular	Hydroxymethylglutaryl -CoA reductase inhibitor	IC_{50} of 28 nM (Istvan and Deisenhofer, 2001)	Thrombocytopenia, Alopecia, hepatic and pancreatic disorders	94%	88%
Galeterone	Cancer	Androgen receptor antagonist	IC_{50} of 384 nM (Handratta et al., 2005)	Hypokalaemia, hypertension, increased levels of alanine aminotransferase and aspartate aminotransferase (Antonarakis and Bastos, 2016)	103%	113%

Ganetespib	Cancer	Heat shock protein 90 inhibitor	IC_{50} of 10 - 14 nM (Ying et al., 2012)	Visual disorders (e.g. blurred vision and night blindness), anaemia, increased pain throughout body (Goldman et al., 2013)	81%	95%
Hydroxychloroquine sulfate	Anti-malarial	Inhibits hemozoin biocrystallization	IC_{50} of 5.8 - 7.8 nM in parasite growth inhibition assays (Delves et al., 2012)	Severe cutaneous reactions, seizures, visual disorders and cardiovascular disorders (e.g. cardiomyopathy)	87%	115%
Hygromycin B	Antibiotic	Inhibits protein synthesis	IC_{50} of 16 µg/mL for inhibition of translation (McGaha and Champney, 2007)	Unknown - not used in humans	87%	104%
Imipramine HCl	Central Nervous	Serotonin-norepinephrine reuptake inhibitor	K_i of 16 nM for NET and 20.3 nM for SERT (Sweetnam et al., 1993)	Cardiac disorders (e.g. arrhythmias and palpitations) and psychological disorders (e.g. hallucinations and delirium)	81%	93%
Iopromide	Contrast Medium	Unknown	Unknown – data not available	Severe cutaneous reactions (e.g. pruritus and urticaria) (García et al., 2014)	82%	109%
Ixazomib	Cancer	Proteasome inhibitor	IC_{50} of 0.93 nM for the β5 site of the 20S proteasome (Kupperman et al., 2010)	Increased risk of infection, peripheral neuropathy and oedema	121%	101%

Ixazomib citrate	Cancer	Proteasome inhibitor	IC_{50} of 0.93 nM for the β5 site of the 20S proteasome (Kupperman et al., 2010)	Increased risk of infection, peripheral neuropathy and oedema	126%	135%
Lacidipine	Cardiovascular	Calcium channel blocker	IC_{50} of 2.76 nM (Spampinato et al., 1993)	Tachycardia, palpitations and peripheral oedema	80%	81%
Lapatinib ditosylate	Cancer	Epidermal growth factor receptor and Erb-β2 tyrosine kinase inhibitor	IC_{50} of 10.2 nM for EGF and 9.8 nM Erb-β2 receptors (Rusnak et al., 2001)	Hepatotoxicity, severe cutaneous reactions and insomnia	106%	90%
Lenalidomide	Cancer	Binds with cereblon to degrade Ikaros transcription factors	IC_{50} of 1.5 μM for cereblon (Matyskiela et al., 2018)	Cardiac disorders (e.g. atrial fibrillation, hyper/hypotension and myocardial infarction), iron overload and severe cutaneous reactions	104%	80%
Lovastatin	Cardiovascular	Hydroxymethylglutaryl -CoA reductase inhibitor	K_i of 0.6 nM and IC_{50} of 20 - 50 nM (Alberts et al., 1980; Jendralla et al., 1990)	N/A	97%	89%
Manidipine	Cardiovascular	Calcium channel blocker	IC_{50} of 8.6 nM (Cho et al., 1989)	Increased palpitations (Ogihara et al., 1992)	120%	89%
Mefloquine HCl	Anti-malarial	Antimalarial MoA = Inhibits protein synthesis by targeting	K_i of 104 nM for A_1 and 675 nM for A_{2A} receptors in	Psychological disorders (e.g. anxiety and depression),	102%	89%

		80S ribosome Other MoA = Adenosine receptor antagonist	humans (Weiss et al., 2003) K_i of 5.2 µM for purine nucleoside phosphorylase in Plasmodium (Dziekan et al., 2019)	sleep and vision disorders		
Menadione	Vitamin	Vitamin K3 analogue - Cofactor in the synthesis of coagulation factors	Unknown – data not available	N/A	100%	80%
Methylene blue	Basic Dye	Nitric oxide synthase and guanylate cyclase inhibitor	Unknown – data not available	Cardiovascular disorders (e.g. decreased cardiac output), gas exchange deterioration and skin discolouration (Ginimuge and Jyothi, 2010)	97%	245%
Mitoxantrone 2HCl	Cancer	Topoisomerase II inhibitor	IC_{50} of 5.3 µM (Hasinoff et al., 2016)	Skin discolouration, acute leukaemia, cardiovascular disorders (e.g. arrhythmias and heart failure)	166%	80%
Nebivolol HCl	Cardiovascular	β-adrenoreceptor inhibitor	pK_i of 9.2 nM for β1, 8.0 nM for β2 and 5.7 nM for β3 (Frazier et al., 2011)	Acute or decompensated heart failure, bradycardia and sleep disorders	92%	107%
Nitazoxanide	Anti-parastic/viral	Inhibition of the pyruvate: ferredoxin/flavodoxin oxidoreductase cycle	IC_{50} of 2.4 µM (Müller et al., 2006)	N/A	96%	94%

Nortriptyline hydrochloride	Central Nervous	Serotonin-norepinephrine reuptake inhibitor	K_i of 6.3 nM for NET and 6.98 nM for SERT (Glennon et al., 2000)	Cardiovascular disorders, psychological disorders, increased risk of infection and hepatic disorders	83%	105%
Olmutinib	Cancer	EGFR tyrosine kinase inhibitor	IC_{50} of 0.1 - 1 µM (Cha et al., 2012)	Severe cutaneous reactions (Kim et al., 2019)	96%	99%
Onalespib	Cancer	Heat shock protein 90 inhibitor	IC_{50} of 27 - 102 nM (Lundsten et al., 2019)	Hepatic toxicity (increased levels of alanine and aspartate aminotransferase) and haematological disorders (e.g. lymphopenia and anaemia) (Do et al., 2015)	85%	109%
Orphenadrine citrate	Central Nervous	Cholinergic receptor blockade	IC_{50} of 16.2 µM (Kornhuber et al., 1995)	Neurological disorders (e.g. hallucinations and seizures) and tachycardia	81%	94%
Oxyclozanide	Anti-parasitic	Uncouples oxidative phosphorylation in flukes	IC_{50} of 13 – 34 µg/mL (Pic, Burgain and Sellam, 2019)	Unknown - not used in humans	111%	99%
Pelitinib	Cancer	EGFR and HER2 inhibitor	IC_{50} of 0.6 - 14.5 nM for EGFR (Rabindran et al., 2004;	Severe cutaneous reactions and anorexia (Erlichman et al., 2006)	120%	82%

			Wissner and Mansour, 2008)			
Penfluridol	Central Nervous	Dopamine receptor antagonist	Ki of 147 nm for D1, 159 nM for D2, 136 nM for D3, 10uM for D4 and 125 nM for D5 (Ashraf-Uz-Zaman et al., 2018)	Cardiovascular disorders (e.g. tachycardia and arrhythmias), neuroleptic malignant syndrome and tremor development (Clarke, 2007)	100%	112%
Perphenazine	Central Nervous	Dopamine (D2) receptor antagonist	K_i of 0.26 - 1.4 nM (Kroeze et al., 2003; Seeman, 2001)	Extrapyramidal reactions (e.g. akathisia and dystonia) (Henao et al., 2014)	96%	107%
Pitavastatin calcium	Cardiovascular	Hydroxymethylglutaryl -CoA reductase inhibitor	K_i of 8.9 µM in rat models (Zhao et al., 2015)	Severe cutaneous reactions (e.g. abnormalities to the scalp and hair)	106%	94%
Pizotifen malate	Central Nervous	Serotonin 5-HT receptor antagonist	K_i of 7.4 for 5-HT_{1A} receptor (Newman-Tancredi et al., 1997)	Psychological disorders (e.g. hallucination and depression) and hepatic disorders	94%	82%
Pracinostat	Cancer	HDAC inhibitor	IC_{50} of 48 nM for HDAC1, 43 nM for HDAC3, 47 nM for HDAC5 and 40 nM for HDAC10 (Novotny-Diermayr et al., 2010)	Haematological disorders (e.g. anaemia, neutropenia and thrombocytopenia) (Quintás-Cardama et al., 2012)	106%	83%

Prochlorperazine dimaleate	Central Nervous	Dopamine receptor antagonist	K_i of 78 nM for D1, 3.6 nM for D2, 4.4 nM for D3 and 810 nM for D4 (Auerbach, DrugMatrix® and ToxFX®, 2014)	Cardiovascular disorders (e.g. QT interval prolongation), haematological disorders (e.g. leucopoenia and agranulocytosis) and sudden death	117%	92%
Prochlorperazine dimaleate salt	Central Nervous	Dopamine receptor antagonist	K_i of 78 nM for D1, 3.6 nM for D2, 4.4 nM for D3 and 810 nM for D4 (Auerbach, DrugMatrix® and ToxFX®, 2014)	Cardiovascular disorders (e.g. arrhythmias, hypotension and QT interval prolongation), haematological disorders (e.g. leucopoenia and agranulocytosis) and sudden death	121%	118%
Quisinostat 2HCl	Cancer	HDAC inhibitor	IC_{50} of 0.11 - 119 nM for HDAC1-10 (Arts et al., 2009)	Cardiac disorders (e.g. tachycardia and ST/T-wave abnormalities) and abnormal liver function (Venugopal et al., 2013)	101%	81%
Quizartinib	Cancer	FLT3 receptor tyrosine kinase inhibitor	IC_{50} of 4.2 nM (Chao et al., 2009; Zarrinkar et al., 2009)	QT prolongation, anaemia and myelosuppression (Levis, 2013)	108%	85%

Ralimetinib	Cancer	p38 MAPK inhibitor	IC_{50} of 7 nM for MAPK14 (Mader et al., 2008)	Haematological disorders (e.g. lymphopenia and leukopenia), anorexia and severe cutaneous reactions (Patnaik et al., 2016)	98%	91%
Regorafenib monohydrate	Cancer	Serine/Threonine kinase inhibitor	IC_{50} of 28 nM for the B-Raf proto-oncogene (Zambon et al., 2012)	Gastrointestinal disorders (e.g. fistulas and perforation), haematological disorders and severe cutaneous reactions	82%	93%
Selinexor	Cancer	Nuclear export protein XPO1 inhibitor	Unknown – data not available	Haematological disorders (e.g. thrombocytopenia and neutropenia) and hyponatremia (Gavriatopoulou et al., 2020)	89%	83%
Sertraline HCl	Central Nervous	Serotonin-epinephrine reuptake inhibitor	K_i of 0.79 nM for SERT (International Union of Basic & Clinical Pharmacology and British Pharmacological Society, 2021b)	Psychological disorders (e.g. anxiety and depersonalisation), cardiac disorders (e.g. arrhythmias and QT interval prolongation) and severe cutaneous reactions	124%	90%
Silmitasertib	Cancer	CK2 inhibitor	IC_{50} of 1 nM for CK2 alpha 1 polypeptide subunit (Pierre et al., 2011)	Haematological disorders (e.g. anaemia and thrombocytopenia) (Borad et al., 2021)	121%	81%

Simvastatin	Cardiovascular	Hydroxymethylglutaryl -CoA reductase inhibitor	IC_{50} of 11 - 12 nM (Istvan and Deisenhofer, 2001)	N/A	87%	80%
Solifenacin succinate	Urological	Muscarinic receptor antagonist	IC_{50} of 573 nM for M2 receptor and 130 nM for M3 receptor (Prat et al., 2011)	Urinary tract infection, hallucinations and cardiac disorders (e.g. arrhythmias and QT interval prolongation)	88%	100%
Tanespimycin	Cancer	Heat shock protein 90 inhibitor	IC_{50} of 780 nM for HSP90 alpha-1 subunit (Li et al., 2014)	Hepatotoxicity and haematological disorders	87%	99%
Thioridazine hydrochloride	Central Nervous	Serotonin 5-HT receptor antagonist	pK_i of 7.4 - 8.0 nM for 5-HT2A receptors and 7.2 - 7.3 nM for 5-HT2C receptors (Herrick-Davis, Grinde and Teitler, 2000; Kongsamut et al., 2002)	Extrapyramidal reactions (e.g. parkinsonism), neuroleptic malignant syndrome and cardiac disorders (e.g. tachycardia) (Feinberg, Fariba and Saadabadi, 2021)	107%	98%
Tocofersolan	Vitamin	Anti-oxidant (water soluble version of Vitamin E)	Unknown – data not available	N/A	91%	104%
Topotecan HCl	Cancer	Topoisomerase I inhibitor	IC_{50} of 7.5 – 60 nM in neuroblastoma cell lines (Chaturvedi et al., 2016)	Haematological disorders (e.g. anaemia, hyperbilirubinemia and leucopoenia), interstitial lung disease and sepsis	101%	81%

Trifluoperazine 2HCl	Central Nervous	Dopamine (D2) receptor antagonist	K_i of 0.96 - 1.3 nM for D2 receptors (Kroeze et al., 2003; Seeman, 2001)	Cardiovascular disorders (e.g. embolism and thrombosis), haematological disorders (e.g. neutropenia and agranulocytosis) and sudden death	107%	109%
Uprosertib	Cancer	AKT serine/threonine kinase inhibitor	K_i of 0.006 nM for kinase 1, 1.4 nM for kinase 2 and 1.5 nM for kinase 3 (Dumble et al., 2014)	Severe cutaneous reactions (Tolcher et al., 2020)	108%	141%
Verteporfin	Photosensitizer	YAP inhibitor	IC_{50} of 1.4 – 7.7 µM (Wei et al., 2017)	Eye disorders (e.g. eye inflammation and retinal detachment), haemorrhage and myocardial infarction	85%	276%
Vinorelbine tartrate	Cancer	Microtubule inhibitor	Unknown – data not available	Haematological disorders (e.g. thrombocytopenia and neutropenia), sepsis and cardiovascular disorders (e.g. hyper/hypotension)	115%	100%
Vitamin D2	Vitamin	Binds to its receptor to maintain calcium balance	Unknown – data not available	N/A	102%	90%

Vortioxentine HBr	Central Nervous	Serotonin 5-HT receptor antagonist	K_i of 7.8 nM for 1A, 7.5 nM for 1B, 6.3 nM for 7 and 8.4 nM 3A (Bang-Andersen et al., 2011)	Neuroleptic malignant syndrome, serotonin syndrome and haemorrhage	128%	107%
Voxtalisib	Cancer	PI3K and mTOR kinase inhibitor	IC_{50} of 39 nM for PI3Kα, 113 nM for β, 9 nM for γ and 43 nM for δ. IC50 of 157 nM for mTOR (Garcia-Echeverria and Sellers, 2008)	Abnormal liver function (e.g. increased alanine aminotransferase) (Awan et al., 2016)	96%	84%

As shown in Figure 3-4, the hits could be broken down into 5 major groups (cancer, cardiovascular, central nervous, anti-microbial and others), according to the current indication they are approved for. None of the 90 hits are currently as a therapeutic to treat dermal scarring or fibrosis.

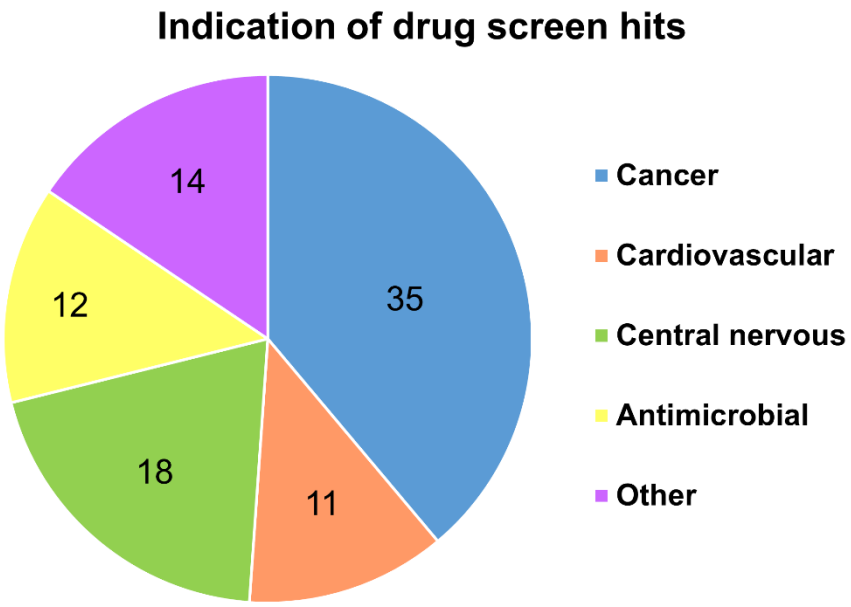

Figure 3-4: Indication of the 90 hits from the screening of 1,954 approved drugs. The hits can be broken down into 13 different indications which they are currently approved for, with drugs used for the treatment of cancers accounting for the majority.

3.3.1. Identification of candidate drugs for further testing

Following the identification of the hit drugs from the screening campaign, an in-depth review of each hit was carried out to identify potential candidates to be taken forward for further testing. Using the criteria set out in section 2.7.1 (Figure 2-3) the first step of the streamlining process was to categorise the hits depending on their safety profile and the number of adverse events experienced by patients who take them. The majority of hits (78) had a number of severe adverse effects associated with them, of which these effects cover a number of different categories. The three most common adverse effects were cardiac disorders (e.g. arrhythmias, QT interval prolongation and cardiomyopathy), neurological disorders (in particular the aggravation of already existing disorders such as depression and anxiety) and haematological disorders (e.g. thrombocytopenia, neutropenia, leucopoenia and agranulocytosis). Furthermore, 21 hits had been associated with the development of severe cutaneous reactions.

Following this, the hits were then filtered using the rest of the criteria outlined in section 3.2.1. Figure 3-5 outlines the criteria and the number of hits that made it through each stage of this process. Of the 90 hits, 12 were identified as exhibiting a desirable safety profile and little-no

adverse effects. Those that had been previously formulated for topical application were identified, which resulted in a list of 10 candidate drugs, across 5 different indications.

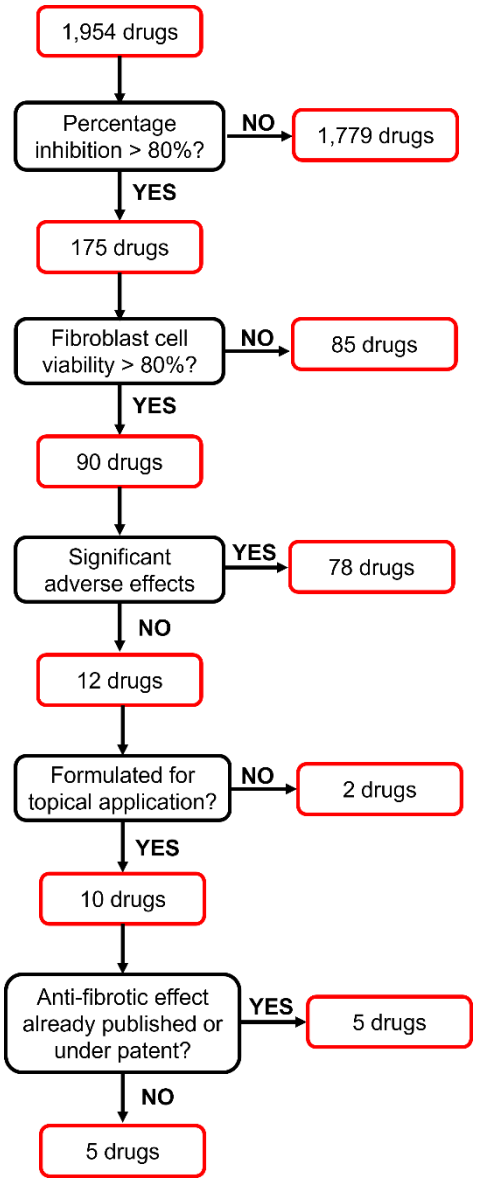

Figure 3-5: Streamlining of hits to identify potential candidate drugs for further testing. 90 drugs were identified as hits (>80% percentage inhibition and >80% cell viability), before excluding hits based on their adverse effect. The final stages of the streamlining process were to identify those that have been previously formulated for topical application, which gave 10 candidate drugs. Literature and patent searches on these 10 drugs were carried out, and 5 drugs were found to not be under patent for hypertrophic scarring and/or fibrosis.

Table 3-3 summarises the 10 candidate drugs with their current indication, mechanism of action, percentage inhibition and the vehicle the drug was dissolved in, in the drug library. Literature and patent searches were then carried out to see if the anti-fibrotic effect of any of the 10 drugs had been reported previously, and/or to see if any were under patent for the treatment of hypertrophic scarring or fibrosis.

Table 3-3: List of potential candidate drugs from the original 90 screening campaign hits, including their current indication, mechanism of action, percentage inhibition, cell viability, vehicle and if the drugs are under patent for fibrosis.

Drug name	Indication category	Mechanism of action	Percentage inhibition	Fibroblast viability	Compound vehicle	Under patent for fibrosis?
Azelastine HCl	Anti-allergy	H1-receptor antagonist	96%	97%	DMSO	No
Ciclopirox	Anti-fungal	Chelator of trivalent cations	99%	106%	DMSO	No
Ciclopirox ethanolamine	Anti-fungal	Chelator of trivalent cations	88%	93%	DMSO	No
Desloratidine	Anti-allergy	H1-receptor antagonist	93%	96%	DMSO	No
Dyclonine HCl	Anaesthetic	Sodium channel blocker	84%	102%	DMSO	No
Lovastatin	Cardiovascular	Hydroxymethylglutaryl-CoA reductase inhibitor	97%	89%	DMSO	Yes - (Mustoe et al., 2020)
Menadione	Vitamin	Vitamin K3 analogue - Cofactor in the synthesis of coagulation factors	100%	80%	DMSO	Yes - (Vermeer, 2016)
Simvastatin	Cardiovascular	Hydroxymethylglutaryl-CoA reductase inhibitor	87%	80%	DMSO	Yes - (Mustoe et al., 2020)
Tocofersolan	Vitamin	Anti-oxidant (water soluble version of Vitamin E)	91%	104%	DMSO	Yes - (Sen et al., 2013)
Vitamin D2	Vitamin	Binds to its receptor to maintain calcium balance	102%	90%	DMSO	Yes - (Mehta, 2006)

As the 10 candidate drugs covered a range of indications and mechanisms of action, the literature search allowed for speculation of the potential mechanism of action which would allow for their evident anti-myofibroblast activity. Figure 3-6 was constructed from this literature search, showing the potential anti-myofibroblast mechanism of these candidate compounds. From the information collected relating to the candidate drugs, it was decided that the anti-fibrotic activity of ciclopirox (CPX) and its ethanolamine (CPXO) would be further investigated. Further details of the rationale of chosing CPX and CPXO can be found in the Chapter 3.4. below.

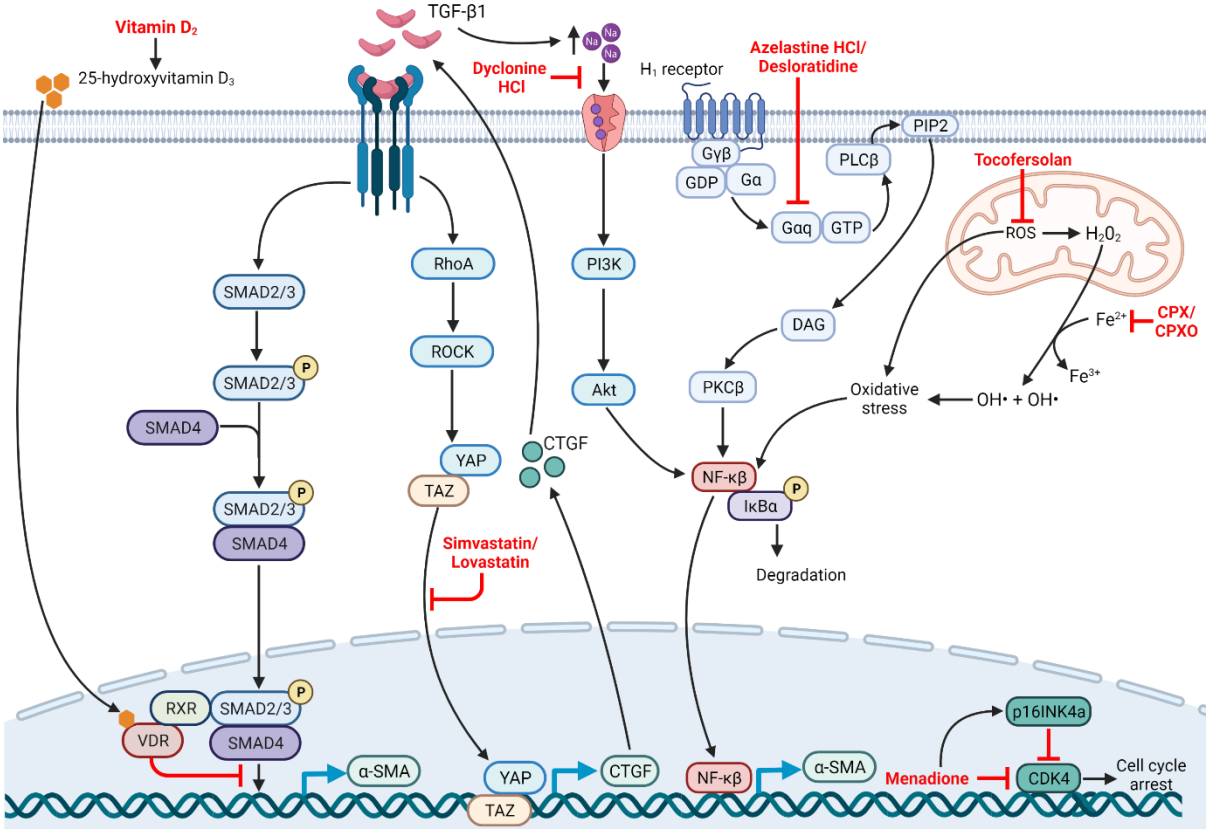

Figure 3-6: Potential mechanism of action for the anti-myofibroblast effect of the ten candidate drugs. Vitamin D2 is first converted to 25-hydroxyvitamin D3 before entering the cell and binding to its receptor (Vitamin D receptor; VDR). VDR binds with (RXR), before binding with the SMAD2/3/4 complex and preventing the activation of pro-fibrotic genes (e.g. α-SMA). Simvastatin and Lovastatin inhibit CTGF production by preventing RhoA/ROCK mediated translocation of YAP/TAZ to the nucleus. TGF-β1 causes an increase in the intra-cellular sodium concentration, which activates the PI3K/Akt pathway and NF-κβ transcription factor. As a sodium channel blocker, dyclonine HCl can block this action. The histamine signalling pathway also activates NF-κβ through GTPases and PKC, which is inhibited by azelastine and desloratidine (H_1 receptor antagonists). Menadione (vitamin K3) has been shown to inhibit fibroblast proliferation through the inhibition of CDK4, and upregulation of CDK inhibitor p16INK4a. Tocofersolan (water soluble version of vitamin E) acts as an anti-oxidant and removes excess reactive oxygen species (ROS), which induce oxidative stress during fibrosis. Finally, as part of the oxidative stress process, ROS generates hydrogen peroxide, which in the presence of iron (Fe^{2+}) converts to hydroxyl radicals. CPX and CPXO are trivalent ion chelators and are able to prevent hydrogen peroxide conversion by chelating iron. Image created using BioRender.

3.4. Discussion

This section of the thesis set out to investigate if this assay can identify any drugs that can inhibit TGF-β1-induced myofibroblast transformation. The following objective was set out to investigate the research question:

1. Screen 1,954 approved drugs to identify any drugs that prevent myofibroblast transformation.

3.4.1. Screening of an approved drug library

Once the developed assay had been deemed suitable for the application of high-throughput screening, the screening of the 1,954 approved drugs could be started. As mentioned previously, the Gilson PipetMAX automated liquid handling system was utilized to minimise human error during the dilution of the drug library, and transfer of the drugs onto the fibroblasts. Working in collaboration with the liquid handling team at Gilson, a three-step protocol was developed and programmed into the PipetMAX (as outlined in Chapter 3.2.1. and Figure 3-1). The drugs were first diluted from a stock concentration of 10 mM to 100 µM in serum free media, before diluting to a working concentration of 10 µM in 1% FCS media. The two-step dilution was utilised to prevent the drugs from precipitating, which can occur when carrying out a large single-step dilution (Popa-Burke and Russell, 2014; Di and Kerns, 2006). 10 µM was chosen as the single concentration to be tested as this is a common concentration used in screening campaigns, with the majority of screens using a concentration between 1 – 10 µM (Hughes et al., 2011). Each drug was tested in duplicate and in all 66 plates used for the screening assay, three sets of control wells were used to control for plate to plate variability. A negative control whereby fibroblasts were left untreated, a positive control whereby fibroblasts were treated with 10 ng/mL of TGF-β1 and a second positive control, whereby fibroblasts were treated with 10 ng/mL TGF-β1 and 1 µM of SB-505124. Prior to the drug screen being carried out on the burn scar fibroblasts, the liquid handling programme was utilised for the screening of the drug library in PD cells (Cellek lab, unpublished observations). This screening campaign was carried out successfully, confirming that the designed programme was functional for the desired purpose.

Following successful completion of the screening campaign in skin-derived fibroblasts, time was spent identifying the best calculation to use to identify the effect each drug had on myofibroblast transformation. Normalised percentage inhibition was chosen (see equation in Chapter 3.2.3.), as this allowed for the normalisation of the drug effect to both the negative control (100% inhibition) and TGF-β1 only positive control (0% inhibition) (Shockley et al., 2019; Gubler, Schopfer and Jacoby, 2013). As seen in the full data set in Figure 3-3, the majority of the 1,954 drugs were found to promote myofibroblast transformation in some way,

denoted by the negative percentage inhibition. Further analysis of these drugs identified 70 with the ability to increase myofibroblast transformation >3-fold compared to the normal TGF-β1 response. A smaller number of drugs were identified as being able to inhibit myofibroblast transformation (positive percentage inhibition), with a hit defined as showing >80% inhibition of α-SMA expression, whilst maintaining >80% cell viability. These parameters were chosen to ensure that the effect seen is due to true inhibition of myofibroblast transformation and not due to the drug being cytotoxic. Futhermore, although it is widely accepted that the cut off for hits is usually an arbitary value selected by the individual, Brideau et al., recommend checking that your chosen value falls within three standard deviations of the postive control value. For this screening assay, SB-505124 (at the 10 μM concentration used for the screen) was utilised as the positive control to check for drug-induced inhibition of myofibroblast transformation. The average percentage inhibition of SB-505124 across the 66 plates used in the drug screen was 106%, with a standard deviation of ±16%. Therefore, three standard deviations of the data would be 58% inhibition. As 80% inhibition falls within these bounds, this confirms that the chosen value is statistically relevant for defining a hit.

Of the drugs that inhibited myofibroblast transformation, 90 hits were identified as showing >80% inhibition of α-SMA expression and >80% cell viability (Table 3-2). The hits were first categorised by the indications that they are currently approved for as a treatment. Thirty five of the hits are currently used as cancer treatments which have been shown to target molecular processes such as the cell cycle and epigenetic changes. The rest of the hits fall into the category of cardiovascular drugs, drugs for the treatment neurological disorders and anti-microbials (e.g. anti-fungals and antibiotics). Drugs in the ‘other’ category include drugs to treat urological disorders, osteoporosis, and allergies. None of the 90 hits are currently licensed as a therapeutic to treat dermal scarring or any other fibrotic disorder.

To my knowledge, this is the first screening campaign which uses the full SelleckChem FDA approved library, of more than 1,000 drugs in any model of skin fibrosis. Out of the 429 citations for the drug library on the SelleckChem website, only 2 papers used the drug library for fibrotic disorders (lung fibrosis and myelofibrosis). However, both studies did not use the full FDA-approved drug library, instead the authors cherry-picked a small number of drugs from the full library (305 for lung fibrosis and 150 for myelofibrosis) (Sieber et al., 2018b; Tomuleasa et al., 2018), with the myelofibrosis paper focussing solely on drugs that had previously shown an inhibitory effect on fibroblast proliferation (Tomuleasa et al., 2018). Regarding screening campaigns for fibrosis using other approved drug libraries, there is one other study that screened the ENZO life sciences library of 640 compounds using murine cardiac fibroblasts (Rehman et al., 2019). The authors identified haloperidol as a hit, and confirmed this in fibroblasts from other tissues, including dermal fibroblasts. Interestingly, in

the screening assay carried out in this thesis, haloperidol was not identified as a hit, as it only showed a 26% inhibition in α-SMA expression. It is hard to compare inhibition between the two screening assays, as Rehamn et al., identified the inhibitory effect of the drugs by calculating the Z-score for each drug and comparing that with the controls (Rehman et al., 2019). Furthermore, the study carried out by Rehman et al., used commercially available dermal fibroblasts and therefore this difference seen between the two drug screens may be due to the differing origins of the cells themselves.

3.4.2. Identification of candidate drugs

To identfy potential candidates for further testing, a series of different criteria were used as outlined in Chapter 3.2.2 (Fig 3-2). The first step of this process was to categorise the hits according to their safety profiles. The benefit of using an approved drug library, is that all the drugs in the library have already been deemed safe to use in humans through completion of clinical trials. Therefore, the purpose of this process was to identify drugs with minimal side effects, or low incidence of side effects, as the patients these drugs are intended for are healthy individuals, aside from their injuries. For example, of the burn patients recruited to this project, the average patient age was 30 years old, with only 3 patients having co-morbidities. Therefore it would be irresponsible to give these patients a drug systemically that could result in severe adverse effects, which may end up being worse than the original injuries themselves. Of the 90 hits, 78 drugs have been associated with severe adverse events, with a large number of the drugs having been associated with multiple severe adverse events. The most common severe adverse events were disorders affecting the cardiovascular and neurological systems, as well as haematological disorders. 21 drugs had also been previously associated with the development of severe cutaneous adverse reactions. As a result of this, these drugs were excluded from being considered as candidate drugs. The next step in the filtering process was to identify any hits that had been previously formulated for topical application. Topical application of the candidate drug would be ideal for dermal scarring, as it would ensure that the drug has a direct effect on the wounded area with minimal systemic effect. Furthermore, the drug could potentially be incorporated into dressings helping to increase patient compliance as they would not have to remember to apply the drug. Of the 12 safe hits, 10 hits were identified as having been previously formulated for topical application, with the drugs falling into 5 different drug classes.

These 10 drugs became the potential candidate drugs and were reviewed extensively before choosing those that would be taking forward for further testing. First, a literature review was carried out to identify if the anti-myofibroblast effect of these drugs had been previously reported. Further, as the drugs cover a wide range of cellular/molecular targets, these

searches allowed for speculation into their potential targets allowing for their anti-myofibroblast effect (Figure 3-6).

Azelastine HCl and desloratidine are second generation anti-histamines, typically used in the treatment of seasonal allergies (Slater, Zechnich and Haxby, 1999). Azelastine HCl is widely available as eyedrops, for the treatment of allergic conditions of the eye (e.g. allergic conjuctivitis) (Williams, Crandall and Sheppard, 2010). Desloratadine, the active metabolite of loratadine, is used to treat more common symptoms of allergys (e.g. allergic rhinitis) (Geha and Meltzer, 2001). Desloratadine is currently available to the population over the counter as an oral medication, however it has been formulated as a topical agent previously to investigate its efficacy against allergic conjunctivitus (Cardelús et al., 1999). Both drugs are histamine receptor-1 (H_1 receptor) antagonists, blocking the action of histamine during an allergic reaction. As H_1 receptors have been shown to be expressed in dermal fibroblasts (Wolak et al., 2017), this would allow azelastine HCl and desloratidine to exert an anti-myofibroblast effect by blocking the histamine signalling cascade. Through the activation of GTPases and PKC, histamine is able to co-ordinate the translocation of the transcription factor NF-κβ to the nucleus (Simons and Simons, 2011). NF-κβ is a pro-inflammatory transcription factor which mediates the induction of various genes involved in a fibrogenic response. In particular, NF-κβ has been shown to induce the expression of α-SMA, helping to co-ordinate myofibroblast transformation (Wang et al., 2017). Therefore, by inhibiting the upstream mediators of the histamine signalling cascade, azelastine HCl and desloratadine exert an anti-myofibroblast effect by preventing the translocation of NF-κβ to the nucleus.

Dyclonine HCl is an anaesthetic that is commonly found in throat lozenges or sprays for the treatment of sore throats (International Union of Basic & Clinical Pharmacology and British Pharmacological Society, 2021a). Dyclonine HCl acts by blocking sodium channels on the neuronal membrane, therefore increasing the threshold for excitation by decreasing the permeability of neuronal membranes (Tikhonov and Zhorov, 2017). The role of sodium in fibrosis has not been widely investigated, however studies focussing on cardiac fibrosis have shown a potential interaction between TGF-β1 and sodium channel signalling. These studies have shown that TGF-β1 causes an increase inward movement of sodium, therefore increasing the intra-cellular sodium concentration (Kaur et al., 2013; Koivumaki et al., 2014; Chatelier et al., 2012). Increased levels of intra-cellular sodium is able to activate the PI3K/Akt signalling pathway, whose downstram mediator is NF-κβ (Fan, Xie and Tian, 2017). As discussed previously, NF-κβ is a pro-inflammatory transcription factor which is able to induce the expression of α-SMA, helping to co-ordinate myofibroblast transformation (Wang et al., 2017). Therefore, dyclonine HCl may be able to exert its anti-myofibroblast effect by blocking the increased inward current of sodium and subsequently, inhibiting the downstream activation

of NF-κβ. However, it is not known whether these sodium channels are expressed and functional in human dermal fibroblasts which would require further investigation.

Ciclopirox (CPX) and ciclopirox ethanolamine (CPXO) are hydroxypyridone anti-fungals, which are commonly used as a topical treatment for fungal skin infections (Jue, Dawson and Brogden, 1985; Subissi et al., 2010; Shen and Huang, 2016). Unlike other anti-fungals who target cell wall synthesis and disrupt the biosynthesis of ergosterol, CPX is a chelator of iron and other ions which are integral for the functioning of different intracellular enzymes (Sonthalia, Agrawal and Sehgal, 2019; Prasad, Shah and Rawal, 2016). Therefore, hydroxypyridone anti-fungals could be inhibiting myofibroblast transformation by chelating intracellular iron. Excessive accumulation of intra-cellular iron has been shown to contribute to the progression of both liver fibrosis and idiopathic pulmonary fibrosis (IPF) (Mehta, Je Farnaud and Sharp, 2019; Ali et al., 2020). It is believed that intracellular iron drives myofibroblast transformation through the production of reactive oxygen species (ROS) and oxidative stress signalling (Philippe, Ruddell and Ramm, 2007). Iron is able to convert hydrogen peroxide to hydroxyl radicals via the Fenton reaction, increasing intracellular levels of ROS, which in turn induces cellular stress and can promote a fibrogenic response in fibroblasts (Winterbourn, 1995; Galaris, Barbouti and Pantopoulos, 2019). Further, iron-induced oxidative stress can induce myofibroblast transformation and subsequent α-SMA expression through the activation of key transcription factors (e.g. NF-κβ/AP-1) (Wang et al., 2017; Hu et al., 2006).

Simvastatin and lovastatin are members of the drug class of 3-hydroxy-3-methyl-glutaryl-coenzyme A (HMG-CoA) reductase inhibitors, which are used in patients to help reduce cholesterol levels (Sizar et al., 2021). Although statins are currently only available on the market as oral medication, a number of studies have formulated them for topical application with some success (Xie et al., 2020; Jia et al., 2017). The anti-scarring effects of statins have been investigated by scientists at Northwestern University (USA), in which they have shown that statins are able to reduce hypertrophic scarring severity in rabbit ear models (Ko et al., 2012; Jia et al., 2017; Xie et al., 2020). Furthermore, they have confirmed an anti-myofibroblast effect with a significant reduction in α-SMA expression seen in histological analysis (Xie et al., 2020). It is believed that statins exert this effect through the inhibition of CTGF, a downstream mediator in the TGF-β1 signalling pathway. During fibrosis, CTGF creates a positive feedback loop with TGF-β1, helping to maintain the myofibroblast phenotype (Kok et al., 2014). Further studies investigating the anti-fibrotic effect of statins have shown that the significant reduction in CTGF is due to statins acting upon the RhoA/ROCK pathway (Milenkovic et al., 2019). Statins have been shown to inhibit the

translocation of YAP/TAZ to the nucleus, preventing the transcription of key fibrotic genes, in particular those for CTGF (Milenkovic et al., 2019).

Vitamin D is an essential vitamin required in a number of bodily functions, in particular bone formation as vitamin D aids in the absorption of calcium (Nair and Maseeh, 2012). Vitamin D can be sourced via our environment (e.g. sunlight) or through our diet and supplementation. Vitamin D2 usually enters our bodies through our diet, where it is converted to the more bioavailable version of vitamin D, 25-hydroxyvitamin D3 (Nair and Maseeh, 2012). The role of vitamin D in fibrosis has been studied extensively and it has been suggested as a therapeutic for many years for hypertrophic scarring, as many burn patients suffer from significant vitamin D deficiency (Ince, Uyar and Dadaci, 2019). Studies have shown that vitamin D is able to interfere with the canonical TGF-β1 signalling pathway, by blocking Smads from inducing pro-fibrotic gene induction (Shany, Sigal-Batikoff and Lamprecht, 2016). Vitamin D binds to its receptor (VDR), which creates a complex with the retinoid x receptor (RXR) which can then interfere with the downstream Smad signalling in two ways. First, the VDR/RXR complex can bind directly with Smad3 and prevent the Smad complex from binding with its genetic target (Zerr et al., 2015). The VDR/RXR complex can also competitively bind to the genetic targets of the Smad complex, also preventing the binding of the Smad complex (Ding et al., 2013). Through this downstream inhibition of the Smad complex, vitamin D2 is able to exert an anti-myofibroblast effect by preventing the expression of key fibrogenic genes (e.g. α-SMA) (Shany, Sigal-Batikoff and Lamprecht, 2016; Zhang et al., 2011).

Tocofersolan is a water soluble version of vitamin E, which is used to treat patients who have a vitamin E deficiency but are unable to absorb fat (Thébaut et al., 2016). Vitamin E is often suggested by clinicians for patients who develop severe scars, as evidence shows that vitamin E oil helps to make the scar more maleable (Baumann and Md, 1999). Vitamin E is an anti-oxidant, which is responsible for removing excess levels of reactive oxygen speices and preventing cells from entering oxidative stress (Burton, Joyce and Ingold, 1983). When a significant injury occurs (e.g. burns), cells undergo oxidative stress, due to the hypoxic conditions created by the injury (Parihar et al., 2008). As a result of the hypoxic conditions, there is an increased production of ROS in the cells, which contributes to the induction of oxidative stress in the cells (Parihar et al., 2008). As discussed previously, oxidative stress is able to mediate the translocation of NF-κβ to the nucleus, where it induces the expression of fibrogenic genes (e.g. α-SMA) (Wang et al., 2017). As vitamin E is able to remove the excess ROS produced during severe injury, it has potential to have an anti-myofibroblast effect by preventing the translocation of NF-κβ.

Menadione (Vitamin K3) is the fat-soluble precurosor to menaquione, which is used to treat hypoprothrombinemia (Cromer and Barker, 1944). Vitamin K is required for the production of a number of different proteins which are involved in key bodily processes (e.g. clotting factors II, VII, IX and X) (Danziger, 2008). The evidence surrounding vitamin K and its anti-fibrotic/anti-myofibroblast ability is contradictory. Regarding its anti-myofibroblast effect as evidenced in the screening assay, a handful of studies have shown that vitamin K3 is able to inhibit fibroblast proliferation *in vitro* (Liu et al., 1996; Pinilla et al., 2014). The authors speculate that vitamin K3 inhibits proliferation in the G1 phase of the cell cycle, through the inhibition of CDK4 and upregulation of pINK6a, a CDK inhibitor (Pinilla et al., 2014; Kuriyama et al., 2005). Further reading suggests that inhibiting cell proliferation at this early stage of the cell cycle, prevents the cells from being able to differentiate into other cell types (Ruijtenberg and van den Heuvel, 2016). Therefore, menadione may be preventing transformation of fibroblasts to myofibroblasts, by inhibiting cell proliferation in the early cell cycle. However, vitamin K is required for the successful production of different proteins, of which a number of these are pro-fibrotic in nature (e.g. periostin) (Kanisicak et al., 2016). This could suggest that increased levels of vitamin K might increase myofibroblast transformation. Therefore it is clear that more research is needed to fully understand the anti-myofibroblast activity of menadione and vitamin K.

Following on from the literature review, a patent search for each drug was carried out to see if any are currently under patent for the treatment of hypertrophic scarring, or other fibrotic disorders. This identified 5 drugs (simvastatin, lovastatin, tocofersolan, menadione and vitamin D2) for which patent applications have been filed for treatment of fibrotic diseases (Vermeer, 2016; Mehta, 2006; Sen et al., 2013; Mustoe et al., 2020). In order to have freedom to operate in this space and not to have issues related to intellectual property in the future development phases, it was decided not to pursue these drugs.

Of the 5 remaining candidate drugs, azelastine HCl and desloratidine were excluded from further testing due to their limited use as a topical agent. Despite azelastine HCl commonly being used for a topical indication, it is mainly formulated as eye drops and desloratidine has only been formulated for topical application in a handful of studies. As a result, this may cause issues further downstream of the drug discovery process regarding the reformulation of the drugs and if they would be able to achieve the desired efficacy needed in a cream/ointment. Dyclonine HCl was also excluded due to its use as an anaethestic. Burn injury patients undergo a number of surgical procedures as part of their standard of care, and so concerns were raised by the clinical team that dyclonine HCl would interfer with the other medications used as part of the standard of care. This meant that CPX and CPXO were chosen as the candidate drugs to be taken forward for further testing in the secondary assays.

In the drug screen, CPX showed 91% inhibition, with 106% cell viability and CPXO showed 88% inhibition and 93% cell viability. These drugs are broad-spectrum anti-fungals, which are effective against multiple species of fungus (e.g. *Dermatophytes* and *Candida*) (Subissi et al., 2010). As a topical treatment, it is currently formulated for use as a wide range of therapeutics, including as a nail lacquer, cream and as a shampoo (Shen and Huang, 2016). In pharmacokinetic studies, CPX has been shown to be a safe topical drug. In penetration studies using a 1% cream, 70-600 μg/mL (~300 μM – 3 mM) of the drug was retained in the stratum corneum of the epidermis and 20 – 30 g/mL (~100 μM) was seen in the dermis, 2 hours after application (Jue, Dawson and Brogden, 1985). After 24 hours of application, 10 μM of CPX was present in the deepest layer of the dermis, with systemic absorption at a maximum of 1.3% of the given dose (Ceschin-Roques et al., 1991). In terms of adverse effects seen, studies have shown that <5% of patients experience any adverse effect, which are limited to slight redness and irritation of the area which the drug is applied to (Gupta and Bluhm, 2004; Gupta, Schouten and Lynch, 2005). CPX is a safe and efficacious drug, which was shown to inhibit myofibroblast transformation, making it the perfect candidate for further testing.

In the last 15 years there has been a resurgence in the repurposing of hydroxypyridone anti-fungals for other disorders. In particular, these drugs have recently been shown to exhibit anticancer and antitumour activity in acute myeloid leukaemia (AML), and other haematologic cancers (Weir et al., 2011; Eberhard et al., 2009). The efforts to repurpose these drugs for other indications gained further traction after it was shown that CPX and CPXO exhibit good safety and tolerability when given systemically (Minden et al., 2014). In some of these studies, CPX and CPXO were shown to reduce collagen production, however this has been limited to histological analysis and not studied in detail (Urquiza et al., 2018; Minden et al., 2014). Interestingly, hydroxypyridone anti-fungals have been found to promote wound healing in chronic ulcers when used in diabetic wound models. CPX and CPXO were both found to increase angiogenesis in the wound site, through the upregulation of multiple angiogenic genes (e.g. VEGF) and through the increased stability and availability of hypoxia inducible factor-1α (HIF-1α) (Linden et al., 2003; Ko et al., 2011). These wound healing enhancing changes subsequently resulted in an increased rate of re-epithelisation and wound closure, with an increase in cellularity in the dermis also observed (Ko et al., 2011).

It is therefore possible that hydroxypyridone anti-fungals are able to exert both a wound healing enhancing and anti-fibrotic effect. Further, their anti-fibrotic effect may not be limited to inhibiting myofibroblast action but may also inhibit other cellular pathologies which contribute to the fibrosis phenotype.

Chapter 4: Investigating the anti-fibrotic effect of hydroxypyridone anti-fungals

4.1. Introduction

The screening campaign identified hydroxypyridone anti-fungals as being able to inhibit myofibroblast transformation, with the literature suggesting that they may have a wider anti-fibrotic effect. This chapter will focus on confirming the anti-myofibroblast activity of hydroxypyridone anti-fungals, as well as investigating their wider anti-fibrotic effect by using a battery of secondary assays. These secondary assays have been designed to measure other aspects of the fibrotic response (ECM production and keratincoyte epithelial-mesenchymal transition), as well as investigate the drugs' effects on various aspects of cell viability. Therefore, these results should provide further understanding as to the extent of the anti-fibrotic effect hydroxypyridone anti-fungals have.

As discussed in previous chapters, myofibroblasts are the key effector cell in the development of hypertrophic scars following burn injury (Sarrazy et al., 2011). To fully investigate the anti-fibrotic effect of the hydroxypyridone anti-fungals, the anti-myofibroblast activity of the drugs needs to be confirmed. This will ensure that the inhibition of myofibroblast transformation seen in the drug screen is reproducible, and will also allow to see if the effect is concentration dependent.

To confirm the anti-myofibroblast effect of hydroxypyridone anti-fungals further, a secondary screening assay measuring ECM production has been developed. Myofibroblasts are responsible for the producing the vast majority of ECM proteins during wound healing. During burn wound healing, the production of ECM is neccessary for the formation of granulation tissue which provides a scaffold for cells to migrate across to aid in wound closure (Frazier et al., 1996; Barker, 2011). Although during the initial proliferation phase of wound healing this production of ECM is crucial, burn injuries result in an extended proliferation phase which leads to the excessive accumulation and production of ECM proteins (Chipp et al., 2017). This is further exacerbated by the delay in the remodelling phase of wound healing, which in some burn injuries may not occur for > 1 year after the initial injury (Gauglitz et al., 2011). Therefore, by measuring myofibroblast ECM production *in vitro*, not only will the anti-myofibroblast effect of the hydroxypyridone anti-fungals be confirmed further but this will also show that the anti-fibrotic effect of the hydroxypyrdone anti-fungals extends to other key myofibroblast functions, as opposed to only a marker protein (α-SMA).

To investigate the anti-fibrotic effect of the hydroxypyridone anti-fungals further, an additional secondary assay was developed to measure keratinocyte epithelial-mesenchymal transition (EMT). Keratinocytes are another key cell population involved in burn wound healing and

subsequent scar formation. These cells mediate re-epithelisation of the wound and restoration of the skin back to its main function as a protective barrier. To achieve re-epithelisation, keratinocytes adopt a mesenchymal phenotype in order to migrate across the wound bed (Stone et al., 2016). During physiological wound healing, the phenotypic plasticity of the EMT process allows keratinocytes to revert back to their epithelial lineage after migrating to a new site(Kalluri and Weinberg, 2009; Kalluri and Neilson, 2003). However, as a result of increased and sustained expression of key cytokines (e.g. TGF-β1) during burn injury, keratinocyte EMT is continuous and does not allow phenotypic plasticity to revert back to their epithelial origin (Kalluri and Neilson, 2003). This causes delayed re-epithelisation of the wound, which has other consequences aside from increased risk of scarring, such as increased risk of infection. Further, whilst converted to their mesenchymal phenotype, kerationcytes are able to produce ECM proteins, in particular fibronectin (Yan et al., 2010). Therefore keratinocytes undergoing EMT provide an additional source of excessive ECM proteins. By investigating the effect of hydroxypyridone anti-fungals on both vimentin and fibronectin expression in keratinocytes undergoing EMT, this will identify if these drugs have a wider anti-fibrotic effect in other key cell populations.

The effect of the hydroxypyridone anti-fungals on cell viability should be assessed fully to ensure that the desired concentrations of the drugs that would be used in the clinic (based on the current pharmacokinetic data) would not cause excessive cytoxicity. When using the In-Cell ELISA, cell viability is assessed by using DRAQ5 which stains nuclear proteins, however this does not give a clear indication as to whether the cells are alive or not. Therefore, two other aspects of cell viability were be measured – cell metabolism and cell membrane permeability. By measuring cell metabolism using the MTT assay, this may indicate a reduced cell number or if the cells are in a state of senescence, induced by the drugs. Cell membrane permeability was measured by using the Sapphire700 stain, which only stains the cytosol of cells whose membranes are no longer intact and undergoing cell death. Comparisons between the MTT and Sapphire700 results allowed for determining if the hydroxypyridone anti-fungals are cytotoxic at the desired concentrations, or if the drugs induce a state of cell senescence without killing the cells.

4.2. Materials and Methods

4.2.1. Cell culture techniques

Fibroblasts and keratinocytes used in the following experiments were passaged and maintained as previously described in Chapter 2.2.2. and Chapter 2.2.3. The patient fibroblast cell lines used in the following experiments were L10FA1, L11FB1 and L12FB1.

Rhabdomyosarcoma (RD) cells (Sigma Aldrich, UK) were used in this chapter as a positive control in the cell viability assays, as the effect of hydroxypyridone anti-fungals had been previously reported in these cells. RD cells were cultured using DMEM containing 10% FCS and 1% Pen/Strep, and passaged/maintained in a same way to the fibroblasts (previously described in Chapter 2.2.2.2.). Unlike the fibroblasts, RD cells did not required any modifications to its media for seeding or drug treatment – therefore these steps were carried out by using DMEM, containing 10% FCS and 1% Pen/Strep.

4.2.1. Immunocytochemistry (ICC)

Immunocytochemsitry to visual keratinocytes undergoing empithelial-mesenchymal transition (EMT), was carried out as previously described in Chapter 2.2.5. The primary and secondary antibodies used in these experiments can be found below in Table 4-1.

Table 4-1: Primary and secondary antibodies used in ICC.

Antibody		Dilution
Primary antibody	Anti-vimentin raised in mouse (Abcam, UK - cat #ab8069)	1:1,000
	Anti-CK-14 raised in rabbit (Abcam, UK – cat #ab181595)	1:1,000
	Anti-fibronectin raised in mouse (eBioscience, UK – cat # 15228197)	1:1,000
Secondary antibody	Donkey anti-mouse IgG antibody, FITC conjugate (Millipore, UK – cat #AP192F)	1:250
	Donkey anti-rabbit IgG antibody, FITC conjugate (Millipore, UK – cat #AP182F)	1:250

4.2.2. In-Cell ELISA (ICE)

The In-Cell ELISA method was carried out in the fibroblasts as previously described in Chapter 2.2.6. For keratinocytes, these were seeded at a density of 4,000 cells per well into black optical 96-well plates and left to adhere for 24 h in the incubator. The next day, keratinocytes were either given fresh blank media or incubated with media containing 10 ng/mL TGF-β1 and/or the desired compounds. The staining of the keratinocytes for their desired proteins was carried out in the same way as the fibroblasts, as described in Chapter 2.2.6. The primary antibodies used for the In-Cell ELISA in the following experiments can be found below in Table 4-2.

Table 4-2: Primary antibodies used in ICE.

Antibody		Dilution
Primary antibody	Anti-α-SMA raised in mouse (Sigma-Aldrich, UK – cat #A5228)	1:3,000
	Anti-vimentin raised in mouse (Abcam, UK - cat #ab8069)	1:3,000
	Anti-fibronectin raised in mouse (eBioscience, UK – cat # 15228197)	1:1,000

4.2.3. Cell viability assays

4.2.3.1. MTT assay

To determine the effects of the drugs on mitochondrial function, an assay utilising 3-(4,5-dimethylthiazol-2-yl)-2,5-diphenyltetrazolium bromide (MTT) was used. Burn scar fibroblasts, normal skin fibroblasts, keratinocytes, and rhabdomyosarcoma cells were seeded at a density of 4,000 cells per well into clear 96-well plates. The plates were incubated at 37°C and 5% CO_2 overnight, to allow the cells to adhere to the plate. The next day, the media on the cells was swapped for either blank media or media containing the desired TGF-β1 and/or drug concentrations. The plates were incubated for 72 h at 37°C and 5% CO_2. MTT (Sigma Aldrich, UK) was prepared in pre-warmed media, at a concentration of 0.5 mg/mL. The old media was removed from each well and replaced with 100 µl of the MTT solution. The plates were covered with aluminum foil and incubated for 2 h at 37°C and 5% CO_2. The MTT solution was removed from the wells and replaced with 100 µl of acidified isopropanol (8% 1 M HCl in Propan-2-ol) to dissolve the formazan crystals. The plates were incubated on an orbital shaker for 5 min at room temperature. Using the Thermo Scientific MultiSkan FC plate reader, absorbance was read at 540 nm and data analysis carried out using Microsoft Excel. To ensure reproducibility of the assay, a standard curve was generated by carrying out a 1:2 dilution series, seeding cell numbers ranging from 39 – 20,000 cells per well. The day after seeding, the same protocol was carried out as described above. Only R^2 values of 0.9 and above, were considered reliable for interpretation of the generated results.

4.2.3.2. Sapphire700 staining

To determine the effect of the candidate drugs on cell membrane permeability, the Sapphire700 stain (Li-Cor, UK) was used. Sapphire700 stains cytoplasmic proteins of cells with compromised membranes. Burn scar fibroblasts, normal skin fibroblasts, keratinocytes, and RD cells were seeded at a density of 4,000 cells per well into black optical 96-well plates. The plates were incubated at 37°C and 5% CO_2 overnight, to allow the cells to adhere to the plate. The next day, the media was replaced with either blank media or media containing the desired TGF-β1 and/or drug concentrations. The plates were incubated for 72 h at 37°C and 5% CO_2. Following this incubation period, the old media was removed from the wells and 50

µl of the Sapphire700 stain (1:500 dilution, in serum free DMEM) was added to each well. The plates were incubated for 30 min at 37°C and 5% CO_2. The plates were scanned using the Li-Cor Odyssey CLx imager in the 700nm channel.

4.2.4. ECM production assay

Fibroblasts were seeded at a density of 4,000 cells per well into black optical 96-well plates and left to adhere overnight at 37°C and 5% CO_2. The following day, the old media was removed and replaced with either fresh blank media or media containing the desired TGF-β1 and/or drug concentrations. The plates were incubated for 7 days at 37°C and 5% CO_2. Following the incubation period, the old media was removed from each well carefully (to prevent disruption of the ECM) and replaced with 100 µl of DRAQ5 diluted in PBS at a dilution of 1:1,000. The plates were incubated at 37°C and 5% CO_2 for 5 min, before removing the DRAQ5 solution and scanning the plate using the Odyssey CLx imager in the 700nm channel. To lyse the cells, 100 µl of 0.25 M ammonium hydroxide in water was added to each well and incubated at 37°C and 5% CO_2 for 10 min. The ammonium hydroxide was removed from the wells and the plates were washed using PBS. Following this, the ECM was fixed using a solution of 50% methanol and 7.5% acetic acid in distilled water. 100 µl of the fixing solution was added to each well, and incubated for 1 h at -20°C. The fixing solution was removed carefully and each well washed with cold PBS.

The ECM was stained using Coomassie blue (Fisher Scientific, UK) to measure total ECM production. 100 µl of Coomassie Blue was added to each well and the plates incubated for 72 h at 4°C. Following incubation with Coomassie blue, the stain was removed, and the wells were washed carefully using 100 µl cold PBS. The plates were scanned using the Odyssey CLx imager in the 700 nm channel. For data analysis, the Coomassie measurements were normalized to the cell number obtained previously.

4.3. Results

4.3.1. Confirmation of anti-myofibroblast activity in candidate drugs

Before investigating the effect of CPX and CPXO using the secondary assays, confirmation of their ability to prevent myofibroblast transformation was carried out. Both drugs were purchased from a different supplier (Sigma-Aldrich, UK) to the drug library supplier (SelleckChem), and full concentration response curves for both CPX (Lot #Y0000040) and CPXO (Lot #C2162700) were constructed which had been pre-dissolved in DMSO (the vehicle used in the drug screen) and in PBS (as both show good solubility in water). Both drugs were given in co-incubation with 10 ng/mL TGF-β1, with concentrations of each compound ranging from 0.3 µM – 300 µM. Figure 4-1 shows that when pre-dissolved in DMSO, CPX generated an inverse sigmoid curve with both upper and lower plateaus and an IC_{50} of 16.7 ± 2.3 µM. A similar response was also seen when CPX was pre-dissolved in PBS (Fig 4-1), generating an inverse sigmoid curve with both upper and lower plateaus, and an IC_{50} of 17.2 ± 2.5 µM was calculated. Statistical analysis of the IC_{50} for each vehicle showed no significant difference in potencies (p=0.94), when using Student's t-test of unpaired means.

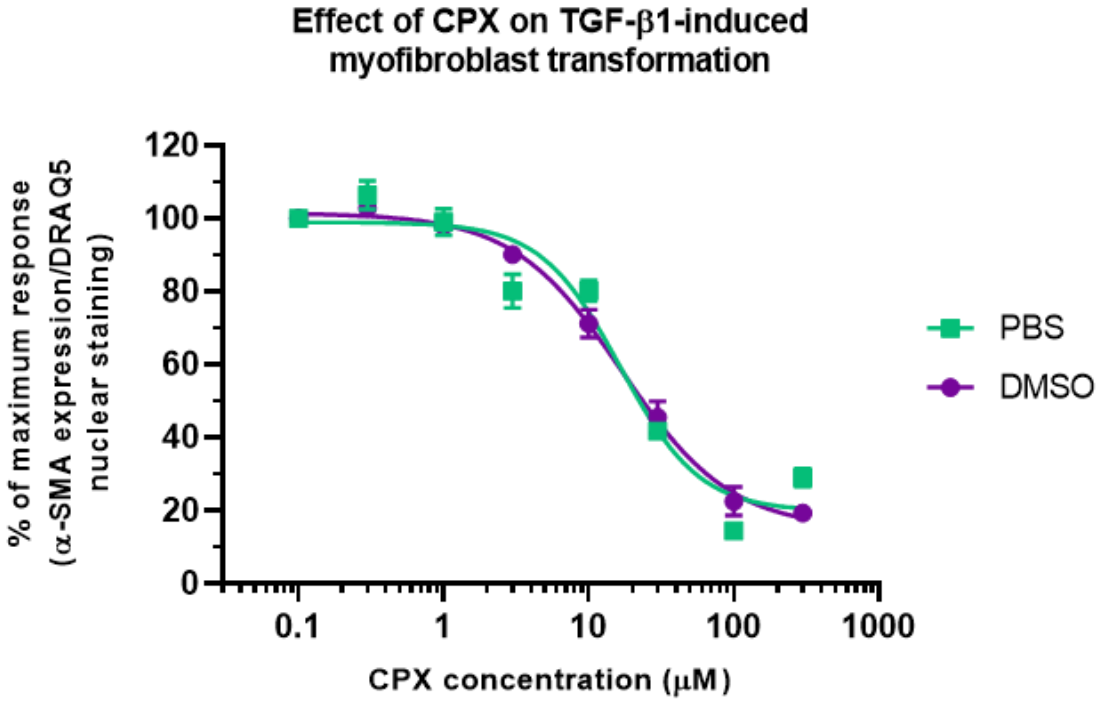

Figure 4-1: Effect of CPX on TGF-β1-induced myofibroblast transformation. A full concentration response curve was generated for CPX, using DMSO and PBS as a vehicle. Burn scar fibroblasts were incubated with 10 ng/mL TGF-β1 and a range of concentrations of CPX (0.1 µM – 300 µM) for 72 h. α-SMA expression was measured using the In-Cell ELISA method. Data points are plotted as average ± SEM, N=3, n=9.

Figure 4-2 shows that when pre-dissolved in DMSO, CPXO did not generate an inverse sigmoid curve and instead exhibited a linear regression, with an IC_{50} of 32.3 ± 3.1 µM. However, when CPXO was pre-dissolved in PBS this generated an inverse sigmoid curve with both upper and lower plateaus, and an IC_{50} of 10.3 µM ± 0.8 µM was calculated. Statistical analysis of the IC_{50} for each vehicle showed a significant difference in potencies ($p<0.001$), when using Student's t-test of unpaired means.

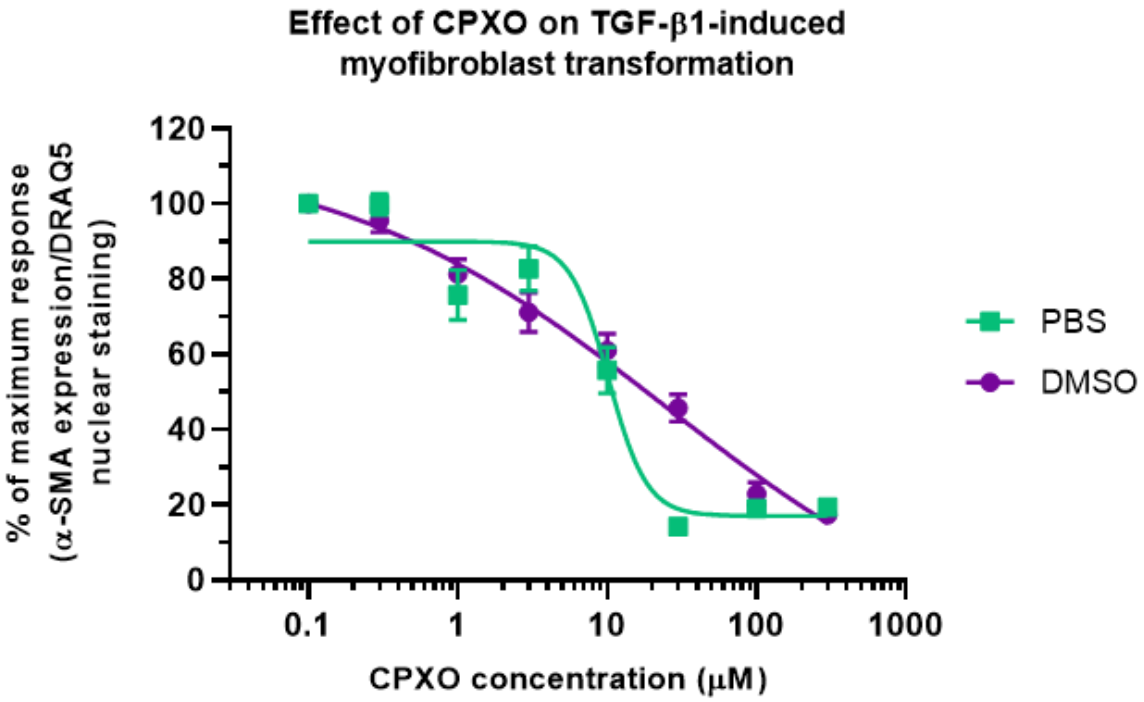

Figure 4-2: Effect of CPXO on TGF-β1-induced myofibroblast transformation. A full concentration response curve was generated for CPXO, using DMSO and PBS as a vehicle. Burn scar fibroblasts were incubated with 10 ng/mL TGF-β1 and a range of concentrations of CPXO (0.1 µM – 300 µM) for 72 h, before measuring α-SMA expression using the In-Cell ELISA method. Data points are plotted as average ± SEM, N=3, n=9.

To identify if the anti-myofibroblast activity seen in CPX and CPXO was an individual drug effect or an effect seen in the whole drug class of hydroxypyridone anti-fungals, another hydroxypyridone anti-fungal piroctone olamine (Octopirox; OPX) was purchased from Sigma Aldrich (Lot #BCBZ5087). Full concentration response curves for OPX (pre-dissolved in DMSO and PBS) were constructed, with OPX given in co-incubation with 10 ng/mL TGF-β1. OPX concentrations ranged from 0.03 µM to 100 µM. When dissolved in both DMSO and PBS (Fig 4-3) OPX generated an inverse sigmoid curve with both upper and lower plateaus, and IC_{50} values of 1.4 ± 0.1 µM and 2.0 ± 0.6 µM, respectively, could be calculated. Statistical analysis of the IC_{50} for each vehicle showed no significant difference in potencies (p=0.32), when using Student's t-test of unpaired means.

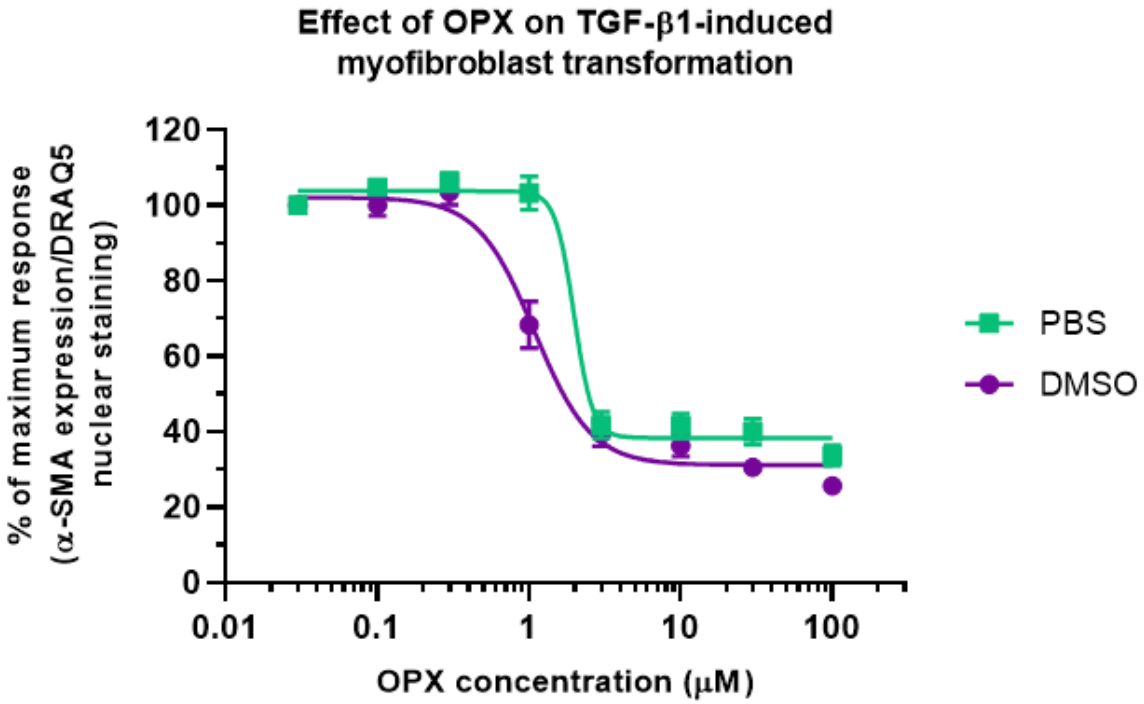

Figure 4-3: Effect of OPX on TGF-β1-induced myofibroblast transformation. A full concentration response curve was generated for OPX, using both DMSO and PBS as a vehicle. Burn scar fibroblasts were incubated with 10 ng/mL TGF-β1 and a range of concentrations of OPX (0.03 µM – 100 µM) for 72 h, before measuring α-SMA expression using the In-Cell ELISA method. Data points are plotted as average ± SEM, where N=3, n=9.

Table 4-3 shows an overview of the IC_{50} for each drug in both DMSO and PBS. For the secondary assays, it was decided that the vehicle used for each drug would be the one that the drug showed the highest potency. Therefore, CPX and OPX were pre-dissolved in DMSO and CPXO was pre-dissolved in PBS.

Table 4-3: IC_{50} of hydroxypyridone anti-fungals, to determine effect on α-SMA expression when dissolved in different vehicles.

Drug name	Vehicle	IC_{50}
Ciclopirox (CPX)	DMSO	16.7 ± 2.3 µM
	PBS	17.3 ± 2.5 µM
Ciclopirox ethanolamine (CPXO)	DMSO	32.3 ± 3.1 µM
	PBS	10.3 ± 0.8 µM
Piroctone olamine (OPX)	DMSO	1.4 ± 0.1 µM
	PBS	2.0 ± 0.6 µM

4.3.2. Effect of candidate drugs on aspects of cell viability

To confirm if the anti-fibrotic effect observed is due to increased cell toxicity, cell viability was investigated by measuring mitochondrial function and cell membrane permeability. To measure mitochondrial function, the 3-(4,5-dimethylthiazol-2-yl)-2,5-diphenyl tetrazolium bromide (MTT) assay was utilized, and standard curves generated for each cell type used. For this, the cells were seeded on a 96-well plate by carrying out a 1:2 serial dilution, starting at 39 cells per well and finishing at 20,000 cells per well. The standard curves were generated by measuring the absorbance at 540nm, with the curve for each cell line obtaining an R^2 of >0.9.

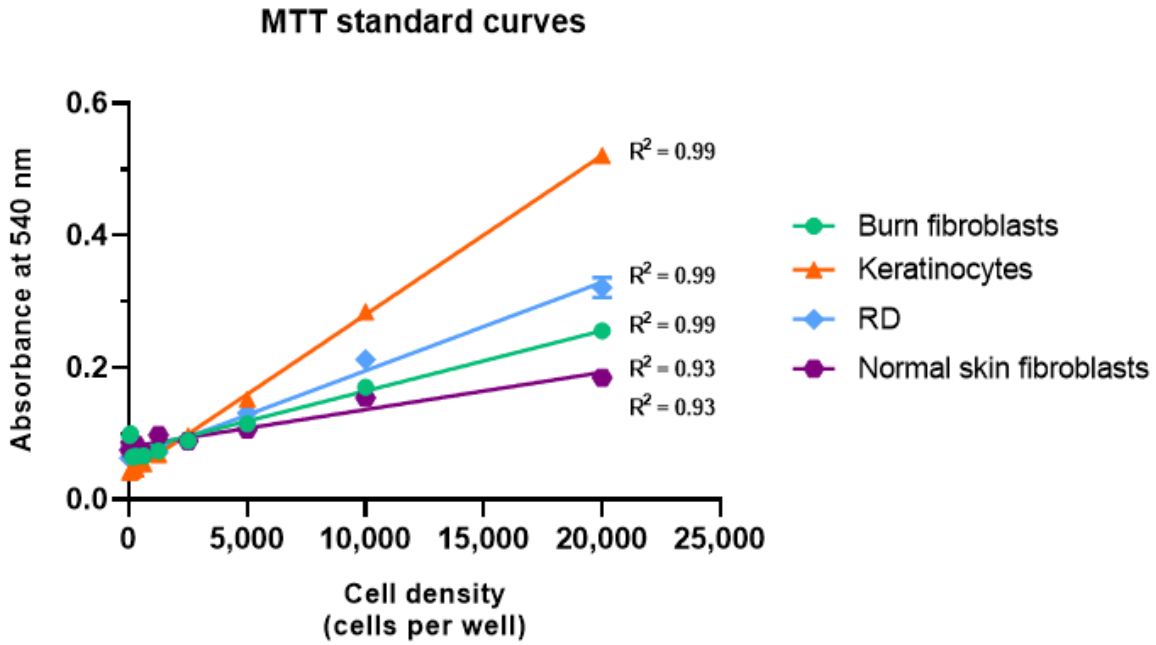

Figure 4-4: Standard curves used for MTT assay. Burn scar derived fibroblasts, keratinocytes, RD cells and fibroblasts derived from normal skin, were seeded into a 96-well plate at varying cell densities (39 – 20,000 cells per well). This was used to generate a standard curve by measuring absorbance at 540nm wavelength. Each standard curve generated an $R^2 > 0.9$.

To observe the effect of the hydroxypyridone anti-fungals on mitochondrial function, each cell type was treated with CPX, CPXO and OPX, in presence and absence of TGF-β1. Concentration response curves for each drug were constructed with concentrations ranging from 0.1 µM – 300 µM for CPX and CPXO, and 0.03 µM – 100 µM for OPX. The IC_{50} and E_{max} (maximum inhibition of mitochondrial function) for each drug (with and without TGF-β1) was calculated and summarized in Table 4-4, 4-5 and 4-6.

Following treatment with CPX only (Fig 4-5A) burn scar fibroblasts and normal skin fibroblasts showed maximum inhibition of mitochondrial function at approximately 40%. In keratinocytes and RD cells CPX showed maximum inhibition at approximately 85% and showed higher potency than in the fibroblast cell lines. When applied in co-incubation with TGF-β1 (Fig 4-5B), the potency of CPX was not affected in burn fibroblasts and keratinocytes. CPX showed greater potency in normal skin fibroblasts and lower potency in RD cells. Maximum inhibition of CPX in the fibroblast cell lines was not affected by co-incubation with TGF-β1, however in keratinocytes and RD cells maximum inhibition was reduced by 20%.

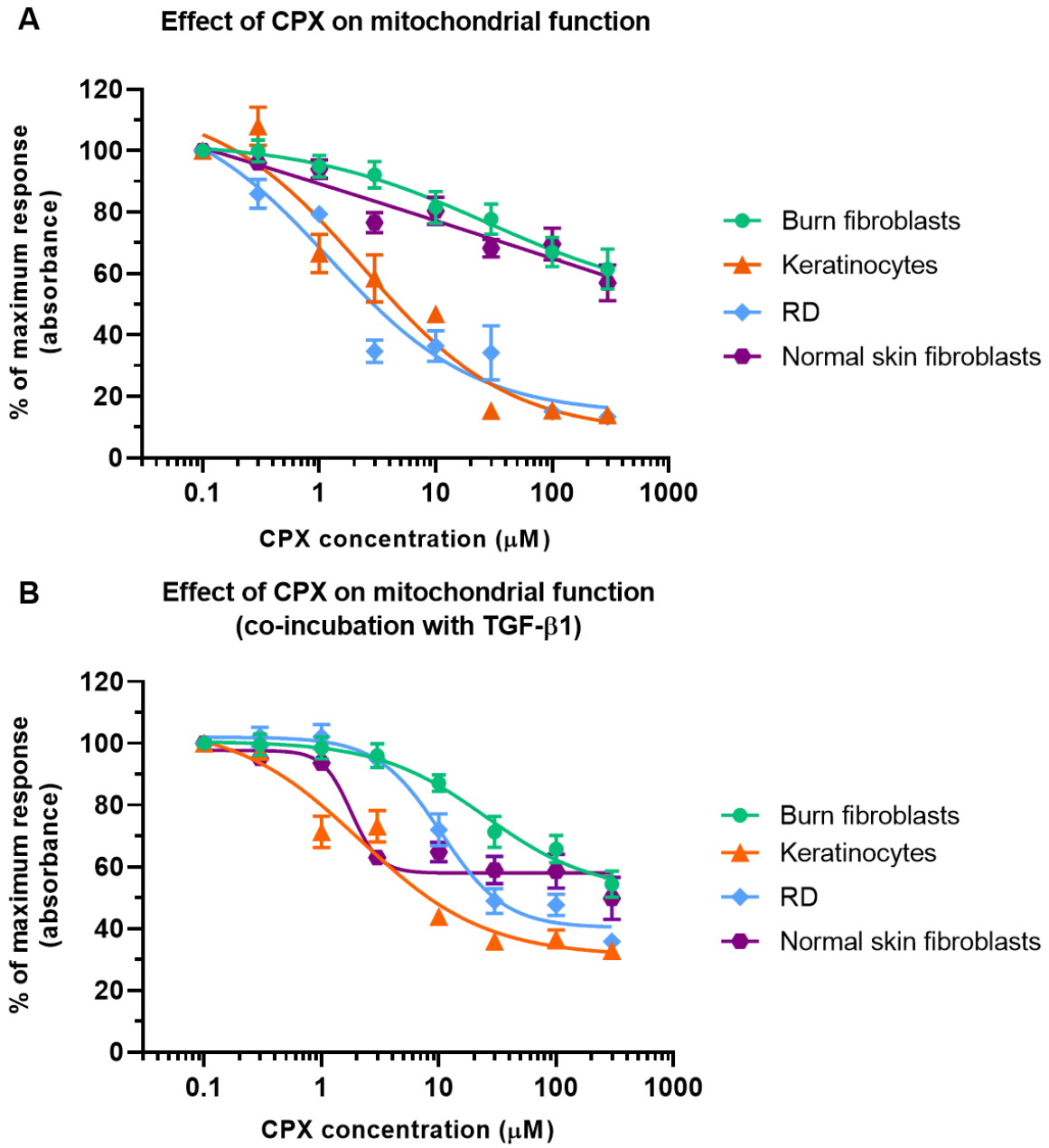

Figure 4-5: Effect of CPX on mitochondrial function when cells are A) untreated and B) treated with 10 ng/mL TGF-β1. A full concentration response curve was generated for CPX, where cells were treated with a range of concentrations of CPX (0.1 μM – 300 μM). Data points are plotted as average ± SEM, where N=3, n=9.

Table 4-4: IC_{50} and E_{Max} of CPX (with and without TGF-β1) when measuring for mitochondrial function.

Cell type	No TGF-β1		10 ng/mL TGF-β1	
	IC_{50}	E_{Max}	IC_{50}	E_{max}
Burn fibroblasts	36.4 ± 12.7 µM	49.8 ± 6.1%	22.4 ± 7.4 µM	48.0 ± 8.1%
RD cells	1.2 ± 0.8 µM	85.8 ± 7.4%	0.4 ± 0.6 µM	59.7 ± 2.8%
Keratinocytes	2.3 ± 1.1 µM	91.8 ± 8.7%	2.1 ± 0.7 µM	68.9 ± 4.6%
Normal skin fibroblasts	31.3 ± 7.2 µM	42.9 ± 4.7%	1.7 ± 0.2 µM	42.0 ± 2.1%

Treatment with CPXO only, exhibited a higher potency and maximum inhibition in keratinocytes and RD cells, compared to the fibroblast cell lines (Fig 4-6A). Further, treatment with CPXO only was more potent in the two fibroblast cell lines, compared to CPX only. In co-incubation with TGF-β1 (Figure 4-6B), CPXO had no effect on the potency and maximum inhibition in burn fibroblasts. In the normal skin fibroblasts, CPXO was less potent but increased maximum inhibition of mitochondrial function by 20% (Table 4-5). In the keratinocyte and RD cells, when applied in co-incubation with TGF-β1, CPXO exhibited reduced potency and the maximum inhibition was also decreased by approximately 20% (Table 4-5).

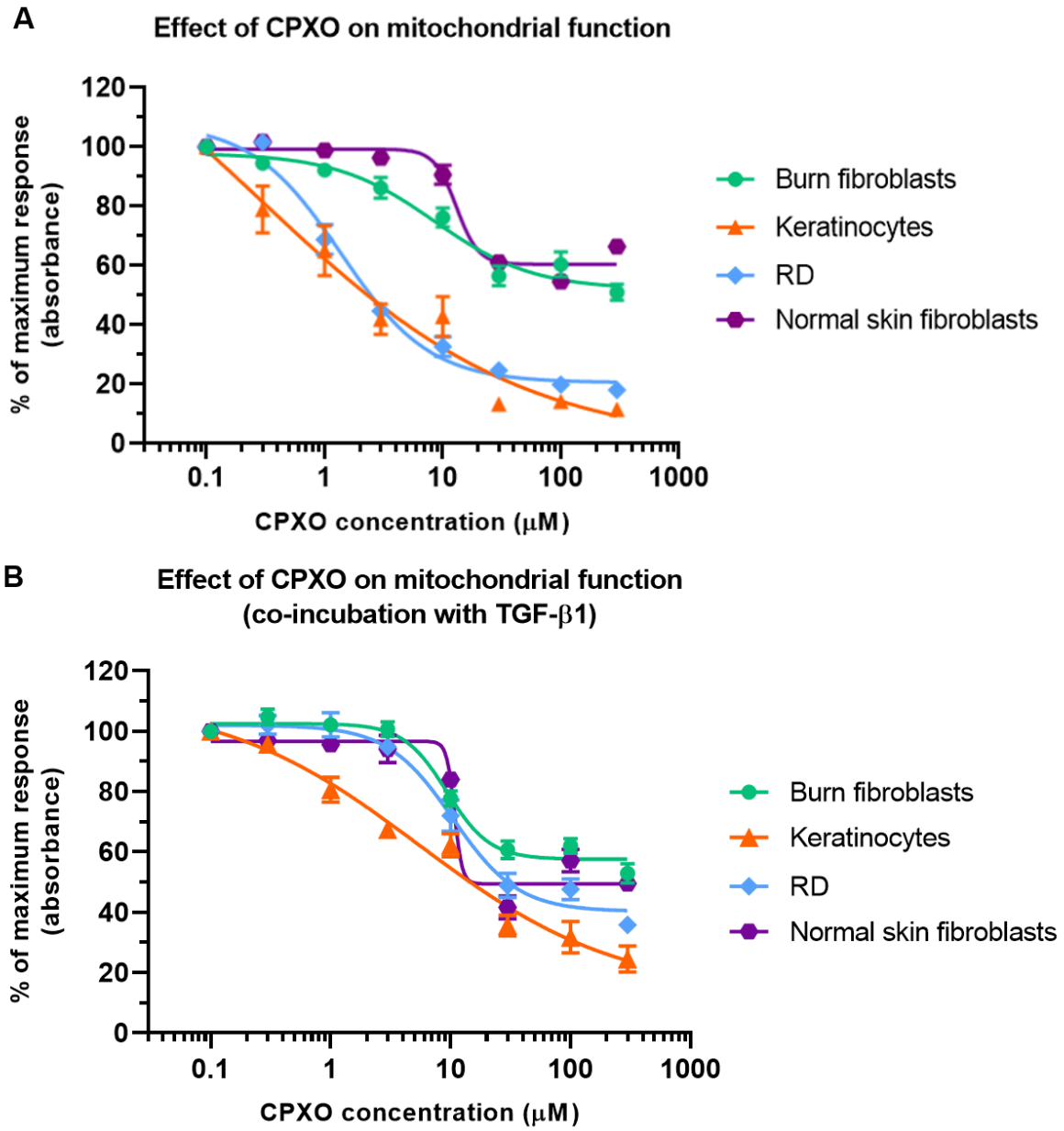

Figure 4-6: Effect of CPXO on mitochondrial function when cells are A) untreated and B) treated with 10 ng/mL TGF-β1. A full concentration response curve was generated for CPXO, where cells were treated with a range of concentrations of CPXO (0.1 μM – 300 μM). Data points are plotted as average ± SEM, where N=3, n=9.

Table 4-5: IC_{50} and E_{Max} of CPXO (with and without TGF-β1) when measuring for mitochondrial function.

Cell type	No TGF-β1		10 ng/mL TGF-β1	
	IC_{50}	E_{Max}	IC_{50}	E_{Max}
Burn fibroblasts	8.5 ± 1.8 µM	47.9 ± 3.4%	9.2 ± 0.8 µM	42.4 ± 1.73%
RD cells	1.3 ± 0.1 µM	79.4 ± 2.2%	10.4 ± 1.4 µM	59.7 ± 2.8%
Keratinocytes	0.31 ± 1.0 µM	100.8 ± 19.5%	5.5 ± 2.1 µM	86.8 ± 13.1%
Normal skin fibroblasts	10.3 ± 1.9 µM	30.1 ± 3.4%	34.1 ± 13.5 µM	50.5 ± 2.6%

Following treatment with OPX only (Fig 4-7A), a similar response to CPX and CPXO was noted in the keratinocytes and RD cells, whereby OPX exhibited greater maximum inhibition of mitochondrial function and was more potent in these cells. In the fibroblast cell lines the maximum inhibition exhibited by OPX was also similar to CPX and CPXO with approximately 30-40% inhibition seen. When applied in co-incubation with TGF-β1, the potency of OPX in RD cells and keratinocytes remained unchanged, however the maximum inhibition of mitochondrial function was reduced by approximately 20% and 10%, respectively (Table 4-6). In the fibroblast cell lines, OPX exhibited greater potency and maximum inhibition of mitochondrial function (increase of approximately 16-20%; Table 4-6).

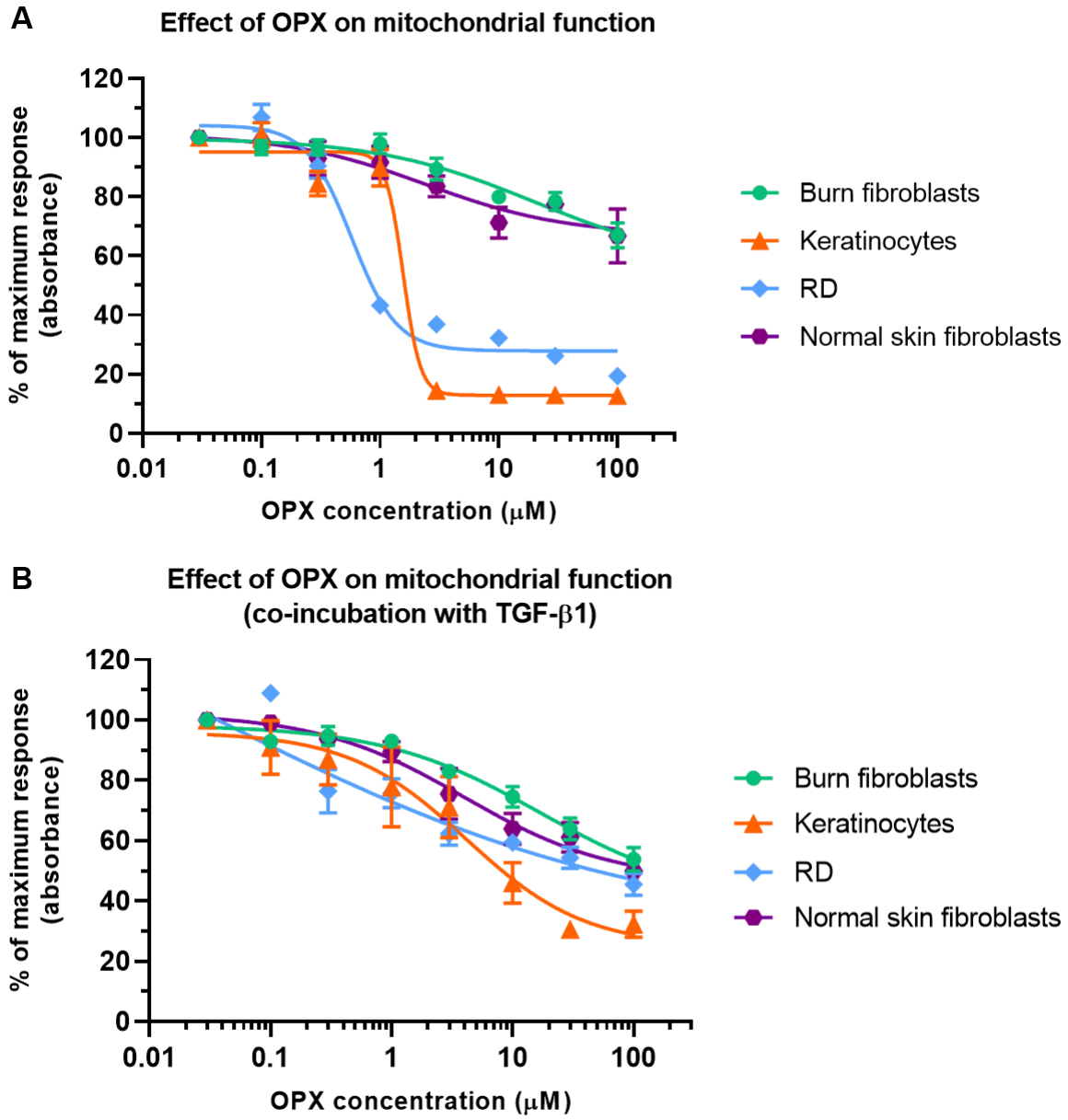

Figure 4-7: Effect of OPX on mitochondrial function when cells are A) untreated and B) treated with 10 ng/mL TGF-β1. A full concentration response curve was generated for OPX, where cells were treated with a range of concentrations of OPX (0.03 μM – 100 μM). Data points are plotted as average ± SEM, where N=3, n=9.

Table 4-6: IC_{50} and E_{Max} of OPX (with and without TGF-β1) when measuring for mitochondrial function.

Cell type	No TGF-β1		10 ng/mL TGF-β1	
	IC_{50}	E_{Max}	IC_{50}	E_{Max}
Burn fibroblasts	20.2 ± 3.6 µM	43.6 ± 3.2%	6.1 ± 1.4 µM	59.8 ± 17.0%
RD cells	0.5 ± 0.1 µM	72.1 ± 2.0%	0.5 ± 0.3 µM	54.5 ± 2.3%
Keratinocytes	2.1 ± 0.3 µM	87.1 ± 2.3%	4.2 ± 2.1 µM	75.1 ± 12.6%
Normal skin fibroblasts	8.5 ± 1.2 µM	32.9 ± 8.9%	4.0 ± 2.3 µM	53.4 ± 9.5%

The second aspect of cell viability that was measured was cell membrane permeability, carried out by using the LiCor Sapphire700 stain. Sapphire700 accumulates in the cytoplasm and nucleus of cells with a compromised membrane. To observe the effect of the hydroxypyridone anti-fungals on cell membrane permeability, each cell type was treated with CPX, CPXO and OPX, with and without TGF-β1 treatment. Concentration response curves for each drug were constructed with concentrations ranging from 0.1 µM – 300 µM for CPX and CPXO, and 0.03 µM – 100 µM for OPX. The IC_{50} and E_{max} for the following figures are summarized in Tables 4-7, 4-8 and 4-9.

CPX exhibited similar responses in each cell line, regardless of whether it was used on its own or in co-incubation with TGF-β1 (Figure 4-8). Furthermore, CPX was shown to have similar potencies across the different cell lines and remained unaffected by TGF-β1 treatment. CPX decreased cell membrane permeability in keratinocytes, by 15-20%. The greatest effect could be observed in the fibroblast cell lines, with a 40-50% increase in cell membrane permeability.

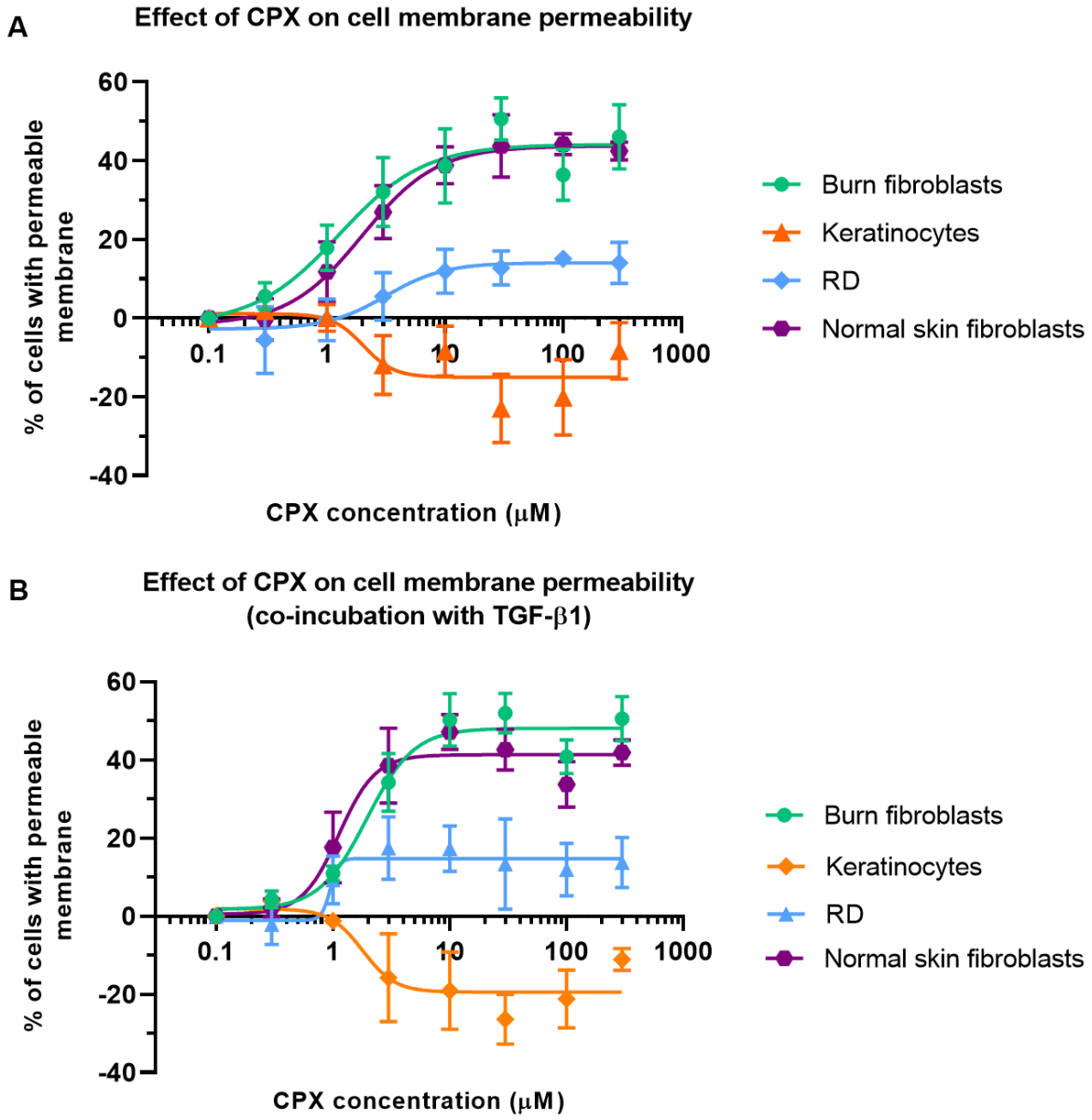

Figure 4-8: Effect of CPX on cell membrane permeability when cells are A) untreated and B) TGF-β1 treated. A full concentration response curve was generated for CPX, where cells were treated with a range of concentrations of CPX (0.1 μM – 300 μM). Data points are plotted as average ± SEM, where N=3, n=9.

Table 4-7: IC_{50} and E_{Max} of CPX (with and without TGF-β1) when measuring for cell membrane permeability.

Cell type	No TGF-β1		10 ng/mL TGF-β1	
	IC_{50}	**E_{Max}**	**IC_{50}**	**E_{max}**
Burn fibroblasts	2.1 ± 1.0 µM	44.1 ± 4.2%	1.8 ± 0.4 µM	48.1 ± 2.5%
RD cells	1.5 ± 0.9 µM	14.1 ± 2.9%	0.7 ± 0.1 µM	14.7 ± 3.0%
Keratinocytes	3.5 ± 1.0 µM	-15.0 ± 3.2%	3.2 ± 1.2 µM	-19.4 ± 3.2%
Normal skin fibroblasts	2.1 ± 0.5 µM	43.7 ± 3.1%	1.1 ± 0.2 µM	41.3 ± 4.5%

CPXO also exhibited similar responses in each cell line, regardless of whether it was used on its own or in co-incubation with TGF-β1 (Figure 4-9). CPXO was shown to have the greatest effect in the fibroblast cell lines, with normal skin fibroblasts having the highest percentage of cells with a permeable membrane at approximately 58%. CPXO also exhibited a similar effect on keratinocytes as CPX did, in which the number of cells with a permeable membrane was decreased by 19% (CPXO only) and 27% (+10 ng/mL TGF-β1).

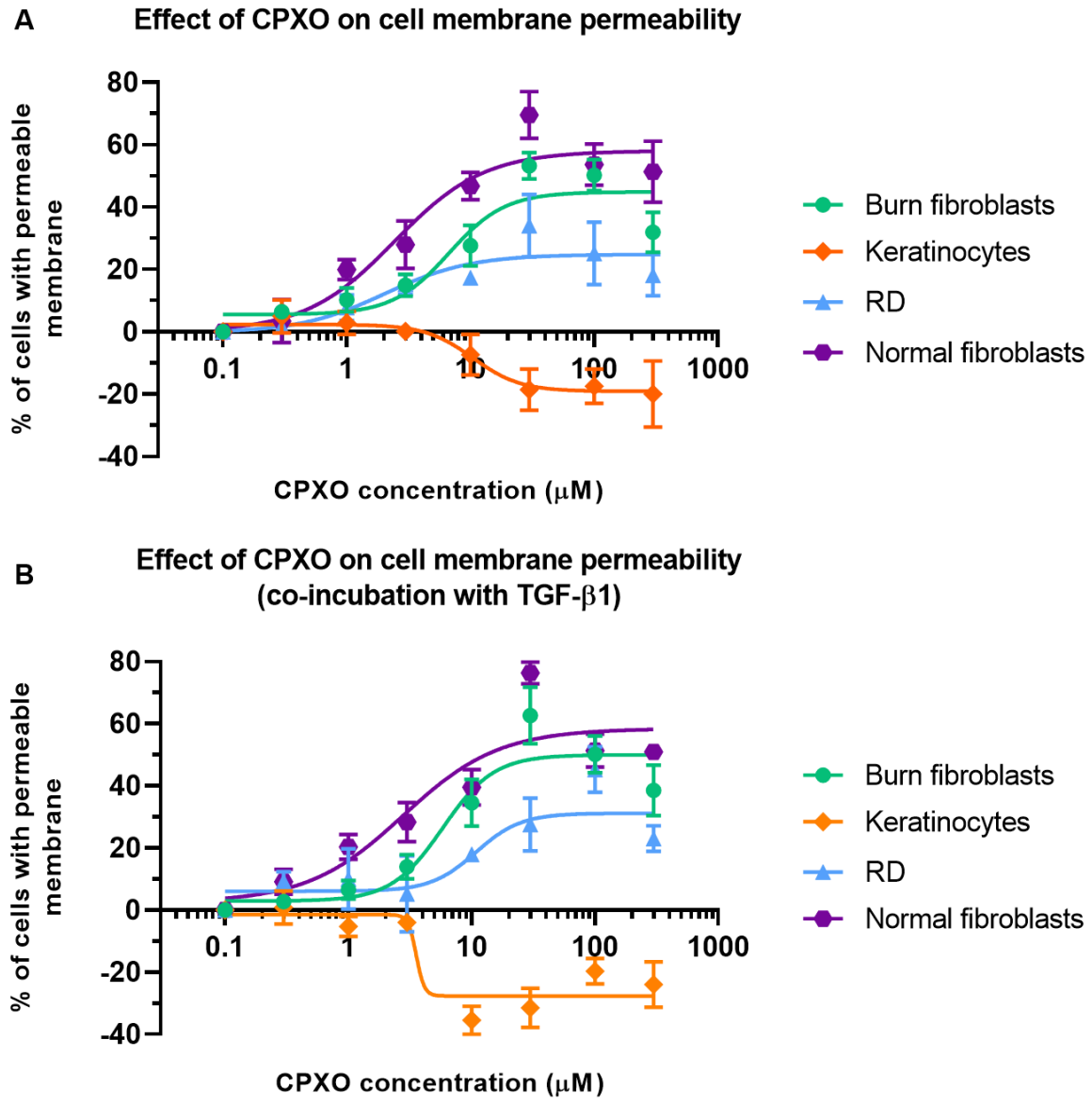

Figure 4-9: Effect of CPXO on mitochondrial function when cells are A) untreated and B) treated with 10 ng/mL TGF-β1. A full concentration response curve was generated for CPXO, where cells were treated with a range of concentrations of CPXO (0.1 μM – 300 μM). Data points are plotted as average ± SEM, where N=3, n=9.

Table 4-8: IC_{50} and E_{Max} of CPXO (with and without TGF-β1) when measuring for cell membrane permeability.

Cell type	No TGF-β1		10 ng/mL TGF-β1	
	IC_{50}	**E_{Max}**	**IC_{50}**	**E_{Max}**
Burn fibroblasts	5.2 ± 1.2 µM	44.8 ± 3.3%	4.6 ± 1.1 µM	50.0 ± 3.9%
RD cells	0.6 ± 0.9 µM	24.8 ± 4.1%	0.3 ± 0.2 µM	31.1 ± 5.2%
Keratinocytes	11.8 ± 0.7 µM	-19.1 ± 3.7%	3.6 ± 0.5 µM	-27.6 ± 2.9%
Normal skin fibroblasts	2.1 ± 0.9 µM	58.0 ± 5.1%	2.8 ± 1.3 µM	58.4 ± 5.5%

The potency of OPX was shown to differ across the different cell lines, dependent on presence or absence of TGF-β1 (Figure 4-10). OPX is more potent in co-incubation with TGF-β1, in both fibroblast cell lines. In the burn fibroblasts the percentage of cells with a permeable membrane was similar between the two treatment groups, whereas in the normal skin fibroblasts, treatment with OPX only increased the percentage of permeable cells by 12%. OPX also exhibited the same effect on keratinocytes, in which the percentage of cells with a permeable membrane was decreased by approximately 15% in both treatment groups.

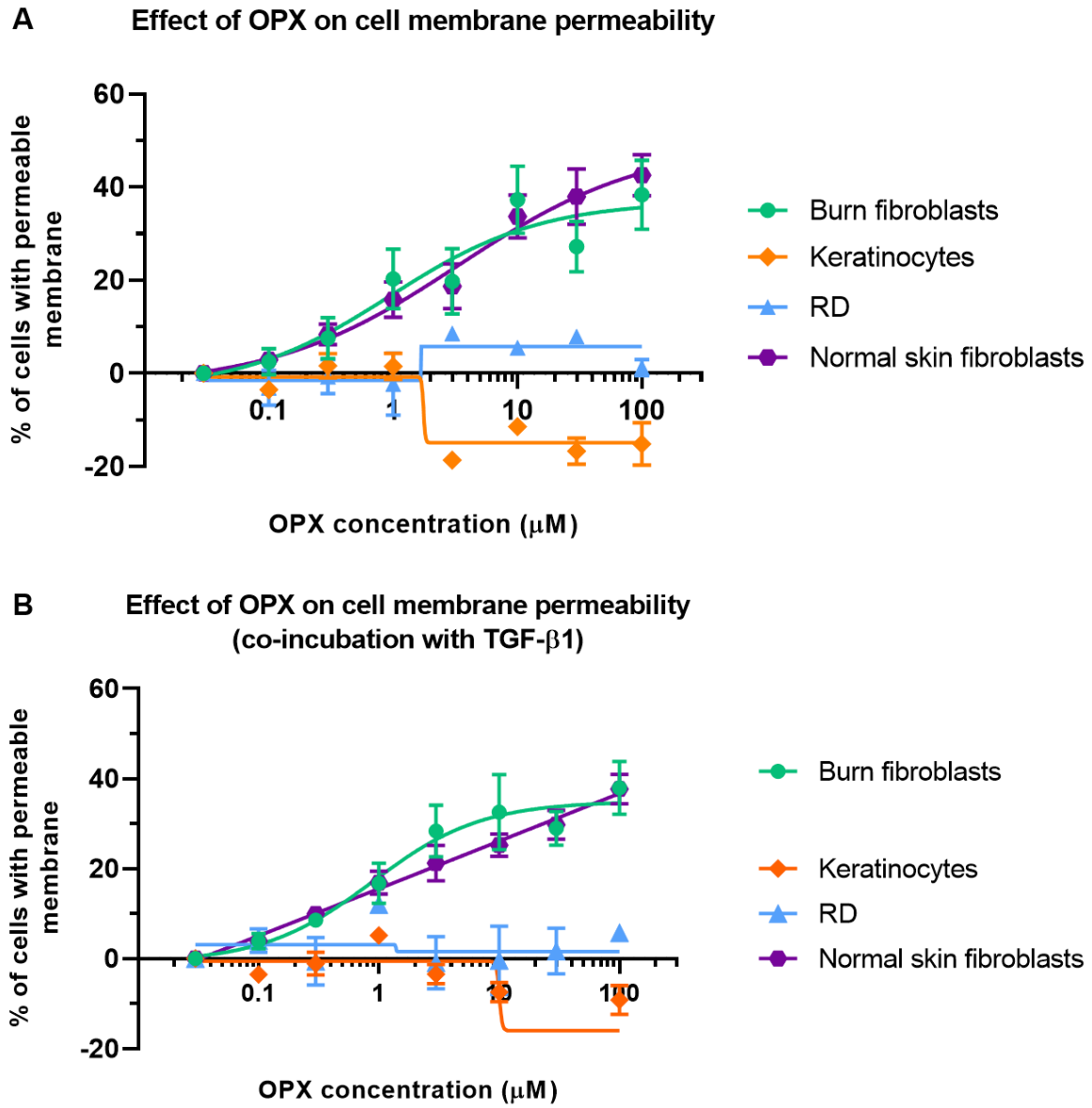

Figure 4-10: Effect of OPX on cell membrane permeability when cells are A) untreated and B) treated with 10 ng/mL TGF-β1. A full concentration response curve was generated for OPX, where cells were treated with a range of concentrations of OPX (0.03 μM – 100 μM). Data points are plotted as average ± SEM, N=3, n=9.

Table 4-9: IC_{50} and E_{Max} of OPX (with and without TGF-β1) when measuring for cell membrane permeability.

Cell type	No TGF-β1		10 ng/mL TGF-β1	
	IC_{50}	**E_{max}**	**IC_{50}**	**E_{Max}**
Burn fibroblasts	1.8 ± 1.2 µM	37.0 ± 7.8%	1.1 ± 4.6 µM	34.9 ± 3.9%
RD cells	0.1 ± 0.7 µM	5.7 ± 1.5%	N/A	1.5 ± 2.4%
Keratinocytes	2.3 ± 1.3 µM	-14.9 ± 1.3%	5.4 ± 4.1µM	-16.0 ± 2.3%
Normal skin fibroblasts	2.5 ± 1.9 µM	49.5 ± 12.1%	2.2 ± 2.1 µM	37.7 ± 2.6%

4.3.3. Effect of candidate drugs on keratinocyte EMT

Another phenotype associated with dermal scarring is excessive keratinocyte EMT. In the presence of TGF-β1, keratinocytes adopt a migratory phenotype and start to express mesenchymal markers (Stone et al., 2016). To confirm that TGF-β1 induced these phenotypic changes, keratinocytes were treated with varying concentrations of TGF-β1 (0.01 ng/mL – 30 ng/mL) and full concentration response curves were constructed for the EMT markers fibronectin and vimentin (Fig 4-11). This generated sigmoid curves for both markers, with both upper and lower plateaus. Maximum expression was at seen at 3 ng/mL for fibronectin and at 10 ng/mL for vimentin, where an EC_{50} of 0.77 ± 0.08 µM was calculated for fibronectin and an EC_{50} of 2.52 ± 0.22 µM was calculated for vimentin.

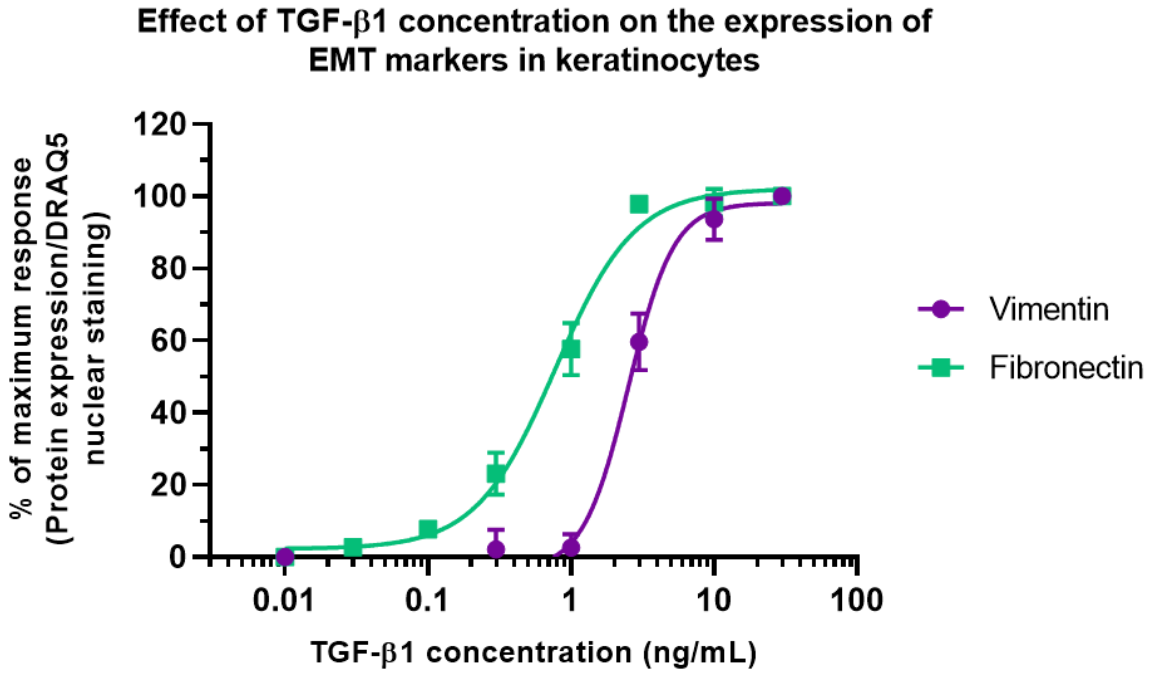

Figure 4-11: Effect of TGF-β1 concentration on expression of EMT markers in keratinocytes. Keratinocytes were incubated with TGF-β1 at varying concentrations (0.01 – 30 ng/mL) for 72 h, before measuring fibronectin and vimentin expression using the In-Cell ELISA method. Data points are plotted as average ± SEM of the percentage of maximum TGF-β1 response, where N=1, n=3.

To further confirm these phenotypic changes, ICC was used to visualize fibronectin (Fig 4-12) and vimentin (Fig 4-13) expression in keratinocytes treated with 10 ng/mL TGF-β1 (to ensure maximum EMT) for 72 h. As well as staining for the markers of interest, the cells were also stained for CK-14 to visualise the cell morphology. Figure 4-12B shows that in the presence of TGF-β1 keratinocytes lose their typical cobblestone morphology and start to lay down extracellular matrix in the form of fibronectin.

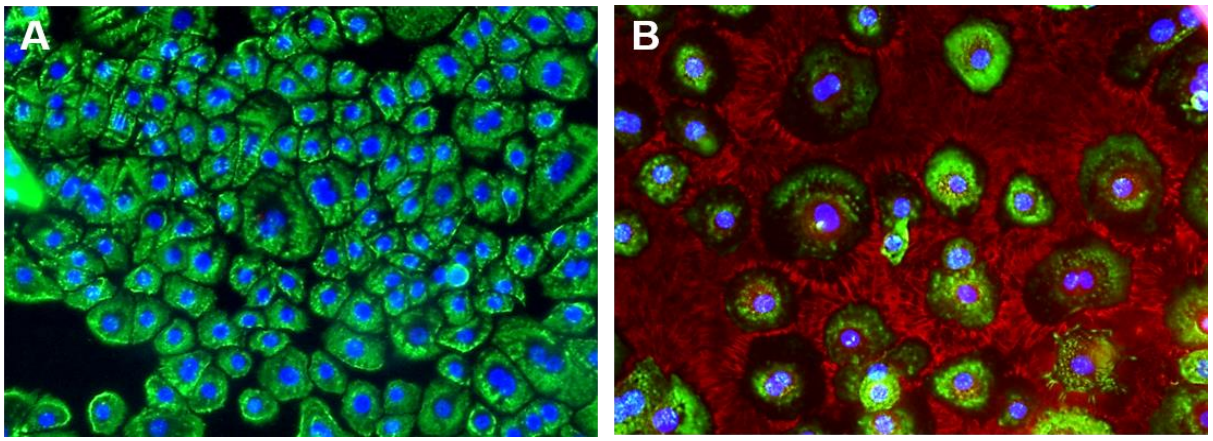

Figure 4-12: Immunocytochemical staining of keratinocytes for fibronectin and CK-14 expression. A) untreated keratinocytes and B) keratinocytes treated with 10 ng/mL TGF-β1 for 72 h. Nuclei were stained with DAPI (blue), CK-14 positive cells stained green, and fibronectin was stained red. Images were obtained using 100X magnification.

Vimentin expression in keratinocytes in the presence or absence of TGF-β1 was visualised in Figure 4-13B. This further confirms that in the presence of TGF-β1, keratinocytes not only lose their cobblestone like morphology, but the individual cells show a more rounded shape. Further, vimentin expression in keratinocytes was only seen in the TGF-β1-treated keratinocytes.

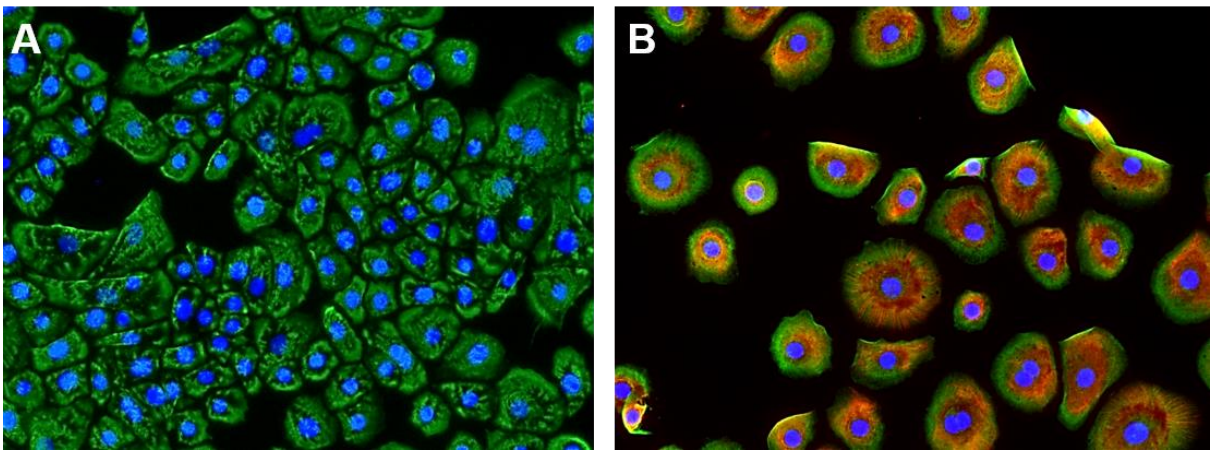

Figure 4-13: Immunocytochemical staining of keratinocytes for vimentin and CK-14 expression. A) untreated keratinocytes and B) keratinocytes treated with 10 ng/mL TGF-β1 for 72 h. Cell nuclei were stained with DAPI (blue), CK-14 positive cells stained green, and vimentin was stained red. Images obtained using 100X magnification.

To identify if drug-induced inhibition of keratinocyte EMT could be achieved, a concentration response curve for SB-505124 was constructed for both fibronectin and vimentin expression (Fig 4-14). SB-505124 was applied in co-incubation with 10 ng/mL TGF-β1, with concentrations ranging from 0.03 µM – 100 µM. This generated an inverse sigmoid curve for both fibronectin and vimentin, with both upper and lower plateaus. An IC_{50} of 1.2 ± 0.6 µM was calculated for fibronectin, and an IC_{50} of 1.0 ± 0.5 µM was calculated for vimentin.

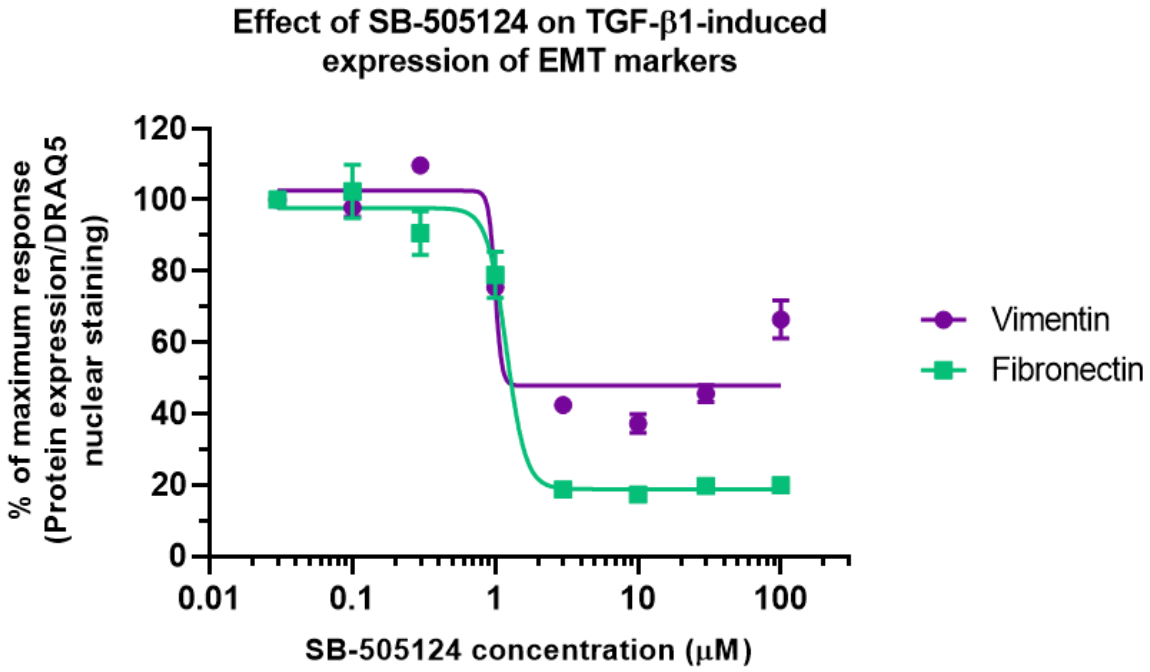

Figure 4-14: Effect of SB-505124 on TGF-β1-induced expression of EMT markers. Keratinocytes were co-treated with 10 ng/mL TGF-β1 and a range of SB-505124 concentrations (0.03 µM – 100 µM) for 72 h, before measuring fibronectin and vimentin expression using the In-Cell ELISA method. A full concentration response curve was generated for both vimentin and fibronectin expression. Data points are plotted as average ± SEM of the percentage of maximum response, where N=1, n=3.

Following this, the effect of the hydroxypyridone anti-fungals on keratinocyte EMT were investigated by constructing concentration response curves for CPX, CPXO and OPX. All three drugs were applied in co-incubation with 10 ng/mL TGF-β1, with concentrations ranging from 0.1 µM – 300 µM for CPX and CPXO, and 0.03 µM – 100 µM for OPX. Following the 72 h incubation with the drugs, expression of fibronectin and vimentin was measured using ICE analysis. Figure 4-15 shows the constructed concentration response curves for CPX, which generated an inverse sigmoid curve for both fibronectin and vimentin, with upper and lower plateaus. An IC_{50} of 1.5 ± 0.2 µM was calculated for fibronectin expression and an IC_{50} of 17.7 ± 3.2 µM was calculated for vimentin expression.

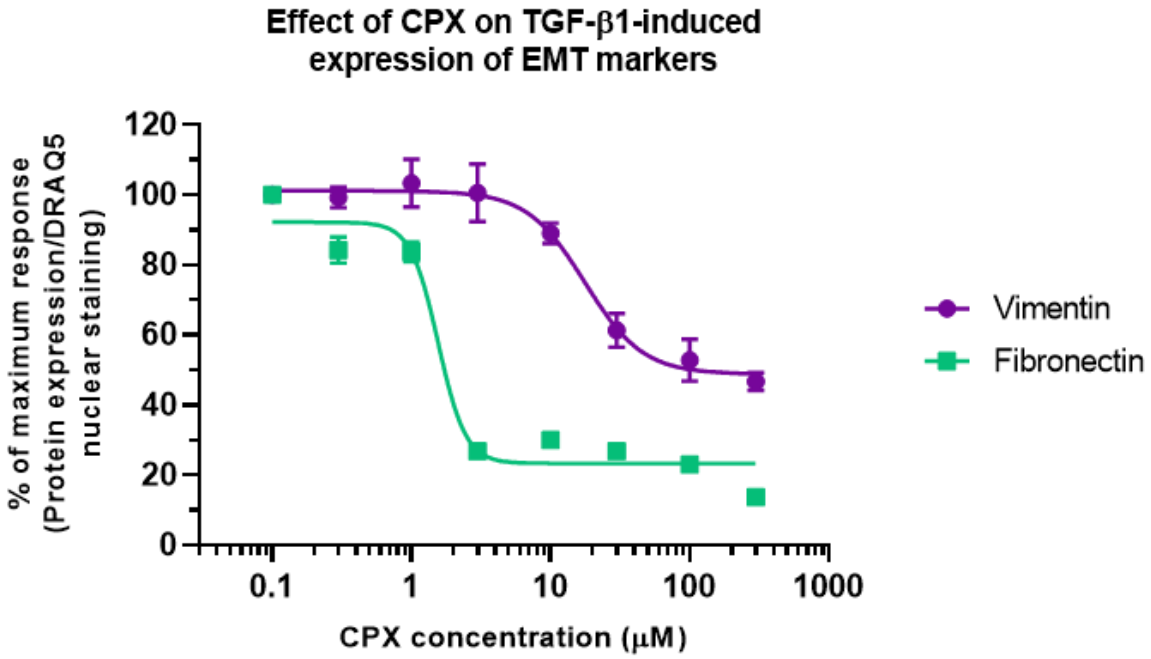

Figure 4-15: Effect of CPX on TGF-β1-induced keratinocyte EMT. A full concentration response curve was generated for CPX, where keratinocytes were incubated with 10 ng/mL TGF-β1 and a range of concentrations of CPX (0.1 µM – 300 µM) for 72 h, before measuring fibronectin and vimentin expression using the In-Cell ELISA method. Data points are plotted as average ± SEM, where N=1, n=3.

Figure 4-16 shows the constructed concentration response curves for CPXO, which generated an inverse sigmoid curve for both fibronectin and vimentin, with upper and lower plateaus. An IC_{50} of 14.4 ± 2.6 µM was calculated for fibronectin expression and an IC_{50} of 21.8 ± 6.9 µM was calculated for vimentin expression.

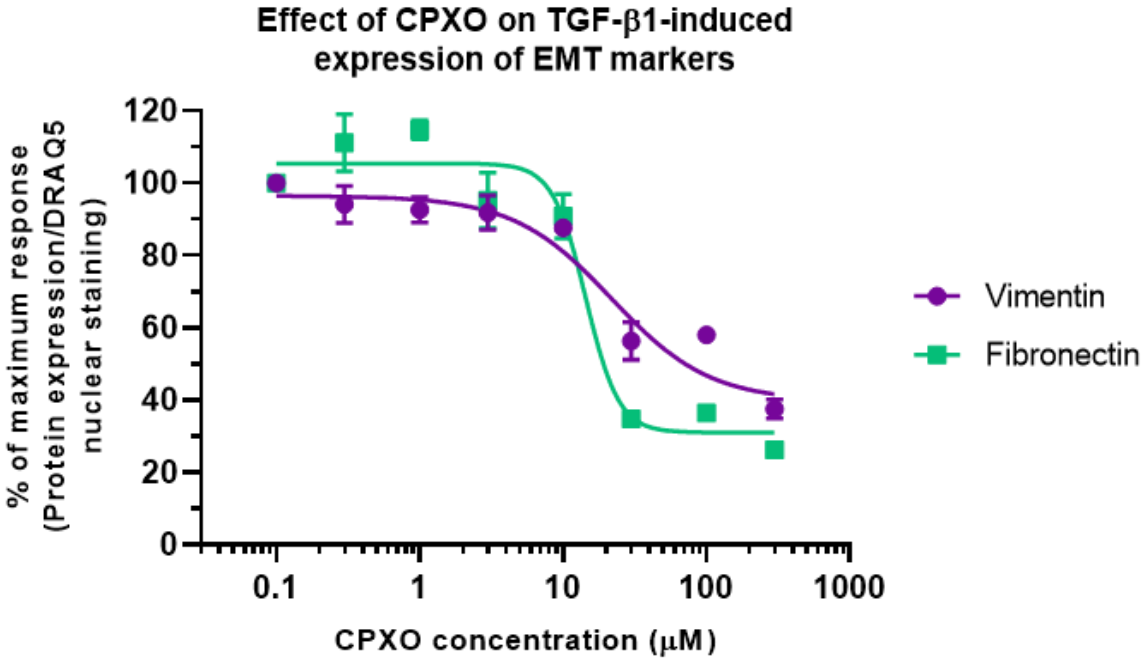

Figure 4-16: Effect of CPXO on TGF-β1-induced keratinocyte EMT. A full concentration response curve was generated for CPXO, where keratinocytes were incubated with 10 ng/mL TGF-β1 and a range of concentrations of CPXO (0.1 µM – 300 µM) for 72 h, before measuring fibronectin and vimentin expression using the In-Cell ELISA method. Data points are plotted as average ± SEM, where N=1, n=3.

Finally, Figure 4-17 shows the constructed concentration response curves for OPX, which generated an inverse sigmoid curve for both fibronectin and vimentin, with upper and lower plateaus. An IC_{50} of 11.1 ± 1.6 µM was calculated for fibronectin expression and an IC_{50} of 9.5 ± 4.1 µM of was calculated for vimentin expression.

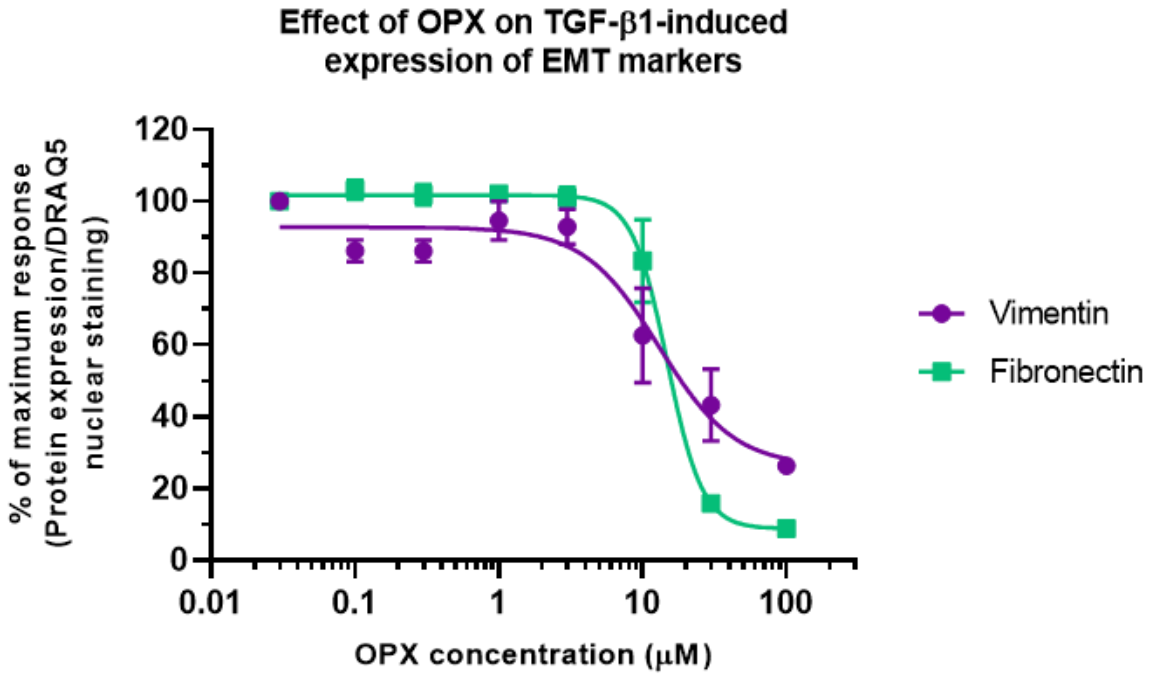

Figure 4-17: Effect of OPX on TGF-β1-induced keratinocyte EMT. A full concentration response curve was generated for OPX, where keratinocytes were incubated with 10 ng/mL TGF-β1 and a range of concentrations of OPX (0.03 µM – 100 µM) for 72 h, before measuring fibronectin and vimentin expression using the In-Cell ELISA method. Data points are plotted as average ± SEM, where N=1, n=3.

Table 4-10 shows an overview of the effect of each drug on TGF-β1-induced fibronectin and vimentin expression, summarising the IC_{50} of each drug.

Table 4-10: IC_{50} for hydroxypyridone anti-fungals and their effect on markers of TGF-β1-induced keratinocyte EMT.

Drug name	IC_{50}	
	Fibronectin	Vimentin
Ciclopirox (CPX)	1.5 ± 0.2 µM	17.7 ± 3.2 µM
Ciclopirox ethanolamine (CPXO)	14.4 ± 2.6 µM	21.8 ± 6.9 µM
Piroctone olamine (OPX)	11.1 ± 1.6 µM	9.5 ± 4.1 µM

4.3.4. Effect of candidate drugs on extracellular matrix production

One of the defining features of fibrosis is the dysregulation in ECM homeostasis, causing an imbalance between ECM production and ECM degradation. As a result of this imbalance, during fibrosis there is an excessive production of ECM. To confirm that TGF-β1 could induce ECM production, fibroblasts were incubated with either blank media or media containing 10 ng/mL TGF-β1 for 7 days. Fibroblasts were lysed, before fixing and staining the ECM with Coomassie blue to measure total ECM production. Figure 4-18A shows that when left untreated, there is no ECM production by quiescent fibroblasts, compared to Figure 4-18B which shows that in the presence of TGF-β1, myofibroblasts will produce and lay down ECM.

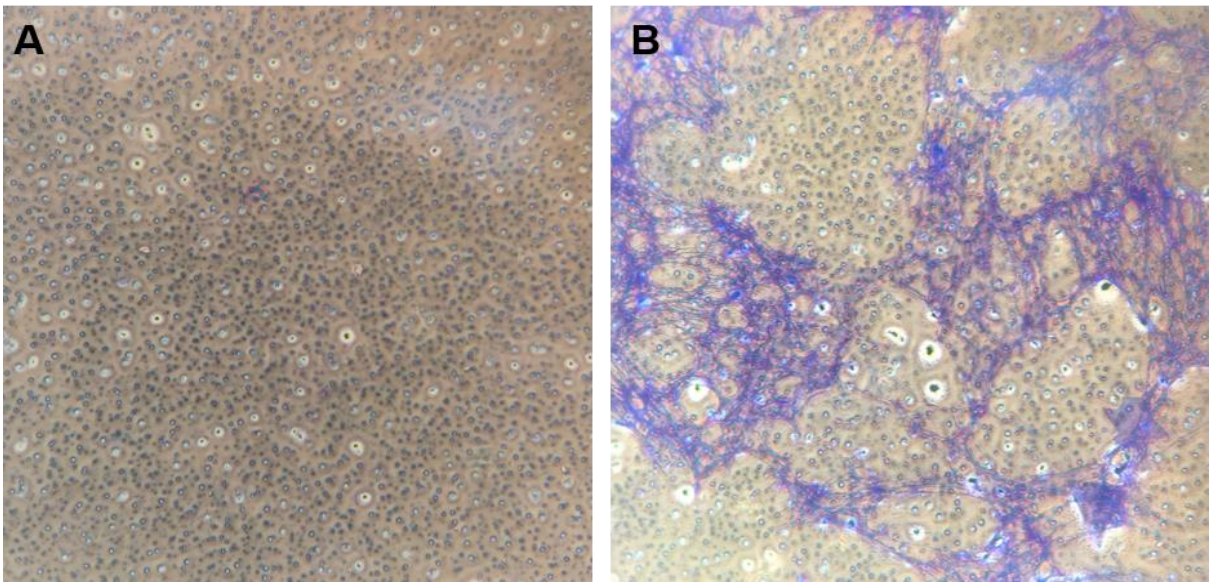

Figure 4-18: Representative images of Coomassie staining of ECM. Burn scar fibroblasts were A) untreated or B) treated with 10 ng/mL TGF-β1 for 7 days, before staining the ECM with Coomassie blue. Images obtained using brightfield microscopy at 100x magnification.

To see if ECM production could be inhibited in a concentration-dependent manner, a full concentration-response curved for the type 1 TGF-β1 receptor inhibitor SB-505124 was constructed, testing a range of concentrations (0.03 μM – 100 μM) in co-incubation with 10 ng/mL TGF-β1 for 72 h. This showed that SB-505124 was able to inhibit ECM production in a concentration-dependent manner and an IC_{50} of 5.9 ± 0.2 μM could be calculated (Fig 4-19).

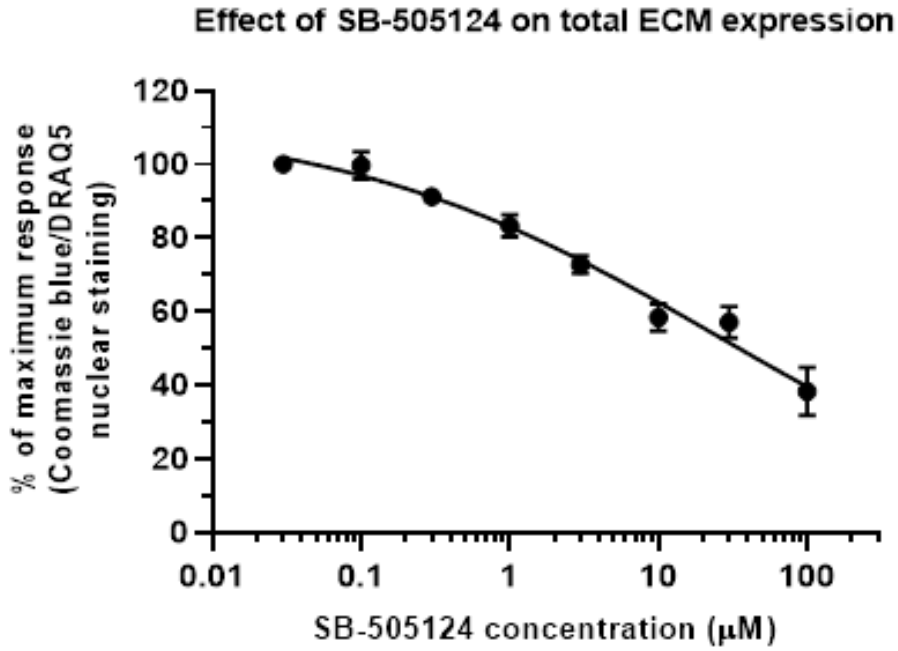

Figure 4-19: Effect of SB-505124 on total ECM production. A full concentration response curve was generated for SB-505124, where fibroblasts were incubated with 10 ng/mL TGF-β1 and a range of concentrations of SB-505124 (0.03 μM – 100 μM) for 7 days before measuring total ECM production by staining with Coomassie blue. Data points are plotted as average ± SEM, where N=3, n=9.

Following this, the effect of the hydroxypyridone anti-fungals on total ECM production were investigated by constructing concentration response curves for CPX, CPXO and OPX. All three drugs were applied in co-incubation with 10 ng/mL TGF-β1, with concentrations ranging from 0.1 µM – 300 µM for CPX and CPXO, and 0.03 µM – 100 µM for OPX. As shown in Figure 4-20, all three drugs inhibited ECM production in a concentration-dependent manner, generating inverse sigmoid curves with upper and lower plateaus. The calculated IC_{50} of each drug has been summarized in Table 4-11.

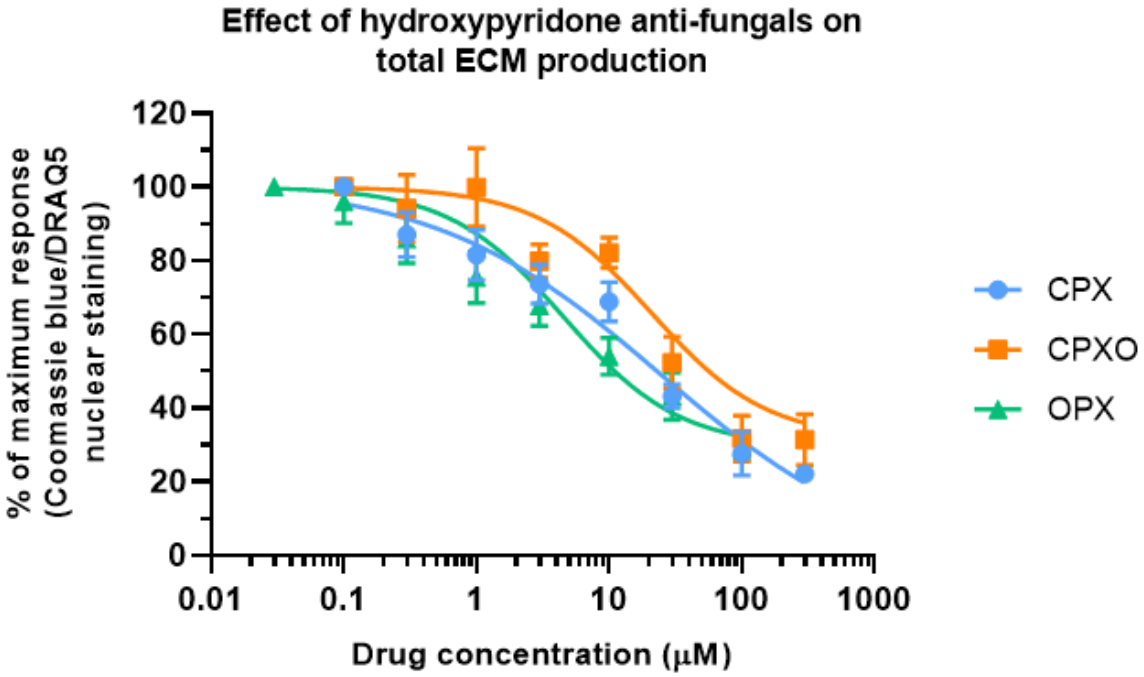

Figure 4-20: Effect of hydroxypyridone anti-fungals on total ECM production. Full concentration response curves were generated for CPX, CPXO and OPX where fibroblasts were incubated with 10 ng/mL TGF-β1 and a range of concentrations of CPX/CPXO (0.1 µM – 300 µM) and OPX (0.03 µM – 100 µM) for 7 days. Total ECM production was measured by staining the ECM with Coomassie blue solution. Data points are plotted as average ± SEM, where N=3, n=9.

Table 4-11: IC_{50} for all hydroxypyridone anti-fungals and their effect on total ECM production.

Drug name	IC_{50}
Ciclopirox (CPX)	20.9 ± 2.5 µM
Ciclopirox ethanolamine (CPXO)	19.9 ± 6.3 µM
Piroctone olamine (OPX)	5.2 ± 3.5 µM

4.4. Discussion

This section of the thesis set out to investigate if any of the hits identified from the screening assay capable of showing other anti-fibrotic effects.

The following objectives were set out to investigate the above hypothesis:

1. Develop secondary screening assays, to measure other common hallmarks of fibrosis and assess cell viability.

2. Investigate the anti-fibrotic activity of the candidate drugs using the secondary assays.

4.4.1. Confirmation of anti-myofibroblast activity

To confirm the anti-myofibroblast effect seen by CPX and CPXO in the screening campaign, both drugs were purchased from a different supplier to that of the drug library supplier. The purpose of this was to ensure that the anti-myofibroblast effect seen in the initial drug screen was not a mistake, ensuring the integrity of the drug library. Further, confirmation of anti-myofibroblast activity ensured this effect was universal, regardless of the supplier. The safety data sheets for both CPX and CPXO showed that both drugs have good solubility in water and in DMSO, and both could be used a vehicle. As a result of this, the anti-myofibroblast activity of both drugs was tested in both vehicles by constructing concentration response curves. Varying concentrations of CPX and CPXO were tested (0.1 µM - 300 µM) in co-incubation with 10 ng/mL TGF-β1. When using both DMSO and PBS as a vehicle, CPX was able to inhibit TGF-β1-induced myofibroblast transformation in a concentration-dependent manner, as shown by the reduction in the α-SMA/DRAQ5 ratio at the higher concentrations of the drug. In DMSO, an IC_{50} of 16.7 ± 2.3 µM could be calculated and in PBS an IC_{50} of 17.2 ± 2.5 µM could be calculated, with no significant difference in potency between the two vehicles. Similarly, CPXO was also able to inhibit TGF-β1-induced myofibroblast transformation in a concentration-dependent manner, however there was a significant difference in potency between the two vehicles. When DMSO was used as a vehicle for CPXO, an IC_{50} of 32.3 ± 3.1 µM could be calculated and when PBS was used as a vehicle, an IC_{50} of 10.3 ± 0.8 µM could be calculated.

To observe if the anti-myofibroblast activity seen in CPX and CPXO was specific to them or a universal effect of the hydroxypyridone anti-fungal drug class, the effect of the other drugs in the drug class was investigated. Two other hydroxypyridone anti-fungals have been discovered – rilopirox and piroctone olamine (Octopirox; OPX). Although rilopirox was found to be efficacious in the treatment of intravaginal fungal infections and exhibited low toxicity in *in vitro* and *in vivo* studies, it never made it to market (Korting and Grundmann-Kollmann, 1997; Raether and Hänel, 1990) and was not available to be purchased from any supplier.

Piroctone olamine however, is commonly found in most anti-dandruff shampoos for the treatment of pityriasis capitis and was available to be purchased from Sigma-Aldrich (Schmidt-Rose et al., 2011; Lodén and Wessman, 2000). It should be noted that OPX was not one of the 1,954 approved drugs in the drug library. Like with CPX and CPXO, concentration response curves for OPX using DMSO and PBS as a vehicle were constructed. Varying concentrations of OPX were used (0.03 μM – 100 μM) in co-incubation with 10 ng/mL TGF-β1. OPX (when using both DMSO and PBS) was able to inhibit TGF-β1-induced myofibroblast transformation in a concentration-dependent manner. When DMSO was used as a vehicle, an IC_{50} of 1.37 ± 0.12 μM could be calculated and an IC_{50} of 2.0 ± 0.62 μM could be calculated when using PBS, with no significant difference between the potencies.

To my knowledge, this is the first study to show that hydroxypyridone anti-fungals have a direct anti-myofibroblast effect in skin fibroblasts. Further, little research has been conducted into the effect of hydroxypyridone anti-fungals on myofibroblast transformation in other fibrotic disorders. In a study published very recently, CPXO was shown to have anti-myofibroblast activity in tissue from polycystic kidney disease (Radadiya et al., 2021). Histological analysis of this tissue showed a reduction in α-SMA expression and reduced intensity of Masson's trichrome staining, signifying a reduction in collagen production and the disease associated fibrosis (Radadiya et al., 2021).

As discussed in Chapter 3, the widely understood mechanism of action of hydroxypyridone anti-fungals is iron chelation. Therefore, as already speculated, these drugs could be inhibiting myofibroblast transformation by removing excess intra-cellular iron, and prevent oxidative stress in these cells. Furthermore, the use of mainstream iron chelators (e.g. deferoxamine, deferiprone and deferasirox) as therapies for liver fibrosis has been suggested, after showing to exhibit an anti-fibrotic effect in both *in vitro* and clinical studies (Jin, Terai and Sakaida, 2007; Wu et al., 2006; Sousos et al., 2018). These drugs were shown to not only inhibit other aspects of the fibrosis pathology but also exert an anti-myofibroblast effect, observed by a reduction in α-SMA expression (Jin, Terai and Sakaida, 2007). Two of these drugs, deferiprone and deferasirox, were present in the approved drug library, however neither exhibited a significant anti-myofibroblast effect with -36% and 28% inhibition of α-SMA expression, respectively. Deferoxamine however, was not present in the approved drug library, and has previously been shown to prevent dermal fibrosis following radiation therapy when used as a prophylactic (Shen et al., 2020). Therefore the effect of deferoxamine on the burn scar fibroblasts should be investigated to see if it exhibits a similar effect to the other iron chelators, or if it exhibits an anti-myofibroblast effect.

Another way that hydroxypyridone anti-fungals could be inhibiting myofibroblast transformation is through the blockade of Wnt/β-catenin signalling. Hydroxypyridone anti-fungals have recently been shown to influence Wnt/β-catenin signalling in a number of cancers. In colorectal cancer, successful blockade of this pathway resulted in the upregulation of β-catenin degradation and in murine models of AML, CPX was shown to inhibit the upregulation of β-catenin associated genes (Song et al., 2011; Kim et al., 2011). Wnt/β-catenin signalling is part of the non-canonical TGF-β1 signalling pathway in fibrosis, in which stabilisation of β-catenin and subsequent nuclear translocation, results in the upregulation of α-SMA (Poon et al., 2009). Small molecule inhibition (ICG-001) of Wnt signalling has been studied as a potential therapy for IPF. In this study, a significant reduction in α-SMA expression was observed when lung resident mesenchymal stem cells were treated with ICG-001, in co-incubation with TGF-β1 (Cao et al., 2018). Therefore, it can be speculated that hydroxypyridone anti-fungals are inhibiting α-SMA expression through the blockade of Wnt/β-catenin signalling, by increasing degradation of cytoplasmic β-catenin and causing the downregulation of β-catenin's target genes, however this requires further investigation.

4.4.2. Effect of candidate drugs on cell viability

In the screening assay and subsequent confirmatory concentration response curves, the hydroxypyridone anti-fungals exhibited suitable cell viability when using DRAQ5, a nuclear stain. To assess the effect of the hydroxypyridone anti-fungals on cell viability further, two other aspects of cell viability were also investigated. For these experiments four different cell lines were utilised – burn scar fibroblasts, as they are the cells of interest; normal fibroblasts from a burn patient, as when given topically there is potential for the drug to diffuse outside of the wound area and affect normal fibroblasts; keratinocytes, as they are the other major cell population involved in wound healing and one of the secondary assays is based on keratinocyte EMT; rhabdomyosarcoma cells, as the effect of hydroxypyridone anti-fungals on their viability has been studied previously.

The first aspect of cell viability that was investigated was mitochondrial function, for which a MTT assay was utilised. The MTT assay is a colorimetric tetrazolium-based assay, which has been shown to be a reliable tool for measuring cell viability and proliferation (Mosmann, 1983; Hansen, Nielsen and Berg, 1989). The assay measures the reduction of MTT to formazan, a NADH and NADPH dependent process, before dissolving the formazan crystals in acid alcohol. Cells with impaired mitochondrial function are unable to reduce the MTT, and so less formazan is produced (Berridge and Tan, 1993). To show that the output signal from the assay correlated to changes in cell number, standard curves for each cell line were constructed. Cells were seeded at a range of cell densities (39 – 20,000 cells per well) for the standard

curve, with an R^2 > 0.9 calculated for each cell type, indicating that the assay is able to accurately associate cell number to the detected signal.

To investigate the effect of each drug on mitochondrial function, concentration response curves were constructed with and without TGF-β1 treatment in all of the cell lines described above. The IC_{50} and E_{max} (maximum mitochondrial inhibition) for all cell lines and conditions are summarised in Chapter 4.3.2. All three drugs exhibited a similar response in both keratinocytes and RD cells, whereby they are most potent in these cells and also show greatest inhibition of mitochondrial function. Hydroxypyridone anti-fungals have recently shown anticancer and antitumour effects in a number of different cancers, including rhabdomyosarcoma. As part of this, previous studies have identified that CPX is able to induce cell cycle arrest of RD cells at the G1 phase, through the upregulation of CKD (Wu et al., 2016). Interestingly, when the drugs were given in co-incubation with TGF-β1, the E_{max} in keratinocytes and RD cells decreased by approximately 20%. Observations in the literature have shown that TGF-β1 is able to inhibit proliferation and induce apoptosis in both keratinocytes and RD cells (Amendt et al., 2002; Ye et al., 2005; Wang et al., 2003). Therefore, it can be assumed that if the initial TGF-β1 effect was removed from the data, the E_{max} for the TGF-β1-treated cells would be similar to that of the untreated results. This suggests that the drugs are able to exert a similar effect in the keratinocytes as the RD effect, which has been previously published, by inducing cell cycle arrest.

In the burn scar and normal fibroblasts, CPX exhibited a similar response across both cell types regardless of TGF-β1 treatment. The E_{max} was observed at 300 μM for untreated and TGF-β1-treated burn fibroblasts, and for untreated normal fibroblasts. The E_{max} was seen at >10 μM in the TGF-β1-treated normal fibroblasts. At the IC_{50} concentration that was calculated for anti-myofibroblast activity (16.7 μM), CPX exhibited ~20% inhibition of mitochondrial function in the burn fibroblasts and ~40% inhibition of mitochondrial function in the normal fibroblasts. When treated with CPXO the E_{max} in both treatment groups can be seen at concentrations >100 μM in burn fibroblasts, and concentrations >30 μM in normal fibroblasts. At the IC_{50} concentration that was calculated for anti-myofibroblast activity (10.3 μM), CPXO exhibited ~20% inhibition of mitochondrial function in burn fibroblasts and normal fibroblasts. Following OPX treatment, the E_{max} was seen at concentrations >30 μM in both burn scar and normal skin fibroblasts, regardless of TGF-β1 treatment. At the IC_{50} concentration that was calculated for anti-myofibroblast activity (1.3 μM), OPX exhibited ~10% inhibition of mitochondrial function in both burn fibroblasts and normal fibroblasts.

These results show that hydroxypyridone anti-fungals have a minimal effect on mitochondrial function in both burn scar and normal fibroblasts at the clinically expected IC_{50} values

(CPX = 16.7 µM, CPXO = 10.3 µM and OPX = 1.3 µM) for each drug. Further, maximum inhibition of mitochondrial function in the fibroblast cells was only seen at higher concentrations of each drug (CPX > 300 µM, CPXO > 30 µM and OPX > 30 µM).

The second aspect of cell viability that was measured was cell membrane permeability. This allowed for the confirmation as to whether the cells were dead, or if the drugs had induced cell senescence. For this, the Sapphire700 stain from LiCor was utilised. The Sapphire700 stain is a non-specific stain that is unable to penetrate intact cell membranes. If a cell has a compromised membrane, Sapphire700 will bind to the intracellular proteins and become fluorescent, allowing for detection using near infrared (Posimo et al., 2014). As with the MTT assays, the effect of CPX, CPXO and OPX on cell membrane permeability was investigated with and without TGF-β1 in all four cell lines, by constructing concentration response curves for each drug. The IC_{50} and E_{max} (maximum percentage of cells with a permeable membrane) for all cell lines and conditions are summarised in Chapter 4.3.3.

In line with previously published data (Zhou et al., 2014), hydroxypyridone anti-fungals not only affect mitochondrial function in RD cells but can also induce cell death by interfering with cell membrane permeability – as indicated by the increased Sapphire700 staining. In the keratinocytes, the hydroxypyridone anti-fungals were found to decrease cell membrane permeability in the untreated and TGF-β1-treated cells. The E_{max} ranged from -14% to -37% across the three drugs (with and without TGF-β1 treatment), indicating an increase in cell viability. Results from a study which investigated the effect of CPX and CPXO on hydrogen peroxide induced apoptosis in keratinocytes, showed that CPX and CPXO exhibited a cytoprotective effect by preventing cell apoptosis (Regdon et al., 2021). Therefore, it can be hypothesised that these drugs are also exhibiting a cytoprotective effect on keratinocytes in this study.

In the burn scar and normal fibroblasts, following treatment with CPX only, the E_{max} was reached at concentrations >30 µM in the burn scar and normal fibroblasts. In the TGF-β1-treated cells, the E_{max} was reached at concentrations >10 µM for burn scar fibroblasts, and concentrations >3 µM for normal fibroblasts. At the IC_{50} concentration that was calculated for anti-myofibroblast activity (16.7 µM), ~45% of cells had a permeable membrane in the burn fibroblasts and ~40% of cells had a permeable membrane in the normal fibroblasts, when treated with CPX. Following CPXO treatment, the E_{max} in the untreated burn scar and normal fibroblasts was achieved at concentrations >100 µM, whereas this was achieved at concentrations >30 µM in the TGF-β1-treated fibroblasts. At the IC_{50} concentration that was calculated for anti-myofibroblast activity (10.3 µM), ~30% of cells had a permeable membrane in the burn fibroblasts and ~45% of cells had a permeable membrane in the normal fibroblasts,

when treated with CPXO. The E_{max} in the burn scar fibroblasts (with and without TGF-β1 treatment) was achieved at concentrations >30 µM. In the normal skin fibroblasts the E_{max} was seen at the highest concentration of OPX tested (100 µM), regardless of TGF-β1 treatment. At the IC_{50} concentration that was calculated for anti-myofibroblast activity (1.3 µM), ~15% of the cells were found to have a permeable membrane (burn scar and normal fibroblasts, with and without TGF-β1) when treated with OPX. These results suggest that overall, all hydroxypyridone anti-fungals were able to maintain a suitable cell viability (~70 – 80 %) at lower concentrations (<30 µM) in the burn scar fibroblasts.

The purpose of carrying out these assays with and without TGF-β1 treatment was to see if hydroxypyridone anti-fungals were capable of selectively killing myofibroblasts. This would have been a favourable observation, as the myofibroblasts present in the active scarring phase are apoptosis resistant. However, both untreated and TGF-β1-treated burn scar fibroblasts showed similar reductions in cell viability in both MTT and the Sapphire700 assays.

Previous pharmacokinetic data has shown that ~10 µM of the drug is retained in the dermis following topical application of 1% CPXO cream (Ceschin-Roques et al., 1991). At 10 µM of CPXO, a 20% inhibition in mitochondrial function was seen, with 30% of cells having a permeable cell membrane in the burn scar fibroblasts. Further, as 10 µM of CPXO was used in the initial drug screen this data showed a reduction of ~10% in the DRAQ5 nuclear staining. With this data it can be deduced that CPXO is able to maintain suitable cell viability (70-80%) at this concentration, and therefore any cytotoxicity seen, should have no major effect on the anti-myofibroblast activity. Furthermore, the pharmacokinetic data showed that 300 µM of CPXO would be retained in the epithelium upon topical application (Ceschin-Roques et al., 1991). At this concentration, CPXO exhibited a cytoprotective effect when looking at cell membrane permeability, despite inhibiting mitochondrial function. Therefore it can be speculated that CPXO induces a state of cell senescence in keratinocytes, without causing cell death; this would require further investigation.

4.4.3. Effect of candidate drugs on keratinocyte EMT

As with myofibroblast transformation, TGF-β1 is able to induce keratinocyte epithelial-mesenchymal transition through both canonical and non-canonical signalling pathways. The downstream effect of this leads to the upregulation of mesenchymal-related transcription factors and proteins, and downregulation of epithelial associated proteins. In particular, keratinocytes have been shown to express the filamentous protein vimentin, and also produce the ECM component fibronectin, when exposed to TGF-β1 (Stone et al., 2016). To confirm these observations *in vitro*, human keratinocytes were exposed to varying concentrations of TGF-β1 (0.01 ng/mL – 30 ng/mL) and concentration response curves measuring both vimentin

and fibronectin were constructed. TGF-β1 exhibited higher potency when inducing fibronectin production (EC_{50} = 0.77 ± 0.08 μM), whilst vimentin expression was induced at higher concentrations of TGF-β1 (EC_{50} = 2.52 ± 0.22 μM). Maximum expression of both fibronectin and vimentin was seen at concentrations >10 ng/mL TGF-β1. To observe any morphological changes in the keratinocytes upon exposure to TGF-β1, keratinocytes were stained for CK-14, and also stained for vimentin and fibronectin using ICC. These cytochemical stainings allowed for visualisation of the morphological changes keratinocytes undergo during EMT. Untreated keratinocytes exhibited their usual cobblestone morphology, with no vimentin or fibronectin expression seen. Upon TGF-β1 treatment, keratinocytes showed significant expression of vimentin and fibronectin and complete loss of their normal morphology, with keratinocytes appearing rounder and larger, with loss of their cell-cell adhesions.

Previous studies have shown that pharmacological blockade of TGFβ receptor 1, and downstream TGF-β1 signalling not only prevented EMT from occurring, but also promoted an enhanced epithelial phenotype (Lamouille and Derynck, 2007; Eger et al., 2004). To confirm if this could be seen using the ICE method, a concentration-response curve for SB-505124 (a selective TGFβ receptor 1 antagonist) was constructed before staining for vimentin and fibronectin. Varying concentrations of SB-505124 were used (0.03 μM – 100 μM) in co-incubation with 10 ng/mL TGF-β1. Successful blockade of TGF-β1 signalling showed that SB-505124 was able to inhibit TGF-β1-induced expression of vimentin and fibronectin, in a concentration-dependent manner. SB-505124 exhibited similar potency for both vimentin and fibronectin, with an IC_{50} of 1.0 ± 0.5 μM and 1.2 ± 0.6 μM, respectively, suggesting that TGF-β1 signalling is equally important for induction of both vimentin, and fibronectin.

Following this, the effect of the hydroxypyridone anti-fungals on TGF-β1-induced keratinocyte EMT was investigated. Varying concentrations of CPX, CPXO and OPX (0.03 μM – 100 μM) were tested in co-incubation with 10 ng/mL TGF-β1, before staining for vimentin and fibronectin. All three drugs were shown to inhibit TGF-β1-induced keratinocyte EMT in a concentration-dependent manner, with varying potencies. CPX was more potent in inhibiting fibronectin expression (IC_{50} = 1.5 ± 0.2 μM) compared to CPXO and OPX (IC_{50} of 14.4 ± 2.6 μM and 11.1 ± 1.6 μM, respectively). Furthermore, OPX was shown to be more potent in inhibiting vimentin expression (IC_{50} = 9.5 ± 4.1 μM) compared to CPX and CPXO (IC_{50} of 17.7 ± 3.2 μM and 21.8 ± 6.9 μM, respectively).

To my knowledge, this is the first study to show that hydroxypyridone anti-fungals are able to directly inhibit TGF-β1-induced keratinocyte EMT. Recent studies investigating metastasis and the role of EMT in tumour invasion (e.g. glioblastoma and colorectal cancer), may have shed light on the potential mechanism of actions that hydroxypyridone anti-fungals work

through to inhibit EMT. Upregulation of EMT associated transcription factors and markers can be initiated through TGF-β1 canonical and non-canonical signalling (Stone et al., 2016). During EMT, activated Wnt signalling inhibits β-catenin phosphorylation and degradation, leading to increased levels of cytoplasmic β-catenin (Xu, Lamouille and Derynck, 2009). As discussed in section 4.5.1. successful blockade of Wnt/β-catenin signalling has shown increased β-catenin degradation and downregulation of β-catenin target genes (Song et al., 2011). SNAIL1/2 are transcription factors that help to co-ordinate the EMT process and are usually activated through the downstream actions of Smad2/3. They have been shown to directly suppress E-cadherin expression and upregulate the expression of vimentin and fibronectin (Cano et al., 2000). A recent study using glioblastoma cells showed that when treated with CPX and CPXO, cell migration (mediated through EMT) was inhibited through the suppression of N-cadherin and SNAIL1 (Su et al., 2021). As well as being activated via Smad2/3, SNAIL1/2 can also be activated via Wnt/β-catenin signalling, with a study showing that overexpression of SNAIL1/2 led to the upregulation of Wnt target genes for EMT (Stemmer et al., 2008). It can therefore be suggested that hydroxypyridone anti-fungals are inhibiting vimentin and fibronectin expression through the blockade of Wnt/β-catenin signalling, and the subsequent suppression of the SNAIL1 transcription factor.

4.4.4. Effect of candidate drugs on ECM production

As described in the introduction (Chapter 1.3), fibrosis is defined as the excessive accumulation of extracellular matrix in the injured area (Nanthakumar et al., 2015; Pakshir and Hinz, 2018). Although a number of different cell types are believed to contribute to the overproduction of ECM during fibrosis, it is widely believed that myofibroblasts are the greatest contributor to this (Hardie, Glasser and Hagood, 2009). To investigate if the anti-myofibroblast activity exhibited by the hydroxypyridone anti-fungals correlated with a reduction in ECM production, a secondary assay was developed to measure total ECM production.

The assay utilised in this study was based upon the established method in the lab, which had adapted other previously published methods so that normalisation of ECM production to total cell number could be carried out (Ilg et al., 2019). The original assay utilised Flamingo dye to stain for total ECM production, but as this could not be detected using the LiCor Odyssey scanner, Coomassie blue was used to stain total ECM production instead (Qureshi et al., 2017; Holdsworth et al., 2017). The protocol was optimised for the burn scar fibroblasts, in which the Coomassie blue stain was left to incubate for 72 h at 4°C instead of 24 h.

Before investigating the effects of the hydroxypyridone anti-fungals, bright-field microscopy was used to visualise ECM production in the TGF-β1-treated fibroblasts. The presence of fibrous ECM strands in the TGF-β1-treated fibroblast wells and lack of in the untreated

fibroblasts, confirms that myofibroblasts are responsible for production of ECM and this is induced upon treatment with TGF-β1. Further, to see if blockade of TGF-β1 signalling would inhibit ECM production, a concentration response curve for SB-505124 was constructed, whereby SB-505124 was tested at varying concentrations (0.3 µM – 100 µM) in co-incubation with 10 ng/mL TGF-β1. SB-505124 was able to inhibit total ECM production in a concentration-dependent manner, and an IC_{50} of 5.9 ± 0.2 µM was calculated. This data is in line with other observations in the literature, where blockade of TGF-β1 signalling using SB-505124 has been shown to inhibit ECM production in other cell types (e.g. chondrocytes) (Tekari et al., 2015). Further, SB-505124 exhibited a similar response when measuring for total ECM production in PD fibroblasts, with an IC_{50} of 3.0 ± 0.5 µM (Ilg et al., 2019).

To investigate the effect of the hydroxypyridone anti-fungals on total ECM production, varying concentrations of each drug (0.03 µM – 300 µM) were tested in co-incubation with 10 ng/mL TGF-β1 and full a concentration response curve for each drug were constructed. CPX, CPXO and OPX were all able to inhibit total ECM production by myofibroblasts in a concentration-dependent manner. OPX was found to be the most potent with an IC_{50} of 5.2 ± 3.5 µM, whereas CPX and CPXO showed similar potencies, with an IC_{50} of 20.9 ± 2.5 µM and 19.9 ± 6.3 µM, respectively.

Using histological analysis, previous studies have identified that treatment with hydroxypyridone anti-fungals could reduce collagen production and disease associated fibrosis (Urquiza et al., 2018; Minden et al., 2014). From the results of this thesis, it could be suggested that the reduction in total ECM is a direct result of the hydroxypyridone anti-fungal inhibition of myofibroblast transformation. However, as hydroxypyridone anti-fungals are iron chelators, it has been shown that they are able to inhibit the post-translational modification of collagen. Prolyl hydroxylase is the enzyme responsible for the production of hydroxyproline, the post-translational modification that allows for collagen stability, as it raises the melting point of collagen (Shoulders and Raines, 2009). As the reaction catalysed by prolyl hydroxylase is dependent on the availability of iron (Fe^{3+}) ions, hydroxypyridone anti-fungals have been found to inhibit this reaction using their chelator activity (Shoulders and Raines, 2009; Maruo et al., 2002; Lim et al., 2013). It is therefore possible that inhibition of total ECM production exerted by hydroxypyridone anti-fungals in this study, is partially due to their iron chelator function and inducing collagen instability, as well as their anti-myofibroblast activity.

Chapter 5: Outlook

This thesis has successfully investigated the research questions and achieved the aims and objectives which were set out prior to this work being undertaken. A phenotypic, high-throughput screening assay which can measure myofibroblast transformation, was fully optimised and validated for use with primary human dermal fibroblasts. Further, this assay was used to screen an approved drug library to find novel therapies that can inhibit TGF-β1-induced myofibroblast transformation. 90 drugs were identified from this screening campaign and following filtering of these hits, one drug class (hydroxypyridone anti-fungals) were taken forward for further investigation. This work showed that the hydroxypyridone anti-fungals were capable of reducing different fibrotic phenotypes, including myofibroblast transformation, keratinocyte EMT and total ECM production. Further, the hydroxypyridone anti-fungals were efficacious at concentrations that maintained suitable cell viability. This work provides the basis for further research to be carried out to investigate the mechanism of action of hydroxypyridone anti-fungals and for their clinical efficacy to be investigated in clinical trials

5.1. Limitations

Many of the limitations associated with this piece of work relate to the primary high-throughput screening assay.

One of the greatest limitations of the screening assay was the use of a single dose, high concentration of TGF-β1. It has been reported that circulating levels of TGF-β1 vary between 0.02 ng/mL – 2 ng/mL, with this increasing after burn injury and during wound healing (Fogel-Petrovic et al., 2007). Although the chosen concentration of TGF-β1 for the assay is likely to mimic the concentration seen during injury, this is given as a single dose and not continually over a certain time period. The lack of continuous exposure to TGF-β1 may affect the assay and fibroblast behaviour in some way. Further, the wound healing environment would be mimicked better if a mixture of different pro-fibrotic cytokines (e.g. IL-1β, PDGF and IL-4), as well as TGF-β1 was used to induce myofibroblast transformation. One other limitation of the assay is that the candidate drugs were given at the same time-point as the TGF-β1 dose, only investigating if the drugs were capable of preventing myofibroblast transformation. Given that the drug would be given later into the wound healing process, the effect of the drugs on fully transformed myofibroblasts and at shorter TGF-β1 exposure times (e.g. 24 and 48 hours) should be investigated.

The severity of scarring experienced by patients can vary based on genetic variation and their ethnicity. The ethnicity of each patient recruited to the study was not made available to the author to ensure anonymity. It is therefore assumed the majority of patients were of white ethnicity, based on the pigmentation of the tissue samples acquired and general population of

Chelmsford and Essex, where St. Andrew's Burn Centre is based. Previous research using the Vancouver Scar Scale to measure scar severity, identified that white patients experience less severe scarring, compared to those of Asian and Black/Afro-Caribbean descent (Thompson et al., 2013). Carrying out this assay using fibroblasts from patients of different ethnicities would be beneficial to ensure that the candidate drugs have a universal effect and not only benefit those from one specific ethnic group.

The thesis investigates the effect of the candidate drugs on different cellular phenotypes associated with dermal scarring, using monolayer cell culture. Given that crosstalk between fibroblasts and different cell populations (e.g. keratinocytes) is likely to drive dermal scarring, the use of a 3-dimensional culture system to investigate the effect of the candidate drugs would be beneficial. Further, seeding of the cells onto a relevant matrix, instead of seeding them onto a plastic plate, would make the assay more physiologically relevant.

5.2. Future work

This study has shown that hydroxypyridone anti-fungals are able to inhibit individual aspects of the fibrosis phenotype. One of the limitations of this work is that it does not consider the potential crosstalk between the different cell types in the skin, with this crosstalk helping to co-ordinate the healing response. *In vivo* animal models would be the first choice to study this, however there are large debates surrounding the ethics of the current animal models for dermal scarring and more specifically, burn injuries themselves. Further, the animal models for dermal scarring are somewhat limited and expensive (typically pig or rabbit), as murine and rodents do not share similar skin architecture and their wound healing responses differ to humans. This has led to the successful development of *ex vivo* models (where patient tissue is kept alive in culture) and 3D human skin equivalents (fibroblasts and keratinocytes are layered upon a transwell insert). These models would allow for the monitoring of how the hydroxypyridone anti-fungals effect other phenotypes associated with fibrosis in a time-course manner. This includes delayed re-epithelisation of the wound site, cell apoptosis and overall scar appearance. Following confirmation of the efficacy of hydroxypyridone anti-fungals on a 3D/*ex vivo* model, the clinical efficacy would need to be investigated. Using patients who have recently suffered a severe cutaneous wound, a placebo-controlled clinical trial should be undertaken.

The mechanism of action of hydroxypyridone anti-fungals in fibrosis is widely unknown. Potential pathways that the drugs may be working through have been speculated throughout this thesis, and therefore a mechanistic study to deconvolute this is needed. The first step in this process would be to see if myofibroblast transformation and keratinocyte EMT are iron-dependent processes. As hydroxypyridone anti-fungals are iron chelators, the

overloading of iron should inhibit their action. Furthermore, other iron chelators (e.g. deferoxamine) could also be investigated. If these drugs are not able to inhibit myofibroblast transformation and keratinocyte EMT, this would indicate that hydroxypyridone anti-fungals are acting through other mechanisms. In this situation, the effect of hydroxypyridone on both canonical TGF-β1 signalling pathways and non-canonical pathways should be investigated, in particular Wnt/β-catenin signalling.

Investigating the effect of the other candidate drugs that were identified from the screeening assay would also be beneficial. Testing of these drugs in combination with the hydroxypyridone anti-fungals may identfy a novel drug combination which further enhance their individual anti-fibrotic effects. Furthermore, investigating the effect of the drugs that were found to increase myofibroblast transformation in the screening campaign, may shed light on novel therapeutics to target chronic wound healing (e.g. diabetic ulcers). The drugs that were able to increase myofibroblast transformation could be repurposed if they were shown to enhance wound healing (e.g. increased rate of re-epithelisation, increased angiogenesis and increased cell infilatration in the wound area).

Even though hydroxypyridone anti-fungals showed good efficacy in inhibiting keratinocyte EMT, the secondary assay developed could be optimised and validated for high-throughput screening. The benefit of carrying out a similar screening campaign in human keratinocytes would allow the identification of other drugs in the library that are capable of inhibiting both TGF-β1-induced keratinocyte EMT and myofibroblast transformation, potentially identifying other mechanisms of fibrosis that can be targeted therapeutically. Further, there is potential for identifying a combination treatment using a drug that can inhibit myofibroblast transformation and one that can inhibit keratinocyte EMT. If this combination were to show a synergistic effect in a relevant model (e.g. a 3D skin model or *in vivo* studies), this would provide key information into the mechanisms that drive dermal scarring.

This is now the second successful screening campaign using the initial assay protocol that was designed, therefore indicating that this assay, and the use of phenotypuc screening, is reliable and robust enough to be adapted for other fibrotic disorders. This assay therefore be adapted for the identification of novel therapeutics for the more life-threatening fibrotic disorders (e.g. lung and liver fibrosis).

5.3. Conclusions

- Primary human fibroblasts were successfully isolated from skin samples, with their identity confirmed by measuring vimentin, desmin and CK-14 expression.
- TGF-β1 was able to induce myofibroblast transformation in these cells, with maximum α-SMA expression seen at concentrations of TGF-β1 > 3 ng/mL.
- The primary screening assay, using the ICE method, was optimised fully to ensure the correct conditions and protocol was used for the skin fibroblasts.
- The primary screening assay was rigorously validated, to determine statistical robustness and reliability for high-throughput screening. This yielded a Z-factor > 0.5 when both manual and automated liquid handling was used. Concentration response curves for SB-505124, DMSO and PBS indicated that the assay could detect compound-induced inhibition of myofibroblast transformation.
- Screening of 1,954 approved drugs identified 90 hits which were capable of inhibiting α-SMA expression by >80%, whilst maintaining >80% cell viability.
- Streamlining of these hits identified 12 with a desirable safety profile, with 10 hits having been previously formulated for topical application.
- Hydroxypyridone anti-fungals (CPX, CPXO and OPX) were chosen for further testing, and shown to inhibit TGF-β1-induced myofibroblast transformation in a concentration-dependent manner.
- When looking at aspects of cell viability, hydroxypyridone anti-fungals were shown to have minimal effect on mitochondrial function in fibroblasts and only affected cell membrane permeability at higher concentrations.
- When investigating the effect of the hydroxypyridone anti-fungals on the expression of EMT markers in keratinocytes, CPX, CPXO and OPX were shown to inhibit both TGF-β1-induced vimentin and fibronectin expression in a concentration-dependent manner.
- CPX, CPXO and OPX reduced total ECM production in a concentration-dependent manner, further confirming their anti-myofibroblast activity.
- This is the first study to identify and investigate the anti-fibrotic effect of hydroxypyridone anti-fungals in dermal scarring. This study has shown that hydroxypyridone anti-fungals could be re-purposed as a potential therapy to prevent the formation of severe scarring following injury and trauma.

6. References

Aarabi, S., Longaker, M.T. and Gurtner, G.C., 2007. Hypertrophic scar formation following burns and trauma: New approaches to treatment. *PLoS Medicine*, 4(9), pp.1464–1470. https://doi.org/10.1371/journal.pmed.0040234.

Aban, C.E., Lombardi, A., Neiman, G., Biani, M.C., la Greca, A., Waisman, A., Moro, L.N., Sevlever, G., Miriuka, S. and Luzzani, C., 2021. Downregulation of E-cadherin in pluripotent stem cells triggers partial EMT. *Scientific Reports*, 11(1), p.2048. https://doi.org/10.1038/s41598-021-81735-1.

Aggarwal, G., Zarrow, J.E., Mashhadi, Z., Flynn, C.R., Vinson, P., Weaver, C.D. and Davies, S.S., 2020. Symmetrically substituted dichlorophenes inhibit N-acyl-phosphatidylethanolamine phospholipase D. *Journal of Biological Chemistry*, 295(21), pp.7289–7300. https://doi.org/10.1074/jbc.RA120.013362.

Akhmetshina, A., Palumbo, K., Dees, C., Bergmann, C., Venalis, P., Zerr, P., Horn, A., Kireva, T., Beyer, C., Zwerina, J., Schneider, H., Sadowski, A., Riener, M.O., MacDougald, O.A., Distler, O., Schett, G. and Distler, J.H.W., 2012. Activation of canonical Wnt signalling is required for TGF-β-mediated fibrosis. *Nature Communications*, 3(735), pp.1–12. https://doi.org/10.1038/ncomms1734.

Akhurst, R.J. and Hata, A., 2012. Targeting the TGFβ signalling pathway in disease. *Nature Reviews Drug Discovery*, 11(10), pp.790–811. https://doi.org/10.1038/nrd3810.

Alberton, F., Corain, M., Garofano, A., Pangallo, L., Valore, A., Zanella, V. and Adani, R., 2014. Efficacy and safety of collagenase Clostridium histolyticum injection for Dupuytren contracture: report of 40 cases. *Musculoskeletal Surgery*, 98(3), pp.225–232. https://doi.org/10.1007/s12306-013-0304-x.

Alberts, A.W., Chen, J., Kuron, G., Hunt, V., Huff, J., Hoffman, C., Rothrock, J., Lopez, M., Joshua, H., Harris, E., Patchett, A., Monaghan, R., Currie, S., Stapley, E., Albers-Schonberg, G., Hensens, O., Hirshfield, J., Hoogsteen, K., Liesch, J. and Springer, J., 1980. Mevinolin: a highly potent competitive inhibitor of hydroxymethylglutaryl-coenzyme A reductase and a cholesterol-lowering agent. *Proceedings of the National Academy of Sciences*, 77(7), pp.3957–3961. https://doi.org/10.1073/pnas.77.7.3957.

Alberts, B., Johnson, A., Lewis, J., Morgan, D., Raff, M., Roberts, K. and Walter, P., 2014. The epidermal-stem cell system maintains a self-renewing waterproof barrier. In: *Molecular Biology of the Cell*, 6th ed. Garland Science.pp.1225–1226.

Ali, M.K., Kim, R.Y., Brown, A.C., Donovan, C., Vanka, K.S., Mayall, J.R., Liu, G., Pillar, A.L., Jones-Freeman, B., Xenaki, D., Borghuis, T., Karim, R., Pinkerton, J.W., Aryal, R., Heidari, M., Martin, K.L., Burgess, J.K., Oliver, B.G., Trinder, D., Johnstone, D.M., Milward, E.A., Hansbro, P.M. and Horvat, J.C., 2020. Critical role for iron accumulation in the pathogenesis of fibrotic lung disease. *Journal of Pathology*, 251(1), pp.49–62. https://doi.org/10.1002/path.5401.

Amendt, C., Mann, A., Schirmacher, P. and Blessing, M., 2002. Resistance of keratinocytes to TGFβ-mediated growth restriction and apoptosis induction accelerates re-epithelialization in skin wounds. *Journal of Cell Science*, 115(10), pp.2189–2198. https://doi.org/10.1242/jcs.115.10.2189.

Andreeff, B., Stone, R., Michaeli, J., Young, C.W., Tong, W.P., Sogoloff, H., Ervin, T., Kufe, D., Rifkind, R.A. and Marks, P.A., 1992. Hexamethylene Bisacetamide in Myelodysplastic

Syndrome and Acute Myelogenous Leukemia: A Phase II Clinical Trial with a Differentiation-Inducing Agent. *Blood*, 80(10), pp.2604–2609.

Andriessen, M., Niessen, F., van de Kerkhof, P. and Schalkwijk, J., 1998. Hypertrophic scarring is associated with epidermal abnormalities: an immunohistochemical study. *Journal of Pathology*, 186, pp.192–200.

Ansel, J.C., Tiesman, J.P., Olerud, J.E., Krueger, J.G., Krane, J.F., Tara, D.C., Shipley, G.D., Gilbertson, D., Usui, M.L. and Hart, C.E., 1993. Human Keratinocytes Are a Major Source of Cutaneous Platelet-derived Growth Factor. *The Journal of Clinical Investigation*, 92, pp.671–678.

Antonarakis, E. and Bastos, D., 2016. Galeterone for the treatment of advanced prostate cancer: the evidence to date. *Drug Design, Development and Therapy*, Volume 10, pp.2289–2297. https://doi.org/10.2147/DDDT.S93941.

Arif, S., Attiogbe, E. and Moulin, V.J., 2021. Granulation tissue myofibroblasts during normal and pathological skin healing: The interaction between their secretome and the microenvironment. *Wound Repair and Regeneration*, 29(4), pp.563–572. https://doi.org/10.1111/wrr.12919.

Armour, A., Scott, P.G. and Tredget, E.E., 2007. Cellular and molecular pathology of HTS: Basis for treatment. *Wound Repair and Regeneration*, 15(Suppl.1), pp.S6–S17. https://doi.org/10.1111/j.1524-475X.2007.00219.x.

Arno, A.I., Gauglitz, G.G., Barret, J.P. and Jeschke, M.G., 2014. Up-to-date approach to manage keloids and hypertrophic scars: A useful guide. *Burns*, 40(7), pp.1255–1266. https://doi.org/10.1016/j.burns.2014.02.011.

Aronson, J. ed., 2016. Dichlorophen. In: *Meyler's Side Effects of Drugs*, Sixteenth. Elsevier.p.942. https://doi.org/10.1016/B978-0-444-53717-1.00612-0.

Arts, J., King, P., Mariën, A., Floren, W., Beliën, A., Janssen, L., Pilatte, I., Roux, B., Decrane, L., Gilissen, R., Hickson, I., Vreys, V., Cox, E., Bol, K., Talloen, W., Goris, I., Andries, L., du Jardin, M., Janicot, M., Page, M., van Emelen, K. and Angibaud, P., 2009. JNJ-26481585, a Novel "Second-Generation" Oral Histone Deacetylase Inhibitor, Shows Broad-Spectrum Preclinical Antitumoral Activity. *Clinical Cancer Research*, 15(22), pp.6841–6851. https://doi.org/10.1158/1078-0432.CCR-09-0547.

Ashraf-Uz-Zaman, M., Sajib, M.S., Cucullo, L., Mikelis, C.M. and German, N.A., 2018. Analogs of penfluridol as chemotherapeutic agents with reduced central nervous system activity. *Bioorganic & Medicinal Chemistry Letters*, 28(23–24), pp.3652–3657. https://doi.org/10.1016/j.bmcl.2018.10.036.

Asilian, A., Darougheh, A. and Shariati, F., 2006. New Combination of Triamcinolone, 5-Fluorouracil, and Pulsed-Dye Laser for Treatment of Keloid and Hypertrophic Scars. *Dermatologic Surgery*, 32(7), pp.907–915.

Asrani, S.K., Devarbhavi, H., Eaton, J. and Kamath, P.S., 2019. Burden of liver diseases in the world Introduction and global burden. *Journal of Hepatology*, 70, pp.151–171.

Atiyeh, B.S., 2007. Nonsurgical management of hypertrophic scars: Evidence-based therapies, standard practices, and emerging methods. *Aesthetic Plastic Surgery*, 31(5), pp.468–492. https://doi.org/10.1007/s00266-006-0253-y.

Atiyeh, B.S., Costagliola, M. and Hayek, S.N., 2005. Keloid or hypertrophic scar: The controversy: Review of the literature. *Annals of Plastic Surgery*, 54(6), pp.676–680. https://doi.org/10.1097/01.sap.0000164538.72375.93.

Attali, P., 1987. Dupuytren's Contracture, Alcohol Consumption, and Chronic Liver Disease. *Archives of Internal Medicine*, 147(6), pp.1065–1067. https://doi.org/10.1001/archinte.1987.00370060061012.

Au, K. and Ehrlich, H.P., 2010. When the Smad signaling pathway is impaired, fibroblasts advance open wound contraction. *Experimental and Molecular Pathology*, 89(3), pp.236–240. https://doi.org/10.1016/j.yexmp.2010.08.002.

Auerbach, S., DrugMatrix® and ToxFX®, 2014. *Prochlorperazine*. National Toxicology Program.

Awan, F.T., Gore, L., Gao, L., Sharma, J., Lager, J. and Costa, L.J., 2016. Phase Ib trial of the PI3K/mTOR inhibitor voxtalisib (SAR245409) in combination with chemoimmunotherapy in patients with relapsed or refractory B-cell malignancies. *British Journal of Haematology*, 175(1), pp.55–65. https://doi.org/10.1111/bjh.14181.

van Baar, M.E., 2020. Epidemiology of Scars and Their Consequences: Burn Scars. In: *Textbook on Scar Management*. Cham: Springer International Publishing.pp.37–43. https://doi.org/10.1007/978-3-030-44766-3_5.

Bakin, A., Rinehart, C., Tomlinson, A. and Arteaga, C., 2002. p38 mitogen-activated protein kinase is required for TGFβ-mediated fibroblastic transdifferentiation and cell migration. *Journal of Cell Science*, 115(15), pp.3193–3206.

Ball, C., Izadi, D., Verjee, L.S., Chan, J. and Nanchahal, J., 2016. Systematic review of non-surgical treatments for early dupuytren's disease. *BMC Musculoskeletal Disorders*, 17(345), pp.1–17. https://doi.org/10.1186/s12891-016-1200-y.

Bang-Andersen, B., Ruhland, T., Jørgensen, M., Smith, G., Frederiksen, K., Jensen, K.G., Zhong, H., Nielsen, S.M., Hogg, S., Mørk, A. and Stensbøl, T.B., 2011. Discovery of 1-[2-(2,4-Dimethylphenylsulfanyl)phenyl]piperazine (Lu AA21004): A Novel Multimodal Compound for the Treatment of Major Depressive Disorder. *Journal of Medicinal Chemistry*, 54(9), pp.3206–3221. https://doi.org/10.1021/jm101459g.

Barf, T. and Kaptein, A., 2012. Irreversible Protein Kinase Inhibitors: Balancing the Benefits and Risks. *Journal of Medicinal Chemistry*, 55(14), pp.6243–6262. https://doi.org/10.1021/jm3003203.

Barker, T.H., 2011. The role of ECM proteins and protein fragments in guiding cell behavior in regenerative medicine. *Biomaterials*, 32(18), pp.4211–4. https://doi.org/10.1016/j.biomaterials.2011.02.027.

Barnes, J.L. and Gorin, Y., 2011. Myofibroblast differentiation during fibrosis: Role of NAD(P)H oxidases. *Kidney International*, 79(9), pp.944–956. https://doi.org/10.1038/ki.2010.516.

Barriere, G., Fici, P., Gallerani, G., Fabbri, F. and Rigaud, M., 2015. Epithelial Mesenchymal Transition: a double-edged sword. *Clinical and Translational Medicine*, 4(14), pp.1–6. https://doi.org/10.1186/s40169-015-0055-4.

Bass, J.J., Wilkinson, D.J., Rankin, D., Phillips, B.E., Szewczyk, N.J., Smith, K. and Atherton, P.J., 2017. *An overview of technical considerations for Western blotting*

applications to physiological research. *Scandinavian Journal of Medicine and Science in Sports*, https://doi.org/10.1111/sms.12702.

Bataller, R. and Brenner, D.A., 2005. Liver fibrosis. *Journal of Clinical Investigation*, [online] 115(2), pp.209–218. https://doi.org/10.1172/JCI200524282.

Baumann, L.S. and Md, J.S., 1999. The Effects of Topical Vitamin E on the Cosmetic Appearance of Scars. *Dermatologic Surgery*, 25(4), pp.311–315. https://doi.org/10.1046/j.1524-4725.1999.08223.x.

Bayat, A., Arscott, G., Ollier, W.E.R., Mc Grouther, D.A. and Ferguson, M.W.J., 2005. Keloid disease: Clinical relevance of single versus multiple site scars. *British Journal of Plastic Surgery*, 58(1), pp.28–37. https://doi.org/10.1016/j.bjps.2004.04.024.

Bayat, A., Cunliffe, E.J. and McGrouther, D.A., 2007. Assessment of clinical severity in Dupuytren's disease. *British Journal of Hospital Medicine*, 68(11), pp.604–609. https://doi.org/10.12968/hmed.2007.68.11.27683.

Bayat, A., McGrouther, D.A. and Ferguson, M.W.J., 2003. Skin scarring. *British Medical Journal*, [online] 326(7380), pp.88–92. https://doi.org/10.1136/bmj.326.7380.88.

Bedossa, P. and Paradis, V., 2003. Liver extracellular matrix in health and disease. *Journal of Pathology*, 200(4), pp.504–515. https://doi.org/10.1002/path.1397.

Bellew, S., Weiss, M. and Weiss, R., 2005. Comparison of intense pulsed light to 595-nm long-pulsed pulsed dye laser for treatment of hypertrophic surgical scars: a pilot study. *Journal of Drugs in Dermatology*, 4(4), pp.448–452.

Berridge, M.V. and Tan, A.S., 1993. Characterization of the Cellular Reduction of 3-(4,5-dimethylthiazol-2-yl)-2,5-diphenyltetrazolium bromide (MTT): Subcellular Localization, Substrate Dependence, and Involvement of Mitochondrial Electron Transport in MTT Reduction. *Archives of Biochemistry and Biophysics*, 303(2), pp.474–482. https://doi.org/10.1006/abbi.1993.1311.

Biernacka, A., Dobaczewski, M. and Frangogiannis, N.G., 2011. TGF-β signaling in fibrosis. *Growth Factors*, 29(5), pp.196–202. https://doi.org/10.3109/08977194.2011.595714.

Boer, M., Duchnik, E., Maleszka, R. and Marchlewicz, M., 2016. Structural and biophysical characteristics of human skin in maintaining proper epidermal barrier function. *Postepy Dermatologii i Alergologii*, 33(1), pp.1–5. https://doi.org/10.5114/pdia.2015.48037.

Bonis, P.A.L., Friedman, S.L. and Kaplan, M.M., 2001. Is Liver Fibrosis Reversible? *New England Journal of Medicine*, 344(6), pp.452–454. https://doi.org/10.1056/NEJM200102083440610.

Bonnans, C., Chou, J. and Werb, Z., 2014. Remodelling the extracellular matrix in development and disease. *Nature Reviews Molecular Cell Biology*, 15(12), pp.786–801. https://doi.org/10.1038/nrm3904.

Bonner, J.C., 2004. Regulation of PDGF and its receptors in fibrotic diseases. *Cytokine and Growth Factor Reviews*, 15(4), pp.255–273. https://doi.org/10.1016/j.cytogfr.2004.03.006.

Borad, M.J., Bai, L.-Y., Chen, M.-H., Hubbard, J.M., Mody, K., Rha, S.Y., Richards, D.A., Davis, S.L., Soong, J., Huang, C.-E.C.-E., Tse, E., Ahn, D.H., Chang, H.-M., Yen, C.-J., Oh, D.-Y., Park, J.O., Hsu, C., Becerra, C.R., Chen, J.-S. and Chen, Y.-Y., 2021. Silmitasertib (CX-4945) in combination with gemcitabine and cisplatin as first-line treatment for patients with locally advanced or metastatic cholangiocarcinoma: A phase Ib/II study. *Journal of*

Clinical Oncology, 39(3_suppl), pp.312–312. https://doi.org/10.1200/JCO.2021.39.3_suppl.312.

Bordeaux, J., Welsh, A.W., Agarwal, S., Killiam, E., Baquero, M.T., Hanna, J.A., Anagnostou, V.K. and Rimm, D.L., 2010. Antibody validation. *BioTechniques*, 48(3), pp.197–209. https://doi.org/10.2144/000113382.

Borthwick, L.A., Wynn, T.A. and Fisher, A.J., 2013. Cytokine mediated tissue fibrosis. *Biochimica et Biophysica Acta (BBA) - Molecular Basis of Disease*, 1832(7), pp.1049–1060. https://doi.org/10.1016/j.bbadis.2012.09.014.

Bower, M., Nelson, M. and Gazzard, B., 1990. Dupuytren's contractures in patients infected with HIV. *British Medical Journal*, 300, pp.164–165.

Bragulla, H.H. and Homberger, D.G., 2009. Structure and functions of keratin proteins in simple, stratified, keratinized and cornified epithelia. *Journal of Anatomy*, 214(4), pp.516–559. https://doi.org/10.1111/j.1469-7580.2009.01066.x.

Bran, G.M., Goessler, U.R., Hormann, K., Riedel, F. and Sadick, H., 2009. Keloids: Current concepts of pathogenesis (Review). *International Journal of Molecular Medicine*, 24(3), pp.283–293. https://doi.org/10.3892/ijmm_00000231.

Brem, H., Kodra, A., Golinko, M.S., Entero, H., Stojadinovic, O., Wang, V.M., Sheahan, C.M., Weinberg, A.D., Woo, S.L.C., Paul Ehrlich, H. and Tomic-Canic, M., 2009. Mechanism of Sustained Release of Vascular Endothelial Growth Factor in Accelerating Experimental Diabetic Healing. *Journal of Investigative Dermatology*, 129(9), pp.2275–2287. https://doi.org/10.1038/jid.2009.26.

Brewster, C.T., Choong, J., Thomas, C., Wilson, D. and Moiemen, N., 2020. Steam inhalation and paediatric burns during the COVID-19 pandemic. *The Lancet*, [online] 395(10238), p.1690. https://doi.org/10.1016/S0140-6736(20)31144-2.

Brusselaers, N., Monstrey, S., Vogelaers, D., Hoste, E. and Blot, S., 2010. Severe burn injury in europe: A systematic review of the incidence, etiology, morbidity, and mortality. *Critical Care*, [online] 14(5), p.R188. https://doi.org/10.1186/cc9300.

Buggy, J.J., Cao, Z.A., Bass, K.E., Verner, E., Balasubramanian, S., Liu, L., Schultz, B.E., Young, P.R. and Dalrymple, S.A., 2006. CRA-024781: a novel synthetic inhibitor of histone deacetylase enzymes with antitumor activity *in vitro* and *in vivo*. *Molecular Cancer Therapeutics*, 5(5). https://doi.org/10.1158/1535-7163.MCT-05-0442.

Burton, G.W., Joyce, A. and Ingold, K.U., 1983. Is vitamin E the only lipid-soluble, chain-breaking antioxidant in human blood plasma and erythrocyte membranes? *Archives of Biochemistry and Biophysics*, 221(1), pp.281–290. https://doi.org/10.1016/0003-9861(83)90145-5.

Cano, A., Pérez-Moreno, M.A., Rodrigo, I., Locascio, A., Blanco, M.J., del Barrio, M.G., Portillo, F. and Angela Nieto, M., 2000. The transcription factor Snail controls epithelial-mesenchymal transitions by repressing E-cadherin expression. *Nature Cell Biology*, 2, pp.76–83.

Cao, H., Wang, C., Chen, X., Hou, J., Xiang, Z., Shen, Y. and Han, X., 2018. Inhibition of Wnt/β-catenin signaling suppresses myofibroblast differentiation of lung resident mesenchymal stem cells and pulmonary fibrosis. *Scientific Reports*, 8(1), p.13644. https://doi.org/10.1038/s41598-018-28968-9.

Cardelús, I., Antón, F., Beleta, J. and Palacios, J.M., 1999. Anticholinergic effects of desloratadine, the major metabolite of loratadine, in rabbit and guinea-pig iris smooth muscle. *European Journal of Pharmacology*, 374(2), pp.249–254. https://doi.org/10.1016/S0014-2999(99)00310-6.

Careta, M.F. and Romiti, R., 2015. Localized scleroderma: Clinical spectrum and therapeutic update. *Anais Brasileiros de Dermatologia*, 90(1), pp.62–73. https://doi.org/10.1590/abd1806-4841.20152890.

Carmeliet, P., 2005. VEGF as a Key Mediator of Angiogenesis in Cancer. *Oncology*, 69(3), pp.4–10. https://doi.org/10.1159/000088478.

Caves, J.M., Cui, W., Wen, J., Kumar, V.A., Haller, C.A. and Chaikof, E.L., 2011. Elastin-like protein matrix reinforced with collagen microfibers for soft tissue repair. *Biomaterials*, 32(23), pp.5371–5379. https://doi.org/10.1016/j.biomaterials.2011.04.009.

Ceschin-Roques, C.G., HÄNel, H., Pruja-Bougaret, S.M., Lagarde, I., Vandermander, J. and Michel, G., 1991. Ciclopiroxolamine cream 1%: In vitro and in vivo penetration into the stratum corneum. *Skin Pharmacology and Physiology*, 4(2), pp.95–99. https://doi.org/10.1159/000210930.

Cha, M., Ha, T., Jeon, J., Jo, M., Kang, S., Kim, M., Kim, M., Kwak, E., Lee, J., Lee, K. and Suh, K., 2012. *Novel fused pyrimidine derivatives for inhibition of tyrosine kinase activity.* WO2011162515A3.

Chao, Q., Sprankle, K.G., Grotzfeld, R.M., Lai, A.G., Carter, T.A., Velasco, A.M., Gunawardane, R.N., Cramer, M.D., Gardner, M.F., James, J., Zarrinkar, P.P., Patel, H.K. and Bhagwat, S.S., 2009. Identification of N-(5-tert-Butyl-isoxazol-3-yl)-N-{4-[7-(2-morpholin-4-yl-ethoxy)imidazo[2,1-b][1,3]benzothiazol-2-yl]phenyl} urea Dihydrochloride (AC220), a Uniquely Potent, Selective, and Efficacious FMS-Like Tyrosine Kinase-3 (FLT3) Inhibitor. *Journal of Medicinal Chemistry*, 52(23), pp.7808–7816. https://doi.org/10.1021/jm9007533.

Chatelier, A., Mercier, A., Tremblier, B., Thériault, O., Moubarak, M., Benamer, N., Corbi, P., Bois, P., Chahine, M. and Faivre, J.F., 2012. A distinct de novo expression of Nav1.5 sodium channels in human atrial fibroblasts differentiated into myofibroblasts. *The Journal of Physiology*, 590(17), pp.4307–4319. https://doi.org/10.1113/jphysiol.2012.233593.

Chaturvedi, N.K., McGuire, T.R., Coulter, D.W., Shukla, A., McIntyre, E.M., Sharp, J.G. and Joshi, S.S., 2016. Improved therapy for neuroblastoma using a combination approach: superior efficacy with vismodegib and topotecan. *Oncotarget*, 7(12), pp.15215–15229. https://doi.org/10.18632/oncotarget.7714.

Chen, M., Huang, J., Yang, X., Liu, B., Zhang, W., Huang, L., Deng, F., Ma, J., Bai, Y., Lu, R., Huang, B., Gao, Q., Zhuo, Y. and Ge, J., 2012. Serum starvation induced cell cycle synchronization facilitates human somatic cells reprogramming. *PLoS ONE*, 7(4), pp.1–9. https://doi.org/10.1371/journal.pone.0028203.

Chen, R., Cheng, Q., Owusu-Ansah, K.G., Chen, J., Song, G., Xie, H., Zhou, L., Xu, X., Jiang, D. and Zheng, S., 2018. Cabazitaxel, a novel chemotherapeutic alternative for drug-resistant hepatocellular carcinoma. *American journal of cancer research*, 8(7), pp.1297–1306.

Chen, X., Chong, C.R., Shi, L., Yoshimoto, T., Sullivan, D.J.† and Liu, J.O., 2006. Inhibitors of Plasmodium falciparum methionine aminopeptidase 1b possess antimalarial activity. *PNAS*, [online] 103(39), pp.14548–14553. Available at: <www.ebi.ac.uk>.

Chiang, R.S., Borovikova, A.A., King, K., Banyard, D.A., Lalezari, S., Toranto, J.D., Paydar, K.Z., Wirth, G.A., Evans, G.R.D. and Widgerow, A.D., 2016. Current concepts related to hypertrophic scarring in burn injuries. *Wound Repair and Regeneration*, 24(3), pp.466–477. https://doi.org/10.1111/wrr.12432.

Chipp, E., Charles, L., Thomas, C., Whiting, K., Moiemen, N. and Wilson, Y., 2017. A prospective study of time to healing and hypertrophic scarring in paediatric burns: every day counts. *Burns & Trauma*, [online] 5(3), pp.1–6. https://doi.org/10.1186/s41038-016-0068-2.

Cho, H., Ueda, M., Shima, K., Mizuno, A., Hayashimatsu, M., Ohnaka, Y., Takeuchi, Y., Hamaguchi, M., Aisaka, K. and Hidaka, T., 1989. Dihydropyrimidines: novel calcium antagonists with potent and long-lasting vasodilative and antihypertensive activity. *Journal of medicinal chemistry*, 32(10), pp.2399–406. https://doi.org/10.1021/jm00130a029.

Chong, C.R., Chen, X., Shi, L., Liu, J.O. and Sullivan, D.J., 2006. A clinical drug library screen identifies astemizole as an antimalarial agent. *Nature Chemical Biology*, 2(8), pp.415–416. https://doi.org/10.1038/nchembio806.

Chong, C.R. and Sullivan, D.J., 2007. New uses for old drugs. *Nature*, 448(7154), pp.645–646. https://doi.org/10.1038/448645a.

Chuang-Tsai, S., Sisson, T.H., Hattori, N., Tsai, C.G., Subbotina, N.M., Hanson, K.E. and Simon, R.H., 2003. Reduction in Fibrotic Tissue Formation in Mice Genetically Deficient in Plasminogen Activator Inhibitor-1. *American Journal of Pathology*, 163(2), pp.445–452.

Cichorek, M., Wachulska, M., Stasiewicz, A. and Tymińska, A., 2013. Skin melanocytes: Biology and development. *Postepy Dermatologii i Alergologii*, 30(1), pp.30–41. https://doi.org/10.5114/pdia.2013.33376.

Clark, A., Imran, J., Madni, T. and Wolf, S.E., 2017. Nutrition and metabolism in burn patients. *Burns & Trauma*, 5. https://doi.org/10.1186/s41038-017-0076-x.

Clarke, Z., 2007. Penfluridol. In: *xPharm: The Comprehensive Pharmacology Reference*. Elsevier.pp.1–4. https://doi.org/10.1016/B978-008055232-3.62384-0.

von Coburg, Y., Kottke, T., Weizel, L., Ligneau, X. and Stark, H., 2009. Potential utility of histamine H3 receptor antagonist pharmacophore in antipsychotics. *Bioorganic & Medicinal Chemistry Letters*, 19(2), pp.538–542. https://doi.org/10.1016/j.bmcl.2008.09.012.

Cocci, A., Russo, G.I., Salamanca, J.I.M., Ralph, D., Palmieri, A. and Mondaini, N., 2020. The End of an Era: Withdrawal of Xiapex (Clostridium histolyticum Collagenase) from the European Market. *European Urology*, 77(5), pp.660–661. https://doi.org/10.1016/j.eururo.2019.11.019.

Connolly, K.L., Chaffins, M. and Ozog, D., 2014. Vascular patterns in mature hypertrophic burn scars treated with fractional CO2 laser. *Lasers in Surgery and Medicine*, 46(8), pp.597–600. https://doi.org/10.1002/lsm.22271.

Connolly, R.M., Rudek, M.A. and Piekarz, R., 2017. Entinostat: a promising treatment option for patients with advanced breast cancer. *Future Oncology*, 13(13), pp.1137–1148. https://doi.org/10.2217/fon-2016-0526.

Coolen, N.A., Verkerk, M., Reijnen, L., Vlig, M., van den Bogaerdt, A.J., Breetveld, M., Gibbs, S., Middelkoop, E. and Ulrich, M.M.W., 2007. Culture of keratinocytes for transplantation without the need of feeder layer cells. *Cell Transplantation*, 16(6), pp.649–661. https://doi.org/10.3727/000000007783465046.

Corbella, X. and Fonollosa, V., 2014. Mortality and survival in systemic sclerosis : Systematic review and. *Seminars in Arthritis and Rheumatism*, [online] 44(2), pp.208–219. https://doi.org/10.1016/j.semarthrit.2014.05.010.

Coulombe, P.A., 2003. Wound epithelialization: accelerating the pace of discovery. *The Journal of investigative dermatology*, 121(2), pp.219–230. https://doi.org/10.1046/j.1523-1747.2003.12387.x.

Cromer, H. and Barker, N., 1944. The effect of large doses of menadione bisulfite (synthetic vitamin K) on excessive hypoprothrombinemia induced by dicumarol. *Proceedings of Staff Meetings of the Mayo Clinic*, 19, pp.217–223.

Cubison, T.C.S., Pape, S.A. and Parkhouse, N., 2006. Evidence for the link between healing time and the development of hypertrophic scars (HTS) in paediatric burns due to scald injury. *Burns*, 32(8), pp.992–999. https://doi.org/10.1016/j.burns.2006.02.007.

DaCosta Byfield, S., Major, C., Laping, N.J. and Roberts, A.B., 2004. SB-505124 Is a Selective Inhibitor of Transforming Growth Factor-β Type I Receptors ALK4, ALK5, and ALK7. *Molecular Pharmacology*, 65(3), pp.744–752. https://doi.org/10.1124/mol.65.3.744.

Dahl, E.L. and Rosenthal, P.J., 2007. Multiple antibiotics exert delayed effects against the Plasmodium falciparum apicoplast. *Antimicrobial agents and chemotherapy*, 51(10), pp.3485–90. https://doi.org/10.1128/AAC.00527-07.

Dalli, J., Montero-Melendez, T., Norling, L. v, Yin, X., Hinds, C., Haskard, D., Mayr, M. and Perretti, M., 2013. Heterogeneity in Neutrophil Microparticles Reveals Distinct Proteome and Functional Properties. *Molecular & Cellular Proteomics*, 12(8), pp.2205–2219. https://doi.org/10.1074/mcp.M113.028589.

Danziger, J., 2008. Vitamin K-dependent Proteins, Warfarin, and Vascular Calcification. *Clinical Journal of the American Society of Nephrology*, 3(5), pp.1504–1510. https://doi.org/10.2215/CJN.00770208.

Darby, I., Skalli, O. and Gabbiani, G., 1990. Alpha-smooth muscle actin is transiently expressed by myofibroblasts during experimental wound healing. *Laboratory investigation; a journal of technical methods and pathology*, 63(1), pp.21–9.

Datta, A., Scotton, C.J. and Chambers, R.C., 2011. Novel therapeutic approaches for pulmonary fibrosis. *British Journal of Pharmacology*, [online] 163, pp.141–172. https://doi.org/10.1111/bph.2011.163.issue-1.

Davis, J. and Molkentin, J.D., 2014. Myofibroblasts: Trust your heart and let fate decide. *Journal of Molecular and Cellular Cardiology*, 70, pp.9–18. https://doi.org/10.1016/j.yjmcc.2013.10.019.

Davis, M.I., Hunt, J.P., Herrgard, S., Ciceri, P., Wodicka, L.M., Pallares, G., Hocker, M., Treiber, D.K. and Zarrinkar, P.P., 2011. Comprehensive analysis of kinase inhibitor selectivity. *Nature Biotechnology*, 29(11). https://doi.org/10.1038/nbt.1990.

Deeks, S.G., Kar, S., Gubernick, S.I. and Kirkpatrick, P., 2008. Raltegravir. *Nature Reviews Drug Discovery*, 7(2), pp.117–118. https://doi.org/10.1038/nrd2512.

Delavary, B.M., van der Veer, W.M., van Egmond, M., Niessen, F.B. and Beelen, R.H.J., 2011. Macrophages in skin injury and repair. *Immunobiology*, 216(7), pp.753–762. https://doi.org/10.1016/j.imbio.2011.01.001.

Delves, M., Plouffe, D., Scheurer, C., Meister, S., Wittlin, S., Winzeler, E.A., Sinden, R.E. and Leroy, D., 2012. The Activities of Current Antimalarial Drugs on the Life Cycle Stages of Plasmodium: A Comparative Study with Human and Rodent Parasites. *PLoS Medicine*, 9(2), p.e1001169. https://doi.org/10.1371/journal.pmed.1001169.

Deng, X., Jin, K., Li, Y., Gu, W., Liu, M. and Zhou, L., 2015. Platelet-Derived Growth Factor and Transforming Growth Factor β1 Regulate ARDS-Associated Lung Fibrosis Through Distinct Signaling Pathways. *Cellular Physiology and Biochemistry*, 36(3), pp.937–946. https://doi.org/10.1159/000430268.

DeSanti, L., 2005. Pathophysiology and current management of burn injury. *Advances in skin & wound care*, 18(6), pp.323–332. https://doi.org/10.1097/00129334-200507000-00014.

Desmouliere, A., Geinoz, A., Gabbiani, F. and Gabbiani, G., 1993. Transforming Growth Factor-β Induces Alpha-Smooth Muscle Actin Expression in Granulation Tissue Myofibroblasts and in Quiescent and Growing Cultured Fibroblasts. *The Journal of Cell Biology*, 122(1), pp.103–111.

Desmoulière, A., Redard, M., Darby, I. and Gabbiani, G., 1995. Apoptosis mediates the decrease in cellularity during the transition between granulation tissue and scar. *The American journal of pathology*, 146(1), pp.56–66.

Di, L. and Kerns, E.H., 2006. Biological assay challenges from compound solubility: strategies for bioassay optimization. *Drug Discovery Today*, 11(9–10), pp.446–451. https://doi.org/10.1016/j.drudis.2006.03.004.

Ding, I. and Peterson, A.M., 2021. Half-life modeling of basic fibroblast growth factor released from growth factor-eluting polyelectrolyte multilayers. *Scientific Reports*, 11(9808), pp.1–13. https://doi.org/10.1038/s41598-021-89229-w.

Ding, N., Yu, R.T., Subramaniam, N., Sherman, M.H., Wilson, C., Rao, R., Leblanc, M., Coulter, S., He, M., Scott, C., Lau, S.L., Atkins, A.R., Barish, G.D., Gunton, J.E., Liddle, C., Downes, M. and Evans, R.M., 2013. A Vitamin D Receptor/SMAD Genomic Circuit Gates Hepatic Fibrotic Response. *Cell*, 153(3), pp.601–613. https://doi.org/10.1016/j.cell.2013.03.028.

Distler, J.H.W., Györfi, A.H., Ramanujam, M., Whitfield, M.L., Königshoff, M. and Lafyatis, R., 2019. Shared and distinct mechanisms of fibrosis. *Nature Reviews Rheumatology*, 15(12), pp.705–730. https://doi.org/10.1038/s41584-019-0322-7.

Distler, O. and Cozzio, A., 2016. Systemic sclerosis and localized scleroderma—current concepts and novel targets for therapy. *Seminars in Immunopathology*, 38(1), pp.87–95. https://doi.org/10.1007/s00281-015-0551-z.

Do, K., Speranza, G., Chang, L.-C., Polley, E.C., Bishop, R., Zhu, W., Trepel, J.B., Lee, S., Lee, M.-J., Kinders, R.J., Phillips, L., Collins, J., Lyons, J., Jeong, W., Antony, R., Chen, A.P., Neckers, L., Doroshow, J.H. and Kummar, S., 2015. Phase I study of the heat shock protein 90 (Hsp90) inhibitor onalespib (AT13387) administered on a daily for 2 consecutive days per week dosing schedule in patients with advanced solid tumors. *Investigational New Drugs*, 33(4), pp.921–930. https://doi.org/10.1007/s10637-015-0255-1.

Dolivo, D.M., Larson, S.A. and Dominko, T., 2019. Crosstalk between mitogen-activated protein kinase inhibitors and transforming growth factor-β signaling results in variable activation of human dermal fibroblasts. *International Journal of Molecular Medicine*, 43(1), pp.325–335. https://doi.org/10.3892/ijmm.2018.3949.

Drews, J. and Ryser, S., 1997. The role of innovation in drug development. *Nature Biotechnology*, [online] 75, pp.1318–1319. Available at: <http://www.nature.com/naturebiotechnology>.

Driskell, R.R., Jahoda, C.A.B., Chuong, C.M., Watt, F.M. and Horsley, V., 2014. Defining dermal adipose tissue. *Experimental Dermatology*, 23(9), pp.629–631. https://doi.org/10.1111/exd.12450.

Dumble, M., Crouthamel, M.-C., Zhang, S.-Y., Schaber, M., Levy, D., Robell, K., Liu, Q., Figueroa, D.J., Minthorn, E.A., Seefeld, M.A., Rouse, M.B., Rabindran, S.K., Heerding, D.A. and Kumar, R., 2014. Discovery of Novel AKT Inhibitors with Enhanced Anti-Tumor Effects in Combination with the MEK Inhibitor. *PLoS ONE*, 9(6), p.e100880. https://doi.org/10.1371/journal.pone.0100880.

Durani, P., Occleston, N., O'Kane, S. and Ferguson, M.W.J., 2008. Avotermin: A Novel Antiscarring Agent. *The International Journal of Lower Extremity Wounds*, 7(3). https://doi.org/10.1177/1534734608322983.

Dziekan, J.M., Yu, H., Chen, D., Dai, L., Wirjanata, G., Larsson, A., Prabhu, N., Sobota, R.M., Bozdech, Z. and Nordlund, P., 2019. Identifying purine nucleoside phosphorylase as the target of quinine using cellular thermal shift assay. *Science Translational Medicine*, 11(473). https://doi.org/10.1126/scitranslmed.aau3174.

Eberhard, Y., McDermott, S.P., Wang, X., Gronda, M., Venugopal, A., Wood, T.E., Hurren, R., Datti, A., Batey, R.A., Wrana, J., Antholine, W.E., Dick, J. and Schimmer, A.D., 2009. Chelation of intracellular iron with the antifungal agent ciclopirox olamine induces cell death in leukemia and myeloma cells. *Blood*, 114(14), pp.3064–3073. https://doi.org/10.1182/blood-2009-03-209965.

Ebrahimi, H., Naderian, M. and Sohrabpour, A.A., 2016. New Concepts on Pathogenesis and Diagnosis of Liver Fibrosis; A Review Article. *Middle East Journal of Digestive Diseases*, 8(3), pp.166–178. https://doi.org/10.15171/mejdd.2016.29.

Eder, J., Sedrani, R. and Wiesmann, C., 2014. The discovery of first-in-class drugs: Origins and evolution. *Nature Reviews Drug Discovery*, 13(8), pp.577–587. https://doi.org/10.1038/nrd4336.

Efstratiadis, G., Divani, M., Katsioulis, E. and Vergoulas, G., 2009. Renal fibrosis. *Hippokratia*, 13(4), pp.224–228.

Eger, A., Stockinger, A., Park, J., Langkopf, E., Mikula, M., Gotzmann, J., Mikulits, W., Beug, H. and Foisner, R., 2004. β-Catenin and TGFβ signalling cooperate to maintain a mesenchymal phenotype after FosER-induced epithelial to mesenchymal transition. *Oncogene*, 23(15), pp.2672–2680. https://doi.org/10.1038/sj.onc.1207416.

Ehrlich, H.P., Desmoulière, A., Diegelmann, R.F., Cohen, I.K., Compton, C.C., Garner, W.L., Kapanci, Y. and Gabbiani, G., 1994. Morphological and immunochemical differences between keloid and hypertrophic scar. *American Journal of Pathology*, 145(1), pp.105–113.

Eming, S.A., Krieg, T. and Davidson, J.M., 2007. Inflammation in wound repair: Molecular and cellular mechanisms. *Journal of Investigative Dermatology*, 127(3), pp.514–525. https://doi.org/10.1038/sj.jid.5700701.

Eming, S.A., Martin, P. and Tomic-Canic, M., 2014. Wound repair and regeneration: Mechanisms, signaling, and translation. *Science Translational Medicine*, 6(265), pp.1–36. https://doi.org/10.1126/scitranslmed.3009337.Wound.

Erlichman, C., Hidalgo, M., Boni, J.P., Martins, P., Quinn, S.E., Zacharchuk, C., Amorusi, P., Adjei, A.A. and Rowinsky, E.K., 2006. Phase I Study of EKB-569, an Irreversible Inhibitor of the Epidermal Growth Factor Receptor, in Patients With Advanced Solid Tumors. *Journal of Clinical Oncology*, 24(15), pp.2252–2260. https://doi.org/10.1200/JCO.2005.01.8960.

Espana, A., Solano, T. and Quintanilla, E., 2001. Bleomycin in the Treatment of Keloids and Hypertrophic Scars by Multiple Needle Punctures. *Dermatologic Surgery*, 27(1), pp.23–27.

European Comission, European Medicines Agency and Heads of Medicines Agencies, 2021. *Proposal for a framework to support not-for-profit organisations and academia in repurposing authorised medicines*.

Faldmo, L. and Kravitz, M., 1993. Management of acute burns and burn shock resuscitation. *AACN clinical issues in critical care nursing*, 4(2), pp.351–66.

Falke, L.L., Gholizadeh, S., Goldschmeding, R., Kok, R.J. and Nguyen, T.Q., 2015. Diverse origins of the myofibroblast-implications for kidney fibrosis. *Nature Reviews Nephrology*, 11(4), pp.233–244. https://doi.org/10.1038/nrneph.2014.246.

Fan, X., Xie, J. and Tian, J., 2017. Reducing Cardiac Fibrosis: Na/K-ATPase Signaling Complex as a Novel Target. *Cardiovascular pharmacology: open access*, 6(1). https://doi.org/10.4172/2329-6607.1000204.

Feinberg, S., Fariba, K. and Saadabadi, A., 2021. *Thioridazine*. StatPearls.

de Felice, B., Garbi, C., Santoriello, M., Santillo, A. and Wilson, R.R., 2009. Differential apoptosis markers in human keloids and hypertrophic scars fibroblasts. *Molecular and Cellular Biochemistry*, 327(1–2), pp.191–201. https://doi.org/10.1007/s11010-009-0057-x.

Fett, N., 2013. Scleroderma: Nomenclature, etiology, pathogenesis, prognosis, and treatments: Facts and controversies. *Clinics in Dermatology*, [online] 31(4), pp.432–437. https://doi.org/10.1016/j.clindermatol.2013.01.010.

Finnerty, C., Jeschke, M., Branksi, L., Barret, J., Dziewulski, P. and Herndon, D., 2017. Hypertrophic scarring: the greatest unmet challenge following burn injury. *The Lancet*, 4(11), pp.1427–1436. https://doi.org/10.1016/S2214-109X(16)30265-0.Cost-effectiveness.

Fischer, A.H., Jacobson, K.A., Rose, J. and Zeller, R., 2008. Hematoxylin and Eosin Staining of Tissue and Cell Sections. *Cold Spring Harbor Protocols*, 2008(6). https://doi.org/10.1101/pdb.prot4986.

Fish, P. v, Deur, C., Gan, X., Greene, K., Hoople, D., Mackenny, M., Para, K.S., Reeves, K., Ryckmans, T., Stiff, C., Stobie, A., Wakenhut, F. and Whitlock, G.A., 2008. Design and synthesis of morpholine derivatives. SAR for dual serotonin & noradrenaline reuptake inhibition. *Bioorganic & medicinal chemistry letters*, 18(8), pp.2562–6. https://doi.org/10.1016/j.bmcl.2008.03.050.

Fletcher, J., Tan, E.S.L., Thomas, M., Taylor, F., Elliott, D. and Bindra, R., 2019. Collagenase injections for Dupuytren's contracture: prospective cohort study in a public health setting. *ANZ Journal of Surgery*, 89(5), pp.573–577. https://doi.org/10.1111/ans.14988.

Fogel-Petrovic, M., Long, J.A., Misso, N.L., Foster, P.S., Bhoola, K.D. and Thompson, P.J., 2007. Physiological concentrations of transforming growth factor β1 selectively inhibit human dendritic cell function. *International Immunopharmacology*, 7(14). https://doi.org/10.1016/j.intimp.2007.07.003.

Frazier, E.P., Michel-Reher, M.B., van Loenen, P., Sand, C., Schneider, T., Peters, S.L.M. and Michel, M.C., 2011. Lack of evidence that nebivolol is a β3-adrenoceptor agonist. *European Journal of Pharmacology*, 654(1), pp.86–91. https://doi.org/10.1016/j.ejphar.2010.11.036.

Frazier, K., Williams, S., Kothapalli, D., Klapper, H. and Grotendorst, G.R., 1996. Stimulation of fibroblast cell growth, matrix production, and granulation tissue formation by connective tissue growth factor. *The Journal of investigative dermatology*, 107(3), pp.404–11. https://doi.org/10.1111/1523-1747.ep12363389.

Freedman, S.B., Patel, S., Marwood, R., Emms, F., Seabrook, G.R., Knowles, M.R. and McAllister, G., 1994. Expression and pharmacological characterization of the human D3 dopamine receptor. *The Journal of pharmacology and experimental therapeutics*, 268(1), pp.417–26.

Freshwater, M.F., 2013. Botulinum toxin for scars: Can it work, does it work, is it worth it? *Journal of Plastic, Reconstructive and Aesthetic Surgery*, [online] 66(3), pp.e92–e93. https://doi.org/10.1016/j.bjps.2012.11.034.

Friend, C., Scher, W., Holland, J.G. and Sato, T., 1971. Hemoglobin Synthesis in Murine Virus-Induced Leukemic Cells In Vitro: Stimulation of Erythroid Differentiation by Dimethyl Sulfoxide. *Proceedings of the National Academy of Sciences*, 68(2), pp.378–382.

Frykberg, R.G. and Banks, J., 2015. Challenges in the Treatment of Chronic Wounds. *Advances in Wound Care*, 4(9), pp.560–582. https://doi.org/10.1089/wound.2015.0635.

Galaris, D., Barbouti, A. and Pantopoulos, K., 2019. *Iron homeostasis and oxidative stress: An intimate relationship*. *Biochimica et Biophysica Acta - Molecular Cell Research*, https://doi.org/10.1016/j.bbamcr.2019.118535.

Gale, A.J., 2011. Current Understanding of Hemostasis. *Toxicologic Pathology*, 39(1), pp.273–280. https://doi.org/10.1177/0192623310389474.

Garaffa, G., Gentile, V., Antonini, G., Tsafrakidis, P., Raheem, A.A. and Ralph, D.J., 2013. Penile reconstruction in the male. *Arab Journal of Urology*, 11(3), pp.267–271. https://doi.org/10.1016/j.aju.2013.04.003.

García, M., Aguirre, U., Martinez, A., Ruiz, B., Lertxundi, U. and Aguirre, C., 2014. Acute adverse reactions to iopromide *vs* iomeprol: a retrospective analysis of spontaneous reporting from a radiology department. *The British Journal of Radiology*, 87(1033), p.20130511. https://doi.org/10.1259/bjr.20130511.

Garcia-Echeverria, C. and Sellers, W.R., 2008. Drug discovery approaches targeting the PI3K/Akt pathway in cancer. *Oncogene*, 27(41), pp.5511–5526. https://doi.org/10.1038/onc.2008.246.

Gauglitz, G., Korting, H., Pavicic, T., Ruzicka, T. and Jeschke, M., 2011. Hypertrophic Scarring and Keloids: Pathomechanisms and Current and Emerging Treatment Strategies. *Molecular Medicine*, 17(1–2), pp.113–125. https://doi.org/10.2119/molmed.2009.00153.

Gavriatopoulou, M., Chari, A., Chen, C., Bahlis, N., Vogl, D.T., Jakubowiak, A., Dingli, D., Cornell, R.F., Hofmeister, C.C., Siegel, D., Berdeja, J.G., Reece, D., White, D., Lentzsch, S., Gasparetto, C., Huff, C.A., Jagannath, S., Baz, R., Nooka, A.K., Richter, J., Abonour, R., Parker, T.L., Yee, A.J., Moreau, P., Lonial, S., Tuchman, S., Weisel, K.C., Mohty, M., Choquet, S., Unger, T.J., Li, K., Chai, Y., Li, L., Shah, J., Shacham, S., Kauffman, M.G. and Dimopoulos, M.A., 2020. Integrated safety profile of selinexor in multiple myeloma:

experience from 437 patients enrolled in clinical trials. *Leukemia*, 34(9), pp.2430–2440. https://doi.org/10.1038/s41375-020-0756-6.

Geha, R.S. and Meltzer, E.O., 2001. Desloratadine: A new, nonsedating, oral antihistamine. *Journal of Allergy and Clinical Immunology*, 107(4), pp.751–762. https://doi.org/10.1067/mai.2001.114239.

Gelbert, L.M., Cai, S., Lin, X., Sanchez-Martinez, C., del Prado, M., Lallena, M.J., Torres, R., Ajamie, R.T., Wishart, G.N., Flack, R.S., Neubauer, B.L., Young, J., Chan, E.M., Iversen, P., Cronier, D., Kreklau, E. and de Dios, A., 2014. Preclinical characterization of the CDK4/6 inhibitor LY2835219: in-vivo cell cycle-dependent/independent anti-tumor activities alone/in combination with gemcitabine. *Investigational New Drugs*, 32(5). https://doi.org/10.1007/s10637-014-0120-7.

Gengo, P., View, M., Giuliano, F., McKenna, K., Chester, A. and Lovenburg, T., 2005. Monoaminergic transport binding and inhibition profile of dapoxetine, a medication for the treatment of premature ejaculation. *The Journal of Urology*, 173(4), p.239.

Gennari, L., 2008. Bazedoxifene for the prevention of postmenopausal osteoporosis. *Therapeutics and Clinical Risk Management*, Volume 4. https://doi.org/10.2147/TCRM.S3476.

Ghahary, A., Shen, Y.], Nedelec, B., Wang, I., Scott, P.G. and Tredget, E.E., 1996. Collagenase Production Is Lower in Post-Burn Hypertrophic Scar Fibroblasts Than in Normal Fibroblasts and Is Reduced by Insulin-Like Growth Factor-1. *The Journal of Investigative Dermatology*, 106(5), pp.476–481.

Ghahary, A., Shen, Y.J., Scott, P.G. and Tredget, E.E., 1995. Immunolocalization of TGF-beta 1 in human hypertrophic scar and normal dermal tissues. *Cytokine*, 7(2), pp.184–90. https://doi.org/10.1006/cyto.1995.1025.

Gilroy, D.W., Saunders, M.A. and Wu, K.K., 2001. COX-2 expression and cell cycle progression in human fibroblasts. *American Journal of Physiology-Cell Physiology*, [online] 281, pp.C188–C194. Available at: <http://www.ajpcell.org>.

Ginimuge, P.R. and Jyothi, S.D., 2010. Methylene blue: revisited. *Journal of anaesthesiology, clinical pharmacology*, 26(4), pp.517–20.

Glennon, R.A., Dukat, M., Grella, B., Hong, S.-S., Costantino, L., Teitler, M., Smith, C., Egan, C., Davis, K. and Mattson, M. v., 2000. Binding of β-carbolines and related agents at serotonin (5-HT2 and 5-HT1A), dopamine (D2) and benzodiazepine receptors. *Drug and Alcohol Dependence*, 60(2), pp.121–132. https://doi.org/10.1016/S0376-8716(99)00148-9.

Godtfredsen, N.S., Lucht, H., Prescott, E., Sørensen, T.I.A. and Grønbæk, M., 2004. A prospective study linked both alcohol and tobacco to Dupuytren's disease. *Journal of Clinical Epidemiology*, 57(8), pp.858–863. https://doi.org/10.1016/j.jclinepi.2003.11.015.

Goel, A. and Shrivastava, P., 2010. Post-burn scars and scar contractures. *Indian Journal of Plastic Surgery*, 43(Suppl), pp.S63-71.

Goldman, J.W., Raju, R.N., Gordon, G.A., El-Hariry, I., Teofilivici, F., Vukovic, V.M., Bradley, R., Karol, M.D., Chen, Y., Guo, W., Inoue, T. and Rosen, L.S., 2013. A first in human, safety, pharmacokinetics, and clinical activity phase I study of once weekly administration of the Hsp90 inhibitor ganetespib (STA-9090) in patients with solid malignancies. *BMC Cancer*, 13(1), p.152. https://doi.org/10.1186/1471-2407-13-152.

Gonzalez, A.C.D.O., Andrade, Z.D.A., Costa, T.F. and Medrado, A.R.A.P., 2016. Wound healing - A literature review. *Anais Brasileiros de Dermatologia*, 91(5), pp.614–620. https://doi.org/10.1590/abd1806-4841.20164741.

Gonzalez-Munoz, A.L., Minter, R.R. and Rust, S.J., 2016. Phenotypic screening: The future of antibody discovery. *Drug Discovery Today*, 21(1), pp.150–156. https://doi.org/10.1016/j.drudis.2015.09.014.

Grant, S., Easley, C. and Kirkpatrick, P., 2007. Vorinostat. *Nature Reviews Drug Discovery*, 6(1), pp.21–22. https://doi.org/10.1038/nrd2227.

Griffith, B.H., Monroe, C.W. and McKinney, P., 1970. A follow-up study on the treatment of keloids with triamicinolone acetonide. *Plastic and Reconstructive Surgery*, 46(2), pp.145–150. https://doi.org/10.1097/00006534-197008000-00006.

Grundlingh, J., Payne, J. and Hassan, T., 2017. Attacks with corrosive substances are increasing in UK. *BMJ (Online)*, 358(j3640), pp.1–2. https://doi.org/10.1136/bmj.j3640.

Gubler, H., Schopfer, U. and Jacoby, E., 2013. Theoretical and experimental relationships between percent inhibition and IC50 data observed in high-throughput screening. *Journal of Biomolecular Screening*, 18(1), pp.1–13. https://doi.org/10.1177/1087057112455219.

Gui, T., Sun, Y., Shimokado, A. and Muragaki, Y., 2012. The Roles of Mitogen-Activated Protein Kinase Pathways in TGF- β -Induced Epithelial-Mesenchymal Transition . *Journal of Signal Transduction*, 2012, pp.1–10. https://doi.org/10.1155/2012/289243.

Gupta, A. and Bluhm, R., 2004. Seborrheic dermatitis. *Journal of the European Academy of Dermatology and Venereology*, 18(1), pp.13–26. https://doi.org/10.1111/j.1468-3083.2004.00693.x.

Gupta, A., Schouten, J. and Lynch, L., 2005. Ciclopirox nail lacquer 8% for the treatment of onychomycosis: a Canadian perspective. *Skin Therapy Letter*, 10(7), pp.1–3.

Häkkinen, L., Koivisto, L. and Larjava, H., 2001. An improved method for culture of epidermal keratinocytes from newborn mouse skin. *Methods in Cell Science*, 23(4), pp.189–196. https://doi.org/10.1023/A:1016385109922.

Handratta, V.D., Vasaitis, T.S., Njar, V.C.O., Gediya, L.K., Kataria, R., Chopra, P., Newman, D., Farquhar, R., Guo, Z., Qiu, Y. and Brodie, A.M.H., 2005. Novel C-17-Heteroaryl Steroidal CYP17 Inhibitors/Antiandrogens: Synthesis, in Vitro Biological Activity, Pharmacokinetics, and Antitumor Activity in the LAPC4 Human Prostate Cancer Xenograft Model. *Journal of Medicinal Chemistry*, 48(8), pp.2972–2984. https://doi.org/10.1021/jm040202w.

Hansen, M.B., Nielsen, S.E. and Berg, K., 1989. Re-examination and further development of a precise and rapid dye method for measuring cell growth/cell kill. *Journal of Immunological Methods*, 119(2), pp.203–210. https://doi.org/10.1016/0022-1759(89)90397-9.

Hanson, K.M., Hernady, E.B., Reed, C.K., Johnston, C.J., Groves, A.M. and Finkelstein, J.N., 2019. Apoptosis Resistance in Fibroblasts Precedes Progressive Scarring in Pulmonary Fibrosis and Is Partially Mediated by Toll-Like Receptor 4 Activation. *Toxicological Sciences*, 170(2), pp.489–498. https://doi.org/10.1093/toxsci/kfz103.

Hardie, W.D., Glasser, S.W. and Hagood, J.S., 2009. Emerging concepts in the pathogenesis of lung fibrosis. *American Journal of Pathology*, 175(1), pp.3–16. https://doi.org/10.2353/ajpath.2009.081170.

Har-Shaii, Y., Amar, M. and Sabo, E., 2003. Intralesional cryotherapy for enhancing the involution of hypertrophic scars and keloids. *Plastic and Reconstructive Surgery*, 111(6), pp.1841–1852.

Hart, M.G. and Hooper, G., 2005. Clinical associations of Dupuytren's disease. *Postgraduate Medical Journal*, 81(957), pp.425–428. https://doi.org/10.1136/pgmj.2004.027425.

Harvey-Kemble, J., 1976. Scanning electron microscopy of hypertrophic and keloid scar. *Postgraduate Medical Journal*, 52, pp.219–221.

Hashimura, H., Kimura, F., Ishibashi-Ueda, H., Morita, Y., Higashi, M., Nakano, S., Iguchi, A., Uotani, K., Sugimura, K. and Naito, H., 2017. Radiologic-pathologic correlation of primary and secondary cardiomyopathies: MR imaging and histopathologic findings in hearts from autopsy and transplantation. *Radiographics*, 37(3), pp.719–736. https://doi.org/10.1148/rg.2017160082.

Hasinoff, B.B., Wu, X., Patel, D., Kanagasabai, R., Karmahapatra, S. and Yalowich, J.C., 2016. Mechanisms of Action and Reduced Cardiotoxicity of Pixantrone; a Topoisomerase II Targeting Agent with Cellular Selectivity for the Topoisomerase II Isoform. *Journal of Pharmacology and Experimental Therapeutics*, 356(2), pp.397–409. https://doi.org/10.1124/jpet.115.228650.

Hayashida, K. and Akita, S., 2017. Surgical treatment algorithms for post-burn contractures. *Burns & Trauma*, [online] 5(1), pp.1–8. https://doi.org/10.1186/s41038-017-0074-z.

Hazuda, D.J., Felock, P., Witmer, M., Wolfe, A., Stillmock, K., Grobler, J.A., Espeseth, A., Gabreylski, L., Schleif, W., Blau, C. and Miller, M.D., 2000. Inhibitors of Strand Transfer That Prevent Integration and Inhibit HIV-1 Replication in Cells. *Science*, 287(5453), pp.646–650. https://doi.org/10.1126/science.287.5453.646.

Hellstrom, W.J.G. and Usta, M.F., 2003. Surgical approaches for advanced Peyronie's disease patients. *International Journal of Impotence Research*, 15(Suppl 5), pp.S121–S124. https://doi.org/10.1038/sj.ijir.3901085.

Henao, J.P., Peperzak, K.A., Lichvar, A.B., Orebaugh, S.L., Skledar, S.J., Pippi, M.A. and Williams, B.A., 2014. Extrapyramidal symptoms following administration of oral perphenazine 4 or 8 mg. *European Journal of Anaesthesiology*, 31(4), pp.231–235. https://doi.org/10.1097/EJA.0000000000000048.

Hernandez, L.A., Grisham, M.B., Twohig, B., Arfors, K.E., Harlan, J.M. and Granger, D.N., 1987. Role of neutrophils in ischemia-reperfusion-induced microvascular injury. *The American journal of physiology*, 253(3 Pt 2), pp.H699-703. https://doi.org/10.1152/ajpheart.1987.253.3.H699.

Herrick-Davis, K., Grinde, E. and Teitler, M., 2000. Inverse agonist activity of atypical antipsychotic drugs at human 5-hydroxytryptamine2C receptors. *The Journal of pharmacology and experimental therapeutics*, 295(1), pp.226–32.

Herum, K.M., Choppe, J., Kumar, A., Engler, A.J. and McCulloch, A.D., 2017. Mechanical regulation of cardiac fibroblast profibrotic phenotypes. *Molecular Biology of the Cell*, 28(14), pp.1871–1882. https://doi.org/10.1091/mbc.e17-01-0014.

Hettiaratchy, S. and Dziewulski, P., 2004. Pathophysiology of burns. *BMJ*, 328, pp.1427–1429.

Hewitson, T.D., 2012. Fibrosis in the kidney: Is a problem shared a problem halved? *Fibrogenesis and Tissue Repair*, 5(Suppl1:S14), pp.1–5. https://doi.org/10.1186/1755-1536-5-S1-S14.

Higgins, P.J., Czekay, R.P., Wilkins-Port, C.E., Higgins, S.P., Freytag, J., Overstreet, J.M., Klein, R.M., Higgins, C.E. and Samarakoon, R., 2011. PAI-1: An integrator of cell signaling and migration. *International Journal of Cell Biology*. https://doi.org/10.1155/2011/562481.

Hinderer, S. and Schenke-Layland, K., 2019. Cardiac fibrosis – A short review of causes and therapeutic strategies. *Advanced Drug Delivery Reviews*, 146, pp.77–82. https://doi.org/10.1016/j.addr.2019.05.011.

Hoffmann, K.F., Cheever, A.W. and Wynn, T.A., 2000. IL-10 and the Dangers of Immune Polarization: Excessive Type 1 and Type 2 Cytokine Responses Induce Distinct Forms of Lethal Immunopathology in Murine Schistosomiasis. *The Journal of Immunology*, 164(12), pp.6406–6416. https://doi.org/10.4049/jimmunol.164.12.6406.

Holdsworth, G., Bon, H., Bergin, M., Qureshi, O., Paveley, R., Atkinson, J., Huang, L., Tewari, R., Twomey, B. and Johnson, T., 2017. Quantitative and organisational changes in mature extracellular matrix revealed through high-content imaging of total protein fluorescently stained in situ. *Scientific Reports*, 7(9963), pp.1–12. https://doi.org/10.1038/s41598-017-10298-x.

Honardoust, D., Varkey, M., Marcoux, Y., Shankowsky, H.A. and Tredget, E.E., 2012. Reduced decorin, fibromodulin, and transforming growth factor-β3 in deep dermis leads to hypertrophic scarring. *Journal of Burn Care & Research*, 33(2), pp.218–27. https://doi.org/10.1097/BCR.0b013e3182335980.

Honig, S.C., 2014. Intralesional collagenase in the treatment of Peyronie's disease. *Therapeutic Advances in Urology*, 6(2), pp.47–53. https://doi.org/10.1177/1756287213509849.

Hu, Y., Peng, J., Feng, D., Chu, L., Li, X., Jin, Z., Lin, Z. and Zeng, Q., 2006. Role of Extracellular Signal-Regulated Kinase, p38 Kinase, and Activator Protein-1 in Transforming Growth Factor-β1–Induced Alpha Smooth Muscle Actin Expression in Human Fetal Lung Fibroblasts In Vitro. *Lung*, 184(1). https://doi.org/10.1007/s00408-005-2560-5.

Huang, C. and Ogawa, R., 2020. Systemic factors that shape cutaneous pathological scarring. *FASEB Journal*, 34(10), pp.13171–13184. https://doi.org/10.1096/fj.202001157R.

Hughes, A. and Wijetunge, S., 1993. The action of amlodipine on voltage-operated calcium channels in vascular smooth-muscle. *British Journal of Pharmacology*, 109, pp.120–125.

Hughes, J.P., Rees, S.S., Kalindjian, S.B. and Philpott, K.L., 2011. Principles of early drug discovery. *British Journal of Pharmacology*, 162(6), pp.1239–1249. https://doi.org/10.1111/j.1476-5381.2010.01127.x.

Hultman, C., Edkins, R., Wu, C., Calvert, C. and Cairns, B., 2013. Prospective, Before-After Cohort Study to Assess the Efficacy of Laser Therapy on Hypertrophic Burn Scars. *Annals of Plastic Surgery*, 70(5), pp.521–526.

Humphreys, B.D., 2018. Mechanisms of Renal Fibrosis. *Annual Review of Physiology*, [online] 80, pp.6.1-6.18. https://doi.org/10.1146/annurev-physiol-022516.

Hussein, A.A., Alwaal, A. and Lue, T.F., 2015. All about Peyronie's disease. *Asian Journal of Urology*, 2(2), pp.70–78. https://doi.org/10.1016/j.ajur.2015.04.019.

Ilg, M.M., Mateus, M., Stebbeds, W.J., Milenkovic, U., Christopher, N., Muneer, A., Albersen, M., Ralph, D.J. and Cellek, S., 2019. Antifibrotic Synergy Between Phosphodiesterase Type 5 Inhibitors and Selective Oestrogen Receptor Modulators in Peyronie's Disease Models. *European Urology*, [online] 75(2), pp.329–340. https://doi.org/10.1016/j.eururo.2018.10.014.

Ilg, M.M., Stafford, S.J., Mateus, M., Bustin, S.A., Carpenter, M.J., Muneer, A., Bivalacqua, T.J., Ralph, D.J. and Cellek, S., 2020. Phosphodiesterase Type 5 Inhibitors and Selective Estrogen Receptor Modulators Can Prevent But Not Reverse Myofibroblast Transformation in Peyronie's Disease. *Journal of Sexual Medicine*, [online] pp.1–17. https://doi.org/10.1016/j.jsxm.2020.06.022.

Ince, B., Uyar, I. and Dadaci, M., 2019. Effect of Vitamin D Deficiency on Hypertrophic Scarring. *Dermatologic Surgery*, 45(2), pp.274–279. https://doi.org/10.1097/DSS.0000000000001680.

International Union of Basic & Clinical Pharmacology and British Pharmacological Society, 2021a. *Dyclonine*. Guide to Pharmacology.

International Union of Basic & Clinical Pharmacology and British Pharmacological Society, 2021b. *Sertraline*. Guide to Pharmacology.

Istvan, E.S. and Deisenhofer, J., 2001. Structural Mechanism for Statin Inhibition of HMG-CoA Reductase. *Science*, 292(5519). https://doi.org/10.1126/science.1059344.

Ivaska, J., 2011. Vimentin: Central hub in EMT induction? *Small GTPases*, 2(1), pp.51–53. https://doi.org/10.4161/sgtp.2.1.15114.

Iversen, P., Beck, B., Chen, Y.-F., Dere, W., Devanarayan, V., Eastwood, B., Farmen, M., Iturria, S., Montrose, C., Moore, R., Weidner, J. and Sittampalam, G., 2012. HTS Assay Validation. In: S. Markossian, G. Sittampalam, A. Grossman, K. Brimacombe, M. Arkin, D. Auld, C. Austin, J. Baell, J. Caaverio, T. Chung, N. Coussens, J. Dahlin, V. Devanaryan, T. Foley, M. Glicksman, M. Hall, J. Haas, S. Hoare, J. Inglese, P. Iversen, S. Kahl, S. Kales, S. Kirshner, M. Lal-Nag, Z. Li, J. McGee, O. McManus, T. Riss, P. Saradjian, O. Trask Jr, J. Weidner, M. Wildey, M. Xia and X. Xu, eds. *The Assay Guidance Manual*. Maryland: Eli Lilly & Company and the National Center for Advancing Translational Sciences.pp.1129–1155.

Jalali, M. and Bayat, A., 2007. Current use of steroids in management of abnormal raised skin scars. *The Surgeon*, 5(3), pp.175–180.

Jang, S.-W., Ihm, S.-H., Choo, E.-H., Kim, O.-R., Chang, K., Park, C.-S., Kim, H.-Y. and Seung, K.-B., 2014. Imatinib mesylate attenuates myocardial remodeling through inhibition of platelet-derived growth factor and transforming growth factor activation in a rat model of hypertension. *Hypertension (Dallas, Tex. : 1979)*, 63(6), pp.1228–34. https://doi.org/10.1161/HYPERTENSIONAHA.113.01866.

Jendralla, H., Baader, E., Bartmann, W., Beck, G., Bergmann, A., Granzer, E., von Kerekjarto, B., Kesseler, K. and Krause, R., 1990. Synthesis and biological activity of new HMG-CoA reductase inhibitors. 2. Derivatives of 7-(1H-pyrrol-3-yl)-substituted-3,5-dihydroxyhept-6(E)-enoic (-heptanoic) acids. *Journal of Medicinal Chemistry*, 33(1), pp.61–70. https://doi.org/10.1021/jm00163a011.

Jeschke, M.G., van Baar, M.E., Choudhry, M.A., Chung, K.K., Gibran, N.S. and Logsetty, S., 2020. Burn injury. *Nature Reviews Disease Primers*, [online] 6(11), pp.1–25. https://doi.org/10.1038/s41572-020-0145-5.

Jia, S., Xie, P., Hong, S.J., Galiano, R.D. and Mustoe, T.A., 2017. Local Application of Statins Significantly Reduced Hypertrophic Scarring in a Rabbit Ear Model. *Plastic and Reconstructive Surgery - Global Open*, 5(6), p.e1294. https://doi.org/10.1097/GOX.0000000000001294.

Jin, H., Terai, S. and Sakaida, I., 2007. The iron chelator deferoxamine causes activated hepatic stellate cells to become quiescent and to undergo apoptosis. *Journal of Gastroenterology*, 42(6). https://doi.org/10.1007/s00535-007-2020-5.

Jue, S.G., Dawson, G.W. and Brogden, R.N., 1985. Ciclopirox Olamine 1% Cream: A Preliminary Review of its Antimicrobial Activity and Therapeutic Use. *Drugs*, 29(4), pp.330–341. https://doi.org/10.2165/00003495-198529040-00002.

Kaddoura, I., Abu-Sittah, G., Ibrahim, A., Karamanoukian, R. and Papazian, N., 2017. Burn injury: review of pathophysiology and therapeutic modalities in major burns. *Annals of burns and fire disasters*, [online] 30(2), pp.95–102. Available at: <http://www.ncbi.nlm.nih.gov/pubmed/29021720%0Ahttp://www.pubmedcentral.nih.gov/articlerender.fcgi?artid=PMC5627559>.

Kahaleh, B. and Mulligan-Kehoe, M.J., 2012. Mechanisms of vascular disease. In: *Scleroderma: From Pathogenesis to Comprehensive Management*. Adelaide: The University of Adelaide, Barr Smith Press.pp.227–246. https://doi.org/10.1007/978-1-4419-5774-0_19.

Kalluri, R. and Neilson, E.G., 2003. Epithelial-mesenchymal transition and its implications for fibrosis. *The Journal of clinical investigation*, 112(12), pp.1776–84. https://doi.org/10.1172/JCI20530.

Kalluri, R. and Weinberg, R.A., 2009. The basics of epithelial-mesenchymal transition. *Journal of Clinical Investigations*, 119(6), pp.1420–1428. https://doi.org/10.1172/JCI39104.1420.

Kamato, D., Burch, M.L., Piva, T.J., Rezaei, H.B., Rostam, M.A., Xu, S., Zheng, W., Little, P.J. and Osman, N., 2013. Transforming growth factor-β signalling: Role and consequences of Smad linker region phosphorylation. *Cellular Signalling*, 25(10), pp.2017–2024. https://doi.org/10.1016/j.cellsig.2013.06.001.

Kanisicak, O., Khalil, H., Ivey, M.J., Karch, J., Maliken, B.D., Correll, R.N., Brody, M.J., J. Lin, S.-C., Aronow, B.J., Tallquist, M.D. and Molkentin, J.D., 2016. Genetic lineage tracing defines myofibroblast origin and function in the injured heart. *Nature Communications*, 7(1), p.12260. https://doi.org/10.1038/ncomms12260.

Kanitakis, J., 2002. Anatomy, histology and immunohistochemistry of normal human skin. *European Journal of Dermatology*, 12(4), pp.390–401.

Karimi, G. and Vahabzadeh, M., 2014. Thioxanthenes. In: P. Wexler, ed. *Encyclopedia of Toxicology*, Third. Academic Press.pp.553–557. https://doi.org/10.1016/B978-0-12-386454-3.00656-4.

Kaur, K., Zarzoso, M., Ponce-Balbuena, D., Guerrero-Serna, G., Hou, L., Musa, H. and Jalife, J., 2013. TGF-β1, Released by Myofibroblasts, Differentially Regulates Transcription and Function of Sodium and Potassium Channels in Adult Rat Ventricular Myocytes. *PLoS ONE*, 8(2), p.e55391. https://doi.org/10.1371/journal.pone.0055391.

Keira, S.M., Ferreira, L.M., Gragnani, A., Da, I. and Duarte, S., 2004. Experimental model for fibroblast culture. *Acta Circurgica Brasileria*, [online] 19(Suppl.1), pp.11–16. Available at: <http://www.scielo.br/acb.>.

Kelly, W.K., Richon, V.M., O'connor, O., Curley, T., Macgregor-Curtelli, B., Tong, W., Klang, M., Schwartz, L., Richardson, S., Rosa, E., Drobnjak, M., Cordon-Cordo, C., Chiao, J.H., Rifkind, R., Marks, P.A. and Scher, H., 2003. Phase I Clinical Trial of Histone Deacetylase Inhibitor: Suberoylanilide Hydroxamic Acid Administered Intravenously 1. *Clinical Cancer Research*, 9, pp.3578–3588.

Khan, M. and Gasser, S., 2016. Generating primary fibroblast cultures from mouse ear and tail tissues. *Journal of Visualized Experiments*, 107(e53565), pp.1–6. https://doi.org/10.3791/53565.

Khan, N., Jeffers, M., Kumar, S., Hackett, C., Boldog, F., Khramtsov, N., Qian, X., Mills, E., Berghs, S.C., Carey, N., Finn, P.W., Collins, L.S., Tumber, A., Ritchie, J.W., Jensen, P.B., Lichenstein, H.S. and Sehested, M., 2008. Determination of the class and isoform selectivity of small-molecule histone deacetylase inhibitors. *The Biochemical journal*, 409(2), pp.581–9. https://doi.org/10.1042/BJ20070779.

Kiil, J., 1977. Keloids Treated with Topical Injections of Triamcinolone Acetonide (Kenalog): Immediate and Long-term Results. *Scandinavian Journal of Plastic and Reconstructive Surgery*, 11(2), pp.169–172. https://doi.org/10.3109/02844317709025514.

Kim, D.-W., Lee, D.H., Han, J.-Y., Lee, J., Cho, B.C., Kang, J.H., Lee, K.H., Cho, E.K., Kim, J.-S., Min, Y.J., Cho, J.Y., An, H.J., Kim, H.-G., Lee, K.H., Kim, B.-S., Jang, I.-J., Yoon, S., Han, O., Noh, Y.S., Hong, K.Y. and Park, K., 2019. Safety, tolerability, and anti-tumor activity of olmutinib in non-small cell lung cancer with T790M mutation: A single arm, open label, phase 1/2 trial. *Lung Cancer*, 135, pp.66–72. https://doi.org/10.1016/j.lungcan.2019.07.007.

Kim, S.W., 2021. Management of keloid scars: noninvasive and invasive treatments. *Archives of Plastic Surgery*, 48(2), pp.149–157. https://doi.org/10.5999/aps.2020.01914.

Kim, Y., Schmidt, M., Endo, T., Lu, D., Carson, D. and Schmidt-Wolf, I., 2011. Targeting the Wnt/Beta-catenin Pathway with the Antifungal Agent Ciclopirox Olamine in a Murine Myeloma Model. *In Vivo*, 25, pp.887–894.

Kin, K., Maziarz, J. and Wagner, G.P., 2014. Immunohistological study of the endometrial stromal fibroblasts in the opossum, Monodelphis domestica: Evidence for Homology with eutherian stromal fibroblasts. *Biology of Reproduction*, 90(5), pp.1–12. https://doi.org/10.1095/biolreprod.113.115139.

King, T.E., Albera, C., Bradford, W.Z., Costabel, U., Hormel, P., Lancaster, L., Noble, P.W., Sahn, S.A., Szwarcberg, J., Thomeer, M., Valeyre, D. and du Bois, R.M., 2009. Effect of interferon gamma-1b on survival in patients with idiopathic pulmonary fibrosis (INSPIRE): a multi-centre, randomised, placebo-controlled trial. *The Lancet*, [online] 374, pp.222–228. https://doi.org/10.1016/S0140.

Kitagawa, D., Yokota, K., Gouda, M., Narumi, Y., Ohmoto, H., Nishiwaki, E., Akita, K. and Kirii, Y., 2013. Activity-based kinase profiling of approved tyrosine kinase inhibitors. *Genes to Cells*, 18(2), pp.110–122. https://doi.org/10.1111/gtc.12022.

Ko, J.H., Kim, P.S., Zhao, Y., Hong, S.J. and Mustoe, T.A., 2012. HMG-CoA Reductase Inhibitors (Statins) Reduce Hypertrophic Scar Formation in a Rabbit Ear Wounding Model. *Plastic and Reconstructive Surgery*, 129(2), pp.252e–261e. https://doi.org/10.1097/PRS.0b013e31823aea10.

Ko, S.H., Nauta, A., Morrison, S.D., Zhou, H., Zimmermann, A., Gurtner, G.C., Ding, S. and Longaker, M.T., 2011. Antimycotic ciclopirox olamine in the diabetic environment promotes

angiogenesis and enhances wound healing. *PLoS ONE*, 6(11), pp.1–9. https://doi.org/10.1371/journal.pone.0027844.

Koivumaki, J.T., Clark, R.B., Belke, D., Kondo, C., Fedak, P.W.M., Maleckar, M.M.C. and Giles, W.R., 2014. Na+ current expression in human atrial myofibroblasts: identity and functional roles. *Frontiers in Physiology*, 5. https://doi.org/10.3389/fphys.2014.00275.

Kok, H.M., Falke, L.L., Goldschmeding, R. and Nguyen, T.Q., 2014. Targeting CTGF, EGF and PDGF pathways to prevent progression of kidney disease. *Nature Reviews Nephrology*, 10(12), pp.700–711. https://doi.org/10.1038/nrneph.2014.184.

Kolarsick, P.A.J., Kolarsick, M.A. and Goodwin, C., 2008. Anatomy and Physiology of the Skin. *Journal of Dermatology Nurse's Association*, 3(4), pp.203–213. https://doi.org/10.1097/JDN.0b013e3182274a98.

Kolodsick, J.E., Peters-Golden, M., Larios, J., Toews, G.B., Thannickal, V.J. and Moore, B.B., 2003. Prostaglandin E2 inhibits fibroblast to myofibroblast transition via E. prostanoid receptor 2 signaling and cyclic adenosine monophosphate elevation. *American journal of respiratory cell and molecular biology*, 29(5), pp.537–44. https://doi.org/10.1165/rcmb.2002-0243OC.

Kongsamut, S., Kang, J., Chen, X.-L., Roehr, J. and Rampe, D., 2002. A comparison of the receptor binding and HERG channel affinities for a series of antipsychotic drugs. *European journal of pharmacology*, 450(1), pp.37–41. https://doi.org/10.1016/s0014-2999(02)02074-5.

Kornek, G., Raderer, M., Depisch, D., Haider, K., Fazeny, B., Dittrich, C. and Scheithauer, W., 1994. Amonafide as first-line chemotherapy for metastatic breast cancer. *European Journal of Cancer*, 30(3). https://doi.org/10.1016/0959-8049(94)90264-X.

Kornhuber, J., Parsons, C.G., Hartmann, S., Retz, W., Kamolz, S., Thome, J. and Riederer, P., 1995. Orphenadrine is an uncompetitive N-methyl-D-aspartate (NMDA) receptor antagonist: binding and patch clamp studies. *Journal of Neural Transmission*, 102(3), pp.237–246. https://doi.org/10.1007/BF01281158.

Korting, H.C. and Grundmann-Kollmann, M., 1997. The hydroxypyridones: a class of antimycotics of its own. *Mycoses*, 40(7–8), pp.243–247. https://doi.org/10.1111/j.1439-0507.1997.tb00227.x.

Krieg, T. and Takehara, K., 2009. Skin disease: a cardinal feature of systemic sclerosis. *Rheumatology (Oxford, England)*, 48 Suppl 3(April), pp.14–18. https://doi.org/10.1093/rheumatology/kep108.

Kroeze, W.K., Hufeisen, S.J., Popadak, B.A., Renock, S.M., Steinberg, S., Ernsberger, P., Jayathilake, K., Meltzer, H.Y. and Roth, B.L., 2003. H1-Histamine Receptor Affinity Predicts Short-Term Weight Gain for Typical and Atypical Antipsychotic Drugs. *Neuropsychopharmacology*, 28(3), pp.519–526. https://doi.org/10.1038/sj.npp.1300027.

Kubo, N., Shirakawa, O., Kuno, T. and Tanaka, C., 1987. Antimuscarinic effects of antihistamines : Quantitative evaluation by receptor-binding assay. *The Japanese Journal of Pharmacology*, 43(3). https://doi.org/10.1254/jjp.43.277.

Kuiper, G.G.J.M., Carlsson, B., Grandien, K., Enmark, E., Häggblad, J., Nilsson, S. and Gustafsson, J.-A., 1997. Comparison of the Ligand Binding Specificity and Transcript Tissue Distribution of Estrogen Receptors α and β. *Endocrinology*, 138(3), pp.863–870. https://doi.org/10.1210/endo.138.3.4979.

Kumar, P., Kumar, S., Udupa, E.P., Kumar, U., Rao, P. and Honnegowda, T., 2015. Role of angiogenesis and angiogenic factors in acute and chronic wound healing. *Plastic and Aesthetic Research*, 2(5), pp.243–249. https://doi.org/10.4103/2347-9264.165438.

Kuppe, C., Ibrahim, M.M., Kranz, J., Zhang, X., Ziegler, S., Perales-Patón, J., Jansen, J., Reimer, K.C., Smith, J.R., Dobie, R., Wilson-Kanamari, J.R., Halder, M., Xu, Y., Kabgani, N., Kaesler, N., Klaus, M., Gernhold, L., Puelles, V.G., Huber, T.B., Boor, P., Menzel, S., Hoogenboezem, R.M., Bindels, E.M.J., Steffens, J., Floege, J., Schneider, R.K., Saez-Rodriguez, J., Henderson, N.C. and Kramann, R., 2020. Decoding myofibroblast origins in human kidney fibrosis. *Nature*, 589, pp.281–286. https://doi.org/10.1038/s41586-020-2941-1.

Kupperman, E., Lee, E.C., Cao, Y., Bannerman, B., Fitzgerald, M., Berger, A., Yu, J., Yang, Y., Hales, P., Bruzzese, F., Liu, J., Blank, J., Garcia, K., Tsu, C., Dick, L., Fleming, P., Yu, L., Manfredi, M., Rolfe, M. and Bolen, J., 2010. Evaluation of the Proteasome Inhibitor MLN9708 in Preclinical Models of Human Cancer. *Cancer Research*, 70(5), pp.1970–1980. https://doi.org/10.1158/0008-5472.CAN-09-2766.

Kuriyama, S., Hitomi, M., Yoshiji, H., Nonomura, T., Tsujimoto, T., Mitoro, A., Akahane, T., Ogawa, M., Nakai, S., Deguchi, A., Masaki, T. and Uchida, N., 2005. Vitamins K2, K3 and K5 exert in vivo antitumor effects on hepatocellular carcinoma by regulating the expression of G1 phase-related cell cycle molecules. *International Journal of Oncology*. https://doi.org/10.3892/ijo.27.2.505.

Kwak, D.H., Bae, T.H., Kim, W.S. and Kim, H.K., 2016. Anti-vascular endothelial growth factor (Bevacizumab) therapy reduces hypertrophic scar formation in a rabbit ear wounding model. *Archives of Plastic Surgery*, 43(6), pp.491–497. https://doi.org/10.5999/aps.2016.43.6.491.

Lamouille, S. and Derynck, R., 2007. Cell size and invasion in TGF-β-induced epithelial to mesenchymal transition is regulated by activation of the mTOR pathway. *Journal of Cell Biology*, 178(3), pp.437–451. https://doi.org/10.1083/jcb.200611146.

Lancaster, L.H., de Andrade, J.A., Zibrak, J.D., Padilla, M.L., Albera, C., Nathan, S.D., Wijsenbeek, M.S., Stauffer, J.L., Kirchgaessler, K.U. and Costabel, U., 2017. Pirfenidone safety and adverse event management in idiopathic pulmonary fibrosis. *European Respiratory Review*, 26(146), pp.1–10. https://doi.org/10.1183/16000617.0057-2017.

Lang, T.C., Zhao, R., Kim, A., Wijewardena, A., Vandervord, J., Xue, M. and Jackson, C.J., 2019. A Critical Update of the Assessment and Acute Management of Patients with Severe Burns. *Advances in Wound Care*, 8(12), pp.607–633. https://doi.org/10.1089/wound.2019.0963.

Laquerre, S., Arnone, M., Moss, K., Yang, J., Fisher, K., Kane-Carson, L., Smitheman, K., Ward, J., Heidrich, B. and Rheault, T., 2009. A selective Raf kinase inhibitor induces cell death and tumor regression of human cancer cell lines encoding B-RafV600E mutation. *Molecular Cancer Therapeutics*, 8(12).

Larrabee Jr, W., East, C., Jaffe, H., Stephenson, C. and Peterson, K., 1990. Intralesional Interferon Gamma Treatment for Keloids and Hypertrophic Scars. *Archives of Otolaryngology Head & Neck Surgery*, 116(10), pp.1159–1162.

Lattouf, R., Younes, R., Lutomski, D., Naaman, N., Godeau, G., Senni, K. and Changotade, S., 2014. Picrosirius Red Staining: A Useful Tool to Appraise Collagen Networks in Normal

and Pathological Tissues. *Journal of Histochemistry and Cytochemistry*, 62(10), pp.751–758. https://doi.org/10.1369/0022155414545787.

Leary, T., Jones, P.L., Appleby, M., Blight, A., Parkinson, K. and Stanley, M., 1992. Epidermal Keratinocyte Self-Renewal Is Dependent upon Dermal Integrity. *Journal of Investigative Dermatology*, 99, pp.422–430.

Lee, H.J. and Jang, Y.J., 2018. Recent understandings of biology, prophylaxis and treatment strategies for hypertrophic scars and keloids. *International Journal of Molecular Sciences*, 19(711), pp.1–19. https://doi.org/10.3390/ijms19030711.

Lee, M.K., Pardoux, C., Hall, M.C., Lee, P.S., Warburton, D., Qing, J., Smith, S.M. and Derynck, R., 2007. TGF-β activates Erk MAP kinase signalling through direct phosphorylation of ShcA. *EMBO Journal*, 26(17), pp.3957–3967. https://doi.org/10.1038/sj.emboj.7601818.

Levine, L.A., 2017. Complications and other concerns with intralesional injection therapy with collagenase clostridium histolyticum for Peyronie's disease. *Translational Andrology and Urology*, 6(1), pp.120–122. https://doi.org/10.21037/tau.2017.01.03.

Levine, L.A., Cuzin, B., Mark, S., Gelbard, M.K., Jones, N.A., Liu, G., Kaufman, G.J., Tursi, J.P. and Ralph, D.J., 2015. Clinical Safety and Effectiveness of Collagenase Clostridium Histolyticum Injection in Patients with Peyronie's Disease: A Phase 3 Open-Label Study. *The Journal of Sexual Medicine*, 12(1), pp.248–258. https://doi.org/10.1111/jsm.12731.

Levis, M., 2013. Quizartinib in acute myeloid leukemia. *Clinical advances in hematology & oncology*, 11(9), pp.586–8.

Lewis, T.A., Young, M.A., Arrington, M.P., Bayless, L., Cai, X., Collart, P., Eckman, J.B., Ellis, J.L., Ene, D.G., Libertine, L., Nicolas, J.-M., Scannell, R.T., Wels, B.F., Wenberg, K. and Wypij, D.M., 2004. Cetirizine and loratadine-based antihistamines with 5-lipoxygenase inhibitory activity. *Bioorganic & Medicinal Chemistry Letters*, 14(22), pp.5591–5594. https://doi.org/10.1016/j.bmcl.2004.08.060.

Lex Medicus Pathologies, 2021. *Dupuytren's contracture*. [online] Available at: <https://pathologies.lexmedicus.com.au/collection/depuytrens-contracture> [Accessed 4 Jan. 2021].

Li, D., Ambrogio, L., Shimamura, T., Kubo, S., Takahashi, M., Chirieac, L.R., Padera, R.F., Shapiro, G.I., Baum, A., Himmelsbach, F., Rettig, W.J., Meyerson, M., Solca, F., Greulich, H. and Wong, K.-K., 2008. BIBW2992, an irreversible EGFR/HER2 inhibitor highly effective in preclinical lung cancer models. *Oncogene*, 27(34). https://doi.org/10.1038/onc.2008.109.

Li, J., Chen, J. and Kirsner, R., 2007. Pathophysiology of acute wound healing. *Clinics in Dermatology*, 25(1), pp.9–18. https://doi.org/10.1016/j.clindermatol.2006.09.007.

Li, X., Zhu, L., Wang, B., Yuan, M. and Zhu, R., 2017. Drugs and targets in fibrosis. *Frontiers in Pharmacology*, 8(855), pp.1–21. https://doi.org/10.3389/fphar.2017.00855.

Lijnen, P. and Petrov, V., 2002. Transforming growth factor-beta 1-induced collagen production in cultures of cardiac fibroblasts is the result of the appearance of myofibroblasts. *Methods and Findings in Experimental and Clinical Pharmacology*, 24(6), p.333. https://doi.org/10.1358/mf.2002.24.6.693065.

Lim, S.H., Kim, C., Aref, A.R., Kamm, R.D. and Raghunath, M., 2013. Complementary effects of ciclopirox olamine, a prolyl hydroxylase inhibitor and sphingosine 1-phosphate on

fibroblasts and endothelial cells in driving capillary sprouting. *Integrative Biology*, 5(12), pp.1474–1484. https://doi.org/10.1039/c3ib40082d.

Limandjaja, G.C., Niessen, F.B., Scheper, R.J. and Gibbs, S., 2021. Hypertrophic scars and keloids: Overview of the evidence and practical guide for differentiating between these abnormal scars. *Experimental Dermatology*, 30(1), pp.146–161. https://doi.org/10.1111/exd.14121.

Linden, T., Katschinski, D.M., Eckhardt, K., Scheid, A., Pagel, H. and Wenger, R.H., 2003. The antimycotic ciclopirox olamine induces HIF-1α stability, VEGF expression, and angiogenesis. *The FASEB Journal*, 17(6), pp.761–763. https://doi.org/10.1096/fj.0586fje.

Lipson, K.E., Wong, C., Teng, Y. and Spong, S., 2012. CTGF is a central mediator of tissue remodeling and fibrosis and its inhibition can reverse the process of fibrosis. *Fibrogenesis & Tissue Repair*, 5(Suppl 1), pp.1–8. https://doi.org/10.1186/1755-1536-5-s1-s24.

Liu, T., Guevara, O.E., Warburton, R.R., Hill, N.S., Gaestel, M. and Kayyali, U.S., 2010. Regulation of vimentin intermediate filaments in endothelial cells by hypoxia. *American Journal of Physiology-Cell Physiology*, 299(2), pp.C363–C373. https://doi.org/10.1152/ajpcell.00057.2010.

Liu, T., Song, D., Dong, J., Zhu, P., Liu, J., Liu, W., Ma, X., Zhao, L. and Ling, S., 2017. Current understanding of the pathophysiology of myocardial fibrosis and its quantitative assessment in heart failure. *Frontiers in Physiology*, 8(283), pp.1–13. https://doi.org/10.3389/fphys.2017.00238.

Liu, X.H., Song, X.W., Xu, Y. and Zhang, C., 1996. The Inhibition of Vitamin K3 on Rabbit Fibroblast Proliferation in vitro. *Ophthalmologica*, 210(3), pp.180–182. https://doi.org/10.1159/000310703.

Liu, Y., 2006. Renal fibrosis: New insights into the pathogenesis and therapeutics. *Kidney International*, 69(2), pp.213–217. https://doi.org/10.1038/sj.ki.5000054.

Lodén and Wessman, 2000. The antidandruff efficacy of a shampoo containing piroctone olamine and salicylic acid in comparison to that of a zinc pyrithione shampoo. *International Journal of Cosmetic Science*, 22(4), pp.285–289. https://doi.org/10.1046/j.1467-2494.2000.00024.x.

Lu, F., Gao, J., Ogawa, R., Hyakusoku, H. and Ou, C., 2007. Fas-mediated apoptotic signal transduction in keloid and hypertrophic scar. *Plastic and Reconstructive Surgery*, 119(6), pp.1714–1721. https://doi.org/10.1097/01.prs.0000258851.47193.06.

Lu, L., Saulis, A.S., Liu, W.R., Roy, N.K., Chao, J.D., Ledbetter, S. and Mustoe, T.A., 2005. The Temporal Effects of Anti-TGF-β1, 2, and 3 Monoclonal Antibody on Wound Healing and Hypertrophic Scar Formation. *Journal of the American College of Surgeons*, 201(3). https://doi.org/10.1016/j.jamcollsurg.2005.03.032.

Lundsten, S., Spiegelberg, D., Stenerl&#65533;w, B. and Nestor, M., 2019. The HSP90 inhibitor onalespib potentiates 177Lu-DOTATATE therapy in neuroendocrine tumor cells. *International Journal of Oncology*. https://doi.org/10.3892/ijo.2019.4888.

MacDonald, B.T., Tamai, K. and He, X., 2009. Wnt/β-Catenin Signaling: Components, Mechanisms, and Diseases. *Developmental Cell*, 17(1), pp.9–26. https://doi.org/10.1016/j.devcel.2009.06.016.

Mader, M., de Dios, A., Shih, C., Bonjouklian, R., Li, T., White, W., López de Uralde, B., Sánchez-Martinez, C., del Prado, M., Jaramillo, C., de Diego, E., Martín Cabrejas, L.M., Dominguez, C., Montero, C., Shepherd, T., Dally, R., Toth, J.E., Chatterjee, A., Pleite, S., Blanco-Urgoiti, J., Perez, L., Barberis, M., Lorite, M.J., Jambrina, E., Nevill, C.R., Lee, P.A., Schultz, R.C., Wolos, J.A., Li, L.C., Campbell, R.M. and Anderson, B.D., 2008. Imidazolyl benzimidazoles and imidazo[4,5-b]pyridines as potent p38alpha MAP kinase inhibitors with excellent in vivo antiinflammatory properties. *Bioorganic & medicinal chemistry letters*, 18(1), pp.179–83. https://doi.org/10.1016/j.bmcl.2007.10.106.

Marieb, E.N. and Hoehn, K.N., 2014. Integumentary System. In: *Human Anatomy & Physiology*, 9th ed. Harlow: Pearson Education Limited.pp.180–203.

Marks, P.A., 2007. Discovery and development of SAHA as an anticancer agent. *Oncogene*, 26(9), pp.1351–1356. https://doi.org/10.1038/sj.onc.1210204.

Martin, P., 1997. Wound Healing - Aiming for Perfect Skin Regeneration. *Science*, 276(5309), pp.75–81. https://doi.org/10.1126/science.276.5309.75.

Martinez, F.J., Collard, H.R., Pardo, A., Raghu, G., Richeldi, L., Selman, M., Swigris, J.J., Taniguchi, H. and Wells, A.U., 2017. Idiopathic pulmonary fibrosis. *Nature Reviews Disease Primers*, 3(17074), pp.1–19. https://doi.org/10.1038/nrdp.2017.74.

Maruo, Y., Gochi, A., Kaihara, A., Shimamura, H., Yamada, T., Tanaka, N. and Orita, K., 2002. The antifungal drug ciclopirox inhibits deoxyhypusine and proline hydroxylation, endothelial cell growth and angiogenesis in vitro. *International Journal of Cancer*, 100(4), pp.491–498. https://doi.org/10.1002/ijc.10515.

Massagué, J., 1998. TGF-β Signal Transduction. *Annu. Rev. Biochem*, [online] 67, pp.753–91. Available at: <www.annualreviews.org>.

Massagué, J., 2012. TGFβ signalling in context. *Nature Reviews Molecular Cell Biology*, 13(10), pp.616–630. https://doi.org/10.1038/nrm3434.

Mateus, M.I.R., 2016. *Understanding the role of myofibroblast differentiation in the development of Peyronie's disease*.

Matyskiela, M.E., Couto, S., Zheng, X., Lu, G., Hui, J., Stamp, K., Drew, C., Ren, Y., Wang, M., Carpenter, A., Lee, C.-W., Clayton, T., Fang, W., Lu, C.-C., Riley, M., Abdubek, P., Blease, K., Hartke, J., Kumar, G., Vessey, R., Rolfe, M., Hamann, L.G. and Chamberlain, P.P., 2018. SALL4 mediates teratogenicity as a thalidomide-dependent cereblon substrate. *Nature Chemical Biology*, 14(10), pp.981–987. https://doi.org/10.1038/s41589-018-0129-x.

McAnulty, R.J., 2007. Fibroblasts and myofibroblasts: Their source, function and role in disease. *International Journal of Biochemistry and Cell Biology*, 39(4), pp.666–671. https://doi.org/10.1016/j.biocel.2006.11.005.

McGaha, S.M. and Champney, W.S., 2007. Hygromycin B inhibition of protein synthesis and ribosome biogenesis in Escherichia coli. *Antimicrobial agents and chemotherapy*, 51(2), pp.591–6. https://doi.org/10.1128/AAC.01116-06.

Mehal, W. and Imaeda, A., 2010. Cell death and fibrogenesis. *Seminars in Liver Disease*, 30(3), pp.226–231. https://doi.org/10.1055/s-0030-1255352.

Mehta, A., 2006. *Method of reducing scars with vitamin d*. WO2006094064A2.

Mehta, K.J., Je Farnaud, S. and Sharp, P.A., 2019. Iron and liver fibrosis: Mechanistic and clinical aspects. *World Journal of Gastroenterology*, 25(5), pp.521–538. https://doi.org/10.3748/wjg.v25.i5.521.

Meng, X.M., Nikolic-Paterson, D.J. and Lan, H.Y., 2016. TGF-β: The master regulator of fibrosis. *Nature Reviews Nephrology*, 12(6), pp.325–338. https://doi.org/10.1038/nrneph.2016.48.

Milenkovic, U., Ilg, M.M., Zuccato, C., Ramazani, Y., de Ridder, D. and Albersen, M., 2019. Simvastatin and the Rho-kinase inhibitor Y-27632 prevent myofibroblast transformation in Peyronie's disease-derived fibroblasts via inhibition of YAP/TAZ nuclear translocation. *BJU International*, 123(4), pp.703–715. https://doi.org/10.1111/bju.14638.

Miller, C.P., Collini, M.D., Tran, B.D., Harris, H.A., Kharode, Y.P., Marzolf, J.T., Moran, R.A., Henderson, R.A., Bender, R.H.W., Unwalla, R.J., Greenberger, L.M., Yardley, J.P., Abou-Gharbia, M.A., Lyttle, C.R. and Komm, B.S., 2001. Design, Synthesis, and Preclinical Characterization of Novel, Highly Selective Indole Estrogens. *Journal of Medicinal Chemistry*, 44(11). https://doi.org/10.1021/jm010086m.

Minden, M.D., Hogge, D.E., Weir, S.J., Kasper, J., Webster, D.A., Patton, L., Jitkova, Y., Hurren, R., Gronda, M., Goard, C.A., Rajewski, L.G., Haslam, J.L., Heppert, K.E., Schorno, K., Chang, H., Brandwein, J.M., Gupta, V., Schuh, A.C., Trudel, S., Yee, K.W.L., Reed, G.A. and Schimmer, A.D., 2014. Oral ciclopirox olamine displays biological activity in a phase I study in patients with advanced hematologic malignancies. *American Journal of Hematology*, 89(4), pp.363–368. https://doi.org/10.1002/ajh.23640.

Mokos, Z.B., Jović, A., Grgurević, L., Dumić-Čule, I., Kostović, K., Čeović, R. and Marinović, B., 2017. Current therapeutic approach to hypertrophic scars. *Frontiers in Medicine*, 4(83), pp.1–11. https://doi.org/10.3389/fmed.2017.00083.

Moll, I., 1994. Merkel cell distribution in human hair follicles of the fetal and adult scalp. *Cell and Tissue Research*, 277(1), pp.131–138. https://doi.org/10.1007/BF00303089.

Moll, R., Divo, M. and Langbein, L., 2008. The human keratins: Biology and pathology. *Histochemistry and Cell Biology*, 129(6), pp.705–733. https://doi.org/10.1007/s00418-008-0435-6.

Mora, A.L., Rojas, M., Pardo, A. and Selman, M., 2017. Emerging therapies for idiopathic pulmonary fibrosis, a progressive age-related disease. *Nature Reviews Drug Discovery*, 16(11), pp.755–772. https://doi.org/10.1038/nrd.2017.170.

Mori, R., Shaw, T.J. and Martin, P., 2008. Molecular mechanisms linking wound inflammation and fibrosis: knockdown of osteopontin leads to rapid repair and reduced scarring. *The Journal of experimental medicine*, 205(1), pp.43–51. https://doi.org/10.1084/jem.20071412.

Moritz, C., 2020. 40 years Western blotting: a scientific birthday toast. *Journal of Proteomics*, 212, pp.103575–103587.

Mor-Vaknin, N., Punturieri, A., Sitwala, K. and Markovitz, D., 2003. Vimentin is secreted by activated macrophages. *Nature Cell Biology*, 5(1), pp.59–63. https://doi.org/10.1038/ncb901.

Mosmann, T., 1983. Rapid colorimetric assay for cellular growth and survival: Application to proliferation and cytotoxicity assays. *Journal of Immunological Methods*, 65(1–2), pp.55–63. https://doi.org/10.1016/0022-1759(83)90303-4.

Moyer, K.E., Saggers, G.C. and Paul Ehrlich, H., 2004. Mast cells promote fibroblast populated collagen lattice contraction through gap junction intercellular communication. *Wound Repair and Regeneration*, 12(3), pp.269–274.

Mulhall, J.P., Schiff, J. and Guhring, P., 2006. An Analysis of the Natural History of Peyronie's Disease. *Journal of Urology*, 175(6), pp.2115–2118. https://doi.org/10.1016/S0022-5347(06)00270-9.

Müller, J., Rühle, G., Müller, N., Rossignol, J.-F. and Hemphill, A., 2006. In vitro effects of thiazolides on Giardia lamblia WB clone C6 cultured axenically and in coculture with Caco2 cells. *Antimicrobial agents and chemotherapy*, 50(1), pp.162–70. https://doi.org/10.1128/AAC.50.1.162-170.2006.

Murrell, G.A.C. and Hooper, G., 1992. An insight into Dupuytren's contracture. *Annals of the Royal College of Surgeons of England*, 74(3), pp.156–161.

Murtha, L.A., Schuliga, M.J., Mabotuwana, N.S., Hardy, S.A., Waters, D.W., Burgess, J.K., Knight, D.A. and Boyle, A.J., 2017. The processes and mechanisms of cardiac and pulmonary fibrosis. *Frontiers in Physiology*, 8(777), pp.1–15. https://doi.org/10.3389/fphys.2017.00777.

Mustoe, T.A., 2008. Evolution of silicone therapy and mechanism of action in scar management. *Aesthetic Plastic Surgery*, 32(1), pp.82–92. https://doi.org/10.1007/s00266-007-9030-9.

Mustoe, T.A., Kim, P., Ko, J., Ding, X. and Zhao, Y., 2020. *Methods for scar prevention*. US20210038564A1.

Naber, H.P.H., Drabsch, Y., Snaar-Jagalska, B.E., ten Dijke, P. and van Laar, T., 2013. Snail and Slug, key regulators of TGF-β-induced EMT, are sufficient for the induction of single-cell invasion. *Biochemical and Biophysical Research Communications*, 435(1), pp.58–63. https://doi.org/10.1016/j.bbrc.2013.04.037.

Naeini, F., Najafian, J. and Ahmadpour, K., 2006. Bleomycin Tattooing as a Promising Therapeutic Modality in Large Keloids and Hypertrophic Scars. *Dermatologic Surgery*, 3(8), pp.1023–1029.

Nair, R. and Maseeh, A., 2012. Vitamin D: The "sunshine" vitamin. *Journal of pharmacology & pharmacotherapeutics*, 3(2), pp.118–26. https://doi.org/10.4103/0976-500X.95506.

Nanthakumar, C.B., Hatley, R.J.D., Lemma, S., Gauldie, J., Marshall, R.P. and Macdonald, S.J.F., 2015. Dissecting fibrosis: Therapeutic insights from the small-molecule toolbox. *Nature Reviews Drug Discovery*, [online] 14(10), pp.693–720. https://doi.org/10.1038/nrd4592.

Newman-Tancredi, A., Conte, C., Chaput, C., Verrièle, L., Audinot-Bouchez, V., Lochon, S., Lavielle, G. and Millan, M.J., 1997. Agonist activity of antimigraine drugs at recombinant human 5-HT1A receptors: potential implications for prophylactic and acute therapy. *Naunyn-Schmiedeberg's Archives of Pharmacology*, 355(6), pp.682–688. https://doi.org/10.1007/PL00005000.

Nguyen, T.Q., Roestenberg, P., van Nieuwenhoven, F.A., Bovenschen, N., Li, Z., Xu, L., Oliver, N., Aten, J., Joles, J.A., Vial, C., Brandan, E., Lyons, K.M. and Goldschmeding, R., 2008. CTGF inhibits BMP-7 signaling in diabetic nephropathy. *Journal of the American Society of Nephrology*, 19(11), pp.2098–2107. https://doi.org/10.1681/ASN.2007111261.

NHS England and Improvement, The Department of Health and Social Care, The Medicines and Healthcare products Regulatory Authority, The National Institute for Health and Care Excellence and The National Institute for Health Research, 2019. *Opportunities to Repurpose Medicines in the NHS in England*.

Nielson, C.B., Duethman, N.C., Howard, J.M., Moncure, M. and Wood, J.G., 2017. Burns: Pathophysiology of Systemic Complications and Current Management. *Journal of Burn Care and Research*, 38(1), pp.e469–e481. https://doi.org/10.1097/BCR.0000000000000355.

Niessen, F.B., Schalkwijk, J., Vos, H. and Timens, W., 2004. Hypertrophic scar formation is associated with an increased number of epidermal langerhans cells. *Journal of Pathology*, 202(1), pp.121–129. https://doi.org/10.1002/path.1502.

Niessen, F.B., Spauwen, P.H.M., Schalkwijk, J. and Kon, M., 1999. On the Nature of Hypertrophic Scars and Keloids: A Review. *Plastic and Reconstructive Surgery*, 104(5), pp.1435–1458.

Noble, J., Heathcote, J. and Cohen, H., 1984. Diabetes mellitus in the aetiology of Dupuytren's disease. *The Journal of Bone and Joint Surgery*, 66(3), pp.322–325. https://doi.org/10.1302/0301-620X.66B3.6725338.

Noli, C. and Miolo, A., 2001. The mast cell in wound healing. *Veterinary Dermatology*, 12, pp.303–313.

Noth, I., Oelberg, D., Kaul, M., Conoscenti, C.S. and Raghu, G., 2018. Safety and tolerability of nintedanib in patients with idiopathic pulmonary fibrosis in the USA. *European Respiratory Journal*, 52(1702106), pp.1–4. https://doi.org/10.1183/13993003.02106-2017.

Novotny-Diermayr, V., Sangthongpitag, K., Hu, C.Y., Wu, X., Sausgruber, N., Yeo, P., Greicius, G., Pettersson, S., Liang, A.L., Loh, Y.K., Bonday, Z., Goh, K.C., Hentze, H., Hart, S., Wang, H., Ethirajulu, K. and Wood, J.M., 2010. SB939, a Novel Potent and Orally Active Histone Deacetylase Inhibitor with High Tumor Exposure and Efficacy in Mouse Models of Colorectal Cancer. *Molecular Cancer Therapeutics*, 9(3), pp.642–652. https://doi.org/10.1158/1535-7163.MCT-09-0689.

Nugteren, H.M., Nijman, J.M., de Jong, I.J. and van Driel, M.F., 2011. The association between Peyronie's and Dupuytren's disease. *International Journal of Impotence Research*, 23(4), pp.142–145. https://doi.org/10.1038/ijir.2011.18.

O'Boyle, C.P., Shayan-Arani, H. and Hamada, M.W., 2017. Intralesional cryotherapy for hypertrophic scars and keloids: a review. *Scars, Burns & Healing*, 3, pp.1–9. https://doi.org/10.1177/2059513117702162.

O'Connor, K.A. and Roth, B.L., 2005. Finding new tricks for old drugs: An efficient route for public-sector drug discovery. *Nature Reviews Drug Discovery*, 4(12), pp.1005–1014. https://doi.org/10.1038/nrd1900.

Ogihara, T., Nakagawa, M., Ishikawa, H., Mikami, H., Takeda, K., Nonaka, H., Nagano, M., Sasaki, S., Kagoshima, T. and Higashimori, K., 1992. Effect of manidipine, a novel calcium channel blocker, on quality of life in hypertensive patients. *Blood pressure. Supplement*, 3, pp.135–9.

O'Hare, T., Walters, D.K., Stoffregen, E.P., Jia, T., Manley, P.W., Mestan, J., Cowan-Jacob, S.W., Lee, F.Y., Heinrich, M.C., Deininger, M.W.N. and Druker, B.J., 2005. In vitro Activity of Bcr-Abl Inhibitors AMN107 and BMS-354825 against Clinically Relevant Imatinib-Resistant

Abl Kinase Domain Mutants. *Cancer Research*, 65(11), pp.4500–4505. https://doi.org/10.1158/0008-5472.CAN-05-0259.

Olbe, L., Carlsson, E. and Lindberg, P., 2003. A proton-pump inhibitor expedition: the case histories of omeprazole and esomeprazole. *Nature Reviews Drug Discovery*, 2(2), pp.132–139. https://doi.org/10.1038/nrd1010.

de Oliveira da Silva, B., Ramos, L.F. and Moraes, K.C.M., 2017. Molecular interplays in hepatic stellate cells: apoptosis, senescence, and phenotype reversion as cellular connections that modulate liver fibrosis. *Cell Biology International*, 41(9), pp.946–959. https://doi.org/10.1002/cbin.10790.

Olson, A.L., Gifford, A.H., Inase, N., Fernández Pérez, E.R. and Suda, T., 2018. The epidemiology of idiopathic pulmonary fibrosis and interstitial lung diseases at risk of a progressive-fibrosing phenotype. *European Respiratory Review*, 27(180077), pp.1–10. https://doi.org/10.1183/16000617.0077-2018.

Ono, I., Akasaka, Y., Kikuchi, R., Sakemoto, A., Kamiya, T., Yamashita, T. and Jimbow, K., 2007. Basic fibroblast growth factor reduces scar formation in acute incisional wounds. *Wound Repair and Regeneration*, 15(5), pp.617–623. https://doi.org/10.1111/j.1524-475X.2007.00293.x.

Overstreet, J.M., Samarakoon, R., Cardona-Grau, D., Goldschmeding, R. and Higgins, P.J., 2015. Tumor suppressor ataxia telangiectasia mutated functions downstream of TGF-β1 in orchestrating profibrotic responses. *FASEB Journal*, 29(4), pp.1258–1268. https://doi.org/10.1096/fj.14-262527.

Overstreet, J.M., Samarakoon, R., Meldrum, K.K. and Higgins, P.J., 2014. Redox control of p53 in the transcriptional regulation of TGF-β1 target genes through SMAD cooperativity. *Cellular Signalling*, 26(7), pp.1427–1436. https://doi.org/10.1016/j.cellsig.2014.02.017.

Pakshir, P. and Hinz, B., 2018. The big five in fibrosis: Macrophages, myofibroblasts, matrix, mechanics, and miscommunication. *Matrix Biology*, [online] 68–69(2017), pp.81–93. https://doi.org/10.1016/j.matbio.2018.01.019.

Parihar, A., Parihar, M.S., Milner, S. and Bhat, S., 2008. Oxidative stress and anti-oxidative mobilization in burn injury. *Burns*, 34(1), pp.6–17. https://doi.org/10.1016/j.burns.2007.04.009.

Parker, W.B., Shaddix, S.C., Chang, C.H., White, E.L., Rose, L.M., Brockman, R.W., Shortnacy, A.T., Montgomery, J.A., Secrist, J.A. and Bennett, L.L., 1991. Effects of 2-chloro-9-(2-deoxy-2-fluoro-beta-D-arabinofuranosyl)adenine on K562 cellular metabolism and the inhibition of human ribonucleotide reductase and DNA polymerases by its 5'-triphosphate. *Cancer research*, 51(9), pp.2386–94.

Patnaik, A., Haluska, P., Tolcher, A.W., Erlichman, C., Papadopoulos, K.P., Lensing, J.L., Beeram, M., Molina, J.R., Rasco, D.W., Arcos, R.R., Kelly, C.S., Wijayawardana, S.R., Zhang, X., Stancato, L.F., Bell, R., Shi, P., Kulanthaivel, P., Pitou, C., Mulle, L.B., Farrington, D.L., Chan, E.M. and Goetz, M.P., 2016. A First-in-Human Phase I Study of the Oral p38 MAPK Inhibitor, Ralimetinib (LY2228820 Dimesylate), in Patients with Advanced Cancer. *Clinical Cancer Research*, 22(5), pp.1095–1102. https://doi.org/10.1158/1078-0432.CCR-15-1718.

Paulin, D. and Li, Z., 2004. Desmin: A major intermediate filament protein essential for the structural integrity and function of muscle. *Experimental Cell Research*, 301(1), pp.1–7. https://doi.org/10.1016/j.yexcr.2004.08.004.

Pechulis, A.D., Beck, J.P., Curry, M.A., Wolf, M.A., Harms, A.E., Xi, N., Opalka, C., Sweet, M.P., Yang, Z., Vellekoop, A.S., Klos, A.M., Crocker, P.J., Hassler, C., Laws, M., Kitchen, D.B., Smith, M.A., Olson, R.E., Liu, S. and Molino, B.F., 2012. 4-Phenyl tetrahydroisoquinolines as dual norepinephrine and dopamine reuptake inhibitors. *Bioorganic & medicinal chemistry letters*, 22(23), pp.7219–22. https://doi.org/10.1016/j.bmcl.2012.09.050.

Petrov, V. v., Fagard, R.H. and Lijnen, P.J., 2002. Stimulation of Collagen Production by Transforming Growth Factor-β1 During Differentiation of Cardiac Fibroblasts to Myofibroblasts. *Hypertension*, 39(2), pp.258–263. https://doi.org/10.1161/hy0202.103268.

Philippe, M., Ruddell, R. and Ramm, G., 2007. Role of iron in hepatic fibrosis: One piece in the puzzle. *World Journal of Gastroenterology*, [online] 13(55), pp.4746–4754. Available at: <http://www.wjgn>.

Pic, E., Burgain, A. and Sellam, A., 2019. Repurposing the anthelminthic salicylanilide oxyclozanide against susceptible and clinical resistant *Candida albicans* strains. *Medical Mycology*, 57(3), pp.387–390. https://doi.org/10.1093/mmy/myy027.

Pierce, G.F., Mustoe, T.A., Altrock, B.W., Deuel, T.F. and Thomason, A., 1991. Role of platelet-derived growth factor in wound healing. *Journal of Cellular Biochemistry*, 45(4), pp.319–326. https://doi.org/10.1002/jcb.240450403.

Pierre, F., Chua, P.C., O'Brien, S.E., Siddiqui-Jain, A., Bourbon, P., Haddach, M., Michaux, J., Nagasawa, J., Schwaebe, M.K., Stefan, E., Vialettes, A., Whitten, J.P., Chen, T.K., Darjania, L., Stansfield, R., Bliesath, J., Drygin, D., Ho, C., Omori, M., Proffitt, C., Streiner, N., Rice, W.G., Ryckman, D.M. and Anderes, K., 2011. Pre-clinical characterization of CX-4945, a potent and selective small molecule inhibitor of CK2 for the treatment of cancer. *Molecular and Cellular Biochemistry*, 356(1–2), pp.37–43. https://doi.org/10.1007/s11010-011-0956-5.

Pinilla, I., Izaguirre, L.B., Gonzalvo, F.J., Piazuelo, E., Garcia-Gonzalez, M.A., Sanchez-Cano, A.I. and Sopeña, F., 2014. In Vitro Vitamin K3 Effect on Conjunctival Fibroblast Migration and Proliferation. *The Scientific World Journal*, 2014, pp.1–5. https://doi.org/10.1155/2014/916713.

Poon, R., Nik, S., Ahn, J., Slade, L. and Alman, B.A., 2009. β-catenin and transforming growth factor β have distinct roles regulating fibroblast cell motility and the induction of collagen lattice contraction. *BMC Cell Biology*, 10(1). https://doi.org/10.1186/1471-2121-10-38.

Popa-Burke, I. and Russell, J., 2014. Compound precipitation in high-concentration DMSO solutions. *Journal of Biomolecular Screening*, 19(9), pp.1302–1308. https://doi.org/10.1177/1087057114541146.

Posimo, J.M., Unnithan, A.S., Gleixner, A.M., Choi, H.J., Jiang, Y., Pulugulla, S.H. and Leak, R.K., 2014. Viability assays for cells in culture. *Journal of Visualized Experiments*, 83(e50645), pp.1–14. https://doi.org/10.3791/50645.

Prakash, J. and Pinzani, M., 2017. Fibroblasts and extracellular matrix: Targeting and therapeutic tools in fibrosis and cancer. *Advanced Drug Delivery Reviews*, 121, pp.1–2. https://doi.org/10.1016/j.addr.2017.11.008.

Prasad, R., Shah, A.H. and Rawal, M.K., 2016. Antifungals: Mechanism of Action and Drug Resistance. In: J. Ramos, H. Sychrová and M. Kschischo, eds. *Yeast Membrane Transport*, 1st ed. Springer. https://doi.org/10.1007/978-3-319-25304-6_14.

Prat, M., Buil, M.A., Fernández, M.D., Castro, J., Monleón, J.M., Tort, L., Casals, G., Ferrer, M., Huerta, J.M., Espinosa, S., López, M., Segarra, V., Gavaldà, A., Miralpeix, M., Ramos, I., Vilella, D., González, M., Córdoba, M., Cárdenas, A., Antón, F., Beleta, J. and Ryder, H., 2011. Discovery of novel quaternary ammonium derivatives of (3R)-quinuclidinyl carbamates as potent and long acting muscarinic antagonists. *Bioorganic & medicinal chemistry letters*, 21(11), pp.3457–61. https://doi.org/10.1016/j.bmcl.2011.03.096.

Procopiou, P.A., Browning, C., Buckley, J.M., Clark, K.L., Fechner, L., Gore, P.M., Hancock, A.P., Hodgson, S.T., Holmes, D.S., Kranz, M., Looker, B.E., Morriss, K.M.L., Parton, D.L., Russell, L.J., Slack, R.J., Sollis, S.L., Vile, S. and Watts, C.J., 2011. The Discovery of Phthalazinone-Based Human H1and H3 Single-Ligand Antagonists Suitable for Intranasal Administration for the Treatment of Allergic Rhinitis. *Journal of Medicinal Chemistry*, 54(7). https://doi.org/10.1021/jm1013874.

Qian, A., Meals, R.A., Rajfer, J. and Gonzalez-Cadavid, N.F., 2004. Comparison of gene expression profiles between Peyronie's disease and Dupuytren's contracture. *Urology*, 64(2), pp.399–404. https://doi.org/10.1016/j.urology.2004.04.006.

Quintás-Cardama, A., Kantarjian, H., Estrov, Z., Borthakur, G., Cortes, J. and Verstovsek, S., 2012. Therapy with the histone deacetylase inhibitor pracinostat for patients with myelofibrosis. *Leukemia Research*, 36(9), pp.1124–1127. https://doi.org/10.1016/j.leukres.2012.03.003.

Qureshi, O.S., Bon, H., Twomey, B., Holdsworth, G., Ford, K., Bergin, M., Huang, L., Muzylak, M., Healy, L.J., Hurdowar, V. and Johnson, T.S., 2017. An immunofluorescence assay for extracellular matrix components highlights the role of epithelial cells in producing a stable, fibrillar extracellular matrix. *Biology Open*, 6(10), pp.1423–1433. https://doi.org/10.1242/bio.025866.

Rabeyrin, M., Thivolet, F., Ferretti, G.R., Chalabreysse, L., Jankowski, A., Cottin, V., Pison, C., Cordier, J.F. and Lantuejoul, S., 2015. Usual interstitial pneumonia end-stage features from explants with radiologic and pathological correlations. *Annals of Diagnostic Pathology*, 19(4), pp.269–276. https://doi.org/10.1016/j.anndiagpath.2015.05.003.

Rabindran, S.K., Discafani, C.M., Rosfjord, E.C., Baxter, M., Floyd, M.B., Golas, J., Hallett, W.A., Johnson, B.D., Nilakantan, R., Overbeek, E., Reich, M.F., Shen, R., Shi, X., Tsou, H.-R., Wang, Y.-F. and Wissner, A., 2004. Antitumor Activity of HKI-272, an Orally Active, Irreversible Inhibitor of the HER-2 Tyrosine Kinase. *Cancer Research*, 64(11), pp.3958–3965. https://doi.org/10.1158/0008-5472.CAN-03-2868.

Radadiya, P.S., Thornton, M.M., Puri, R. v, Yerrathota, S., Dinh-Phan, J., Magenheimer, B., Subramaniam, D., Tran, P. v, Zhu, H., Bolisetty, S., Calvet, J.P., Wallace, D.P. and Sharma, M., 2021. Ciclopirox olamine induces ferritinophagy and reduces cyst burden in polycystic kidney disease. *JCI Insight*, [online] 6(9), pp.1–14. https://doi.org/10.1172/jci.

Rae, L., Fidler, P. and Gibran, N., 2016. The Physiologic Basis of Burn Shock and the Need for Aggressive Fluid Resuscitation. *Critical Care Clinics*, 32(4), pp.491–505. https://doi.org/10.1016/j.ccc.2016.06.001.

Raether, W. and Hänel, H., 1990. Rilopirox - a New Hydroxypyridone Antifungal with Fungicidal Properties. *Mycoses*, 33(4), pp.191–202. https://doi.org/10.1111/myc.1990.33.4.191.

Raghu, G., Behr, J., Brown, K., Egan, J., Kawut, S., Flaherty, K., Martinez, F., Nathan, S., Wells, A., Collard, H., Costabel, U., Richeldi, L., de Andrade, J., Khalil, N., Morrison, L., Lederer, D., Shao, L., Li, X., Pedersen, P., Montgomery, A., Chien, J. and O'Riordan, T., 2013. Treatment of Idiopathic Pulmonary Fibrosis With Ambrisentan. *Annals of Internal Medicine*, 158(9), pp.641–649. https://doi.org/10.7326/0003-4819-158-9-201305070-00003.

Ratziu, V., Charlotte, F., Bernhardt, C., Giral, P., Halbron, M., Lenaour, G., Hartmann-Heurtier, A., Bruckert, E. and Poynard, T., 2010. Long-term efficacy of rosiglitazone in nonalcoholic steatohepatitis: Results of the Fatty Liver Improvement by Rosiglitazone Therapy (FLIRT 2) extension trial. *Hepatology*, 51(2), pp.445–453. https://doi.org/10.1002/hep.23270.

Ravikanth, M., Manjunath, K., Ramachandran, C., Soujanya, P. and Saraswathi, T., 2011. Heterogenecity of fibroblasts. *Journal of Oral and Maxillofacial Pathology*, 15(2), pp.247–250. https://doi.org/10.4103/0973-029X.84516.

Reaume, A.G., 2011. Drug repurposing through nonhypothesis driven phenotypic screening. *Drug Discovery Today: Therapeutic Strategies*, 8(3–4), pp.85–88. https://doi.org/10.1016/j.ddstr.2011.09.007.

Regdon, Z., Demény, M.A., Kovács, K., Hajnády, Z., Nagy-Pénzes, M., Bakondi, E., Kiss, A., Hegedűs, C. and Virág, L., 2021. High-content screening identifies inhibitors of oxidative stress-induced parthanatos: cytoprotective and anti-inflammatory effects of ciclopirox. *British Journal of Pharmacology*, 178(5), pp.1095–1113. https://doi.org/10.1111/bph.15344.

Rehman, M., Vodret, S., Braga, L., Guarnaccia, C., Celsi, F., Rossetti, G., Martinelli, V., Battini, T., Long, C., Vukusic, K., Kocijan, T., Collesi, C., Ring, N., Skoko, N., Giacca, M., del Sal, G., Confalonieri, M., Raspa, M., Marcello, A., Myers, M.P., Crovella, S., Carloni, P. and Zacchigna, S., 2019. High-throughput screening discovers antifibrotic properties of haloperidol by hindering myofibroblast activation. *JCI Insight*, 4(8). https://doi.org/10.1172/jci.insight.123987.

Renò, F., Grazianetti, P. and Cannas, M., 2001. Effects of mechanical compression on hypertrophic scars: prostaglandin E 2 release. *Burns*, [online] 27, pp.215–218. Available at: <www.elsevier.com>.

Rhelnwald, J.G. and Green, H., 1975. Serial Cultivation of Strains of Human Epidermal Keratinocytes: the Formation of Keratinizing Colonies from Single Cells. *Cell*, 6, pp.331–344.

Ribrag, V., Kim, W.S., Bouabdallah, R., Lim, S.T., Coiffier, B., Illes, A., Lemieux, B., Dyer, M.J.S., Offner, F., Felloussi, Z., Kloos, I., Luan, Y., Vezan, R., Graef, T. and Morschhauser, F., 2017. Safety and efficacy of abexinostat, a pan-histone deacetylase inhibitor, in non-Hodgkin lymphoma and chronic lymphocytic leukemia: results of a phase II study. *Haematologica*, 102(5). https://doi.org/10.3324/haematol.2016.154377.

Richon, V.M., Emiliani, S., Verdin, E., Webb, Y., Breslow, R., Rifkind, R.A. and Marks, P.A., 1998. A class of hybrid polar inducers of transformed cell differentiation inhibits histone deacetylases. *Cell Biology*, [online] 95, pp.3003–3007. Available at: <www.pnas.org.>.

Riley, K.N. and Herman, I.M., 2005. Collagenase promotes the cellular responses to injury and wound healing in vivo. *Journal of burns and wounds*, 4, p.e8.

Rippa, A.L., Kalabusheva, E.P. and Vorotelyak, E.A., 2019. Regeneration of Dermis: Scarring and Cells Involved. *Cells*, 8(6), p.607. https://doi.org/10.3390/cells8060607.

Riviera, K., 2018. *Burn accidents costing NHS £20 million per annum, show latest statistics on National Burn Awareness Day*. [online] Children's Burn Trust. Available at: <https://www.cbtrust.org.uk/news-and-events/burn-accidents-costing-the-nhs-20-million-per-annum-show-latest-statistics-released-on-national-burn-awareness-day/>.

Rodrigues, J.N., Becker, G.W., Ball, C., Zhang, W., Giele, H., Hobby, J., Pratt, A.L. and Davis, T., 2015. Surgery for Dupuytren's contracture of the fingers. *Cochrane Database of Systematic Reviews*, (12), pp.1–86. https://doi.org/10.1002/14651858.CD010143.pub2.

Rowley, M., 2008. The Discovery of Raltegravir, an Integrase Inhibitor for the Treatment of HIV Infection. In: G. Lawton and D. Witty, eds. *Progress in Medicinal Chemistry*. https://doi.org/10.1016/S0079-6468(07)00001-X.

Rubinstein, E., 2001. History of Quinolones and Their Side Effects. *Chemotherapy*, 47(3). https://doi.org/10.1159/000057838.

Ruijtenberg, S. and van den Heuvel, S., 2016. Coordinating cell proliferation and differentiation: Antagonism between cell cycle regulators and cell type-specific gene expression. *Cell Cycle*, 15(2), pp.196–212. https://doi.org/10.1080/15384101.2015.1120925.

Rusnak, D.W., Lackey, K., Affleck, K., Wood, E.R., Alligood, K.J., Rhodes, N., Keith, B.R., Murray, D.M., Knight, W.B., Mullin, R.J. and Gilmer, T.M., 2001. The effects of the novel, reversible epidermal growth factor receptor/ErbB-2 tyrosine kinase inhibitor, GW2016, on the growth of human normal and tumor-derived cell lines in vitro and in vivo. *Molecular cancer therapeutics*, 1(2), pp.85–94.

Rutan, T., Herdon, D., Osten, T. and Abston, S., 1986. Metabolic Rate Alterations in Early Excision and Grafting versus Conservative Treatment. *The Journal of Trauma: Injury, Infection, and Critical Care*, 26(2), pp.140–142. https://doi.org/10.1097/00005373-198602000-00007.

Safe and Timely Access to Medicines for Patients (STAMP) expert group, 2019. *Proposal for a framework to support not-for-profit organisations and academia (institutions and individuals) in drug repurposing*.

Sahdeo, S., Scott, B.D., McMackin, M.Z., Jasoliya, M., Brown, B., Wulff, H., Perlman, S.L., Pook, M.A. and Cortopassi, G.A., 2014. Dyclonine rescues frataxin deficiency in animal models and buccal cells of patients with Friedreich's ataxia. *Human molecular genetics*, 23(25), pp.6848–62. https://doi.org/10.1093/hmg/ddu408.

Sakamoto, S., Matsuura, K., Masuda, S., Hagiwara, N. and Shimizu, T., 2020. Heart-derived fibroblasts express LYPD-1 and negatively regulate angiogenesis in rat. *Regenerative Therapy*, 15, pp.27–33. https://doi.org/10.1016/j.reth.2020.03.010.

Sams-Dodd, F., 2005. Target-based drug discovery: is something wrong? *Drug Discovery Today*, 10(2), pp.139–147.

Sapitro, J., Dunmire, J.J., Scott, S.E., Sutariya, V., Geldenhuys, W.J., Hewit, M., Yue, B.Y.J.T. and Nakamura, H., 2010. Suppression of transforming growth factor-β effects in rabbit subconjunctival fibroblasts by activin receptor-like kinase 5 inhibitor. *Molecular Vision*, [online] 16, pp.1880–1892. Available at: <http://www.molvis.org/molvis/v16/a204>.

Sarrazy, V., Billet, F., Micallef, L., Coulomb, B. and Desmoulière, A., 2011. Mechanisms of pathological scarring: Role of myofibroblasts and current developments. *Wound Repair and Regeneration*, 19(SUPPL. 1), pp.10–15. https://doi.org/10.1111/j.1524-475X.2011.00708.x.

Sato, M., Shegogue, D., Gore, E.A., Smith, E.A., McDermott, P.J. and Trojanowska, M., 2002. Role of p38 MAPK in transforming growth factor β stimulation of collagen production by scleroderma and healthy dermal fibroblasts. *Journal of Investigative Dermatology*, 118(4), pp.704–711. https://doi.org/10.1046/j.1523-1747.2002.01719.x.

Schlossberg, D. and Rafik, S., 2017. BITIN (Bithionol). In: *Antibiotics Manual*. Chichester, UK: John Wiley & Sons, Ltd.pp.57–57. https://doi.org/10.1002/9781119220787.ch26.

Schmid, P., Itin, P., Cherry, G., Bi, C. and Cox, D.A., 1998. Enhanced Expression of Transforming Growth Factor Type I and Type 11 Receptors in Wound Granulation Tissue and Hypertrophic Scar. *American Journal of Pathology*, 152(2), pp.485–493.

Schmidt-Rose, T., Braren, S., Fölster, H., Hillemann, T., Oltrogge, B., Philipp, P., Weets, G. and Fey, S., 2011. Efficacy of a piroctone olamine/climbazol shampoo in comparison with a zinc pyrithione shampoo in subjects with moderate to severe dandruff. *International Journal of Cosmetic Science*, 33(3), pp.276–282. https://doi.org/10.1111/j.1468-2494.2010.00623.x.

Seeman, P., 2001. Antipsychotic drugs, dopamine receptors, and schizophrenia. *Clinical Neuroscience Research*, 1(1–2), pp.53–60. https://doi.org/10.1016/S1566-2772(00)00007-4.

Selman, M., Thannickal, V.J., Pardo, A., Zisman, D.A., Martinez, F.J. and Lynch III, J.P., 2004. Idiopathic Pulmonary Fibrosis Pathogenesis and Therapeutic Approaches. *Drugs*, 64(4), pp.405–430.

Sen, C., Roy, S., Khanna, S. and Rink, C., 2013. *Treating scar injury using tocotrienol*. EP2858639B1.

Shah, G., 1999. Why do we still use serum in the production of biopharmaceuticals? *Developments in Biological Standardization*, 99, pp.17–22.

Shah, M., Foreman, D.M. and Ferguson, M.W.J., 1992. Control of scarring in adult wounds by neutralising antibody to transforming growth factor β. *The Lancet*, 339(8787). https://doi.org/10.1016/0140-6736(92)90009-R.

Shany, S., Sigal-Batikoff, I. and Lamprecht, S., 2016. Vitamin D and Myofibroblasts in Fibrosis and Cancer: At Cross-purposes with TGF-β/SMAD Signaling. *Anticancer Research*, 36(12), pp.6225–6234. https://doi.org/10.21873/anticanres.11216.

Shen, A.H., Borrelli, M.R., Adem, S., Deleon, N.M.D., Patel, R.A., Mascharak, S., Yen, S.J., Sun, B.Y., Taylor, W.L., Januszyk, M., Nguyen, D.H., Momeni, A., Gurtner, G.C., Longaker, M.T. and Wan, D.C., 2020. Prophylactic treatment with transdermal deferoxamine mitigates radiation-induced skin fibrosis. *Scientific Reports*, 10(12346), pp.1–11. https://doi.org/10.1038/s41598-020-69293-4.

Shen, T. and Huang, S., 2016. Repositioning the Old Fungicide Ciclopirox for New Medical Uses. *Current Pharmaceutical Design*, 22(28), pp.4443–4450.

Shimbori, C., Bellaye, P.S., Xia, J., Gauldie, J., Ask, K., Ramos, C., Becerril, C., Pardo, A., Selman, M. and Kolb, M., 2016. Fibroblast growth factor-1 attenuates TGF-β1-induced lung fibrosis. *Journal of Pathology*, 240(2), pp.197–210. https://doi.org/10.1002/path.4768.

Shindel, A.W., Sweet, G., Thieu, W., Durbin-Johnson, B., Rothschild, J. and Szabo, R., 2017. Prevalence of Peyronie's Disease-Like Symptoms in Men Presenting With Dupuytren Contractures. *Sexual Medicine*, 5(3), pp.e135–e141. https://doi.org/10.1016/j.esxm.2017.06.001.

Shi-Wen, X., Leask, A. and Abraham, D., 2008. Regulation and function of connective tissue growth factor/CCN2 in tissue repair, scarring and fibrosis. *Cytokine and Growth Factor Reviews*, 19(2), pp.133–144. https://doi.org/10.1016/j.cytogfr.2008.01.002.

Shockley, K.R., Gupta, S., Harris, S.F., Lahiri, S.N. and Peddada, S.D., 2019. Quality control of quantitative high throughput screening data. *Frontiers in Genetics*, 10(387), pp.1–12. https://doi.org/10.3389/fgene.2019.00387.

Shoulders, M.D. and Raines, R.T., 2009. Collagen structure and stability. *Annual Review of Biochemistry*, 78, pp.929–958. https://doi.org/10.1146/annurev.biochem.77.032207.120833.

Siani, A., Khaw, R.R., Manley, O.W.G., Tirella, A., Cellesi, F., Donno, R. and Tirelli, N., 2015. Fibronectin localization and fibrillization are affected by the presence of serum in culture media. *Scientific Reports*, 5(9278), pp.1–10. https://doi.org/10.1038/srep09278.

Sieber, P., Schäfer, A., Lieberherr, R., le Goff, F., Stritt, M., Welford, R.W.D., Gatfield, J., Peter, O., Nayler, O. and Lüthi, U., 2018a. Novel high–throughput myofibroblast assays identify agonists with therapeutic potential in pulmonary fibrosis that act via EP 2 and EP 4 receptors. *PLoS ONE*, 13(11), pp.1–27. https://doi.org/10.1371/journal.pone.0207872.

Sieber, P., Schäfer, A., Lieberherr, R., le Goff, F., Stritt, M., Welford, R.W.D., Gatfield, J., Peter, O., Nayler, O. and Lüthi, U., 2018b. Novel high–throughput myofibroblast assays identify agonists with therapeutic potential in pulmonary fibrosis that act via EP2 and EP4 receptors. *PLOS ONE*, 13(11), p.e0207872. https://doi.org/10.1371/journal.pone.0207872.

Simons, F.E.R. and Simons, K.J., 2011. Histamine and H1-antihistamines: Celebrating a century of progress. *Journal of Allergy and Clinical Immunology*, 128(6), pp.1139-1150.e4. https://doi.org/10.1016/j.jaci.2011.09.005.

Simpson, R., Alon, R., Kobzik, L., Valeri, C.R., Shepro, D. and Hechtman, H.B., 1993. Neutrophil and nonneutrophil-mediated injury in intestinal ischemia-reperfusion. *Annals of surgery*, 218(4), pp.444–53; discussion 453-4. https://doi.org/10.1097/00000658-199310000-00005.

Sindrilaru, A., Peters, T., Wieschalka, S., Baican, C., Baican, A., Peter, H., Hainzl, A., Schatz, S., Qi, Y., Schlecht, A., Weiss, J.M., Wlaschek, M., Sunderkötter, C. and Scharffetter-kochanek, K., 2011. An unrestrained proinflammatory M1 macrophage population induced by iron impairs wound healing in humans and mice. 121(3), pp.985–997. https://doi.org/10.1172/JCI44490DS1.

Singer, A.J. and Clark, R.A.F., 1999. Cutaneous Wound Healing. *New England Journal of Medicine*, 341(10), pp.738–746. https://doi.org/10.1056/NEJM199909023411006.

Sinnegger-Brauns, M.J., Huber, I.G., Koschak, A., Wild, C., Obermair, G.J., Einzinger, U., Hoda, J.-C., Sartori, S.B. and Striessnig, J., 2009. Expression and 1,4-Dihydropyridine-Binding Properties of Brain L-Type Calcium Channel Isoforms. *Molecular Pharmacology*, 75(2). https://doi.org/10.1124/mol.108.049981.

Sizar, O., Khare, S., Jamil, R.T. and Talati, R., 2021. *Statin Medications*. StatPearls Publishing.

Slater, J.W., Zechnich, A.D. and Haxby, D.G., 1999. Second-Generation antihistamines: a comparative review. *Drugs*, 57(1), pp.31–47. https://doi.org/10.2165/00003495-199957010-00004.

Smith, C., Smith, J. and Finn, M., 1987. The possible role of mast cells (allergy) in the production of keloid and hypertrophic scarring. *Journal of Burn Care & Rehabilitation*, 8(2), pp.126–131.

Smith, J.F., Walsh, T.J. and Lue, T.F., 2008. Peyronie's disease: A critical appraisal of current diagnosis and treatment. *International Journal of Impotence Research*, 20(5), pp.445–459. https://doi.org/10.1038/ijir.2008.30.

Smith, L.L., Burnet, S.P. and McNeil, J.D., 2003. Musculoskeletal manifestations of diabetes mellitus. *British Journal of Sports Medicine*, 37(1), pp.30–35. https://doi.org/10.1136/bjsm.37.1.30.

Sokoloff, P., Andrieux, M., Besançon, R., Pilon, C., Martres, M.-P., Giros, B. and Schwartz, J.-C., 1992. Pharmacology of human dopamine D3 receptor expressed in a mammalian cell line: comparison with D2 receptor. *European Journal of Pharmacology: Molecular Pharmacology*, 225(4), pp.331–337. https://doi.org/10.1016/0922-4106(92)90107-7.

Somogyi, V., Chaudhuri, N., Torrisi, S.E., Kahn, N., Müller, V. and Kreuter, M., 2019. The therapy of idiopathic pulmonary fibrosis: What is next? *European Respiratory Review*, 28(190021), pp.1–20. https://doi.org/10.1183/16000617.0021-2019.

Song, E., Ouyang, N., Hörbelt, M., Antus, B., Wang, M. and Exton, M.S., 2000. Influence of alternatively and classically activated macrophages on fibrogenic activities of human fibroblasts. *Cellular Immunology*, 204(1), pp.19–28. https://doi.org/10.1006/cimm.2000.1687.

Song, S., Christova, T., Perusini, S., Alizadeh, S., Bao, R.Y., Miller, B.W., Hurren, R., Jitkova, Y., Gronda, M., Isaac, M., Joseph, B., Subramaniam, R., Aman, A., Chau, A., Hogge, D.E., Weir, S.J., Kasper, J., Schimmer, A.D., Al-Awar, R., Wrana, J.L. and Attisano, L., 2011. Wnt inhibitor screen reveals iron dependence of β-catenin signaling in cancers. *Cancer Research*, 71(24), pp.7628–7639. https://doi.org/10.1158/0008-5472.CAN-11-2745.

Sonthalia, S., Agrawal, M. and Sehgal, V., 2019. Topical ciclopirox olamine 1%: Revisiting a unique antifungal. *Indian Dermatology Online Journal*, 10(4), pp.481–485. https://doi.org/10.4103/idoj.idoj_29_19.

Sorg, H., Tilkorn, D.J., Hager, S., Hauser, J. and Mirastschijski, U., 2017. Skin Wound Healing: An Update on the Current Knowledge and Concepts. *European Surgical Research*, 58(1–2), pp.81–94. https://doi.org/10.1159/000454919.

Sorrell, J.M. and Caplan, A.I., 2004. Fibroblast heterogeneity: More than skin deep. *Journal of Cell Science*, 117(5), pp.667–675. https://doi.org/10.1242/jcs.01005.

Sorrentino, A., Thakur, N., Grimsby, S., Marcusson, A., von Bulow, V., Schuster, N., Zhang, S., Heldin, C.H. and Landström, M., 2008. The type I TGF-β receptor engages TRAF6 to activate TAK1 in a receptor kinase-independent manner. *Nature Cell Biology*, 10(10), pp.1199–1207. https://doi.org/10.1038/ncb1780.

Sousos, N., Sinakos, E., Klonizakis, P., Adamidou, D., Daniilidis, A., Gigi, E., Vetsiou, E., Tsioni, K., Mandala, E. and Vlachaki, E., 2018. Deferasirox improves liver fibrosis in beta-

thalassaemia major patients. A five-year longitudinal study from a single thalassaemia centre. *British Journal of Haematology*, 181(1). https://doi.org/10.1111/bjh.14509.

Spampinato, S., Bachetti, T., Carboni, L., Ratti, E., van Amsterdam, F.T. and Ferri, S., 1993. Ca2+ channel blocking activity of lacidipine and amlodipine in A7r5 vascular smooth muscle cells. *European journal of pharmacology*, 244(2), pp.139–44. https://doi.org/10.1016/0922-4106(93)90019-6.

Stebbeds, W.J.D., 2015. *In vitro studies of myofibroblasts: disease association and identification of novel therapeutic compounds*.

Stekelenburg, C.M., Marck, R.E., Tuinebreijer, W.E., de Vet, H.C.W., Ogawa, R. and van Zuijlen, P.P.M., 2015. A systematic review on burn scar contracture treatment: searching for evidence. *Journal of Burn Care and Research*, 36(3), pp.153–161.

Stemmer, V., de Craene, B., Berx, G. and Behrens, J., 2008. Snail promotes Wnt target gene expression and interacts with β-catenin. *Oncogene*, 27(37), pp.5075–5080. https://doi.org/10.1038/onc.2008.140.

Stone, R., Pastar, I., Ojeh, N., Chen, V., Liu, S., Garzon, K. and Tomic-Canic, M., 2016. Epithelial-Mesenchymal Transition in Tissue Repair and Fibrosis. *Cell and Tissue Research*, 365(3), pp.495–506.

Stuart, D., Li, N., Poon, D., Aardalen, K., Kaufman, S., Merritt, H., Salangsang, F., Lorenzana, E., Li, A. and Ghoddusi, M., 2012. Preclinical profile of LGX818: A potent and selective RAF kinase inhibitor. *Cancer Research*, 72(8 (Supplement 1)).

Stylianou, N., Buchan, I. and Dunn, K.W., 2015. A review of the international Burn Injury Database (iBID) for England and Wales: descriptive analysis of burn injuries 2003-2011. *BMJ open*, 5(e006184), pp.1–11. https://doi.org/10.1136/bmjopen-2014-006184.

Su, Z., Han, S., Jin, Q., Zhou, N., Lu, J., Shangguan, F., Yu, S., Liu, Y., Wang, L., Lu, J., Li, Q., Cai, L., Wang, C., Tian, X., Chen, L., Zheng, W. and Lu, B., 2021. Ciclopirox and bortezomib synergistically inhibits glioblastoma multiforme growth via simultaneously enhancing JNK/p38 MAPK and NF-κB signaling. *Cell Death and Disease*, 12(3). https://doi.org/10.1038/s41419-021-03535-9.

Subissi, A., Monti, D., Togni, G. and Mailland, F., 2010. Ciclopirox: Recent nonclinical and clinical data relevant to its use as a topical antimycotic agent. *Drugs*, 70(16), pp.2133–2152. https://doi.org/10.2165/11538110-000000000-00000.

Sultana, J., Crisafulli, S., Gabbay, F., Lynn, E., Shakir, S. and Trifirò, G., 2020. Challenges for Drug Repurposing in the COVID-19 Pandemic Era. *Frontiers in Pharmacology*, 11. https://doi.org/10.3389/fphar.2020.588654.

Summa, V., Petrocchi, A., Bonelli, F., Crescenzi, B., Donghi, M., Ferrara, M., Fiore, F., Gardelli, C., Gonzalez Paz, O., Hazuda, D.J., Jones, P., Kinzel, O., Laufer, R., Monteagudo, E., Muraglia, E., Nizi, E., Orvieto, F., Pace, P., Pescatore, G., Scarpelli, R., Stillmock, K., Witmer, M. v. and Rowley, M., 2008. Discovery of Raltegravir, a Potent, Selective Orally Bioavailable HIV-Integrase Inhibitor for the Treatment of HIV-AIDS Infection. *Journal of Medicinal Chemistry*, 51(18), pp.5843–5855. https://doi.org/10.1021/jm800245z.

Sunahara, R.K., Guan, H.C., O'Dowd, B.F., Seeman, P., Laurier, L.G., Ng, G., George, S.R., Torchia, J., van Tol, H.H. and Niznik, H.B., 1991a. Cloning of the gene for a human dopamine D5 receptor with higher affinity for dopamine than D1. *Nature*, 350(6319), pp.614–9. https://doi.org/10.1038/350614a0.

Sunahara, R.K., Guan, H.-C., O'Dowd, B.F., Seeman, P., Laurier, L.G., Ng, G., George, S.R., Torchia, J., van Tol, H.H.M. and Niznik, H.B., 1991b. Cloning of the gene for a human dopamine D5 receptor with higher affinity for dopamine than D1. *Nature*, 350(6319), pp.614–619. https://doi.org/10.1038/350614a0.

Sweetnam, P.M., Caldwell, L., Lancaster, J., Bauer, C., McMillan, B., Kinnier, W.J. and Price, C.H., 1993. The Role of Receptor Binding in Drug Discovery. *Journal of Natural Products*, 56(4), pp.441–455. https://doi.org/10.1021/np50094a001.

Swinney, D.C., 2013. Phenotypic vs. Target-based drug discovery for first-in-class medicines. *Clinical Pharmacology and Therapeutics*, 93(4), pp.299–301. https://doi.org/10.1038/clpt.2012.236.

Swinney, D.C. and Anthony, J., 2011. How were new medicines discovered? *Nature Reviews Drug Discovery*, 10(7), pp.507–519. https://doi.org/10.1038/nrd3480.

Swinney, D.C. and Lee, J.A., 2020. Recent advances in phenotypic drug discovery. *F1000Research*, 9(944), pp.1–9. https://doi.org/10.12688/f1000research.25813.1.

Takashima, A., 1998. Establishment of Fibroblast Cultures. *Current Protocols in Cell Biology*, 2(2.1). https://doi.org/10.1002/0471143030.cb0201s00.

Tan, E.M.L., Qin, H., Kennedy, S.H., Rouda, S., Fox, J.W. and Moore, J.H., 1995. Platelet-derived growth factors-AA and-BB regulate collagen and collagenase gene expression differentially in human fibroblasts. *Journal of Biochemistry*, [online] 310, pp.585–588. Available at: <http://portlandpress.com/biochemj/article-pdf/310/2/585/617875/bj3100585.pdf>.

Tanaka, M., Levy, J., Terada, M., Breslow, R., Rifkind, R.A. and Marks, P.A., 1975. Induction of Erythroid Differentiation in Murine Virus Infected Erythroleukemia Cells by Highly Polar Compounds. *Proceedings of the National Academy of Sciences*, 72(3), pp.1003–1006.

Tatsumi, M., Groshan, K., Blakely, R.D. and Richelson, E., 1997. Pharmacological profile of antidepressants and related compounds at human monoamine transporters. *European Journal of Pharmacology*, 340(2–3), pp.249–258. https://doi.org/10.1016/S0014-2999(97)01393-9.

Tekari, A., Luginbuehl, R., Hofstetter, W. and Egli, R.J., 2015. Transforming growth factor beta signaling is essential for the autonomous formation of cartilage-like tissue by expanded chondrocytes. *PLoS ONE*, 10(3), pp.1–17. https://doi.org/10.1371/journal.pone.0120857.

Terstappen, G.C., Schlüpen, C., Raggiaschi, R. and Gaviraghi, G., 2007. Target deconvolution strategies in drug discovery. *Nature Reviews Drug Discovery*, 6(11), pp.891–903. https://doi.org/10.1038/nrd2410.

Thébaut, A., Nemeth, A., le Mouhaër, J., Scheenstra, R., Baumann, U., Koot, B., Gottrand, F., Houwen, R., Monard, L., de Micheaux, S.L., Habes, D. and Jacquemin, E., 2016. Oral Tocofersolan Corrects or Prevents Vitamin E Deficiency in Children With Chronic Cholestasis. *Journal of Pediatric Gastroenterology & Nutrition*, 63(6), pp.610–615. https://doi.org/10.1097/MPG.0000000000001331.

Theilgaard-Mönch, K., Knudsen, S., Follin, P. and Borregaard, N., 2004. The Transcriptional Activation Program of Human Neutrophils in Skin Lesions Supports Their Important Role in Wound Healing. *The Journal of Immunology*, 172(12), pp.7684–7693. https://doi.org/10.4049/jimmunol.172.12.7684.

Thompson, C.M., Hocking, A.M., Honari, S., Muffley, L.A., Ga, M. and Gibran, N.S., 2013. Genetic risk factors for hypertrophic scar development. *Journal of Burn Care and Research*, 34(5), pp.477–482. https://doi.org/10.1097/BCR.0b013e3182a2aa41.

Tiede, S., Ernst, N., Bayat, A., Paus, R., Tronnier, V. and Zechel, C., 2009. Basic fibroblast growth factor: A potential new therapeutic tool for the treatment of hypertrophic and keloid scars. *Annals of Anatomy*, 191(1), pp.33–44. https://doi.org/10.1016/j.aanat.2008.10.001.

Tikhonov, D.B. and Zhorov, B.S., 2017. Mechanism of sodium channel block by local anesthetics, antiarrhythmics, and anticonvulsants. *The Journal of general physiology*, 149(4), pp.465–481. https://doi.org/10.1085/jgp.201611668.

Tolcher, A.W., Kurzrock, R., Valero, V., Gonzalez, R., Heist, R.S., Tan, A.R., Means-Powell, J., Werner, T.L., Becerra, C., Wang, C., Leonowens, C., Kalyana-Sundaram, S., Kleha, J.F., Gauvin, J., D'Amelio, A.M., Ellis, C., Ibrahim, N. and Yan, L., 2020. Phase I dose-escalation trial of the oral AKT inhibitor uprosertib in combination with the oral MEK1/MEK2 inhibitor trametinib in patients with solid tumors. *Cancer Chemotherapy and Pharmacology*, 85(4), pp.673–683. https://doi.org/10.1007/s00280-020-04038-8.

Tomuleasa, C., Selicean, S., Gafencu, G., Petrushev, B., Pop, L., Berce, C., Jurj, A., Trifa, A., Rosu, A., Pasca, S., Magdo, L., Zdrenghea, M., Dima, D., Tanase, A., Frinc, I., Bojan, A., Berindan-Neagoe, I., Ghiaur, G. and Ciurea, S.O., 2018. Fibroblast dynamics as an in vitro screening platform for anti-fibrotic drugs in primary myelofibrosis. *Journal of Cellular Physiology*, 233(1), pp.422–433. https://doi.org/10.1002/jcp.25902.

Tracy, L.E., Minasian, R.A. and Caterson, E.J., 2016. Extracellular Matrix and Dermal Fibroblast Function in the Healing Wound. *Advances in Wound Care*, 5(3), pp.119–136. https://doi.org/10.1089/wound.2014.0561.

Tran, C., Ouk, S., Clegg, N.J., Chen, Y., Watson, P.A., Arora, V., Wongvipat, J., Smith-Jones, P.M., Yoo, D., Kwon, A., Wasielewska, T., Welsbie, D., Chen, C.D., Higano, C.S., Beer, T.M., Hung, D.T., Scher, H.I., Jung, M.E. and Sawyers, C.L., 2009. Development of a Second-Generation Antiandrogen for Treatment of Advanced Prostate Cancer. *Science*, 324(5928), pp.787–790. https://doi.org/10.1126/science.1168175.

Trautmann, A., Toksoy, A., Engelhardt, E., Brocker, E.-B. and Gillitzer, R., 2000. Mast cell involvement in normal human skin wound healing: expression of monocyte chemoattractant protein-1 is correlated with recruitment of mast cells which synthesize interleukin-4 in vivo. *The Journal of Pathology*, 190(1), pp.100–106. https://doi.org/10.1002/(SICI)1096-9896(200001)190:1<100::AID-PATH496>3.0.CO;2-Q.

Tredget, E.E., Shankowsky, H.A., Pannu, R., Nedelec, B., Iwashina, T., Ghahary, A., Taerum, T. v and Scott, P.G., 1998. Transforming growth factor-beta in thermally injured patients with hypertrophic scars: effects of interferon alpha-2b. *Plastic and reconstructive surgery*, 102(5), pp.1317–28; discussion 1329-30. https://doi.org/10.1097/00006534-199810000-00001.

Tsatmali, M., Ancans, J. and Thody, A.J., 2002. Melanocyte function and its control by melanocortin peptides. *Journal of Histochemistry and Cytochemistry*, 50(2), pp.125–133. https://doi.org/10.1177/002215540205000201.

Tzouvelekis, A., Bonella, F. and Spagnolo, P., 2015. Update on therapeutic management of idiopathic pulmonary fibrosis. *Therapeutics and Clinical Risk Management*, 11, pp.359–370. https://doi.org/10.2147/TCRM.S69716.

Ud-Din, S. and Bayat, A., 2013. Strategic management of keloid disease in ethnic skin: A structured approach supported by the emerging literature. *British Journal of Dermatology*, 169(Suppl.3), pp.71–81. https://doi.org/10.1111/bjd.12588.

Uitto, J., Olsen, D.R. and Fazio, M.J., 1989. Extracellular Matrix of the Skin: 50 Years of Progress. *The Journal of Investigative Dermatology*, 92(4), pp.61S-77S.

Umemoto, S., Ogihara, T., Rakugi, H., Matsumoto, M., Kitagawa, K., Shimada, K., Higaki, J., Ito, S., Suzuki, H., Ohashi, Y., Saruta, T. and Matsuzaki, M., 2013. Effects of a benidipine-based combination therapy on the risk of stroke according to stroke subtype: the COPE trial. *Hypertension Research*, 36(12). https://doi.org/10.1038/hr.2013.100.

Urquiza, P., Laín, A., Sanz-Parra, A., Moreno, J., Bernardo-Seisdedos, G., Dubus, P., González, E., Gutiérrez-de-Juan, V., García, S., Eraña, H., San Juan, I., Macías, I., ben Bdira, F., Pluta, P., Ortega, G., Oyarzábal, J., González-Muñiz, R., Rodríguez-Cuesta, J., Anguita, J., Díez, E., Blouin, J.-M., de Verneuil, H., Mato, J.M., Richard, E., Falcón-Pérez, J.M., Castilla, J. and Millet, O., 2018. Repurposing ciclopirox as a pharmacological chaperone in a model of congenital erythropoietic porphyria. *Science Translational Medicine*, [online] 10, pp.1–9. Available at: <http://stm.sciencemag.org/>.

Vangipuram, M., Ting, D., Kim, S., Diaz, R. and Schüle, B., 2013. Skin punch biopsy explant culture for derivation of primary human fibroblasts. *Journal of visualized experiments*, e3779(77), pp.1–3. https://doi.org/10.3791/3779.

Venugopal, B., Baird, R., Kristeleit, R.S., Plummer, R., Cowan, R., Stewart, A., Fourneau, N., Hellemans, P., Elsayed, Y., Mcclue, S., Smit, J.W., Forslund, A., Phelps, C., Camm, J., Evans, T.R.J., de Bono, J.S. and Banerji, U., 2013. A Phase I Study of Quisinostat (JNJ-26481585), an Oral Hydroxamate Histone Deacetylase Inhibitor with Evidence of Target Modulation and Antitumor Activity, in Patients with Advanced Solid Tumors. *Clinical Cancer Research*, 19(15), pp.4262–4272. https://doi.org/10.1158/1078-0432.CCR-13-0312.

Vermeer, C., 2016. *Compositions for treating or preventing cardiovascular disease*. US20160250160A1.

Villegas, J. and McPhaul, M., 2005. Establishment and Culture of Human Skin Fibroblasts. *Current Protocols in Molecular Biology*, 71(1). https://doi.org/10.1002/0471142727.mb2803s71.

Vincent, F., Loria, P., Pregel, M., Stanton, R., Kitching, L., Nocka, K., Doyonnas, R., Steppan, C., Gilbert, A., Schroeter, T. and Peakman, M.-C., 2015. Developing predictive assays: The phenotypic screening “rule of 3.” *Science Translational Medicine*, 7(293), pp.293ps15-293ps15. https://doi.org/10.1126/scitranslmed.aab1201.

Vogel, B., Siebert, H., Hofmann, U. and Frantz, S., 2015. Determination of collagen content within picrosirius red stained paraffin-embedded tissue sections using fluorescence microscopy. *MethodsX*, 2, pp.124–134. https://doi.org/10.1016/j.mex.2015.02.007.

Wahab, N.A., Weston, B.S. and Mason, R.M., 2005. Connective tissue growth factor CCN2 interacts with and activates the tyrosine kinase receptor TrkA. *Journal of the American Society of Nephrology*, 16(2), pp.340–351. https://doi.org/10.1681/ASN.2003100905.

Wang, H., Yang, G.-H., Bu, H., Zhou, Q., Guo, L.-X., Wang, S.-L. and Ye, L. v, 2003. Systematic analysis of the TGF-b/Smad signalling pathway in the rhabdomyosarcoma cell line RD. *International Journal of Experimental Pathology*, 84, pp.153–163.

Wang, J., Zohar, R. and McCulloch, C.A., 2006. Multiple roles of α-smooth muscle actin in mechanotransduction. *Experimental Cell Research*, 312(3), pp.205–214. https://doi.org/10.1016/j.yexcr.2005.11.004.

Wang, Q., Wang, J., Wang, J., Hong, S., Han, F., Chen, J. and Chen, G., 2017. HMGB1 induces lung fbroblast to myofbroblast differentiation through NF-κB-mediated TGF-β1 release. *Molecular Medicine Reports*, 15(5), pp.3062–3068. https://doi.org/10.3892/mmr.2017.6364.

Wang, S., Wilkes, M.C., Leof, E.B. and Hirschberg, R., 2005. Imatinib mesylate blocks a non-Smad TGF-beta pathway and reduces renal fibrogenesis in vivo. *FASEB journal : official publication of the Federation of American Societies for Experimental Biology*, 19(1), pp.1–11. https://doi.org/10.1096/fj.04-2370com.

Wei, H., Wang, F., Wang, Y., Li, T., Xiu, P., Zhong, J., Sun, X. and Li, J., 2017. Verteporfin suppresses cell survival, angiogenesis and vasculogenic mimicry of pancreatic ductal adenocarcinoma via disrupting the YAP-TEAD complex. *Cancer Science*, 108(3), pp.478–487. https://doi.org/10.1111/cas.13138.

Wei, J., Bhattacharyya, S., Tourtellotte, W.G. and Varga, J., 2011. Fibrosis in systemic sclerosis: Emerging concepts and implications for targeted therapy. *Autoimmunity Reviews*, 10(5), pp.267–275. https://doi.org/10.1016/j.autrev.2010.09.015.Fibrosis.

Weir, S.J., Patton, L., Castle, K., Rajewski, L., Kasper, J. and Schimmer, A.D., 2011. The repositioning of the anti-fungal agent ciclopirox olamine as a novel therapeutic agent for the treatment of haematologic malignancy. *Journal of Clinical Pharmacy and Therapeutics*, 36(2), pp.128–134. https://doi.org/10.1111/j.1365-2710.2010.01172.x.

Weiss, S.M., Benwell, K., Cliffe, I.A., Gillespie, R.J., Knight, A.R., Lerpiniere, J., Misra, A., Pratt, R.M., Revell, D., Upton, R. and Dourish, C.T., 2003. Discovery of nonxanthine adenosine A2A receptor antagonists for the treatment of Parkinson's disease. *Neurology*, 61(Issue 11, Supplement 6), pp.S101–S106. https://doi.org/10.1212/01.WNL.0000095581.20961.7D.

West, H.C. and Bennett, C.L., 2018. Redefining the role of langerhans cells as immune regulators within the skin. *Frontiers in Immunology*, 8(1941), pp.1–8. https://doi.org/10.3389/fimmu.2017.01941.

Wilgus, T.A., Roy, S. and McDaniel, J.C., 2013. Neutrophils and Wound Repair: Positive Actions and Negative Reactions. *Advances in Wound Care*, 2(7), pp.379–388. https://doi.org/10.1089/wound.2012.0383.

Wilkins, E., Wilson, L., Wickramasinghe, P., Bhatnagar, P., Leal, J., Luengo-Fernandez, R., Burns, R., Rayner, M. and Townsend, N., 2017. *European Cardiovascular Disease Statistics 2017*. Brussels.

Williams, P., Crandall, E. and Sheppard, J., 2010. Azelastine hydrochloride, a dual-acting anti-inflammatory ophthalmic solution, for treatment of allergic conjunctivitis. *Clinical Ophthalmology*, 4, pp.993–1001. https://doi.org/10.2147/OPTH.S13479.

Winterbourn, C.C., 1995. Toxicity of iron and hydrogen peroxide: the Fenton reaction. *Toxicology Letters*, 82–83. https://doi.org/10.1016/0378-4274(95)03532-X.

Wipff, P.-J., Rifkin, D.B., Meister, J.-J. and Hinz, B., 2007. Myofibroblast contraction activates latent TGF-β1 from the extracellular matrix. *Journal of Cell Biology*, 179(6), pp.1311–1323. https://doi.org/10.1083/jcb.200704042.

Wiśniowska, B., Mendyk, A., Fijorek, K., Glinka, A. and Polak, S., 2012. Predictive model for L-type channel inhibition: multichannel block in QT prolongation risk assessment. *Journal of Applied Toxicology*, 32(10). https://doi.org/10.1002/jat.2784.

Wissner, A. and Mansour, T.S., 2008. The Development of HKI-272 and Related Compounds for the Treatment of Cancer. *Archiv der Pharmazie*, 341(8), pp.465–477. https://doi.org/10.1002/ardp.200800009.

Wolak, M., Bojanowska, E., Staszewska, T., Ciosek, J., Juszczak, M. and Drobnik, J., 2017. The role of histamine in the regulation of the viability, proliferation and transforming growth factor β1 secretion of rat wound fibroblasts. *Pharmacological Reports*, 69(2), pp.314–321. https://doi.org/10.1016/j.pharep.2016.11.006.

Wolfram, D., Tzankov, A., Pülzl, P. and Piza-Katzer, H., 2009. Hypertrophic scars and keloids - A review of their pathophysiology, risk factors, and therapeutic management. *Dermatologic Surgery*, 35(2), pp.171–181. https://doi.org/10.1111/j.1524-4725.2008.34406.x.

Wong, R., Geyer, S., Weninger, W., Guimberteau, J.C. and Wong, J.K., 2016. The dynamic anatomy and patterning of skin. *Experimental Dermatology*, 25(2), pp.92–98. https://doi.org/10.1111/exd.12832.

Wu, J., Liu, H., Zhang, G., Gu, L., Zhang, Y., Gao, J., Wei, Y. and Ma, Z., 2016. Antileukemia effect of Ciclopirox olamine is mediated by downregulation of intracellular ferritin and inhibition β-catenin-c-Myc signaling pathway in glucocorticoid resistant T-ALL cell lines. *PLoS ONE*, 11(8), pp.1–14. https://doi.org/10.1371/journal.pone.0161509.

Wu, S.-F., Peng, C.-T., Wu, K.-H. and Tsai, C.-H., 2006. Liver Fibrosis and Iron Levels During Long-Term Deferiprone Treatment of Thalassemia Major Patients. *Hemoglobin*, 30(2). https://doi.org/10.1080/03630260600642534.

Wynn, T. a and Ramalingam, T., 2013. Mechanism of fibrosis: therapeutic translation for fibrotic disease. *Nature Medicine*, 18(7), pp.1028–1040. https://doi.org/10.1038/nm.2807.Mechanisms.

Wynn, T.A., 2004. Fibrotic disease and the TH1/TH2 paradigm. *Nature Reviews Immunology*, 4(8), pp.583–594. https://doi.org/10.1038/nri1412.

Wynn, T.A., 2007. Common and unique mechanisms regulate fibrosis in various fibroproliferative diseases. *The Journal of Clinical Investigation*, 117(3), pp.524–529.

Wynn, T.A. and Vannella, K.M., 2016. Macrophages in Tissue Repair, Regeneration, and Fibrosis. *Immunity*, [online] 44(3), pp.450–462. https://doi.org/10.1016/j.immuni.2016.02.015.

Xiao, Z., Zhang, F. and Cui, Z., 2009. Treatment of hypertrophic scars with intralesional botulinum toxin type a injections: A preliminary report. *Aesthetic Plastic Surgery*, 33(3), pp.409–412. https://doi.org/10.1007/s00266-009-9334-z.

Xie, J.L., Bian, H.N., Qi, S.H., Chen, H. de, Li, H.D., Xu, Y. bin, Li, T.Z., Liu, X.S., Liang, H.Z., Xin, B.R. and Huan, Y., 2008. Basic fibroblast growth factor (bFGF) alleviates the scar of the rabbit ear model in wound healing. *Wound Repair and Regeneration*, 16(4), pp.576–581. https://doi.org/10.1111/j.1524-475X.2008.00405.x.

Xie, P., Dolivo, D.M., Jia, S., Cheng, X., Salcido, J., Galiano, R.D., Hong, S.J. and Mustoe, T.A., 2020. Liposome-encapsulated statins reduce hypertrophic scarring through topical

application. *Wound Repair and Regeneration*, 28(4), pp.460–469. https://doi.org/10.1111/wrr.12811.

Xu, C., Qin, Z., Liang, M., Chen, H., Yang, L., Luo, X., Luo, J., Xu, H., Cui, J., Lu, S. and Lu, K., 2013. Effect of Dimethyl Sulfoxide on Cell Cycle Synchronization of in vitro Cultured Monkey (Maccaca fascicularis) Ear Skin Fibroblats. *Journal of Animal and Veterinary Advances*, 12(2), pp.242–247.

Xu, J., Lamouille, S. and Derynck, R., 2009. TGF-B-induced epithelial to mesenchymal transition. *Cell Research*, 19(2), pp.156–172. https://doi.org/10.1038/cr.2009.5.

Xue, H., McCauley, R.L., Zhang, W. and Martini, D.K., 2000. Altered interleukin-6 expression in fibroblasts from hypertrophic burn scars. *The Journal of burn care & rehabilitation*, 21(2), pp.142–6. https://doi.org/10.1097/00004630-200021020-00010.

Xue, M. and Jackson, C.J., 2015. Extracellular Matrix Reorganization During Wound Healing and Its Impact on Abnormal Scarring. *Advances in Wound Care*, 4(3), pp.119–136. https://doi.org/10.1089/wound.2013.0485.

Yan, C., Grimm, W.A., Garner, W.L., Qin, L., Travis, T., Tan, N. and Han, Y.-P., 2010. Epithelial to Mesenchymal Transition in Human Skin Wound Healing Is Induced by Tumor Necrosis Factor-α through Bone Morphogenic Protein-2. *The American Journal of Pathology*, 176(5), pp.2247–2258. https://doi.org/10.2353/ajpath.2010.090048.

Yang, S., Sun, Y., Geng, Z., Ma, K., Sun, X. and Fu, X., 2016. Abnormalities in the basement membrane structure promote basal keratinocytes in the epidermis of hypertrophic scars to adopt a proliferative phenotype. *International Journal of Molecular Medicine*, 37(5), pp.1263–1273. https://doi.org/10.3892/ijmm.2016.2519.

Ye, L., Zhang, H.-Y., Yang, G.-H., Bu, H. and Guo, H., 2005. Effects of transforming growth factor-beta/Smad signaling on the growth and apoptosis of human rhabdomyosarcoma cell line. *Chinese Journal of Pathology*, 34(7), pp.407–412.

Ying, H.Z., Chen, Q., Zhang, W.Y., Zhang, H.H., Ma, Y., Zhang, S.Z., Fang, J. and Yu, C.H., 2017. PDGF signaling pathway in hepatic fibrosis pathogenesis and therapeutics (Review). *Molecular Medicine Reports*, 16(6), pp.7879–7889. https://doi.org/10.3892/mmr.2017.7641.

Ying, W., Du, Z., Sun, L., Foley, K.P., Proia, D.A., Blackman, R.K., Zhou, D., Inoue, T., Tatsuta, N., Sang, J., Ye, S., Acquaviva, J., Ogawa, L.S., Wada, Y., Barsoum, J. and Koya, K., 2012. Ganetespib, a Unique Triazolone-Containing Hsp90 Inhibitor, Exhibits Potent Antitumor Activity and a Superior Safety Profile for Cancer Therapy. *Molecular Cancer Therapeutics*, 11(2), pp.475–484. https://doi.org/10.1158/1535-7163.MCT-11-0755.

Yoshidas, M., Kijima, M., Akita, M. and Beppu, T., 1990. Potent and Specific Inhibition of Mammalian Histone Deacetylase Both in Vivo and in Vitro by Trichostatin A*. *The Journal of Biological Chemistry*, 265(28), pp.17174–17179.

Yu-Yun Lee, J., Yang, C.-C., Chao, S.-C. and Wong, T.-W., 2004. Histopathological Differential Diagnosis of Keloid and Hypertrophic Scar. *American Journal of Dermatopathology*, [online] 26(5), pp.379–384. Available at: <http://journals.lww.com/amjdermatopathology>.

Zambon, A., Niculescu-Duvaz, I., Niculescu-Duvaz, D., Marais, R. and Springer, C.J., 2012. Small molecule inhibitors of BRAF in clinical trials. *Bioorganic & medicinal chemistry letters*, 22(2), pp.789–92. https://doi.org/10.1016/j.bmcl.2011.11.060.

Zarrinkar, P.P., Gunawardane, R.N., Cramer, M.D., Gardner, M.F., Brigham, D., Belli, B., Karaman, M.W., Pratz, K.W., Pallares, G., Chao, Q., Sprankle, K.G., Patel, H.K., Levis, M., Armstrong, R.C., James, J. and Bhagwat, S.S., 2009. AC220 is a uniquely potent and selective inhibitor of FLT3 for the treatment of acute myeloid leukemia (AML). *Blood*, 114(14), pp.2984–2992. https://doi.org/10.1182/blood-2009-05-222034.

Zerr, P., Vollath, S., Palumbo-Zerr, K., Tomcik, M., Huang, J., Distler, A., Beyer, C., Dees, C., Gela, K., Distler, O., Schett, G. and Distler, J.H.W., 2015. Vitamin D receptor regulates TGF-β signalling in systemic sclerosis. *Annals of the Rheumatic Diseases*, 74(3), pp.e20–e20. https://doi.org/10.1136/annrheumdis-2013-204378.

Zhang, G.Y., Cheng, T., Luan, Q., Liao, T., Nie, C.L., Zheng, X., Xie, X.G. and Gao, W.Y., 2011. Vitamin D: a novel therapeutic approach for keloid, an in vitro analysis. *British Journal of Dermatology*, 164(4), pp.729–737. https://doi.org/10.1111/j.1365-2133.2010.10130.x.

Zhang, G.Y., Wu, L.C., Liao, T., Chen, G., Chen, Y.H., Meng, X.C., Wang, A.Y., Chen, S.Y., Lin, K., Lin, D.M., Gao, W.Y. and Li, Q.F., 2016a. Altered circulating endothelial progenitor cells in patients with keloid. *Clinical and Experimental Dermatology*, 41(2), pp.152–155. https://doi.org/10.1111/ced.12695.

Zhang, J., Chung, T. and Oldenburg, K., 1999. A Simple Statistical Parameter for Use in Evaluation and Validation of High Throughput Screening Assays. *Journal of Biomolecular Screening*, 4(2), pp.67–73.

Zhang, S., Liu, Z., Su, G. and Wu, H., 2016b. Comparative Analysis of KnockOut ™ Serum with Fetal Bovine Serum for the In Vitro Long-Term Culture of Human Limbal Epithelial Cells. *Journal of Ophthalmology*, 2016, pp.1–10. https://doi.org/10.1155/2016/7304812.

Zhao, J., Yan, H., Li, Y., Wang, J., Han, L., Wang, Z., Tang, M., Zhang, W., Zhang, Y. and Zhong, M., 2015. Pitavastatin calcium improves endothelial function and delays the progress of atherosclerosis in patients with hypercholesterolemia. *Journal of Zhejiang University-SCIENCE B*, 16(5), pp.380–387. https://doi.org/10.1631/jzus.B1400181.

Zhong, Z., Sassi, M., Heaton, S., Koch, S., de Block, G., Conlon, D., Lochead, J., Dreja, H., Munro, M., Solache, A. and Hamilton, B., 2018. Large-scale use of knockout validation to confirm antibody specificity. *The Journal of Immunology*, 200(1 Supplement), pp.120.18-undefined.

Zhou, D., Tan, R.J., Fu, H. and Liu, Y., 2016. Wnt/β-catenin signaling in kidney injury and repair: A double-edged sword. *Laboratory Investigation*, 96(2), pp.156–167. https://doi.org/10.1038/labinvest.2015.153.

Zhou, H., Shen, T., Shang, C., Luo, Y., Liu, L., Yan, J., Li, Y. and Huang, S., 2014. Ciclopirox induces autophagy through reactive oxygen species-mediated activation of JNK signaling pathway. *Oncotarget*, [online] 5(20), pp.10140–10150. Available at: <www.impactjournals.com/oncotarget/>.

Zhou, X., Tan, F.K., Reveille, J.D., Wallis, D., Milewicz, D.M., Ahn, C., Wang, A. and Arnett, F.C., 2002. Association of novel polymorphisms with the expression ofSPARC in normal fibroblasts and with susceptibility to scleroderma. *Arthritis & Rheumatism*, 46(11), pp.2990–2999. https://doi.org/10.1002/art.10601.

Zhu, H., Huang, M., Yang, F., Chen, Y., Miao, Z.-H., Qian, X.-H., Xu, Y.-F., Qin, Y.-X., Luo, H.-B., Shen, X., Geng, M.-Y., Cai, Y.-J. and Ding, J., 2007. R16, a novel amonafide

analogue, induces apoptosis and G $_2$ -M arrest via poisoning topoisomerase II. *Molecular Cancer Therapeutics*, 6(2). https://doi.org/10.1158/1535-7163.MCT-06-0584.

Zhu, Z., Ding, J. and Tredget, E.E., 2016. The molecular basis of hypertrophic scars. *Burns & Trauma*, 4(2), pp.1–12. https://doi.org/10.1186/s41038-015-0026-4.

Appendix I: Ethical information

NHS
Health Research Authority

East of England - Cambridge Central Research Ethics Committee
Royal Standard Place
Nottingham
NG1 6FS

Please note: This is the favourable opinion of the REC only and does not allow you to start your study at NHS sites in England until you receive HRA Approval

21 March 2018

Prof Selim Cellek
Anglia Ruskin University
Faculty of Medical Science
Bishop Hall Lane, Chelmsford
CM1 1SQ

Dear Professor Cellek

Study title:	**Development of novel anti-fibrotic medicines through phenotypic screening to prevent scar formation.**
REC reference:	**18/EE/0072**
IRAS project ID:	**238766**

The Research Ethics Committee reviewed the above application at the meeting held on 09 March 2018. Thank you for attending along with Alice Lapthorn and Professor Peter Dzwielski to discuss the application.

We plan to publish your research summary wording for the above study on the HRA website, together with your contact details. Publication will be no earlier than three months from the date of this favourable opinion letter. The expectation is that this information will be published for all studies that receive an ethical opinion but should you wish to provide a substitute contact point, wish to make a request to defer, or require further information, please contact hra.studyregistration@nhs.net outlining the reasons for your request. Under very limited circumstances (e.g. for student research which has received an unfavourable opinion), it may be possible to grant an exemption to the publication of the study.

Ethical opinion

The members of the Committee present gave a favourable ethical opinion of the above research on the basis described in the application form, protocol and supporting documentation, subject to the conditions specified below. .

Conditions of the favourable opinion

The REC favourable opinion is subject to the following conditions being met prior to the start of the study.

1. The following detail should be added to the final paragraph of page 1 of the Participant Information Sheet following the sentence ending 'some cells will be isolated': 'Cells from these samples will be cultured before being tested.'

You should notify the REC once all conditions have been met (except for site approvals from host organisations) and provide copies of any revised documentation with updated version numbers. Revised documents should be submitted to the REC electronically from IRAS. The REC will acknowledge receipt and provide a final list of the approved documentation for the study, which you can make available to host organisations to facilitate their permission for the study. Failure to provide the final versions to the REC may cause delay in obtaining permissions.

Management permission must be obtained from each host organisation prior to the start of the study at the site concerned.

Management permission should be sought from all NHS organisations involved in the study in accordance with NHS research governance arrangements. Each NHS organisation must confirm through the signing of agreements and/or other documents that it has given permission for the research to proceed (except where explicitly specified otherwise).

Guidance on applying for HRA Approval (England)/ NHS permission for research is available in the Integrated Research Application System, at www.hra.nhs.uk or at http://www.rdforum.nhs.uk.

Where a NHS organisation's role in the study is limited to identifying and referring potential participants to research sites ("participant identification centre"), guidance should be sought from the R&D office on the information it requires to give permission for this activity.

For non-NHS sites, site management permission should be obtained in accordance with the procedures of the relevant host organisation.

Sponsors are not required to notify the Committee of management permissions from host organisations.

Registration of Clinical Trials

All clinical trials (defined as the first four categories on the IRAS filter page) must be registered on a publically accessible database. This should be before the first participant is recruited but no later than 6 weeks after recruitment of the first participant.

There is no requirement to separately notify the REC but you should do so at the earliest opportunity e.g. when submitting an amendment. We will audit the registration details as part of the annual progress reporting process.

To ensure transparency in research, we strongly recommend that all research is registered but for non-clinical trials this is not currently mandatory.

If a sponsor wishes to request a deferral for study registration within the required timeframe, they should contact hra.studyregistration@nhs.net. The expectation is that all clinical trials will be registered, however, in exceptional circumstances non registration may be permissible with prior agreement from the HRA. Guidance on where to register is provided on the HRA website.

It is the responsibility of the sponsor to ensure that all the conditions are complied with before the start of the study or its initiation at a particular site (as applicable).

Ethical review of research sites

NHS Sites

The favourable opinion applies to all NHS sites taking part in the study taking part in the study, subject to management permission being obtained from the NHS/HSC R&D office prior to the start of the study (see "Conditions of the favourable opinion" below).

Summary of discussion at the meeting

- **Social or scientific value; scientific design and conduct of the study**

  The Committee commented on the applicants wishing to apply 1400 different drugs to the collected samples and asked them where they will start with such a large library of drugs. *The applicants responded they are also working with another student who is using the same drug libraries and they are hoping he will help with the process.* The Committee was content with the applicants' response.

- **Recruitment arrangements and access to health information, and fair participant selection**

  The Committee queried why the upper age limit for inclusion has been capped at 75. *The applicants responded the upper age limit was chosen because in general patients tend to have higher mortality. In addition scars tend not to be as aggressive.* The Committee enquired if the healing process is slower over the age of 75. *The applicants explained that it is not the healing process which becomes slower but the scarring that lessens. Cells also grow less in people over the age of 75.* The Committee was content with the applicants' response.

- **Care and protection of research participants; respect for potential and enrolled participants' welfare and dignity**

  The Committee sought clarification as to whether the laboratories where the samples will be stored are accredited. *The applicants confirmed they would not be using accredited laboratories.* The Committee queried whether this would have any bearing on the applicant being able to utilise the samples. *The applicants responded they will be able to publish the results of the study. They will not be using the tissue for human trial at this point, but if they did want to do so later they would move to an accredited lab and submit an*

amendment as appropriate. The Committee was content with the applicants' response.

The Committee questioned whether retention of the study data for a period of 3 years was adequate. *The applicants responded this timeframe is recommended by the university in their policy. If they needed a longer retention period they would need to return to the ethics committee at later date with an amendment*. The Committee suggested a longer period for retention may be advisable at this point particularly as the study is being conducted for the purposes of gaining a PhD. *The applicants acknowledged the Committee's advice*.

- **Informed consent process and the adequacy and completeness of participant information**

  The Committee commented that the fact that the cells from tissue which will be taken from participants will be cultured and grown is not detailed in the Participant Information Sheet and agreed this detail should be added. *The applicants agreed*.

Please contact the REC Manager if you feel that the above summary is not an accurate reflection of the discussion at the meeting.

Approved documents

The documents reviewed and approved at the meeting were:

Document	*Version*	*Date*
IRAS Application Form [IRAS_Form_18012018]		18 January 2018
Letter from sponsor [Sponsorhip letter]	v01	04 December 2017
Other [PIS CF Breast Constr]	v01	10 November 2017
Participant information sheet (PIS) [PIS CF Burns]	v01	10 November 2017
Research protocol or project proposal [Study Protocol]	v01	10 November 2017
Summary CV for Chief Investigator (CI) [Cellek CV]	v01	09 November 2017
Summary CV for student [Student CV]	v01	02 January 2018
Summary CV for supervisor (student research) [Peter D CV]	v01	13 December 2017

Membership of the Committee

The members of the Ethics Committee who were present at the meeting are listed on the attached sheet.

The Committee is constituted in accordance with the Governance Arrangements for Research Ethics Committees and complies fully with the Standard Operating Procedures for Research Ethics Committees in the UK.

After ethical review

Reporting requirements

The attached document "After ethical review – guidance for researchers" gives detailed guidance on reporting requirements for studies with a favourable opinion, including:

- Notifying substantial amendments
- Adding new sites and investigators
- Notification of serious breaches of the protocol
- Progress and safety reports
- Notifying the end of the study

The HRA website also provides guidance on these topics, which is updated in the light of changes in reporting requirements or procedures.

User Feedback

The Health Research Authority is continually striving to provide a high quality service to all applicants and sponsors. You are invited to give your view of the service you have received and the application procedure. If you wish to make your views known please use the feedback form available on the HRA website: http://www.hra.nhs.uk/about-the-hra/governance/quality-assurance/

HRA Training

We are pleased to welcome researchers and R&D staff at our training days – see details at http://www.hra.nhs.uk/hra-training/

18/EE/0072	Please quote this number on all correspondence

With the Committee's best wishes for the success of this project.

Yours sincerely

pp C Hardwicke

Revd Dr Derek Fraser
Alternate Vice-Chair

E-mail: NRESCommittee.EastofEngland-CambridgeCentral@nhs.net

Enclosures: *List of names and professions of members who were present at the meeting and those who submitted written comments*

"After ethical review – guidance for researchers"

Copy to: *Prof Roderick Watkins*
Miss Lauren Perkins, Mid Essex Hospitals Trust

East of England - Cambridge Central Research Ethics Committee

Attendance at Committee meeting on 09 March 2018

Committee Members:

Name	*Profession*	*Present*	*Notes*
Dr Gusztav Belteki	Consultant Neonatologist	No	
Mr Andrew Bush	Director	Yes	
Dr Joseph Cheriyan	Consultant Physician	No	
Ms Anita Chhabra	Clinical Trials Pharmacist	Yes	
Dr Lydia Drumright	University Lecturer in Clinical Informatics	No	
Revd Dr Derek Fraser (Acting Chair)	Chaplain	Yes	
Mr Stewart Fuller	Head Nurse	Yes	
Dr James Goodman	Registrar in clinical pharmacology and general medicine	No	
Miss Giselle Kerry	Data Access and Regulatory Support Officer	Yes	
Mr David Lewin	Retired Research Officer	Yes	
Ms Moira Malfroy	Retired Senior Research Nurse/Clinical Trial Manager	Yes	
Miss Emma McManus	Research Associate in Health Economics and Health Technology Assessment	Yes	
Mrs Beth Midgley	Public Speaker	No	
Professor Sumantra Ray	Senior Medical Advisor/Scientist	Yes	
Dr Mary-Beth Sherwood	Research Governance Assistant	Yes	

Also in attendance:

Name	*Position (or reason for attending)*
Ms Carolyn Halliwell	REC Manager
Aoibhinn McDonnell	Observer

Ymchwil Iechyd a Gofal Cymru
Health and Care Research Wales

NHS
Health Research Authority

Prof Selim Cellek
Anglia Ruskin University
Faculty of Medical Science
Bishop Hall Lane, Chelmsford
CM1 1SQ

Email: hra.approval@nhs.net
Research-permissions@wales.nhs.uk

19 April 2018

Dear Prof Cellek

HRA and Health and Care Research Wales (HCRW) Approval Letter

Study title:	**Development of novel anti-fibrotic medicines through phenotypic screening to prevent scar formation.**
IRAS project ID:	**238766**
REC reference:	**18/EE/0072**
Sponsor	**Anglia Ruskin University**

I am pleased to confirm that HRA and Health and Care Research Wales (HCRW) Approval has been given for the above referenced study, on the basis described in the application form, protocol, supporting documentation and any clarifications received. You should not expect to receive anything further relating to this application.

How should I continue to work with participating NHS organisations in England and Wales?
You should now provide a copy of this letter to all participating NHS organisations in England and Wales*, as well as any documentation that has been updated as a result of the assessment.

*'In flight studies' which have already started an SSI (Site Specific Information) application for NHS organisations in Wales will continue to use this route. Until 10 June 2018, applications on either documentation will be accepted in Wales, but after this date all local information packs should be shared with NHS organisations in Wales using the Statement of Activities/Schedule of Events for non-commercial studies and template agreement/ Industry costing template for commercial studies.

Following the arranging of capacity and capability, participating NHS organisations should **formally confirm** their capacity and capability to undertake the study. How this will be confirmed is detailed in the "*summary of assessment*" section towards the end of this letter.

You should provide, if you have not already done so, detailed instructions to each organisation as to how you will notify them that research activities may commence at site following their confirmation of capacity and capability (e.g. provision by you of a 'green light' email, formal notification following a site

initiation visit, activities may commence immediately following confirmation by participating organisation, etc.).

It is important that you involve both the research management function (e.g. R&D office) supporting each organisation and the local research team (where there is one) in setting up your study. Contact details of the research management function for each organisation can be accessed here.

How should I work with participating NHS/HSC organisations in Northern Ireland and Scotland?
HRA/HCRW Approval does not apply to NHS/HSC organisations within the devolved administrations of Northern Ireland and Scotland.

If you indicated in your IRAS form that you do have participating organisations in either of these devolved administrations, the final document set and the study wide governance report (including this letter) has been sent to the coordinating centre of each participating nation. You should work with the relevant national coordinating functions to ensure any nation specific checks are complete, and with each site so that they are able to give management permission for the study to begin.

Please see IRAS Help for information on working with NHS/HSC organisations in Northern Ireland and Scotland.

How should I work with participating non-NHS organisations?
HRA/HCRW Approval does not apply to non-NHS organisations. You should work with your non-NHS organisations to obtain local agreement in accordance with their procedures.

What are my notification responsibilities during the study?
The document "*After Ethical Review – guidance for sponsors and investigators*", issued with your REC favourable opinion, gives detailed guidance on reporting expectations for studies, including:

- Registration of research
- Notifying amendments
- Notifying the end of the study

The HRA website also provides guidance on these topics, and is updated in the light of changes in reporting expectations or procedures.

I am a participating NHS organisation in England or Wales. What should I do once I receive this letter?
You should work with the applicant and sponsor to complete any outstanding arrangements so you are able to confirm capacity and capability in line with the information provided in this letter.

The sponsor contact for this application is as follows:

Prof Roderick Watkins
Email: roderick.watkins@anglia.ac.uk
Tel: 01223698077

Who should I contact for further information?
Please do not hesitate to contact me for assistance with this application. My contact details are below.

IRAS project ID	238766

Your IRAS project ID is **238766**. Please quote this on all correspondence.

Yours sincerely

Rekha Keshvara
Senior Assessor

Email: hra.approval@nhs.net

Copy to: *Prof Roderick Watkins*
Miss Lauren Perkins, Mid Essex Hospitals Trust

IRAS project ID	238766

List of Documents

The final document set assessed and approved by HRA/HCRW Approval is listed below.

	Version	*Date*
Contract/Study Agreement template [MTA ARU]		
Evidence of Sponsor insurance or indemnity (non NHS Sponsors only)		15 July 2017
HRA Schedule of Events	1	19 April 2018
HRA Statement of Activities	1	19 April 2018
IRAS Application Form [IRAS_Form_18012018]		18 January 2018
Letter from sponsor [Sponsorhip letter]	v01	04 December 2017
Participant information sheet (PIS) [Burns Info Consent]	2	21 March 2018
Participant information sheet (PIS) [Breast Recon Info]	2	21 March 2018
Research protocol or project proposal [Study Protocol]	v01	10 November 2017
Summary CV for Chief Investigator (CI) [Cellek CV]	v01	09 November 2017
Summary CV for student [Student CV]	v01	02 January 2018
Summary CV for supervisor (student research) [Peter D CV]	v01	13 December 2017

Anglia Ruskin University
Cambridge Chelmsford Peterborough

24th April 2018

Dear Alice

Principal Investigator: *Alice Lapthorn*
FREP number: *FMSFREP/17/18 187*
Project Title: *Development of novel anti-fibrotic medicines through phenotypic screening to prevent scar formation.*

I am pleased to inform you that your ethics application has been approved by the Faculty Research Ethics Panel (FREP) under the terms of Anglia Ruskin University's Research Ethics Policy (Dated 8 September 2016, Version 1.7).

Ethical approval is given for 3 years from Tuesday 24th April 2018. If your research will extend beyond this period, it is your responsibility to apply for an extension before your approval expires.

It is your responsibility to ensure that you comply with Anglia Ruskin University's Research Ethics Policy and the Code of Practice for Applying for Ethical Approval at Anglia Ruskin University available at www.anglia.ac.uk/researchethics including the following.

- The procedure for submitting substantial amendments to the committee, should there be any changes to your research. You cannot implement these amendments until you have received approval from FREP for them.
- The procedure for reporting accidents, adverse events and incidents.
- The Data Protection Act (1998) and General Data Protection Requirement from 25 May 2018.
- Any other legislation relevant to your research. You must also ensure that you are aware of any emerging legislation relating to your research and make any changes to your study (which you will need to obtain ethical approval for) to comply with this.
- Obtaining any further ethical approval required from the organisation or country (if not carrying out research in the UK) where you will be carrying the research out. This includes other Higher Education Institutions if you intend to carry out any research involving their students, staff or premises. Please ensure that you send the FREP copies of this documentation if required, prior to starting your research.
- Any laws of the country where you are carrying the research and obtaining any other approvals or permissions that are required.
- Any professional codes of conduct relating to research or requirements from your funding body (please note that for externally funded research, where the funding has been obtained via Anglia Ruskin University, a Project Risk Assessment must have been carried out prior to starting the research).
- Completing a Risk Assessment (Health and Safety) if required and updating this annually or if any aspects of your study change which affect this.
- Notifying the FREP Secretary when your study has ended.

As an ARU sponsored HRA/REC approved study, you are required to submit an Annual Progress Report and Completion Report once the study has ended. The Completion Report MUST be submitted to the Research Ethics Committee (REC) that gave a favourable opinion of the research within 90 days of the conclusion of the study or within 15 days of early termination.

Please also note that your research may be subject to monitoring.

Should you have any queries, please do not hesitate to contact me. May I wish you the best of luck with your research.

Yours sincerely,

FREP Chair
Date 6.10.17
V1.2

Anglia Ruskin University

Mid Essex Hospital Services NHS
NHS Trust

Patient Information Sheet, version 1
Date: November 2017
Indication: Burns

Development of novel medicines to prevent scar formation.

You are being invited to take part in a research study. Before you decide it is important for you to understand why the research is being done and what it will involve. Please take time to read the following information carefully and discuss it with friends, relatives and your doctor if you wish. Ask us if there is anything that is not clear or if you would like more information. Take time to decide whether or not you wish to take part.

Thank you for reading this.

What is the purpose of the study?

We are carrying out a research project in collaboration with Anglia Ruskin University. The aim of this research project is to understand how we can prevent scarring in burn injuries, by developing new medicines. By understanding the scarring process better, we believe that we may be able to develop new and better treatment approaches for this disease.

Why have I been chosen?

You are going to be operated for the treatment of burn injuries. During the surgery, the affected tissue will be removed and non-affected tissue, will also be removed for the skin graft. Much of the affected tissue is usually discarded, with excess normal tissue being discarded as well. We are seeking your permission to use this tissue for the research project mentioned above. **If you do not give your consent, this tissue will be discarded.**

The tissue obtained from you with your permission will be transferred to the research laboratories at Anglia Ruskin University, Essex where the cellular structure and protein content will be analysed. The cells from these samples will be cultured before being tested..

The tissue obtained from you will NOT be used for any genetic research that involves your DNA. At the end of the research project, the tissue we have obtained from you will be destroyed by incineration.

There is no other reason for choosing you to take part in this study. We intend to study material from a number of different patients, until we are able to draw proper conclusions.

Do I have to take part?
It is up to you to decide whether or not to take part. If you do decide to take part you will be given this information sheet to keep and be asked to sign a consent form. If you decide to take part, you are free to withdraw at any time and without giving a reason. This will not affect the standard of care you receive.

What will happen to me if I take part?
You will undergo exactly the same surgery and receive exactly the same medical care as you would normally. No additional drugs or procedures will be used. This means that there are no additional risks, disadvantages or side effects.

What will happen to me if I do not take part?
Your decision of not taking part in this study will not affect the care you will receive. You will undergo exactly the same surgery and receive exactly the same medical care as you would normally.

What are the possible benefits of taking part?
You will not receive any direct benefit from participating in this study, but the results of this study may contribute towards a better understanding of wound healing in burn injuries, and as a result, we may be able to identify a drug to prevent this process. You will not receive any payment for taking part in this study, now or in the future.

Will my taking part in this study be kept confidential?
All information which is collected about you during the course of this research project will be kept strictly confidential. Any information about you which leaves the hospital will have your name and address removed so that you cannot be recognised from it. To protect your privacy, your sample that is transferred to Anglia Ruskin University will be labelled only with a study subject number, not your name. We are not going to keep a link between the subject number and your hospital records meaning that the sample cannot be traced back to you. This total anonymisation process is to ensure that your private data is kept confidential at all times. Only your age, what type of tissue has been taken (burn/unaffected), burn wound depth & size, time to healing, time of biopsy post wound healing, any other diseases (if any) and your medication (if any) will be linked to the subject number.

What happens if I withdraw my consent after the operation?
You are free to withdraw your consent at any time, before or after the surgery. However once the tissue is anonymised as explained above and transferred to the research laboratories, we will not be able to trace them back so it will not be possible to destroy the tissue.

What will happen to the results of the research study?
We hope to publish the results so that as many of our findings as possible will be made available to the medical and scientific community. You will not be personally identified in any publication. Because of the exploratory nature of the work, none of the results will be provided to you or to the physicians who are treating you or may treat you in the future. The timing of any publication will depend mostly on the speed with which we collect the data and cannot be predicted with certainty.

Who is organising and funding the research?
This is a joint programme of research collaboration between Prof Peter Dziewulski and his surgical team at Broomfield Hospital and the research scientists headed by Prof Selim Cellek at Anglia Ruskin University. The doctors are not paid for including you in this study.

Who has reviewed the study?
This study has been reviewed and approved by the Anglia Ruskin University Faculty Research Ethics Panel (XXX) and XXXX NHS Research Ethics Committee (XXXX).

Contact details for further information:

Prof Peter Dziewulski
St Andrews Centre for Plastic Surgery & Burns
Broomfield Hospital
Chelmsford, Essex
CM1 7ET
Phone: 01245 513914
E-mail: peter.dziewulski@meht.nhs.uk

Prof Selim Cellek
Michael Salmon Building
Faculty of Medical Science
Anglia Ruskin University
Chelmsford, Essex
CM1 1SQ
Phone: 01245 684654
E-mail: selim.cellek@anglia.ac.uk

For complaints or if you are unhappy with how you have been treated, please contact
Email address: complaints@anglia.ac.uk
Postal address: Office of the Secretary and Clerk, Anglia Ruskin University, Bishop Hall Lane, Chelmsford, Essex, CM1 1SQ.

Anglia Ruskin University

Mid Essex Hospital Services NHS
NHS Trust

Version: 1
Date: September 2017

CONSENT FORM

Title of Project: Development of novel medicines to prevent scar formation.

Name of Researchers: Prof Peter Dziewulski, Broomfield Hospital and Prof Selim Cellek, Anglia Ruskin University

Please initial box

1. I confirm that I have read and understand the information sheet dated November 2017 (version 1) for the above study and have had the opportunity to ask questions. ☐

2. I understand that my participation is voluntary and that I am free to withdraw at any time, without giving any reason. ☐

3. I understand that sections of any of my medical notes may be looked at by the surgical team with respect to age, sex, condition and treatment at admission. I have been assured that all data relating to my person will be treated with absolute confidentiality at all times and will not be made public. I give permission for these individuals to have access to my records. ☐

4. I understand that my tissue will be totally anonymised, meaning that there will be no link between my tissue and my medical records including my private data so that the tissue cannot be traced back to me. ☐

5. I agree to take part in the above programme of work. ☐

Name of Patient	Signature & Date
Name of Person obtaining consent *(if different from surgeon)*	Signature & Date
Surgeon	Signature & Date

(1 for patient; 1 for surgeon; 1 to be kept with hospital notes)

APPENDIX I

Accompanying note with the tissue sample:

Please complete clearly

Date of surgery:

Age of the patient:

Surgery undergone:

Breast Reconstruction ☐

Burn Injury ☐

Type of tissue:

Burn tissue (< 3-6 months) ☐ Burn tissue (> 2 years) ☐

Burn tissue (6 months – 2 years) ☐ Unaffected tissue ☐

Burn wound information:

Depth of Wound: Time to healing:

Size of Wound: Time of biopsy post-healing:

Any other disease (e.g. diabetes):

Any medication:

Anglia Ruskin University

Mid Essex Hospital Services NHS
NHS Trust

Patient Information Sheet, version 1
Date: November 2017
Indication: Breast Reconstruction

Development of novel medicines to prevent scar formation.

You are being invited to take part in a research study. Before you decide it is important for you to understand why the research is being done and what it will involve. Please take time to read the following information carefully and discuss it with friends, relatives and your doctor if you wish. Ask us if there is anything that is not clear or if you would like more information. Take time to decide whether or not you wish to take part.

Thank you for reading this.

What is the purpose of the study?

We are carrying out a research project in collaboration with Anglia Ruskin University. The aim of this research project is to understand how we can prevent scarring in burn injuries, by developing new medicines. By understanding the scarring process better, we believe that we may be able to develop new and better treatment approaches for this disease.

Why have I been chosen?

You are going to be operated for breast reconstruction, during which excess skin tissue will be removed. This excess tissue is usually discarded and so, we are seeking your permission to use this tissue for the research project mentioned above. Your tissue will be used as a comparison against burn tissue which will be obtained from patients with burns. As burn tissue undergoes 'abnormal' scarring, we wish to use your normal tissue as a comparison, to see why or what causes this scarring to occur. If you do not give your consent, this tissue will be discarded.

The tissue obtained from you with your permission will be transferred to the research laboratories at Anglia Ruskin University, Essex where the cellular structure and protein content will be analysed. The cells from these samples will be cultured before being tested.

The tissue obtained from you will NOT be used for any genetic research that involves your DNA. At the end of the research project, any tissue we have obtained from you will be destroyed by incineration.

There is no other reason for choosing you to take part in this study. We intend to study material from a number of different patients, until we are able to draw proper conclusions.

Do I have to take part?
It is up to you to decide whether or not to take part. If you do decide to take part you will be given this information sheet to keep and be asked to sign a consent form. If you decide to take part, you are free to withdraw at any time and without giving a reason. This will not affect the standard of care you receive.

What will happen to me if I take part?
You will undergo exactly the same surgery and receive exactly the same medical care as you would normally. No additional drugs or procedures will be used. This means that there are no additional risks, disadvantages or side effects.

What will happen to me if I do not take part?
Your decision of not taking part in this study will not affect the care you will receive. You will undergo exactly the same surgery and receive exactly the same medical care as you would normally.

What are the possible benefits of taking part?
You will not receive any direct benefit from participating in this study, but the results of this study may contribute towards a better understanding of wound healing in burn injuries, and as a result, we may be able to identify a drug to prevent this process. Therefore, your tissues may help others who are unfortunate enough to be affected by burns. You will not receive any payment for taking part in this study, now or in the future.

Will my taking part in this study be kept confidential?
All information which is collected about you during the course of this research project will be kept strictly confidential. Any information about you which leaves the hospital will have your name and address removed so that you cannot be recognised from it. To protect your privacy, your sample that is transferred to Anglia Ruskin University will be labelled only with a study subject number, not your name. We are not going to keep a link between the subject number and your hospital records meaning that the sample cannot be traced back to you. This total anonymisation process is to ensure that your private data is kept confidential at all times. Only your age, what surgery you have undergone (breast reconstruction or burn treatment), diseases (if any) and your medication (if any) will be linked to the subject number.

What happens if I withdraw my consent after the operation?
You are free to withdraw your consent at any time, before or after the surgery. However once the tissue is anonymised as explained above and transferred to the research laboratories, we will not be able to trace them back so it will not be possible to destroy the tissue.

What will happen to the results of the research study?
We hope to publish the results so that as many of our findings as possible will be made available to the medical and scientific community. You will not be personally identified in any publication. Because of the exploratory nature of the work, none of the results will be provided to you or to the physicians who are treating you or may treat you in the future. The timing of any publication will depend mostly on the speed with which we collect the data and cannot be predicted with certainty.

Who is organising and funding the research?
This is a joint programme of research collaboration between Prof Peter Dziewulski and his surgical team at Broomfield Hospital and the research scientists headed by Prof Selim Cellek at Anglia Ruskin University. The doctors are not paid for including you in this study.

Who has reviewed the study?
This study has been reviewed and approved by the Anglia Ruskin University Research Ethics Committee (XXX) and XXX NHS Research Ethics Committee (XXXX).

Contact details for further information:

Prof Peter Dziewulski
St Andrews Centre for Plastic Surgery & Burns
Broomfield Hospital
Chelmsford, Essex
CM1 7ET
Phone: 01245 513914
E-mail: peter.dziewulski@meht.nhs.uk

Prof Selim Cellek
Michael Salmon Building
Faculty of Medical Science
Anglia Ruskin University
Chelmsford, Essex
CM1 1SQ
Phone: 01245 684654
E-mail: selim.cellek@anglia.ac.uk

For complaints or if you are unhappy with how you have been treated, please contact
Email address: complaints@anglia.ac.uk
Postal address: Office of the Secretary and Clerk, Anglia Ruskin University, Bishop Hall Lane, Chelmsford, Essex, CM1 1SQ

Anglia Ruskin University

Mid Essex Hospital Services NHS
NHS Trust

Version: 1
Date: September 2017

CONSENT FORM

Title of Project: Development of novel medicines to prevent scar formation.

Name of Researchers: Prof Peter Dziewulski, Broomfield Hospital and Prof Selim Cellek, Anglia Ruskin University

Please initial box

1. I confirm that I have read and understand the information sheet dated November 2017 (version 1) for the above study and have had the opportunity to ask questions. ☐

2. I understand that my participation is voluntary and that I am free to withdraw at any time, without giving any reason. ☐

3. I understand that sections of any of my medical notes may be looked at by the surgical team with respect to age, sex, condition and treatment at admission. I have been assured that all data relating to my person will be treated with absolute confidentiality at all times and will not be made public. I give permission for these individuals to have access to my records. ☐

4. I understand that my tissue will be totally anonymised, meaning that there will be no link between my tissue and my medical records including my private data so that the tissue cannot be traced back to me. ☐

5. I agree to take part in the above programme of work. ☐

Name of Patient	Signature & Date
Name of Person obtaining consent *(if different from surgeon)*	Signature & Date
Surgeon	Signature & Date

(1 for patient; 1 for surgeon; 1 to be kept with hospital notes)

APPENDIX I

Accompanying note with the tissue sample:

Please complete clearly

Date of surgery:

Age of the patient:

Surgery undergone:

Breast Reconstruction ☐

Burn Injury ☐

Type of tissue:

Burn tissue (< 3-6 months) ☐ Burn tissue (> 2 years) ☐

Burn tissue (6 months – 2 years) ☐ Unaffected tissue ☐

Burn wound information:

Depth of Wound: Time to healing:

Size of Wound: Time of biopsy post-healing:

Any other disease (e.g. diabetes):

Any medication:

Appendix II: Supplementary information – Raw data

Raw data for experiments using the ICE method can be found through Anglia Ruskin University's Figshare website, using the following link:

https://figshare.com/s/c9db78e87e1b757013cb

Appendix III: Supplementary figures

Appendix III.I. Statistical validation of fibroblast passages

To ensure that the passages used in the main screening assay would be suitable for high-throughput screening, a Z-factor for each passage (2 – 5) was calculated.

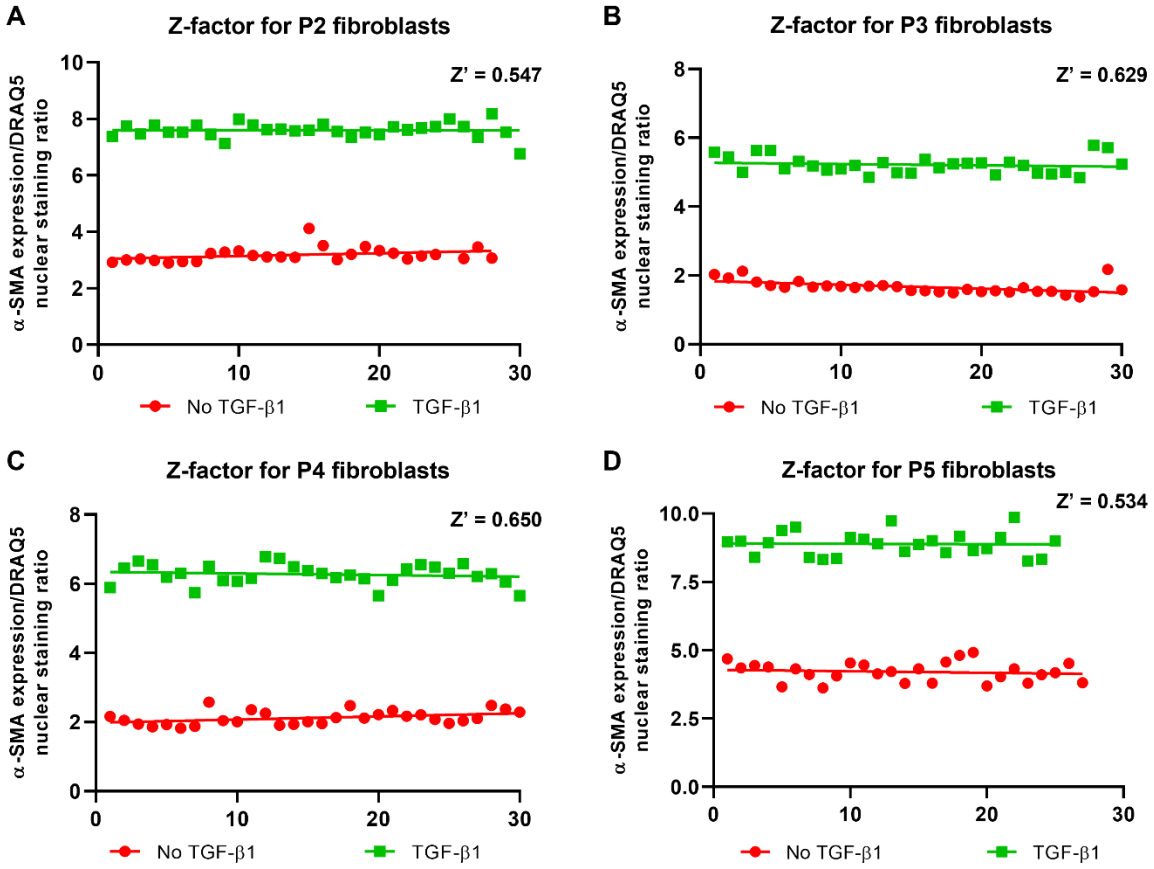

Supplementary figure 1: Statistical validation of different fibroblast passages using the ICE screening assay, measuring the effect of TGF-β1-induced myofibroblast transformation. A,B,C&D: Quantification of the In-Cell ELISA, with resulting Z-factor from the assay for fibroblasts at passage A) 2, B) 3, C) 4 and D) 5. The positive controls are TGF-β1-treated cells, and the negative controls are untreated cells. Data is presented as mean ± SEM, N=1 n=4.

Appendix III.II. IC_{50} of drugs

To accurately calculate the IC_{50} for all concentration response curves the pharmacological effect of the drugs were also calculated.

Appendix III.II.I. High-throughput screening assay validation

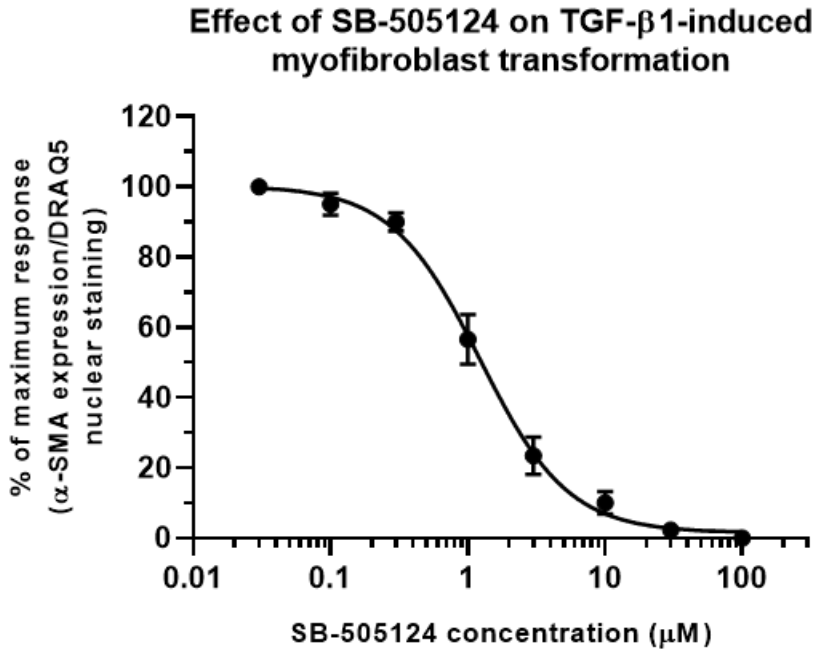

Supplementary figure 2: Effect of SB-505124 on TGF-β1-induced myofibroblast transformation. Burn scar fibroblasts were co-treated with 10 ng/mL TGF-β1 and a range of SB-505124 concentrations (0.03 µM – 100 µM) for 72 h, before measuring α-SMA expression using the In-Cell ELISA method. A full concentration response curve was generated. Data points are plotted as average ± SEM of the percentage of maximum response, N=3, n=9.

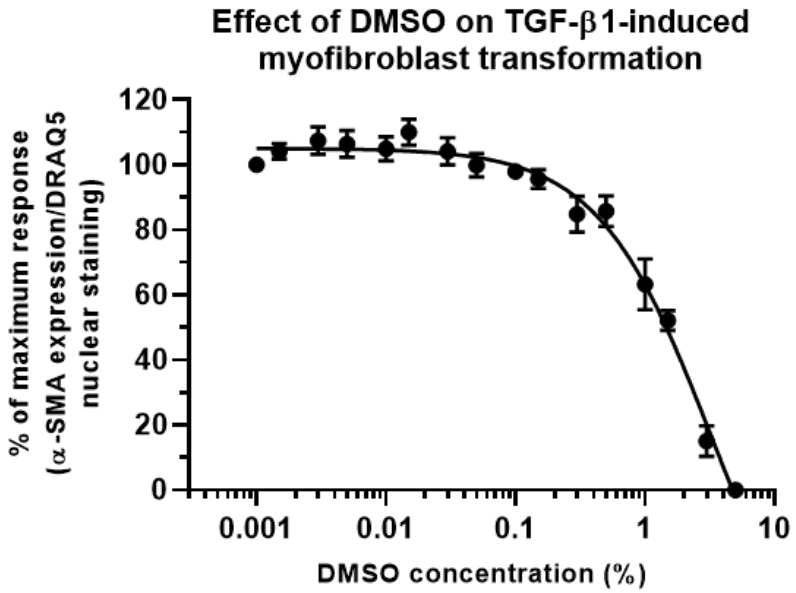

Supplementary figure 3: Effect of DMSO on TGF-β1-induced myofibroblast transformation. Burn scar fibroblasts were co-treated with 10 ng/mL TGF-β1 and a range of concentrations (0.001% – 5%) of DMSO for 72 h, before measuring α-SMA expression using the In-Cell ELISA method. Full concentration response curves were generated. Data points are plotted as average ± SEM of the percentage of maximum response, N=3, n=9.

Appendix III.II.II. Confirmation of anti-myofibroblast activity in candidate drugs

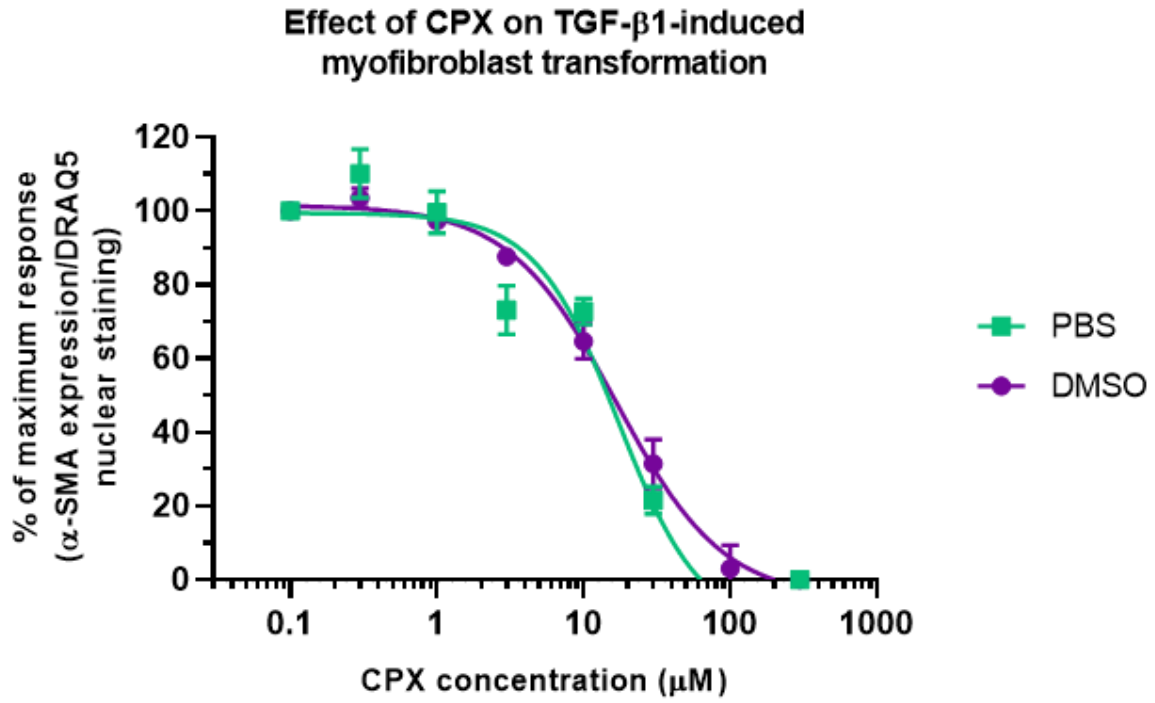

Supplementary figure 4: Effect of CPX on TGF-β1-induced myofibroblast transformation. A full concentration response curve was generated for CPX, using DMSO and PBS as a vehicle. Burn scar fibroblasts were incubated with 10 ng/mL TGF-β1 and a range of concentrations of CPX (0.1 μM – 300 μM) for 72 h. α-SMA expression was measured using the In-Cell ELISA method. Data points are plotted as average ± SEM, N=3, n=9.

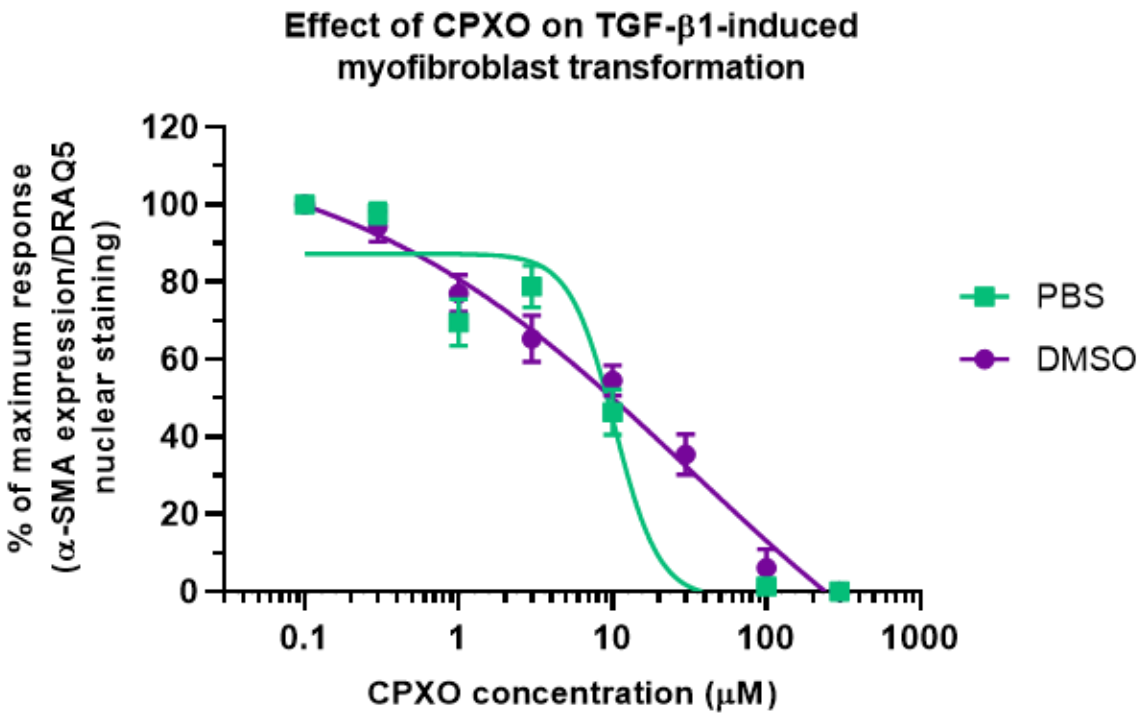

Supplementary figure 5: Effect of CPXO on TGF-β1-induced myofibroblast transformation. A full concentration response curve was generated for CPXO, using DMSO and PBS as a vehicle. Burn scar fibroblasts were incubated with 10 ng/mL TGF-β1 and a range of concentrations of CPXO (0.1 μM – 300 μM) for 72 h, before measuring α-SMA expression using the In-Cell ELISA method. Data points are plotted as average ± SEM, N=3, n=9.

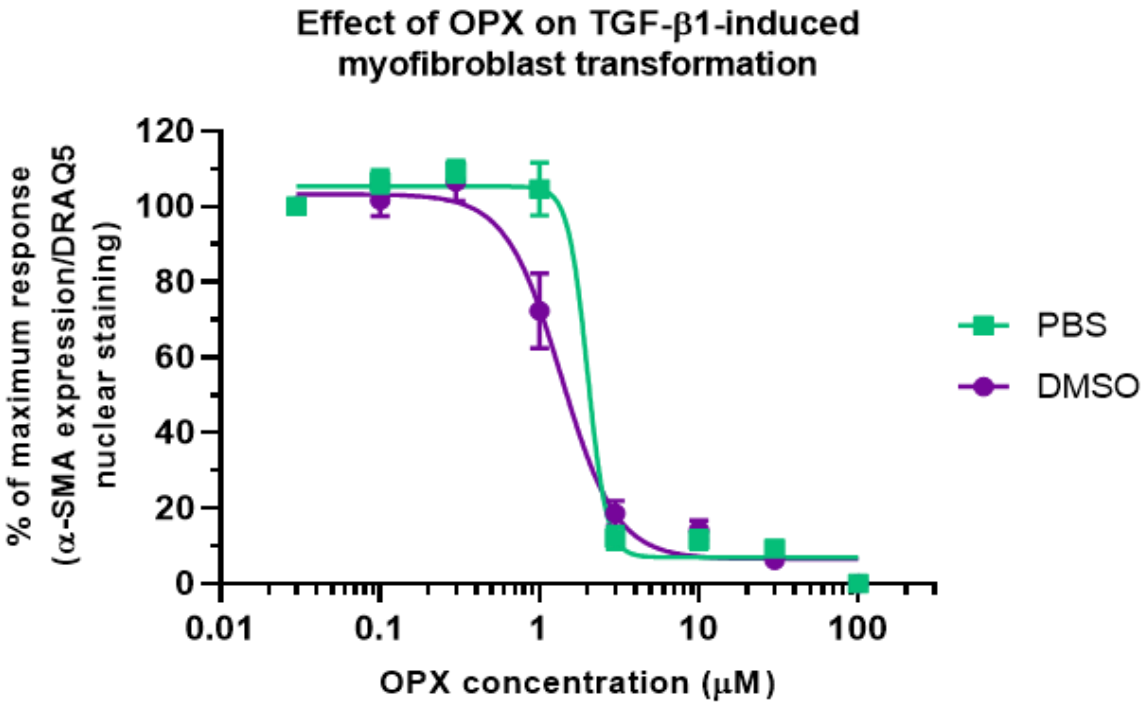

Supplementary figure 6: Effect of OPX on TGF-β1-induced myofibroblast transformation. A full concentration response curve was generated for OPX, using both DMSO and PBS as a vehicle. Burn scar fibroblasts were incubated with 10 ng/mL TGF-β1 and a range of concentrations of OPX (0.1 μM – 300 μM), before measuring α-SMA expression using the In-Cell ELISA method. Data points are plotted as average ± SEM, N=3, n=9.

Appendix IV.III. Effect of candidate drugs on mitochondrial function

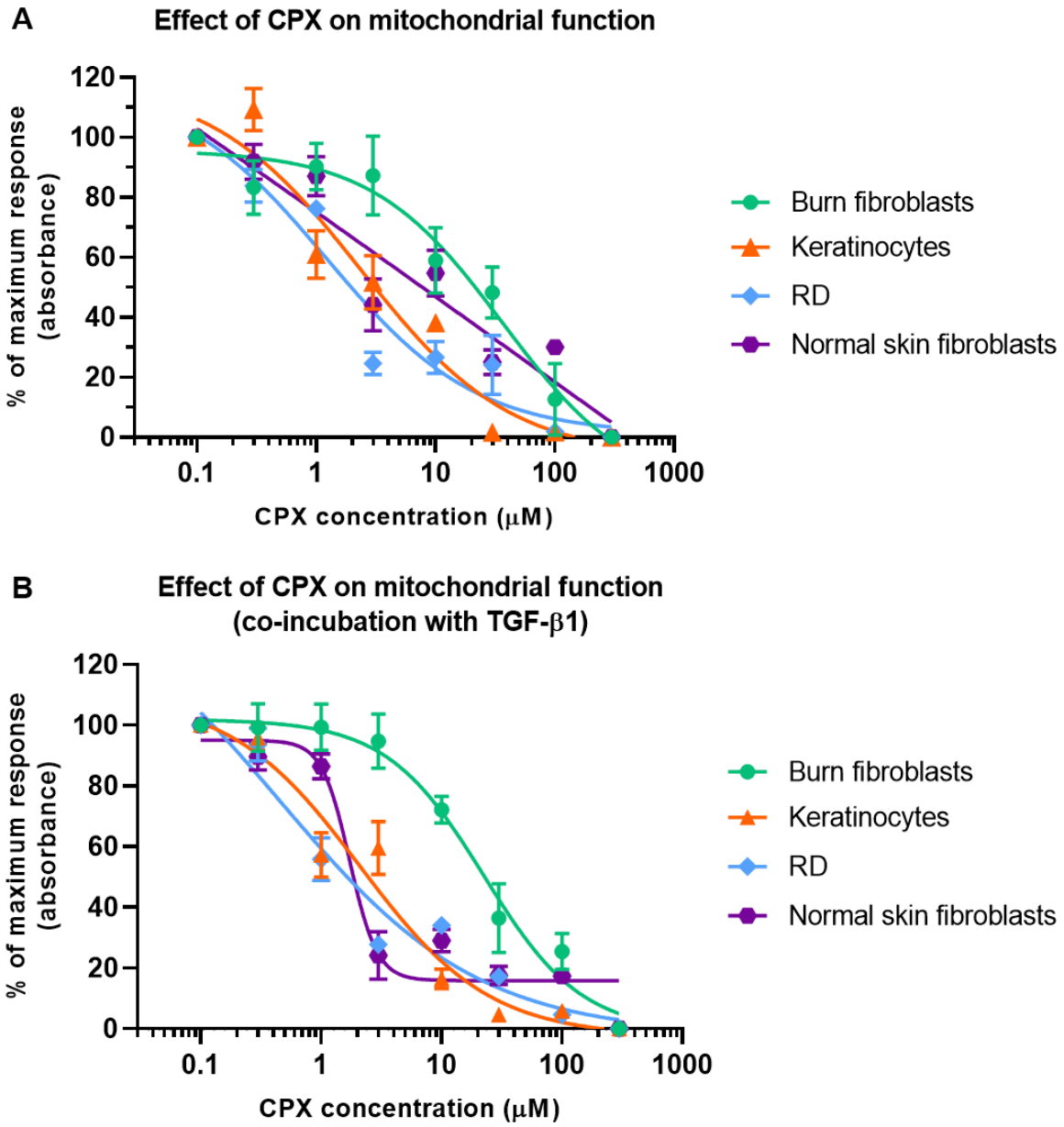

Supplementary figure 7: Effect of CPX on mitochondrial function when cells are A) untreated and B) treated with 10 ng/mL TGF-β1. A full concentration response curve was generated for CPX, where cells were treated with a range of concentrations of CPX (0.1 μM – 300 μM). Data points are plotted as average ± SEM, N=3, n=9.

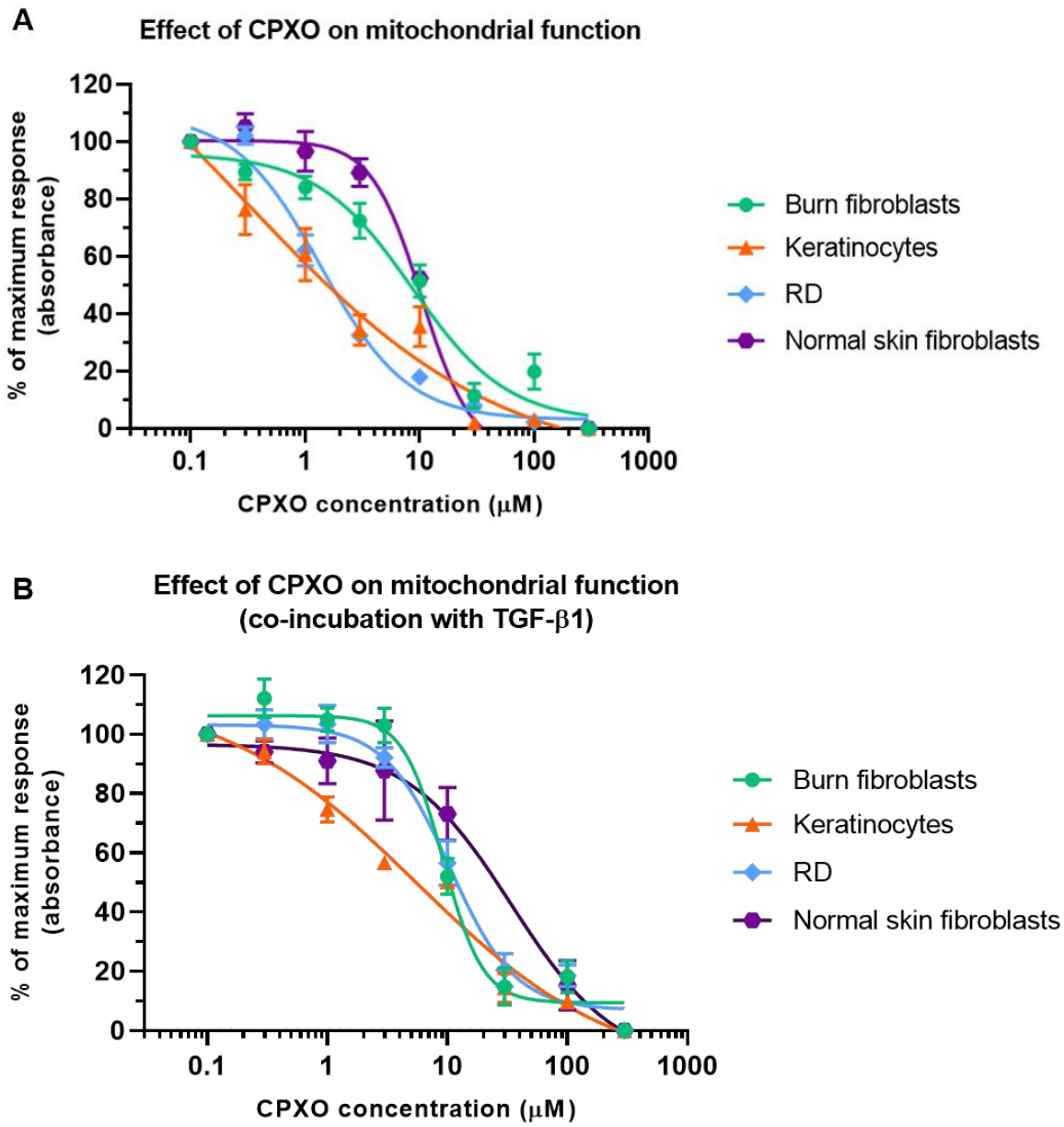

Supplementary figure 8: Effect of CPXO on mitochondrial function when cells are A) untreated and B) treated with 10 ng/mL TGF-β1. A full concentration response curve was generated for CPXO, where cells were treated with a range of concentrations of CPXO (0.1 μM – 300 μM). Data points are plotted as average ± SEM, N=3, n=9.

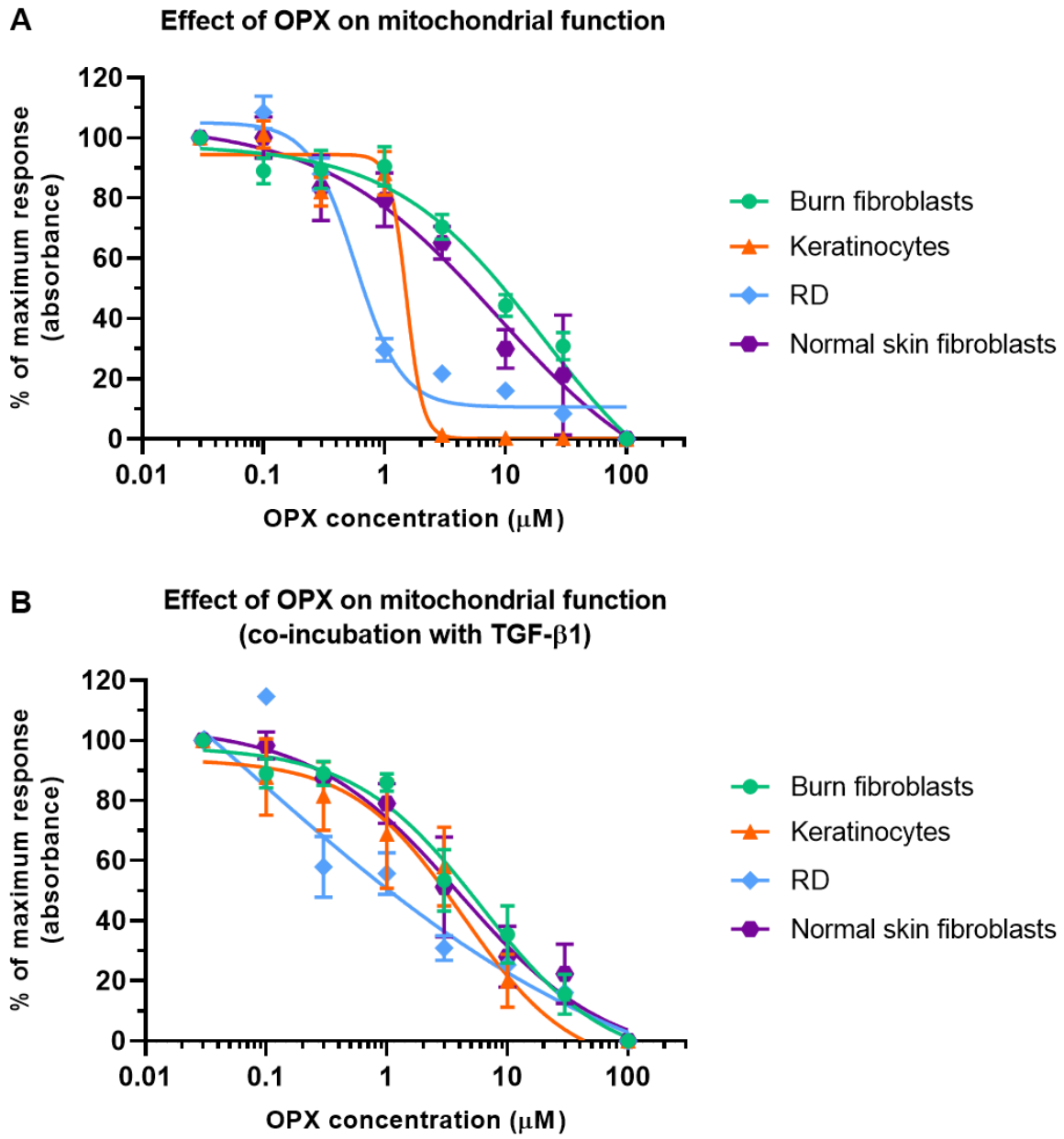

Supplementary figure 9: Effect of OPX on mitochondrial function when cells are A) untreated and B) treated with 10 ng/mL TGF-β1. A full concentration response curve was generated for OPX, where cells were treated with a range of concentrations of OPX (0.03 μM – 100 μM). Data points are plotted as average ± SEM, N=3, n=9.

Appendix III.II.IV. Effect of candidate drugs on cell membrane permeability

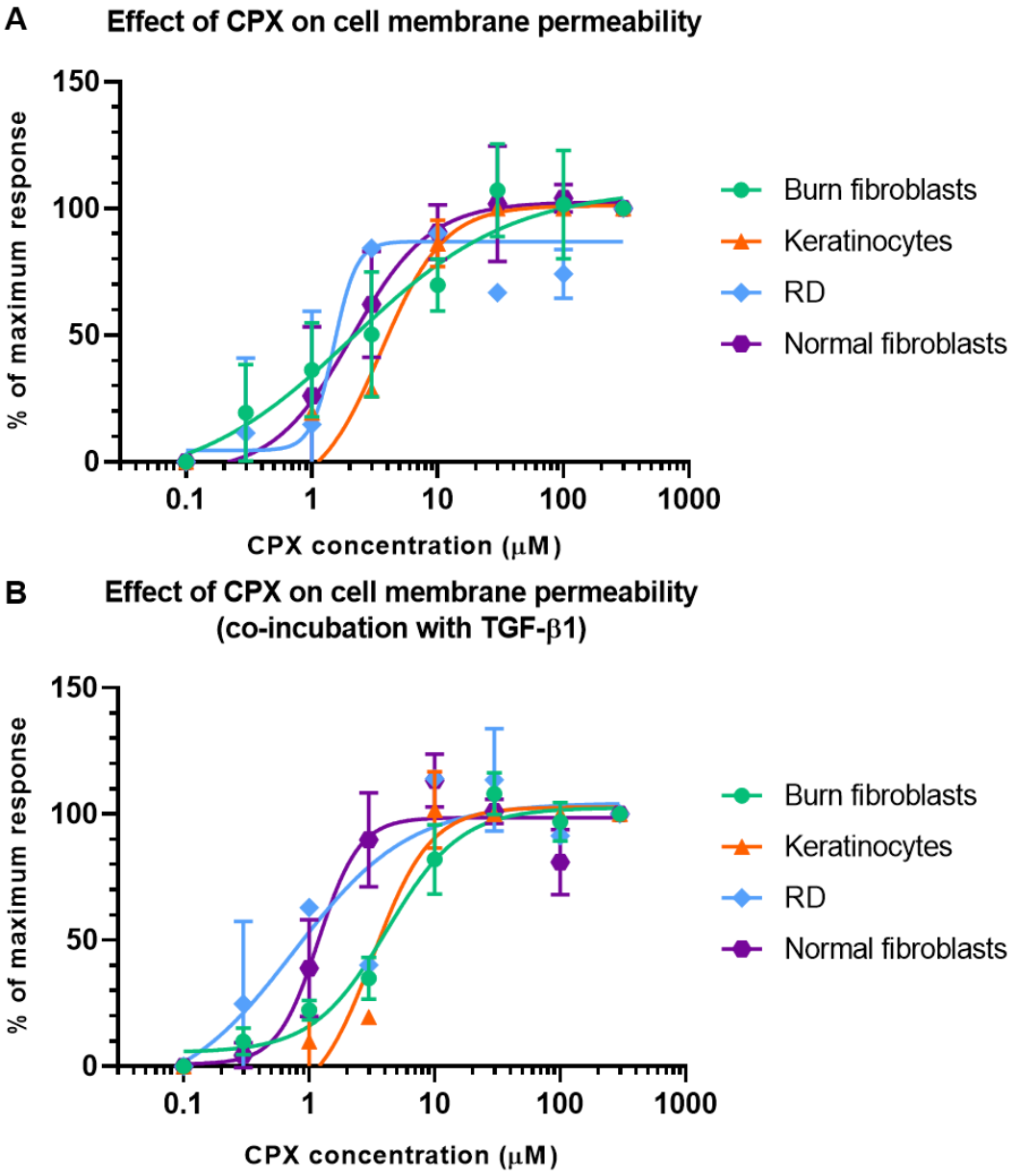

Supplementary figure 10: Effect of CPX on cell membrane permeability when cells are A) untreated and B) treated with 10 ng/mL TGF-β1. A full concentration response curve was generated for CPX, where cells were treated with a range of concentrations of CPX (0.1 μM – 300 μM). Data points are plotted as average ± SEM, where N=3, n=9.

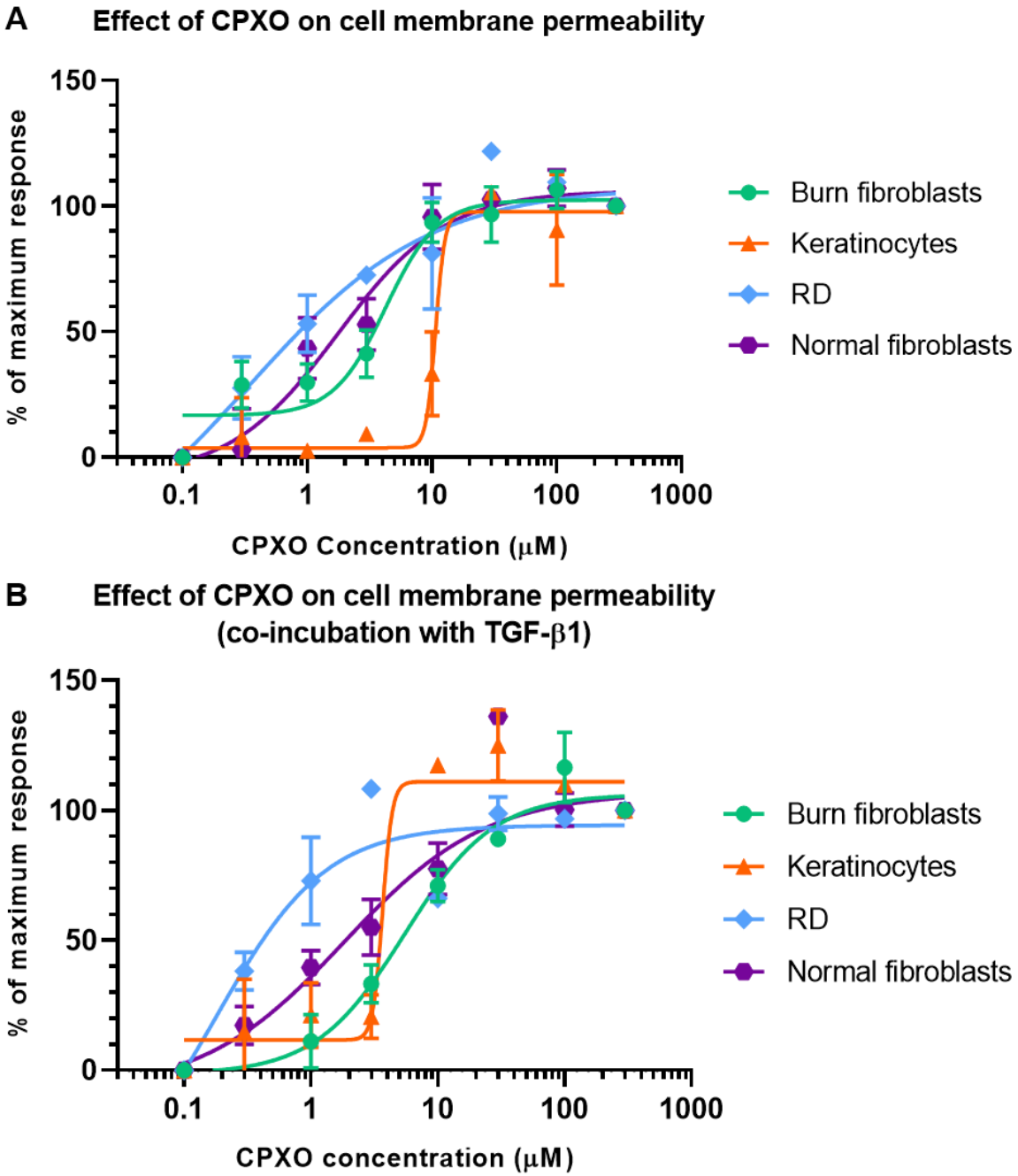

Supplementary figure 11: Effect of CPXO on cell membrane permeability when cells are A) untreated and B) treated with 10 ng/mL TGF-β1. A full concentration response curve was generated for CPXO, where cells were treated with a range of concentrations of CPXO (0.1 μM – 300 μM). Data points are plotted as average ± SEM, where N=3, n=9.

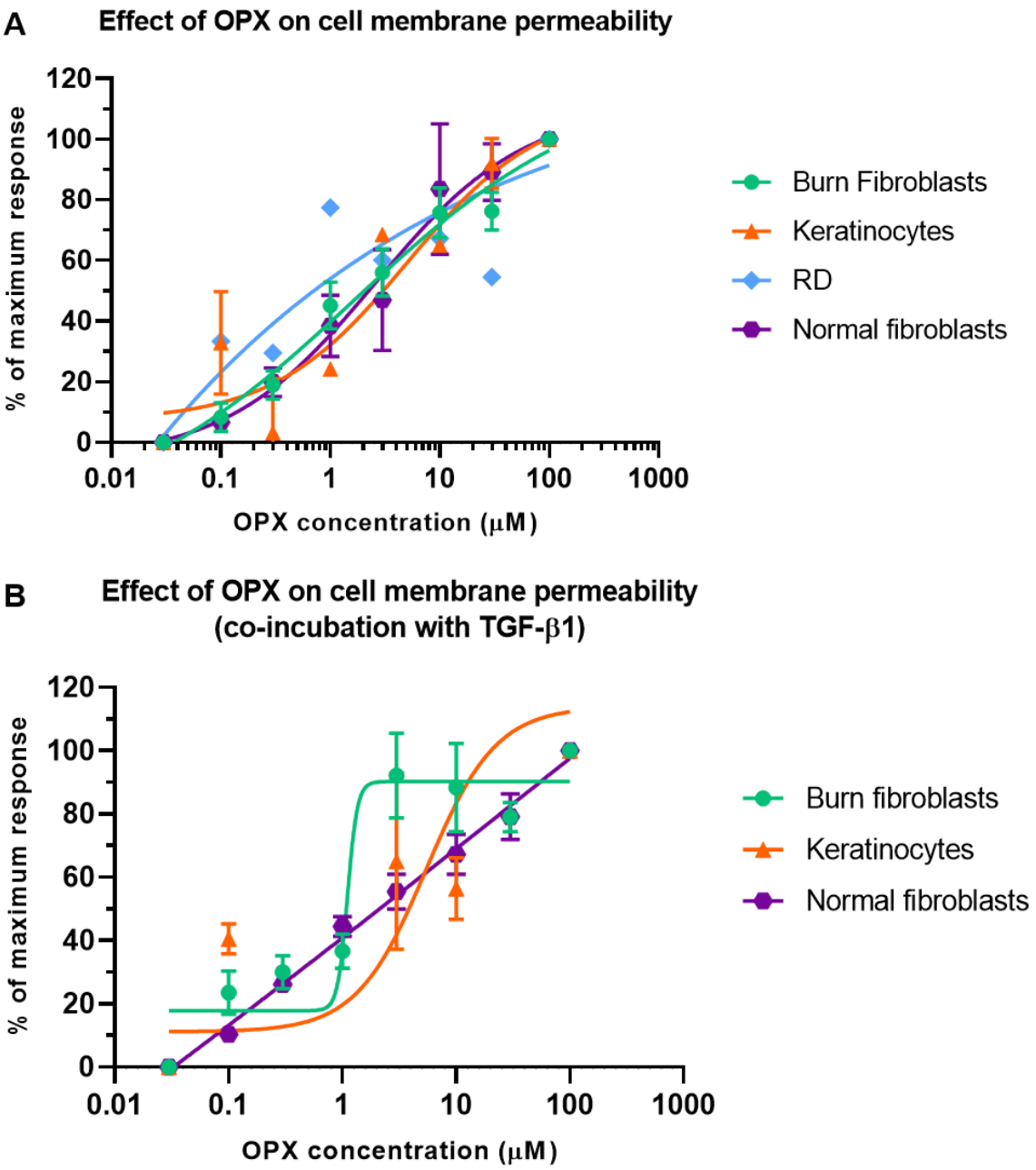

Supplementary figure 12: Effect of OPX on cell membrane permeability when cells are A) untreated and B) treated with 10 ng/mL TGF-β1. A full concentration response curve was generated for OPX, where cells were treated with a range of concentrations of OPX (0.03 µM – 100 µM). Data points are plotted as average ± SEM, where N=3, n=9.

Appendix III.II.V. Effect of candidate drugs on keratinocyte EMT

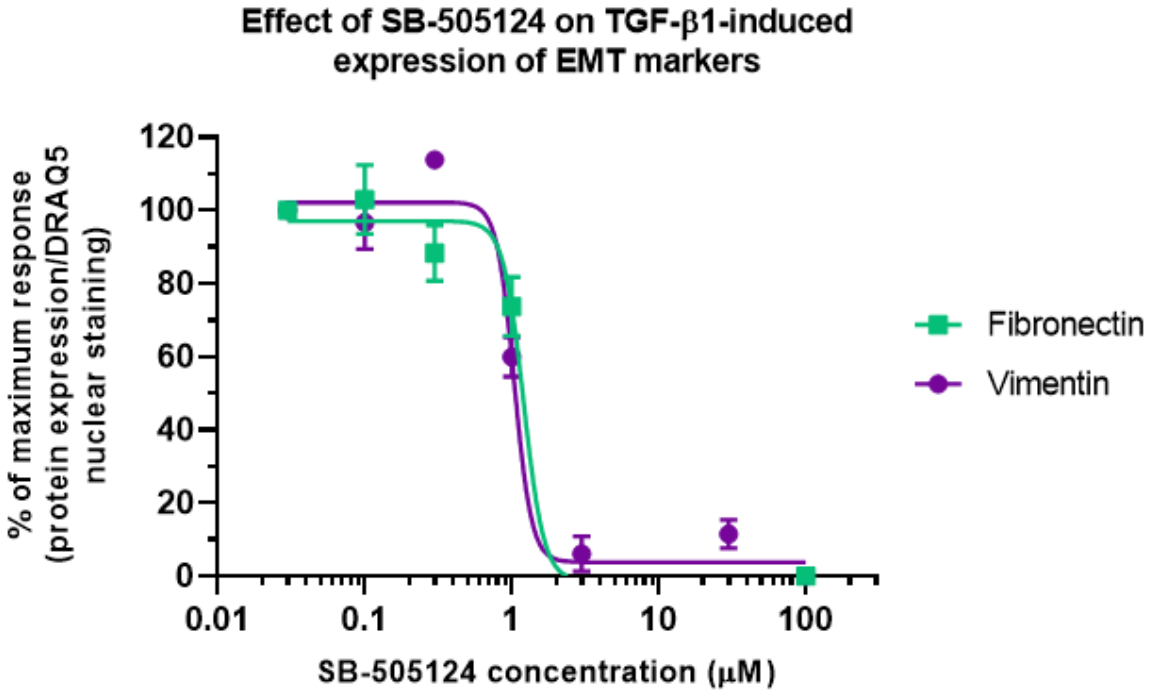

Supplementary figure 13: Effect of SB-505124 on TGF-β1-induced expression of EMT markers. Keratinocytes were co-treated with 10 ng/mL TGF-β1 and a range of SB-505124 concentrations (0.03 μM – 100 μM) for 72 h. A full concentration response curve was generated for both vimentin and fibronectin expression. Data points are plotted as average ± SEM of the percentage of maximum response, where N=1, n=3.

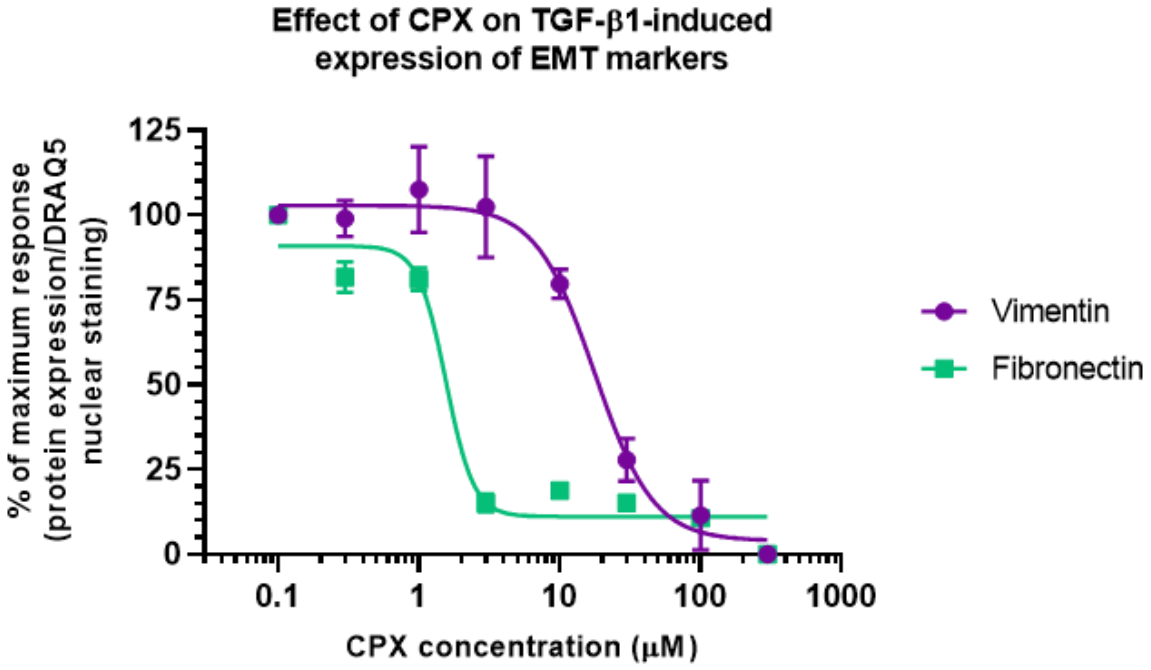

Supplementary figure 14: Effect of CPX on TGF-β1-induced keratinocyte EMT. A full concentration response curve was generated for CPX, where keratinocytes were incubated with 10 ng/mL TGF-β1 and a range of concentrations of CPX (0.1 μM – 300 μM), before measuring fibronectin and vimentin expression using the In-Cell ELISA method. Data points are plotted as average ± SEM, N=1, n=3.

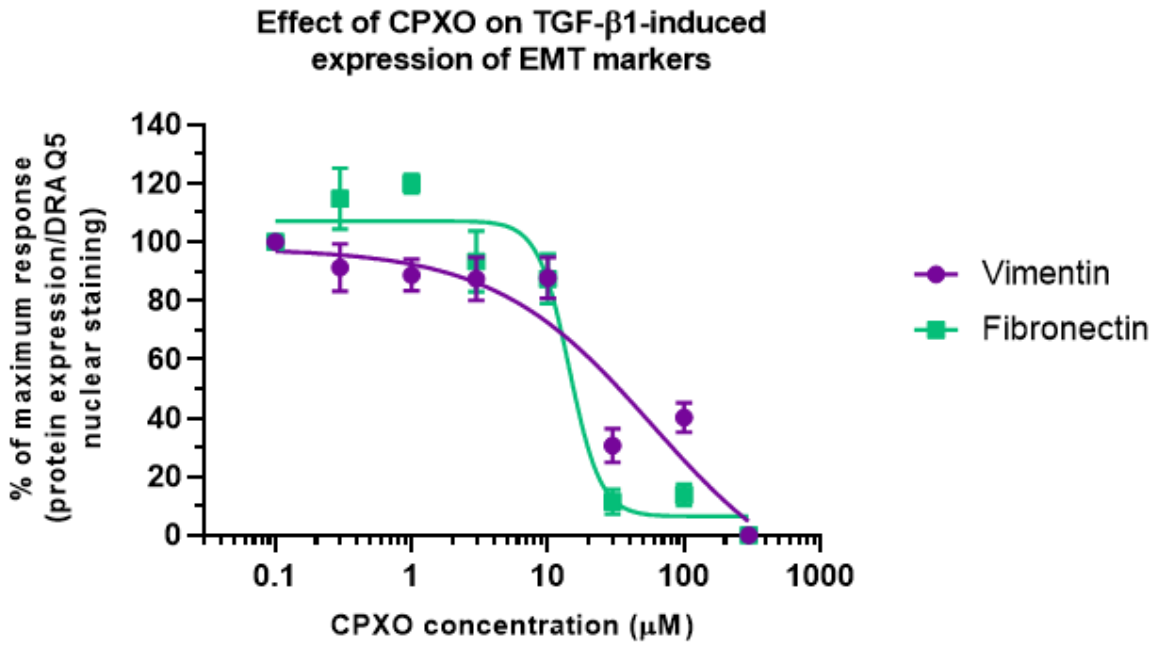

Supplementary figure 15: Effect of CPXO on TGF-β1-induced keratinocyte EMT. A full concentration response curve was generated for CPXO, where keratinocytes were incubated with 10 ng/mL TGF-β1 and a range of concentrations of CPXO (0.1 μM – 300 μM), before measuring fibronectin and vimentin expression using the In-Cell ELISA method. Data points are plotted as average ± SEM, N=1, n=3.

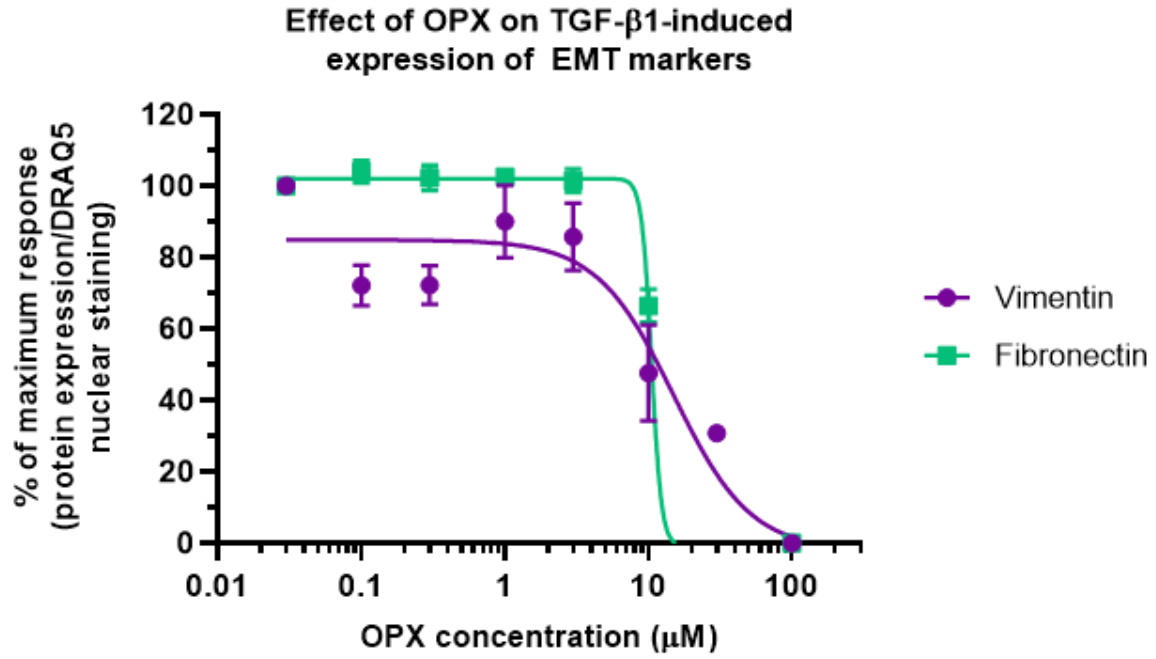

Supplementary figure 16: Effect of OPX on TGF-β1-induced keratinocyte EMT. A full concentration response curve was generated for OPX, where keratinocytes were incubated with 10 ng/mL TGF-β1 and a range of concentrations of OPX (0.03 μM – 100 μM), before measuring fibronectin and vimentin expression using the In-Cell ELISA method. Data points are plotted as average ± SEM, N=1, n=3.

Appendix III.II.VI. Effect of candidate drugs on ECM production

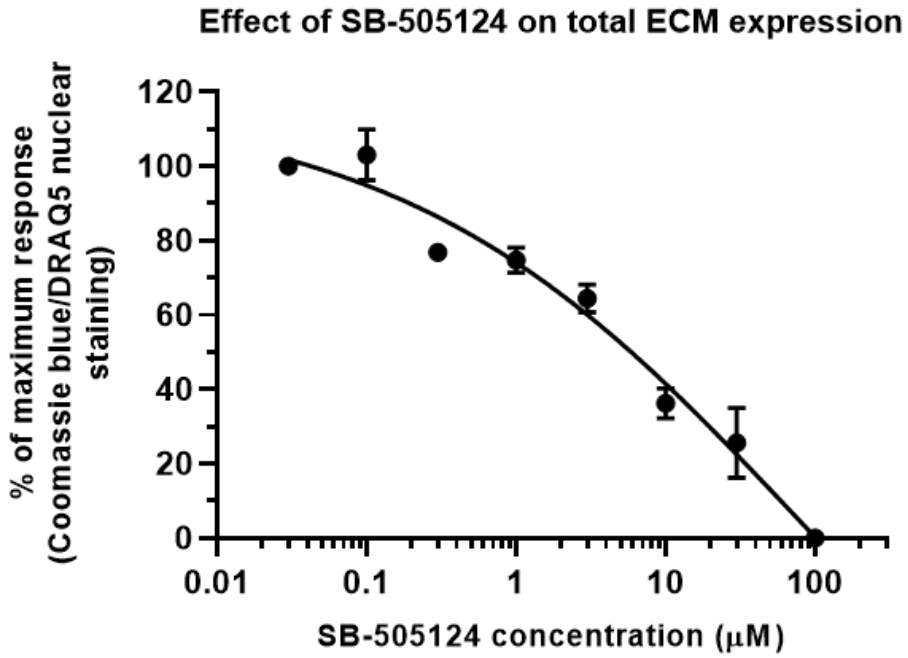

Supplementary figure 17: Effect of SB-505124 on total ECM production. A full concentration response curve was generated for SB-505124 where fibroblasts were incubated with 10 ng/mL TGF-β1 and a range of concentrations of SB-505124 (0.3 μM – 100 μM) for 7 days. Total ECM production was measured by staining the ECM with Coomassie blue solution. Data points are plotted as average ± SEM, N=3, n=9.

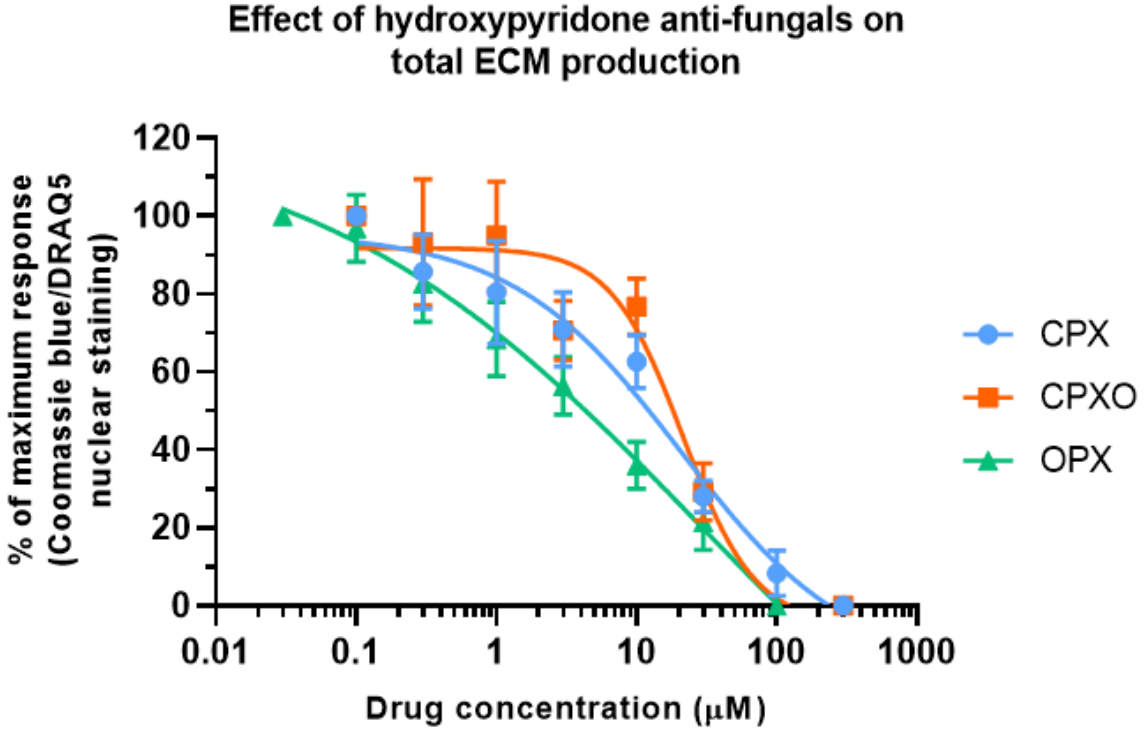

Supplementary figure 18: Effect of hydroxypyridone anti-fungals on total ECM production. A full concentration response curve was generated for CPX, CPXO and OPX where fibroblasts were incubated with 10 ng/mL TGF-β1 and a range of concentrations of CPX/CPXO (0.1 μM – 300 μM) and OPX (0.03 μM – 100 μM) for 7 days. Total ECM production was measured by staining the ECM with Coomassie blue solution. Data points are plotted as average ± SEM, N=3, n=9.

Appendix IV: Abstracts of presentations arisen from this thesis

Marcus M. Ilg, Alice R. Lapthorn, Justine V. Sullivan, Peter Dziewulski, Odhran P. Shelley, Asif Muneer, David J. Ralph, Selim Cellek. Identification of novel therapeutics for fibrotic diseases using phenotypic screening. Presented at the British Pharmacological Society and ELRIG joint meeting: Translating Ideas into Therapies (June 2021).

Marcus M. Ilg, Alice R. Lapthorn, Justine V. Sullivan, Peter Dziewulski, Odhran P. Shelley, Asif Muneer, David J. Ralph, Selim Cellek. Phenotypic screening as a tool to identify novel therapeutics for fibrotic diseases. Presented at the British Pharmacological Society and Society for Medicines Research joint meeting: Current Trends in Drug Discovery (June 2021).

Alice R. Lapthorn, Marcus M. Ilg, Sophie L. Harding, Justine V. Sullivan, Peter Dziewulski, Odhran P. Shelley, Asif Muneer, David J. Ralph, Selim Cellek. Using phenotypic screening to identify novel treatments for fibrotic disorders. International Journal of Experimental Pathology. 2021;102:A1-A17.

Alice R. Lapthorn, Marcus M. Ilg, Justine V. Sullivan, Peter Dziewulski, Odhran P. Shelley, Selim Cellek. High-throughput screening reveals 90 hits that can inhibit myofibroblast transformation in an *in vitro* model of dermal scarring. Presented at the British Society for Investigative Dermatology Annual Meeting (March 2021).

Alice R. Lapthorn, Marcus M. Ilg, Justine V. Sullivan, Peter Dziewulski, Odhran P. Shelley, Selim Cellek. Screening of 1,954 FDA-approved drugs reveals 90 hits with anti-myofibroblast activity using an *in vitro* model of cutaneous scarring. British Journal of Pharmacology. 2019;178(2):411. DOI:10.1111/bph.15316

Marcus M. Ilg, Alice R. Lapthorn, Asif Muneer, Nim Christopher, Selim Cellek, David J. Ralph. High-throughput phenotypic screening campaign of 1,954 FDA-approved drugs reveals 41 hits with anti-myofibroblast activity in an in vitro model of Peyronie's disease. Journal of Sexual Medicine. 2020;17(6):S129. DOI: 10.1016/j.jsxm.2020.04.035

Alice R. Lapthorn, Marcus M. Ilg, Justine V. Sullivan, Peter Dziewulski, Selim Cellek. Development of a high-throughput, cell-based phenotypic assay to identify novel anti-fibrotic medicines to prevent scar formation after burn injury. Journal of Investigative Dermatology. 2019;139(5):S122. DOI: 10.1016/j.jid.2019.03.785